EXAMINATION OF HYDRODYNAMIC SOIL-PLANT WATER RELATIONS WITH A NEW SPAC MODEL AND REMOTE SENSING EXPERIMENTS

By

ZIJUAN DENG

As a requirement in full for the degree of

Doctorate of Philosophy

The School of the Environment,
Faculty of Science and Engineering,
Flinders University of South Australia, Adelaide

December, 2014

TABLE OF CONTENTS

SUMMARY

Understanding soil-plant water relations is important for water resources management and ecosystem conservation in a changing environment. Simulating the water transfer in the soil-plant-atmosphere continuum (SPAC) is one of the key ecohydrological subjects which illustrates land surface mass and energy exchanges and provides meaningful guidance for future scenarios. Barriers, however, exist in SPAC modelling in terms of data sharing and methodology integration among the communities of hydrology and eco-physiology.

This study focuses on developing a new SPAC model (namely v-SPAC model) to enhance the communications between the communities. Unlike hydrologic models which lack representation of key plant hydraulic processes or eco-physiological models which usually assume steady-state environment, the new model integrates both root-zone hydrological processes and vegetation controls on plant water use. For the first time, a model of such type is parameterized with reduces uncertainty in hydrologic model calibration. Testing of the v-SPAC model was conducted on two native species: *Acacia pycnantha* in the natural field and potted *Eucalyptus crenulata* saplings in a water controlled experiment. The results show that the v-SPAC model performs well in reproducing the dynamics of both plant and soil water status and water flux.

Equipped with the new model, we are able to explore several hot topics in ecohydrology. For example, nocturnal transpiration has attracted continuous attention in the eco-physiology group, which, however, is ignored in the zero flux boundary in the hydrologic models. The v-SPAC model is capable to quantify the observed hydraulic disequilibrium between soil and plant which cannot be explained with

hydrologic models. The v-SPAC model is also used to evaluate the associated uncertainties in the nocturnal transpiration calculation with existing methods in the eco-physiology group.

Based on the v-SPAC modelling experiments, the robustness of a novel method (RWRC method) to depict root zone soil water retention curve is tested. With simulations under various plant, soil, atmosphere scenarios, the v-SPAC model helps to identify favourable conditions for the RWRC application. The new method provides an important complement to the tradition methods which may only capture the soil hydraulic properties at the centimetre scale. In some cases, this can be done over metre scale but with high cost. The new method characterizes the root-zone averaged hydrological properties (in metre scale) which are more appropriate for root-zone hydrologic modelling and land surface modelling.

Finally, the usefulness of thermal remote sensing technique is tested on detecting plant water stress. The v-SPAC model is indirectly applied by gap-filling the benchmark water stress time series. The work serves as an important extension to previous components as thermal remote sensing is a common up-scaling tool for land surface modelling. The experiment provides important insight into upscaling individual tree properties to ecosystem level with remote sensing technique. The results suggest that the linear upscaling scheme commonly used in remote sensing may not be valid under all atmospheric conditions.

This thesis demonstrates the great benefits of integrating knowledge, data and methodology from both hydrology and eco-physiology fields. The preliminary application of the v-SPAC model has illustrated its robust capacity in explaining some ecohydrological phenomena and is expected to continue contributing to the field.

DECLARATION

I certify that this thesis does not incorporate without acknowledgment any material previously submitted for a degree or diploma in any university; and that to the best of my knowledge and belief it does not contain any material previously published or written by another person except where due reference is made in the text

—————————————————

ACKNOWLEDGEMENTS

LIST OF TABLES

LIST OF FIGURES

LIST OF SYMBOLS AND ABBREVATIONS

Notation (Variables)	Description
Flux terms	
PET (mm/d)	Potential evapo-transpiration
PT (mm/d)	Potential transpiration
T (mm/d)	Actual transpiration
PE (mm/d)	Potential evaporation
E (mm/d)	Actual evaporation
ET (mm/d)	Actual evapo-transpiration
RWU (mm/d)	Root water uptake from soil moisture
SAP (mm/d)	Sap flux normalized by land surface
SAP (cm/hr)	Sap velocity in tree stem xylem
nSAP (cm/hr)	Average raw sap velocity measured in tree stem xylem in night-time (without radiation)
dSAP (cm/hr)	Average raw sap velocity measured in tree stem xylem in day time
Tn (cm/hr)	Night-time transpiration calculated from sap flow measurement
IN (mm/d)	Rainfall or irrigation infiltration to soil surface
RO (mm/d)	Surface runoff
D (mm/d)	Drainage below root zone
$\Delta S(r/s/L)$ (mm/d)	Storage change in (root/stem/leaf)
SAPmax (cm/hr)	Maximum sap velocity at day time
Water state terms	
θ_s (/)	Soil moisture content at saturation
θ_r (/)	Residual soil moisture content
Θ (/)	Soil moisture saturation
ψ_s (MPa)	Soil water potential
$\psi_{s,v}$ (MPa)	The equivalent soil water potential interception of xylem water potential at zero sap flow rate
ψ_x (MPa)	Xylem water potential

$\Psi_{x(rc)}$ (MPa)	Xylem water potential at root collar
$\psi_{r,m}$ (MPa)	Root xylem water potential at node m
$\psi_{x(s)}$ (MPa)	Xylem water potential at stem
$\psi_{x,pd}$ (MPa)	(Stem) xylem water potential at predawn
ψ_{L} (MPa)	Leaf water potential
$\psi_{L,min}$ (MPa)	Minimum leaf water potential
$\psi_{r,min}$ (MPa)	Minimum root water potential allowed in LEACHM and v-SPAC model

Resistance or conductance terms (d is day)

K (mm/d)	Soil hydraulic conductivity
K_s (mm/d)	Saturated soil hydraulic conductivity
k_s (mmol·s^{-1}·MPa^{-1})	Maximum plant hydraulic conductance
K_{sr} (mm/d)	Soil to root hydraulic conductivity
R_{sr} (d)	Soil to root interfacial resistance
$R_{sr,i}$ (d)	Soil-root interfacial resistance in soil layer i
R_p (d)	Plant resistance of water transport from soil-root interface to stem xylem
R_{min} (d)	Minimum plant resistance/ inverse of maximum hydraulic conductance
$R_{r,t}$ (d)	Total resistance of root system
$R_{r,i}$ (d)	Effective root resistance in soil layer i normalized by land surface area
R_{rr} (d)	Radial root resistance; resistance of water transfer from root surface to root xylem.
$R_{x(r/s/L)}$ (d)	Xylem resistance in longitudinal direction; resistance of water transfer within root, stem or leaf conduit (such as vessel, tracheids).
R_c (/)	Friction loss in the root in LEACHM (not used in v-SPAC model)
$R_{s\,(r/s/L)}$ (d)	Resistance of water transfer from root/stem/leaf storage component to water transpiration stream

Other terms

HC	Abbreviation for Hydraulic conductivity
HCL	Abbreviation for Hydraulic conductivity loss
VC	Abbreviation for Vulnerability curve, to describe the plant resistance change with plant water status

IVC	Abbreviation for Integrated vulnerability curve
d (MPa)	parameter in the vulnerability curve
b (/)	parameter in the vulnerability curve
C (mm/MPa)	Capacitance of tree storage (lumped)
Δx (mm)	The effective distance from measured bulk soil to root surface
RDF	Root length density distribution function
L (mm)	Maximum root depth
β(/) (in RDF)	Shape parameter in RDF
λ(/) (in RDF)	Normalization factor to constrain sum of RDF all soil layers to unit one.
$f(\psi_x)$	Reduction function for transpiration
p_1 (MPa) (in $f(\psi_x)$)	The point of ψ_x above which the sap flow rate equals that under fully available water.
p_2 (MPa) (in $f(\psi_x)$)	The point of ψ_x below which the sap flow rate equals zero.
WRC	Abbreviation for Water Retention Curve: relation between water content and water potential
α (1/kPa) (in soil WRC)	Parameter in Van Genuchten WRC function
n (/) (in soil WRC)	Parameter in Van Genuchten WRC function
m (/) (in soil WRC)	Parameter in Van Genuchten WRC function
VPD (kPa)	Vapour pressure deficit
dVPD (kPa)	Day time average VPD
nVPD (kPa)	Night-time average VPD
Rg (W·m^{-2})	Global radiation
g_s(mol·m^{-2}·s^{-1})	Stomata conductance
g_c(mol·m^{-2}·s^{-1})	Canopy conductance
LAI (m^2·m^{-2})	Leaf Area Index
LAD (m^2·m^{-2})	Leaf Area Distribution
RAI (m·m^{-2})	Root area index
Gs	Abbreviation for Stomata Conductance
UB	Abbreviation for Upper Boundary
LB	Abbreviation for Lower Boundary
SS plot	Plot of sap flow rate (SAP) versus stem ψ_x

1 INTRODUCTION

Mechanistic understanding of plant water relations is essential to understand how ecosystems interacts with the environments, and survive and evolve with the climate variation and changes, and the consequences in water resources, carbon budget, and land surface and the atmosphere interaction. The major attributes of plant water relations include leaf water potential, transpiration rate, root water uptake etc. (Aroca, 2012). Water flow in plant and plant water strategies under water-limited environment are century-old topics (Kramer and Boyer, 1995) and challenges remain such as prediction of ecosystem vulnerability and resilience to drought (McDowell et al., 2008). Plant's response to a changing climate and its feedback to climate and land water balance are shared concerns in ecology, physiology and hydrology communities (Adams et al., 2012; Anderegg et al., 2013; Bond et al., 2008). Recently, it has raised world-wide awareness of the great loss in land-scape scale tree mortality caused by the extreme climate (McDowell et al., 2011). The recent worst in a millennium drought in California (2012-2014) again brought the research subject and the hydrological, agricultural, ecological and social-economic consequences into the centre of the public attention (Griffin and Anchukaitis, 2014).

Plant water relation is a multi-discipline subject that requires combined efforts between the communities. Evidence has shown that factors on water relations in the soil, plant and climate system are interdependent and the cause-effect is hard to quantify. For example, McDowell et al. (2013) found out that no threshold (in tree properties) for tree mortality to drought can be clearly identified, rather, the intensity and duration of climate drought is more important. Bucci et al. (2009) reported that

soil water availability and rooting depth are determinant of plant hydraulic conductivity of Patagonian woody species. Yunusa et al. (2010) noted a plant adaption in hydraulic properties to the local soil and water conditions, from observation that less wood density variation across tree species in long water stressed sites than variation between two neighbouring sites of the same tree species. Plant's structure can also feedback to soil water balance, such as different root architecture can result in different soil moisture profile (Doussan et al., 2006), thus influence the soil water balance. Catchment scale water balance can be influenced by disturbance events in forest ecosystem and the different stages of ecosystem such as the aged ecosystem may reduce evapotranspiration than the regenerated ecosystem (Bond et al., 2008).

However, the barriers to fusing the knowledge, skills (such as modelling) and data resources between the communities are apparent. SPAC models are useful tools to integrate the processes involved in the water interaction between soil, plant and atmosphere and provide meaningful guidance for ecosystem response and consequences in future climate and land-cover scenarios. Most SPAC models, however, focus either in soil hydrology or plant physiology component (see table 1 below), while neglecting the detailed process in the other component. For example, the mechanisms that are observed in plant are usually in descriptive way and the observation data are not compatible in scale with hydrological models. While hydrological models have strengths on simulating dynamic soil flux under various climate conditions but ignores the plant water use strategy. For example, potential transpiration and a reduction function are commonly used to represent all of the plant's role in water consumption in hydrologic models, while plant physiologic models may treat soil part as simple water potential boundaries (such as (Chuang et al., 2006; Holtta et al., 2009)). The mechanic plant models are usually confined for hypothetical test

and can be only practically validated in lab experiment (e.g. Doussan et al., 2006). To transfer the knowledge to field condition and to provide insight into scenarios with various combinations of water, energy environment, the bridging between the disciplines needs to be advanced (Anderegg et al., 2013).

Therefore, models that are capable of integrating multiple data sources and consider both the transient environment conditions and plant eco-physiology are valuable in terms of application for field conditions. A good example is demonstrated in King and Caylor (2011), who showcased an enhanced understanding of the plant's behaviour by the marriage of the two disciplines, combining the modelling strengths from hydrology and the control experimental skills from ecology. A brief review is given below on models for simulating water transfer in SPAC and the current capacity of modelling is discussed.

1.1 Water transfer in SPAC

SPAC describes the water transfer in the continuum from soil, root, stem and leaf to the atmosphere. Water transport in plant is governed by the cohesion-tension theory (Dixon and Joly, 1895) which views the transport as a passive process driven by evaporation depletion at leaf level (Dixon and Joly 1895; Kramer and Boyer, 1995; Tyree and Zimmermann, 2002). The detail description of mechanisms and processes involved in water transport in vascular plant can be found in (Sack and Holbrook, 2006; Tyree and Zimmermann, 2002). Figure 1-1 gives the numerical representation of the key resistances and capacitance terms considered in SPAC models.

SPAC models have different focuses and capacities for specific research questions and application purposes. For example, root models focus on water and solute transport in root zone. The root architecture are described in 3D space and the water transport

between root and soil cubic elements are explicitly simulated, while the above ground part are simplified as flux or potential boundaries (e.g. Doussan et al. (2006)). The xylem models focus on water transport in stem trunks in which the trunk is treated as porous media similarly as the soil porous media, and the storage of the trunk is considered as the difference between the input and the output flux. 3D Root models usually do not consider the storage compartment as in xylem models but only view the root as water conduit. Another type of models is based on analogy to resistance-capacitance circuit which are usually 1D models that can embrace all resistance and storage components (Chuang et al., 2006). These models have advantages in greater computing efficiency, but may result in unreasonably large water flux (Chuang et al., 2006; Janott et al., 2011). In this study, we built a model that explicitly described soil-root water transport in porous media but analogize the water flow in plant to RC circuit. The treatment can avoid unreasonable large water flux by constraining the water flux of the below ground processes while represent the above ground processes simple and effective.

Representing the root hydraulics in SPAC model is the key to predict plant water status (Bucci et al., 2009; Jackson et al., 2000). The underground processes involving the roots are most unknown part due to the difficulty of data acquisition. The root was observed more vulnerable than stem to water stress (Jackson et al., 2000). The impact of root shrinkage on soil-root contact and further the change of total resistance to water transfer has been observed (Carminati et al., 2009; Nobel and Cui, 1992). In the following subsection, different models that simulate water transfer processes in different components of SPAC are introduced with emphasis on root water uptake. The associated challenges facing the research of soil-plant water relations are highlighted.
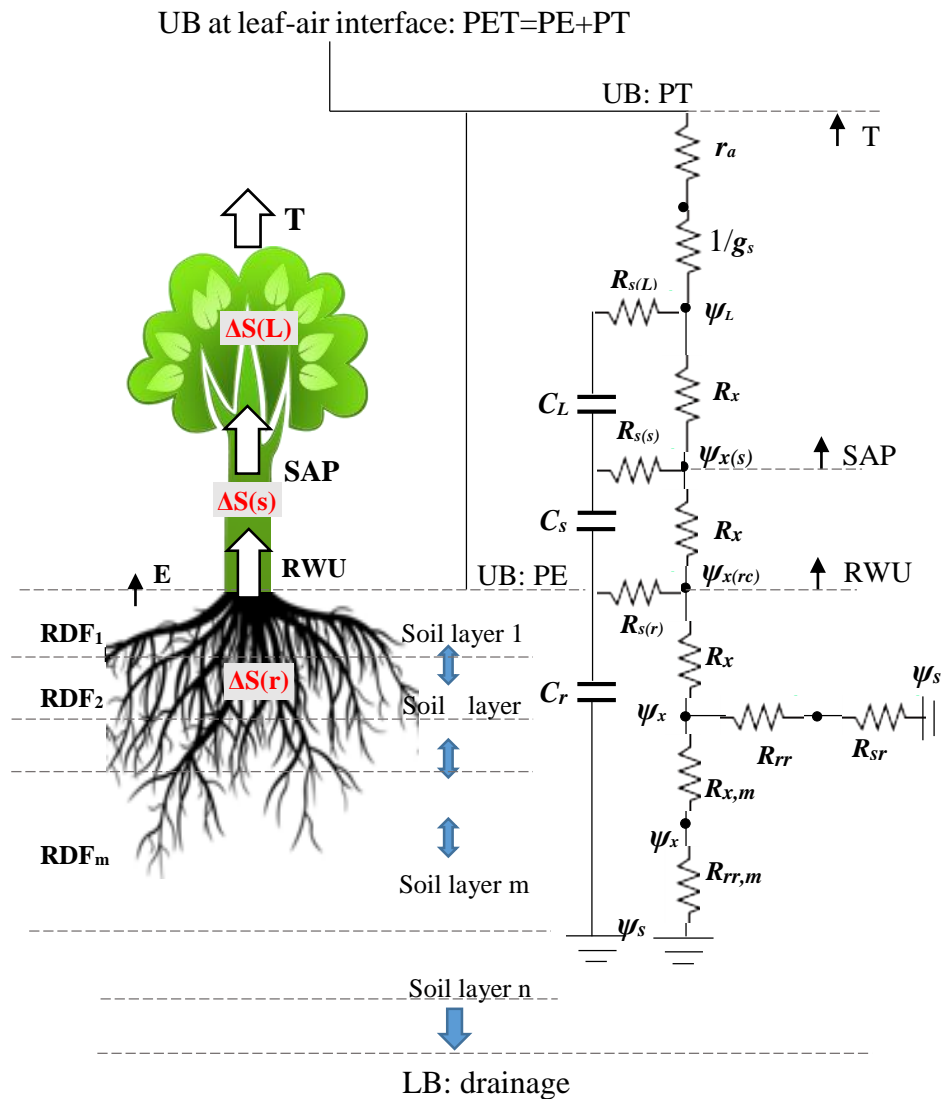
Figure 1-1: Schematic illustration of water transfer in SPAC (modified from (Sack and Holbrook, 2006), refer to the list of symbols and abbreviations on page xiii)

1.1.1 Current modelling capacity for SPAC models and the need

SPAC models are differentiated in terms of model focuses and coupling extent of the components from soil through root, stem, and leaf to atmosphere. SPAC models include **root models** that focus on root water transport such as 3D root models where upper flux boundaries are usually prescribed as potential transpiration or fixed root pressure (e.g. Javaux et al., (2008)). **Xylem models** describe water transport in xylem porous media (from tree xylem to atmosphere). Such models include storage release

which can simulate the lag time of transpiration and storage refilling.

Models that describe complete water path through soil-root-stem-leaf-atmosphere are **fully coupled ones**. Such models aid us to understand the tree water use restrictions, such as those by Sperry et al. (1998) and Holtta et al. (2009). The two models are ideal for theoretical studies, but not applicable to predict transient plant water status and water flux with climate forcing. Practical ones that were validated in field conditions include SiSPAT (Braud et al., 1995), SWIM (Verburg et al., 1996), SPA (Williams et al., 1996) and XFM (Janott et al., 2011). However, the first three models assign constant plant resistances (see table 1-1) and the last one has high data requirement (see Table 1-1 below).

Table 1-1: Summary of coupled SPAC models applicable to predict plant water status and water flux in field cases

Models	Minimal forcing data*
1) SiSPAT	WRC(soil), K_s, R_r, R_x, RDF, LAI,
2) SWIM	WRC(soil), K_s, root radius, root length, RDF, R_r
3) SPA	WRC(soil), K_s, root radius, root length, LAD (similar to RDF), R_a, R_b, $\psi_{L,min}$, , C
4) XFM	WRC(soil), K_s, Root radius, root length, RDF, R_{rr}, R_{xr}, $R_{xs,}$ R_{xL}, VC, WRC(plant), LAI, LAD, RAI, …
5) v-SPAC (this study)	WRC(soil), K_s, R_{min}, RDF, LAI, VC, C

Note: * VC is used to describe transient plant resistance with plant water potential, without VC, plant resistance are not considered or prescribed an empirical constant value. Only XMF and v-SPAC consider transient plant resistance. The capacitance (C) of XMF is included in WRC (plant) function, while our model and SPA use constant C. See definition in the list of symbols and abbreviations on page xiii.

With reviewing the detailed mechanic processes involved, the key processes in SPAC models are identified and targeted for improving their numerical representation in the

new model – a vegetation focused SPAC model (v-SPAC). The v-SPAC model is designed at tree scale for one dimensional soil/plant water transport simulation under different

1.1.1.1 Root models

Root models fall into two categories: macroscopic and microscopic (Hopmans and Bristow, 2002). Macroscopic models describe root water flux as a sink term in Richards equation: the soil water extraction by root are either constrained with empirical stress functions (such as Feddes et al. (1978) stress functions used in Hydrus model (Šimůnek et al. 1998)) or driven by water potential gradient with resistance terms linked to soil or root hydraulic properties (such as scheme of (Nimah and Hanks, 1973) used in LEACHM (Hutson and Wagenet, 1995) and Campbell's 1985 scheme in Sperry et al. (1998) and SWIM (Verburg et al., 1996)). As all models constrain the total soil water extraction with the potential transpiration flux boundaries, when the flux boundary is prescribed, the different root uptake schemes are actually partitioning scheme of water extraction from the soil profile. For example, in Hydrus, the proportion of soil water extraction will follow the stress function that is based on soil water potential/ moisture. The root resistances are ignored, thus Hydrus cannot predict the water potential of root which is needed to calculate plant water balance. Although, Rings et al. (2013) attempted to produce plant water balance by introducing to Hydrus a similar stress function for tree xylem, the temporal root water reservoir at the plant bottom boundary may become inappropriate for simulation under water stressed conditions. LEACHM and SWIM can predict root water potential that bridges the plant and soil hydraulic measurement. The issue with LEACHM is that it does not include root resistance, thus may heavily overestimate water contribution from deep soil layers due to the exponentially increasing soil hydraulic conductivity with

commonly higher soil moisture content with depth. SWIM incorporates root resistance that is linked to root length density and root diameter. The root is only viewed as conducting compartment and the resistance is fixed; the root length density and root diameter in detail are usually not available in natural field conditions.

3D root models with detail root hydraulic architecture help us to understand root water uptake in sub-meter spatial scales over transient soil water conditions. Different from macroscopic root models that only consider root radial resistance (such as SWIM, SiSPAT), 3D root models account for both radial and axial root resistances. However, Doussan et al. (2006) show that radial root resistances are the major resistance and the axial resistance can be ignored for most cases (Doussan et al. 2006). Recent 3D root models include those developed by Dossuan et al. (2006), R-SWMS by (Javaux et al., 2008) and by Schröder (2009). Dunbabin et al. (2013) offered a good review on 3D root models. The models till now, mostly remain in lab validation or indirectly validated. For example, Vrugt et al., (2001) shows one validation with 3D soil moisture measurement (different depths and distances to one tree trunk) without plant validation. Besharat et al. (2010) also validated the root water uptake functions with 3D soil moisture measurement. Doussan et al. (2006) validated the model with constrained pot roots in the lab. The data requirement of such models or experiments are usually not fulfilled in field scale and the models are computationally intense for landscape scale modelling.

Root resistances were observed or indirectly inferred to vary with root water potential diurnally (Nobel and Cui, 1992; Domec et al. 2006), suggesting daily discharge and recharge of root water storage (Scholz et al. 2011). However, representation of such root traits is lacking in both microscopic and macroscopic models, which otherwise, is

required to capture the sub-daily to seasonal plant water status dynamics (Domec et al. 2006).

1.1.1.2 Xylem models

Xylem models focus on water transport in the tree stem. There are two types of xylem models in terms of modelling method (Chuang et al., 2006): one is called Resistance-Capacitance (RC) models that analogize the water transport as electric circuit system (Phillips et al., 1997; Verbeeck et al., 2007) or porous media (PM) models that describe tree xylem as porous media of which the water transport is governed with Richards equation (Chuang et al., 2006; Janott et al., 2011). The PM models, similar to 3D root models, require large amount of tree allometric data such as tree branching and xylem hydraulic conductivity of stem, branches and roots. This complex PM model is hard to apply on cases without thorough measurement of the tree canopy structure, plant hydraulic properties etc. RC models seems more commonly used to quantify tree water use than PM models, but PM models are recently increasingly used to explain tree water use limitation due to plant hydraulic properties (Chuang et al., 2006; Holtta et al., 2009; Janott et al., 2011). To describe the hydraulic properties of the xylems, vulnerability curves and plant water retention curves need to be characterized in the PM models (Janott et al., 2011).

1.1.1.3 Storage term

Tree **storage** not only plays crucial role in desiccation but also plays a diurnal routine: quick depletion of storage for early transpiration at sunrise and storage refilling in late day (Cermak et al., 2007; Chuang et al., 2006; Verbeeck et al., 2007). The storage may contribute from either the rigid xylem or elastic cells (such as bark) or both (Pirson and Zimmermann, 1982). The water is released through processes such as capillary, xylem cavitation and cell shrinkage etc. (Micco and Aronne, 2012). The capacitance

that describes the release of water per change of water potential varies even on one xylem segments (Tyree and Zimmermann, 2002). For example, capacitance was largest when capillary water was released above -0.5 MPa, and reduced between -0.5 and -2.5 MPa, then the capacitance rise again due to xylem cavitation effect (Tyree and Zimmermann, 2002). Cermak et al. (2007) stated that the major contribution is from rigid xylem and that of elastic compartment (bark) is limited in big trees. Numerical discrimination of the storage release phases seem not considered. The storage term is usually described as one lumped term of whole tree capacitance (Sperry et al., 1998) or as constant for different components: leaf, stem or root (Hunt and Nobel, 1987; Sack and Holbrook, 2006). Most RC models use this lumped capacitance. PM models assumes decreasing capacity with decreasing water potential (e.g Chuang et al. (2006) and Kumagai (2001)) since the models assume water release majorly from capillary water.

1.2 Challenges in plant water relation research

1.2.1 Plant hydraulic properties in models and its validation

Concerns on plant response to a changing climate is increasing with the awareness of the world wide tree mortality (McDowell et al., 2013). The loss of forest are magnificent that can result in forest transition from carbon sink to source, water regime transition etc. (Adams et al., 2012). Hydraulic loss of trees was identified as one major reason that accounts for tree mortality during climatic droughts (McDowell et al., 2013). To evaluate the vulnerability and resilience of ecosystems during and after disturbance events are challenges to predict future maps of ecosystem in a changing climate. The hydraulic properties can indicate global convergence of vulnerability of forests (Choat et al., 2012), emphasizing the importance of measuring and incorporating tree hydraulic properties in models. The dynamic response of hydraulic

conductivity to various water conditions, especially the drought conditions are the key points. Cases that simulate and validate tree scale plant hydraulic properties are rare. Observations are usually conducted on tree segment and formed the so-called vulnerability curves (VC). VC describes the hydraulic resistance of water transfer at various water state in vascular plant. The governing function serves in the plant water balance calculation as the same as soil hydraulic function in hydrologic models. VC is usually compared between pre-drought and after-drought conditions to assess plant response to drought (Jackson and Sperry, 2002). While, continuous inference of hydraulic conductivity is not common. VC acquisition is labour intensive and hard to conducted on all segments, especially on roots. A direct method to derive VC for the whole tree is thus valuable to study the plant water relations.

1.2.2 Plant water balance and nocturnal transpiration

Nocturnal transpiration is not a rare phenomenon (Caird et al., 2007) and has been observed in diverse ecosystems (Dawson et al., 2007). The night-time stomata conductance can be as high as day-time conductance, and the total nocturnal transpiration flux amounts to 5-30% of daily transpiration (Caird et al., 2007). Ignoring this component will definitely miscalculate water requirement of ecosystem. The mechanisms of the nocturnal transpiration till now are not clear (Dawson et al., 2007; Snyder et al., 2003; Zeppel et al., 2013).

Direct measurement of tree nocturnal transpiration is a big challenge or is fulfilled at high cost (Buckley et al., 2011). The nocturnal transpiration were majorly calculated from sap flow calculation (Dawson et al., 2007; Caird et al., 2007). However, sap flow is comprised of both nocturnal transpiration and tree storage refilling. Therefore, partitioning the sap flux should be conducted for nocturnal transpiration calculation.

In hydrologic models, day-time sap flow is usually assumed to be transpiration and night-time sap flow is set to zero flux. Under well water conditions, the sap flow can be used to validate models on daily basis as the plant water storage is likely balanced. However, under water stress condition, tree storage may keep depleting that the sap flux may outnumber transpiration significantly (Verbeeck et al., 2007). SPAC models are capable to simulate plant water balance and water status, thus can be used to examine the contribution of storage refilling to the sap flow. However, as SPAC models are driven by potential transpiration boundary conditions, without proper representation of the nocturnal transpiration, night-time sap flow may not be properly interpreted. Energy-based methods such as Penman-Monteith equation are not suitable to constrain the upper flux boundary of SPAC models since it assumes zero stomata conductance in the night. It then requires to combine the eco-physiological methods with hydrologic models for the quantification of the nocturnal transpiration flux or for the validation of the hydrologic models with sub-daily sap flow measurement.

1.2.3 Plant water status monitoring using leaf temperature

Monitoring plant water status is essential for water and yield management (Moran et al., 1994). Plant water status is the basis for stomata conductance modelling and the dependent variable to estimate plant resistance from the vulnerability curve. Plant water status can be revealed from leaf water potential, relative water content, soil water potential/content, stomata conductance etc. (Micco and Aronne, 2012). Soil water content is relatively easy to obtain but need to be carefully manipulated to represent the whole root zone water status. Pre-dawn leaf water potential is viewed as a standard way to indicate plant water status. However, it is not practical to use pre-dawn leaf water potential as a daily routine due to its labour cost (Jones et al., 2007). Leaf temperature shows great potential for plant water stress monitoring in large scale

(Jones et al., 2007). The experience of the ground-based method are mostly applied on homogenous agriculture field but not in native vegetated landscape. The usefulness of the method may be impeded by leaf distribution (Fuchs et al., 1990), contamination of the non-leaf background temperature (Maes, et al., 2012), high VPD (Villalobos et al., 2009) or windy conditions (Moran et al., 1994). It then requires comprehensive study to examine the reliability of method under variable conditions and to derive effective procedure to improve the performance of the method.

Leaf or canopy temperature based thermal indices can indicate root zone water status (Moran et al., 1994), to scale the soil wetness or transpiration temporally (Anderson et al., 2012) and spatially (Yang and Shang, 2013) with satellite products. The scaling is commonly conducted with linear interpolating between the wet and dry reference temperatures. Most of leaf/canopy temperatures studies are conducted at fixed time window or one snapshot. High-temporal and continuous observation during a day and over the seasons of leaf/canopy temperature is rare, but provides valuable dataset to examine the linear upscaling scheme from point to day, and for the gap-filling between the two satellite bypass times.

1.2.4 The scaling issues in ecohydrology

Scaling transpiration from individual trees to the whole ecosystem is an outstanding challenge (Asbjornsen et al., 2011). Jarvis and McNaughton (1986) demonstrated a great example of how plant stomata and atmosphere conditions alternate to dominate the transpiration from stomata, to leaf, to canopy and to regional scales. It suggests that the controlling mechanisms and the domains could shift across scales which obscures simple aggregation of flux from small to large scales. Practically, however, only simple scalars are used for the upscaling task. For example, leaf area and sapwood

area have been commonly used to upscale the tree to stand transpiration. It was noted, however, that the stand transpiration and the leaf area could be decoupled on sandy soils under moisture limited conditions (Donovan and Sperry, 2002). The stand transpiration may be also controlled by the local micro-topography and the soil heterogeneity (Yunusa et al., 2012).

Upscaling of soil hydraulic properties has also been a long-standing challenge that involves integrating hydraulic properties at measurement scale to describe an effective homogeneous soil column that can be used in large scale (Mohanty and Zhu, 2007). The areal soil heterogeneity has now been increasingly tackled with remote sensing technique, but the vertical heterogeneity of soil layers' impact on soil hydraulic properties is much less explored and remains a challenging issue (Mohanty and Zhu, 2007; Shin et al., 2012). The root zone processes will further complicate the upscaling with unknown root distribution and its modification of the soil water balance. Root zone processes, to be described in one vertical dimension for land surface modelling, requires characterizing the effective root zone hydraulic properties (Vrugt et al. 2001; Mohanty and Skaggs, 2001; Shin et al., 2012). Viewing the soil and plant as a while and take the advantages of plant's

1.3 Objectives and outlines of the thesis

The thesis focuses on developing a vegetation-focused Soil-Plant-Atmosphere Continuum (v-SPAC) model. Unlike hydrologic models, which is only interested in simulating tree water flux, the v-SPAC model allows the simulation and assimilation of tree water potential such that, it can be used to explore some concerned ecohydrologic research questions. For example, why some trees response to water stress in isohydric way, while others are anisohydric in terms of leaf water potential;

why some trees showed immediate rise of stem water potential after a rain event while others do not. These questions requires a model with good characterization of plant hydraulic properties and the mechanisms that connects the soil and the plant hydraulically.

The model aims to simulate soil/plant water flux and water status with easy parameterization for field application. Model calibration with limited data in the field commonly occurred. Combining the multiple data sources, such as those of plant and soil will not only promote the confidence of model calibration but also enhance the understanding in the soil-plant water relations. The v-SPAC model is introduced and tested in Chapter 2.

Based on the v-SPAC model, we explore some interesting topics in soil-plant water relation research field. In Chapter 3, we investigate the nocturnal transpiration of two tree species with sap flow measurement. The uncertainties of existing methods in calculating nocturnal transpiration is evaluated with v-SPAC simulation. In Chapter 4, we propose a novel method to derive effective root zone water retention curve from stem-soil hydraulic continuum. The method is tested with synthetic numerical experiments with v-SPAC model and with real cases of two study sites. The new method could be used to describe the effective root zone hydraulic properties. In Chapter 5, we test the usefulness of leaf temperature on detecting soil/plant water status with ground-based thermography technique over two native tree species. The leaf temperature based thermal indices are compared to benchmark water stress indicators: soil moisture and stem water potential, of which the observation gap is filled with v-SPAC simulation.

References

Adams, H.D. et al., 2012. Ecohydrological consequences of drought- and infestation- triggered tree die-off: insights and hypothesis. Ecohydrology, 5(2): 145-159.

Anderegg, L., Anderegg, W., Berry, J., 2013. Not all droughts are created equal: translating meteorological drought into woody plant mortality. Tree Physiology, 33(7): 701-712.

Anderson, M. C., Allen, R. G., Morse, A., and Kustas, W. P. 2012. Use of Landsat thermal imagery in monitoring evapotranspiration and managing water resources. Remote Sensing of Environment, 122, 50-65.

Aroca, R. (Ed.). (2012). Plant responses to drought stress: from morphological to molecular features. Springer.

Asbjornsen, H. et al., 2011. Ecohydrological advances and applications in plant-water relations research: a review. Journal of Plant Ecology, 4(1-2): 3-22.

Ballester, C., Jimenez-Bello, M.A., Castel, J.R., Intrigliolo, D.S., 2013. Usefulness of thermography for plant water stress detection in citrus and persimmon trees. Agricultural and Forest Meteorology, 168: 120-129.

Berni, J., Zarco-Tejada, P., Sepulcre-Canto, G., Fereres, E., Villalobos, F., 2009. Mapping canopy conductance and CWSI in olive orchards using high resolution thermal remote sensing imagery. Remote Sensing of Environment, 113(11): 2380-2388.

Besharat, S., Nazemi, A.H., Sadraddini, A.A., 2010. Parametric modeling of root length density and root water uptake in unsaturated soil. Turkish Journal of Agriculture and Forestry, 34(5): 439-449.

Bond, B.J., Meinzer, F.C., Brooks, J.R. (Eds.), 2008. Chapter 2. How Trees Influence the Hydrological Cycle in Forest Ecosystems. John Wiley & Sons, Ltd, Chichester, UK.

Bond, B. J., Meinzer, F. C. and Brooks, J. R. (2008) How Trees Influence the Hydrological Cycle in Forest Ecosystems, in Hydroecology and Ecohydrology: Past, Present and Future (eds P. J. Wood, D. M. Hannah and J. P. Sadler), John Wiley & Sons, Ltd, Chichester, UK. doi: 10.1002/9780470010198.ch2.

Braud, I., Dantasantonino, A.C., Vauclin, M., Thony, J.L., Ruelle, P., 1995. A simple soil-plant-atmosphere transfer model (sispat) development and field verification. Journal of Hydrology, 166(3-4): 213-250.

Bucci, S.J., Scholz, F.G., Goldstein, G., Meinzer, F.C., Arce, M.E., 2009. Soil water availability and rooting depth as determinants of hydraulic architecture of Patagonian woody species. Oecologia, 160(4): 631-641.

Buckley, T., Turnbull, T., Pfautsch, S., Adams, M. 2011. Nocturnal water loss in mature subalpine Eucalyptus delegatensis tall open forests and adjacent E. pauciflora woodlands. Ecology and Evolution, 1(3), 435-450.

Caird, M. A., Richards, J. H., and Donovan, L. A. 2007. Nighttime stomatal conductance and transpiration in C3 and C4 plants. Plant Physiology, 143(1), 4-10.

Campbell, G.S., Norman, J.M., 1998. An Introduction to Environmental Biophysics.

Carminati, A., Vetterlein, D., Weller, U., Vogel, H.-J., Oswald, S.E., 2009. When Roots Lose Contact. Vadose Zone Journal, 8(3): 805-809.

Cermak, J., Kucera, J., Bauerle, W.L., Phillips, N., Hinckley, T.M., 2007. Tree water storage and its diurnal dynamics related to sap flow and changes in stem volume in old-growth Douglas-fir trees. Tree Physiology, 27(2): 181-198.

Choat B, Jansen S, Brodribb TJ, Cochard H, Delzon S, Bhaskar R, Bucci SJ, Feild TS, Gleanson SM, Hacke UG, Jacobsen AL, Lens F, Maherali H, Martinez-Vilalta J, Mayr S, Mencuccini M, Mitchel PJ, Nardini A, Pittermann J, Pratt RB, Sperry JS, Westoby M, Wright IJ, Zanne AE 2012. Global convergence in the vulnerability of forests to drought. Nature 491:752-755

Chuang, Y.L., Oren, R., Bertozzi, A.L., Phillips, N., Katul, G.G., 2006. The porous media model for the hydraulic system of a conifer tree: Linking sap flux data to transpiration rate. Ecological Modelling, 191(3-4): 447-468.

Dawson, T. E., Burgess, S. S., Tu, K. P., Oliveira, R. S., Santiago, L. S., Fisher, J. B., and Ambrose, A. R. 2007. Nighttime transpiration in woody plants from contrasting

ecosystems. Tree Physiology, 27(4), 561-575.

Dixson, H. H., and Joly, J. 1895. The path of the transpiration-current. Annals of Botany, (3), 403-420.

Donovan, L. A., and Sperry, J. 2000. Scaling the soil–plant–atmosphere continuum: from physics to ecosystems. Trends in plant science, 5(12), 510-512.

Doussan, C., Pierret, A., Garrigues, E., Pages, L., 2006. Water uptake by plant roots: II - Modelling of water transfer in the soil root-system with explicit account of flow within the root system - Comparison with experiments. Plant and Soil, 283(1-2): 99-117.

Dunbabin, V.M. et al., 2013. Modelling root-soil interactions using three-dimensional models of root growth, architecture and function. Plant and Soil, 372(1-2): 93-124.

Feddes, R.A., Kowalik, P.J., Zaradny, H., 1978. Simulation of Field Water Use and Crop Yield. John Wiley & Sons, New York.

Fuchs, M., 1990. Infrared measurement of canopy temperature and detection of plant water-stress. Theoretical and Applied Climatology, 42(4): 253-261.

Gartner, B.L. and F.C. Meinzer. 2005. Structure-function relationships in sapwood water transport and storage. In: Vascular Transport in Plants. N.M. Holbrook and M. Zwieniecki, Editors. Elsevier Academic Press, pp. 307-331.

Gonzalez-Dugo, V. et al., 2012. Almond tree canopy temperature reveals intra-crown variability that is water stress-dependent. Agricultural and Forest Meteorology, 154: 156-165.

Gonzalez-Dugo, V. et al., 2013. Using high resolution UAV thermal imagery to assess the variability in the water status of five fruit tree species within a commercial orchard. Precision Agriculture, 14(6): 660-678.

Grant, O.M., Tronina, L., Jones, H.G., Chaves, M.M., 2007. Exploring thermal imaging variables for the detection of stress responses in grapevine under different irrigation regimes. Journal of Experimental Botany, 58(4): 815-825.

Griffin, D., and Anchukaitis, K. J. 2014. How unusual is the 2012–2014 California drought?. Geophysical Research Letters, 41(24), 9017-9023.

Holtta, T., Cochard, H., Nikinmaa, E., Mencuccini, M., 2009. Capacitive effect of cavitation in xylem conduits: results from a dynamic model. Plant Cell and Environment, 32(1): 10-21.

Hopmans, J.W., Bristow, K.L., 2002. Current capabilities and future needs of root water and nutrient uptake modeling. Advances in Agronomy, Vol 77, 77: 103-183.

Hunt, E. R., & Nobel, P. S. (1987). Non-steady-state water flow for three desert perennials with different capacitances. Functional Plant Biology, 14(4), 363-375.

Hutson, J.L., Wagenet, R.J., 1995. A multiregion model describing water-flow and solute transport in heterogeneous soils. Soil Science Society of America Journal, 59(3): 743-751.

Idso, S., 1982. Non-water-stressed baselines- a key to measure and interpreting plant water-stress. Agricultural Meteorology, 27(1-2): 59-70.

Idso, S., Jackson, R., Pinter, P., Reginato, R., Hatfield, J., 1981. Normalizing the stress-degree-day parameter for environtal variability Agricultural Meteorology, 24(1): 45-55.

Idso, S. et al., 1980. A generalization of the stress-degree-day concept of yield prediction to accommodate a diversity of crops. Agricultural Meteorology, 21(3): 205-211.

Jackson, R.B., Sperry, J.S., Dawson, T.E., 2000. Root water uptake and transport: using physiological processes in global predictions. Trends in Plant Science, 5(11): 482-488.

Jackson, R.D., 1982. Soil-moisture inferences from thermal-infrared measurements of vegetation temperatures. Ieee Transactions on Geoscience and Remote Sensing, 20(3): 282-286.

Jackson, R.D., Idso, S.B., Reginato, R.J., Pinter, P.J., 1981. Canopy temperature as a crop water-stress indicator. Water Resources Research, 17(4): 1133-1138.

Janott, M. et al., 2011. A one-dimensional model of water flow in soil-plant systems based on plant architecture. Plant and Soil, 341(1-2): 233-256.

Jarvis, P.G. and McNaughton, K.G., 1986. Stomatal control of transpiration: scaling up from leaf to region. Advances in Ecological Research, 15: 1-49.

Javaux, M., Schroeder, T., Vanderborght, J., Vereecken, H., 2008. Use of a three-dimensional detailed modeling approach for predicting root water uptake. Vadose Zone Journal, 7(3): 1079-1088.

Jones, H.G., 2007. Monitoring plant and soil water status: established and novel methods revisited and their relevance to studies of drought tolerance. Journal of Experimental Botany, 58(2): 119-130.

Jones, H.G. et al., 2002. Use of infrared thermography for monitoring stomatal closure in the field: application to grapevine. Journal of Experimental Botany, 53(378): 2249-2260.

King, E., Caylor, K., 2011. Ecohydrology in practice: strengths, conveniences, and opportunities. Ecohydrology, 4(4): 608-612.

Kramer, P.J., Boyer, J.S., 1995. Water Relations of Plants and Soils. Nature.

Lange, O. L., Ullmann, I., Tenhunen, J. D., and Bannister, P. 1987. Stomatal conductance and transpiration of the two faces of Acacia phyllodes. Trees,1(2), 110-122.

Maes, W. H., and Steppe, K. 2012. Estimating evapotranspiration and drought stress with ground-based thermal remote sensing in agriculture: a review.Journal of experimental botany, 63(13), 4671-4712.

McDowell, N. et al., 2008. Mechanisms of plant survival and mortality during drought: why do some plants survive while others succumb to drought? New Phytologist, 178(4): 719-739.

McDowell, N.G. et al., 2011. The interdependence of mechanisms underlying climate-driven vegetation mortality. Trends in Ecology & Evolution, 26(10): 523-532.

McDowell, N.G. et al., 2013. Evaluating theories of drought-induced vegetation mortality using a multimodel-experiment framework. New Phytologist, 200(2): 304-321.

Micco, V.D., Aronne, G., 2012. Morpho-Anatomical Traits for Plant Adaptation to Drought Plant Responses to Drought Stress. Springer Berlin Heidelberg.

Mohanty, B.P., Skaggs, T.H., 2001. Spatio-temporal evolution and time-stable characteristics of soil moisture within remote sensing footprints with varying soil, slope, and vegetation. Advances in Water Resources, 24(9-10): 1051-1067.

Mohanty, B. P., & Zhu, J. 2007. Effective hydraulic parameters in horizontally and vertically heterogeneous soils for steady-state land-atmosphere interaction.Journal of Hydrometeorology, 8(4), 715-729.

Moran, M.S., Clarke, T.R., Inoue, Y., Vidal, A., 1994. Estimating crop water-deficit using the relation between surface-air temperature and spectral vegetation index. Remote Sensing of Environment, 49(3): 246-263.

Nimah, M.N., Hanks, R.J., 1973. Model for estimating soil-water, plant, and atmospheric interrelations. 1. description and sensitivity. Soil Science Society of America Journal, 37(4): 522-527.

Nobel, P.S., Cui, M., 1992. Shrinkage of attached roots of opuntia ficus-indica in response to lowered water potentials predicted consequences for water-uptake or loss to soil. Annals of Botany, 70(6): 485-491.

Pirson, A., Zimmermann, M.H. (Eds.), 1982. Encyclopedia of Plant Physiology. Physiological Plant Ecology II, Water relations and carbon assimillation, 12B, New York, 747 pp.

Phillips, N., Nagchaudhuri, A., Oren, R., Katul, G., 1997. Time constant for water transport in loblolly pine trees estimated from time series of evaporative demand and stem sapflow. Trees-Structure and Function, 11(7): 412-419.

Rings, J. et al., 2013. Bayesian inference of tree water relations using a Soil-Tree-Atmosphere Continuum model. Four Decades of Progress in Monitoring and Modeling of Processes in the Soil-Plant-Atmosphere System: Applications and Challenges, 19: 26-36.

Sack, L., Holbrook, N.M., 2006. Leaf hydraulics, Annual Review of Plant Biology. Annual Review of Plant Biology. Annual Reviews, Palo Alto, pp. 361-381.

Scharnagl, B., Vrugt, J.A., Vereecken, H., Herbst, M., 2011. Inverse modelling of in situ soil water dynamics: investigating the effect of different prior distributions of the soil hydraulic parameters. Hydrology and Earth System Sciences, 15(10): 3043-3059.

Scholz, F. G., Phillips, N. G., Bucci, S. J., Meinzer, F. C., & Goldstein, G. 2011. Hydraulic

capacitance: biophysics and functional significance of internal water sources in relation to tree size. In Size-and age-related changes in tree structure and function (pp. 341-361). Springer Netherlands.

Schröder, T. (2009). Three-dimensional modelling of soil-plant interactions: Consistent coupling of soil and plant root systems (Vol. 1). Forschungszentrum Jülich.

Shin, Y., Mohanty, B.P., Ines, A.V.M., 2012. Soil hydraulic properties in one-dimensional layered soil profile using layer-specific soil moisture assimilation scheme. Water Resources Research, 48.

Šimůnek, J., K. Huang, and M. Th. van Genuchten, The HYDRUS code for simulating the one-dimensional movement of water, heat, and multiple solutes in variably-saturated media. Version 6.0, Research Report No. 144, U.S. Salinity Laboratory, USDA, ARS, Riverside, California, 164 pp., 1998.

Sperry, J.S., Adler, F.R., Campbell, G.S., Comstock, J.P., 1998. Limitation of plant water use by rhizosphere and xylem conductance: results from a model. Plant Cell and Environment, 21(4): 347-359.

Snyder, K. A., Richards, J. H., & Donovan, L. A. (2003). Night-time conductance in C3 and C4 species: do plants lose water at night?. Journal of Experimental Botany, 54(383), 861-865.

Tyree, M. T., & Zimmermann, M. H. (2002). Xylem structure and the ascent of sap. Springer.

Verbeeck, H. et al., 2007. Model analysis of the effects of atmospheric drivers on storage water use in Scots pine. Biogeosciences, 4(4): 657-671.

van Genuchten, M. Th., 1980. A closed-form equation for predicting the hydraulic conductivity of unsaturated soils, Soil Sci. Soc. Am. J., 44, 892-898.

Verburg, K., Ross, P., Bristow, K.L., 1996. SWIMv2.1 user manual, CSIRO Division of Soils, Adelaide.

Villalobos, F.J., Testi, L., Moreno-Perez, M.F., 2009. Evaporation and canopy conductance of citrus orchards. Agricultural Water Management, 96(4): 565-573

Vrugt, J.A., van Wijk, M.T., Hopmans, J.W., Simunek, J., 2001. One-, two-, and three-dimensional root water uptake functions for transient modeling. Water Resources Research, 37(10): 2457-2470.

Vrugt, J.A., Stauffer, P.H., Woehling, T., Robinson, B.A., Vesselinov, V.V., 2008. Inverse modeling of subsurface flow and transport properties: A review with new developments. Vadose Zone Journal, 7(2): 843-864.

Wang, X., Yang, W., Wheaton, A., Cooley, N., Moran, B., 2010. Automated canopy temperature estimation via infrared thermography: A first step towards automated plant water stress monitoring. Computers and Electronics in Agriculture, 73(1): 74-83.

Williams, M., E.B. Rastetter, D.N. Fernandes, M.L. Goulden, S.C. Wofsy, G.R. Shaver, J.M. Melillo, J.W. Munger, S.-M. Fan and K.J. Nadelhoffer. 1996. Modelling the soil–plant–atmosphere continuum in a Quercus–Acer stand at Harvard Forest: the regulation of stomatal conductance by light, nitrogen and soil/plant hydraulic properties. Plant Cell Environ. 19:911–927.

Yang, Y., and Shang, S. 2013. A hybrid dual-source scheme and trapezoid framework–based evapotranspiration model (HTEM) using satellite images: Algorithm and model test. Journal of Geophysical Research: Atmospheres,118(5), 2284-2300.

Yunusa, I. et al., 2010. Topographical and seasonal trends in transpiration by two co-occurring Eucalyptus species during two contrasting years in a low rainfall environment. Agricultural and Forest Meteorology, 150(9): 1234-1244.

Zeppel, M., Logan, B., Lewis, J. D., Phillips, N., & Tissue, D. (2013, June). Why lose water at night? disentangling the mystery of nocturnal sap flow, transpiration and stomatal conductance-when, where, who?. In IX International Workshop on Sap Flow 991 (pp. 307-312).

2 A NEW SOIL-PLANT-ATMOSPHERE-CONTINUUM (V-SPAC) MODEL TO STUDY HYDRODYNAMIC SOIL-PLANT WATER RELATIONS: MODEL DESCRIPTION AND COMPARISON

Abstract

This chapter presents a new simple soil-plant-atmospheric-continuum model that emphasizes the role of vegetation in controlling water balance (v-SPAC). It aims to incorporate both plant and soil hydrological measurements into plant water relation modelling. The model is different from previous SPAC models in that (1) the root resistance is treated in a unique way so that no measurement of root hydraulic properties are required, and (2) a plant capacitance is introduced to buffer the effects of day-time transpiration on root water uptake. The root resistance is constrained by an integrated vulnerability curve that can be easily obtained from sap flow and stem xylem water potential time series. The plant capacitance is assumed to be a lumped constant, which determines loss or gain of tree water storage as a function of xylem water potential. The unique representation of root resistance and capacitance allows the model to embrace SPAC hydraulic pathways from bulk soil, to soil-root interface, to root xylem and finally to stem xylem where the xylem water potential is measured.

The comparison of v-SPAC with soil-focused SPAC model LEACHM underscores the importance of incorporating root resistance into SPAC models and the significance of plant regulation in soil water balance. The v-SPAC model is tested on two native vegetation species, an *Acacia pycnantha* tree in a natural environment and *Eucalyptus crenulata* potted saplings with controlled drought treatment. The v-SPAC model simulations, calibrated with dynamic xylem water potential data, are in good

agreement with the observed sap flow and xylem water potential time series, as well as soil moisture variation for the two sets of experiments. This preliminary testing highlights the benefit of using continuous xylem water potential measurement to constrain SPAC modelling, and the necessity to have a vegetation-focused SPAC model, such as v-SPAC, to incorporate such measurements.

2.1 Introduction

Plant–water relations concern how plants extract water from soil, transport water within the plants and lose water by transpiration from the leaves (Passioura, 2010). The water transfer path from soil to plant and finally to the atmosphere is called SPAC (soil-plant-atmosphere continuum). SPAC models quantify water states and water fluxes which have long been a focus of agricultural research (Kramer and Boyer, 1995). Land surface water flux quantification is essential in meteorological and hydrologic modelling as it is often a boundary condition. Thus, soil-plant water relations are a key subject in agriculture, hydrology, and atmospheric science. Soil-plant water relation research is inevitability a multi-discipline task. It is thus important to integrate knowledge, skills and data from multiple disciplines: such as combining modelling strengths from hydrology and control experimental skills from ecology (King and Caylor, 2011). Draye et al. (2010) showed the advantage of using of hydrological models to assist in understanding root-water uptake in the plant physiological field, and emphasized the importance of reflecting plant's role in hydrologic models. SPAC models are developed to meet such needs. They are useful to explain factors that may dominate or limit plant water use, including soil/plant hydraulic properties or atmospheric and soil water conditions. Sperry et al. (1998) showed that maximum tree water use could be limited by hydraulic properties of both soil and plant.

Root water uptake functions in SPAC models are crucial to link soil–plant water status to water flux. Hopmans and Bristow (2002) classified root water uptake functions into two types: microscopic and macroscopic. In a microscopic model, roots are explicitly described as assembled pipes that have axial and radial resistances. A macroscopic model represents root water uptake as a sink term in the Richards equation. LEACHM (Hutson and Wagenet, 1995) and Hydrus (Šimůnek et al. 1998) are two commonly used macroscopic SPAC models that simulate water flow in the vadose zone. The two models use different types of macroscopic root water uptake functions. Hydrus employs a stress function (such as Feddes et al. (1978)) to impose the constraint of soil moisture deficit on transpiration; the root water uptake is thus determined by soil moisture condition, the prescribed stress function, and atmospheric demand. LEACHM applies Darcy's law to describe water flow in the soil-root continuum, the root water uptake rate depends on soil hydraulic conductivity and the soil to root water potential gradient. Both models use an atmospheric boundary condition. Root water uptake is constrained by a defined potential transpiration, neglecting the plant's role in transpiration regulation. Recent advances in 3D microscopic root models and experimental evidence emphasize the significant role of root resistance in manipulating soil water extraction (Doussan et al., 2006; Dunbabin et al., 2013). However, microscopic root models require complex parameterization, such as root architecture, root length and root/stem xylem hydraulic conductivity. They are difficult to apply in field conditions.

Therefore, there is a need to develop a new SPAC model in which the role of vegetation and its response to environmental conditions are represented and can be parameterized with commonly available measurements. A few SPAC models have coupled soil and root /plant resistance, such as SWIM (Verburg et al., 1996) and SiSPAT (Braud et al.,

1995). However, these models treat root resistance as a fixed empirical value that is invariant with root water potential, and neglect water storage in the plant xylem, so fail to simulate the transient process of plant water potential. In order to better represent the role of vegetation in SPAC water transfer and its response to the environmental conditions, a new vegetation-focused soil-plant-atmospheric continuum model (v-SPAC) is developed in this study.

Until now, soil-focused hydrologic models such as LEACHM and Hydrus are commonly parameterized and validated using soil moisture (Besharat et al., 2010; Vrugt et al., 2001). Soil moisture is easy to measure but may not be representative of root zone water status (Jones, 2004; Jones, 2008). In addition, soil moisture varies slowly with time and thus does not reflect diurnal variations of plant water state in SPAC. However, stem xylem water potential provides valuable information as its diurnal magnitude is influenced by the magnitude of SPAC water transfer, plant storage capacitance, and the soil/plant hydraulic properties. Plant water potential characteristics are key to understanding plant water use strategy (Aroca, 2012). For example, why trees behave differently to water stress in terms of leaf water potential (isohydric or anisohydric)? Are these characteristics an adaption to the environment? Very few studies explore the information of plant water potential (Kumagai, 2001; Rings et al., 2013) which could be due to the difficulty of continuous, consistent data acquisition and the lack of a SPAC model capable of utilising plant water potential dynamics. Stem psychrometers have been used for successful continuous monitoring of stem water potential and these data have contributed to enhancing the significance of plant water status in transpiration prediction (Yang et al. 2013, Wang et al. 2014). The v-SPAC model, here, provides a tool to integrate the stem water potential dataset into hydrologic modelling.

Tree scale is the smallest level for integrating mechanisms such as stomata conductance and also the largest intergradation level at which manipulated experiment can be used for the base of modelling test (Tardieu and Simonneau 1998). v-SPAC model aims to simulate water transport in soil and plant in tree scale (several metre squares). All plant resistances and capacitance are parameterized assuming tree plant hydraulic continuum as a whole; the plant water flux and water state are predicted at the tree scale. The v-SAPC model bears unique features including that (1) vegetation control on SPAC water transfer is represented by a resistance network composed of root and stem, which depends on plant water state, (2) root and stem resistance are lumped, so can easily be parameterized with stem water potential and sap flow measurements, (3) a capacitance term is introduced for tree water storage to buffer the effects of daytime transpiration on root water uptake.

The rest of the chapter is organised as follows: section 2 describes the v-SPAC model structure; section 3 describes two field experiments: one on an *Acacia pycnantha* tree and the other on potted *Eucalyptus crenulata* saplings; section 4 shows the parameterization of the plant resistance in the form of a vulnerability curve and model training with an optimization tool; section 5 presents the calibration and prediction results on the two experiments; and the comparison between v-SPAC and LEACHM modelling; conclusions are summarized in section 6.

2.2 Model conceptualization and formulation

2.2.1 Model description

2.2.1.1 Model conceptualization

The new model is developed from LEACHM, used to simulate water and solute transport in the unsaturated zone (Hutson and Wagenet, 1995). Water flow in the soil

matrix remains the same in LEACHM, including infiltration, irrigation, runoff and drainage. Water transport in plant is simulated in the new model in which, the total resistance in soil to root continuum is composed of a soil-root interfacial resistance which is stripped from RWU function in LEACHM and a plant resistance which is superimposed into the RUW function. A capacitance term is also added in the new model to calculate the storage contribution to the transpiration stream together with soil water extraction by the root. As the roles of vegetation on root water uptake are emphasized in this new model, we name it as vegetation-focused SPAC model (v-SPAC) (see Figure 2-1).
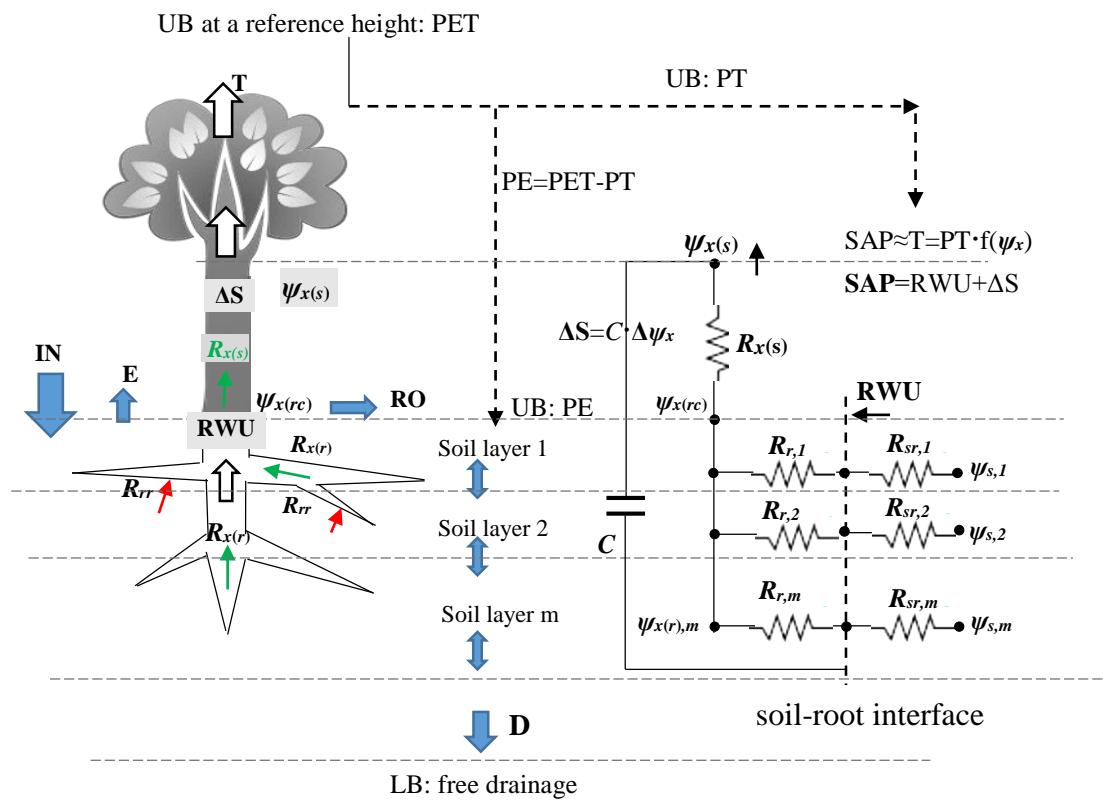
Figure 2-1: Illustration of water flow in the v-SPAC model (see the list of symbols and abbreviations in page vxi to vxii).
Note: the blue arrows in the left section of the figure show the hydrological processes modelled in LEACHM. Other arrows show the processes and parameters modified or added in the v-SPAC model compared to LEACHM.

2.2.1.2 Soil water transport and root water uptake function

The water transport in soil is governed by Richards equation (and the root water uptake is described with the scheme of Nimah and Hanks (1973) in LEACHM).

$$\frac{\partial \theta}{\partial t} = \frac{\partial}{\partial}[K(\theta)\frac{\partial \psi_s}{\partial z} + 1] - \text{RWU}(z,t) \qquad (2\text{-}1)$$

where θ (m$^3 \cdot$m^{-3}) is volumetric water content, ψ_s (mm) is soil water pressure head, K (mm/d) is soil hydraulic conductivity, t (d) is time, z (mm) is depth, positive downwards and RWU is a sink term representing water lost per unit time by root water uptake (d^{-1}). The original RWU (Nimah and Hanks (1973)) function in LEACHM is shown in Eq. 2-2 as follows.

$$\text{RWU}(z,t) = -K(\theta) \cdot \frac{[\psi_s(z,t) - \psi_x(t) - z \cdot (R_c + 1)] \cdot \text{RDF}(z)}{\Delta x \Delta z} \qquad (2\text{-}2)$$

where, $K(\theta)$ (mm/d) is soil hydraulic conductivity. ψ_x (mm) is water potential at root or stem xylem (water potential at root collar in original LEACHM), R_c (mm) accounts for friction loss in the root, "+1" accounts the hydraulic head loss due to gravity, RDF is the fraction of the total active root density in the soil depth increment Δz (mm), Δx is the conceptual distance from a point in the soil where ψ_s is measured, to the plant root. Soil hydraulic conductivity K is calculated following Mualem (1976):

$$K(\theta) = K_s \Theta^{0.5}[1 - (1 - \Theta^{1/m})^m]^2 \qquad (2\text{-}3)$$

where, K_s is saturated hydraulic conductivity, Θ is soil moisture saturation, which is calculated following van Genuchten (1980) water retention function

$$\Theta = \frac{\theta - \theta_r}{\theta_s - \theta_r} = \frac{1}{[1 + (\alpha h)^n]^m} \qquad (2\text{-}4)$$

26

where, θ is soil moisture, θ_s is moisture content at soil saturation, θ_r is the residual moisture content; h is the soil water pressure head (positive) (in kPa). α, n, m are parameters in van Genuchten water retention function and m=1-1/n.

2.2.1.3 The resistance terms

Root diameter changes diurnally and root resistance itself changes with root water potential which also varies with time (Nobel and Cui, 1992). In v-SPAC, it is assumed that the overall root resistance depends on its xylem water potential (ψ_x), the shrinkage is accompanied with a drop of root water content. Therefore, water potential links the resistance and the storage component. In v-SPAC model, the resistance of water flow from soil to plant xylem is described in two parts: the soil-root interfacial resistance transformed from the original RWU function in LEACHM (Eq 2-2) and the resistance of water transfer from the soil-root interface to root (and to stem) xylem. The latter is lumped into an integrated vulnerability curve described later.

The resistance in the soil-root interface

The resistance of water transfer from the bulk soil to the root surface is transformed into Eq. 2-5 from the original RWU in LEACHM (see Eq 2-2):

$$R_{sr}(z,t) = \frac{\Delta x}{RDF(z) \cdot K(\theta)} \tag{2-5}$$

where R_{sr} is described by soil hydraulic conductivity ($K(\theta)$) and an equivalent path length (Δx) for water transfer from soil to root ($\Delta x = 10$ mm is the usual default in LEACHM). The SWIM model sets Δx as dependent on RDF at each soil layer, that is, Δx becomes shorter and R_{sr} is smaller if there is a larger root density. In Janott et al. (2011), Δx is 2 mm inferred from an independent microscopic experiment, while K is weighted between soil hydraulic conductivity of the bulk soil and that at root surface

water potential. In v-SPAC model, Δx is a calibrated parameter rather than an arbitrary constant.

R_c in the original RWU function in LEACHM (see Eq 2-2) is also difficult to determine. From its definition, it should be primarily dependent on the axial root resistance and the overall ratio of radial to axial root resistances at the corresponding soil depth. Since the root resistance is simulated in v-SPAC, R_c is not used in the modelling, i.e. R_c is zero.

The root distribution function RDF is described by an exponential function similar to Hentschel et al.(2013), so that the root density decreases from shallow to deep soils.

$$\mathrm{RDF}(z) = \lambda \beta^{(z/\mathrm{L})} \tag{2-6}$$

where β is the shape parameter at range of 0 to 1, when equals to 1, RDF corresponds to a uniform root density, when close to 0, RDF shows steep exponential decreasing of root length density from soil surface to the bottom root zone. L is the root zone depth and λ is a parameter that is used to normalize total RDF as unit one ($\sum_{z=0}^{L}\mathrm{RDF}(z)=1$), so that $\lambda = 1 / \sum_{z=0}^{L} \beta^{(z/\mathrm{L})}$.

Resistance in the plant: the integrated vulnerability curve

The resistance in plant is added in v-SPAC. A vulnerability curve is introduced to characterize the dynamic resistance in plant with its water status. The vulnerability curve is originally used to describe the hydraulic conductivity loss (HCL) with reduction of xylem water potential of a stem or root segment. Here, we propose an "integrated vulnerability curve (IVC)" to represent the whole plant resistance (R_p)

change with plant water status (ψ_x). IVC defines the overall change of R_p, made up of resistance components through soil-root interface, root cortex, root xylem, root collar and finally in the stem xylem.

The curve takes the form of the Weibull function (e.g. Sperry et al., 1998).

$$R_{\mathrm{p}} = R_{\mathrm{min}} \cdot \exp[(\text{-}\psi_{\mathrm{x}}/\mathrm{d})^{\mathrm{b}}]$$

(2-7)

where R_{min} is the minimum plant resistance (equivalent to the maximum hydraulic conductance at full hydration). The parameters d and b can be obtained by the dehydration method, air injection method, and centrifuge method for single root/ stem segment or the vacuum chamber method for entire shoot or root system (Sperry Lab Methods, http://biologylabs.utah.edu/sperry/methods.html). Each root may have different d and b values, and are dependent on root length, age which is only practical for lab experiment and 3D modelling such as in Doussan et al., (2006). The vacuum chamber is a destructive method, and limited by the size of the chamber. These traditional methods thus cannot be used to determine a vulnerability curve for big trees in field conditions. In our experiments, the parameters are obtained from in-situ measurements on trees, thus representing the hydrodynamics of the whole plant in the field. By analysing concurrent measurements of night-time sap flow and stem xylem water potential, the total plant resistance can be derived (see detail in the following section on deriving IVC parameters).

The plant resistance (R_p) in the model is described as the sum of the total root resistance ($R_{r,t}$) and the stem xylem resistance $R_{x(s)}$.

$$R_{\mathrm{p}} = R_{\mathrm{r,t}} + R_{\mathrm{x(s)}} \qquad\qquad (2\text{-}8)$$

Both $R_{r,t}$ and $R_{x(s)}$ should be described by vulnerability curves, each has three parameters (see Eq. 2-7). To reduce the dimension of the model, stem resistance $R_{x(s)}$ is neglected, and $R_{r,t}$ is approximated as R_p for both tree species in our experiments. The approximation is reasonable as $R_{r,t}$ usually dominates over $R_{x(s)}$ (Hunt et al., 1991; Jackson et al., 2000; Micco and Aronne, 2012; Tyree and Zimmermann, 2002).

The effective root resistances in each soil layer ($R_{r,i}$) is assumed to be in parallel and inversely proportional to RDF (as in LEACHM and SiSPAT).

$$R_{r,i} = \frac{R_{r,t}}{RDF_i} \approx \frac{R_p}{RDF_i} \tag{2-9}$$

Note that $R_{r,i}$ is not simply the sum of the axial root resistance $R_{x(r),i}$ and the radial root resistance $R_{rr,i}$ in soil layer i. $R_{r,i}$ is an effective root resistance, so that the root water uptake is described by Darcy's law with corresponding average soil water potential (ψ_s).

Finally, the root water uptake (RWU) is calculated following:

$$RWU_i = \frac{\psi_{s,i} - \psi_{r,i}}{R_{r,i} + R_{sr,i}} \tag{2-10}$$

Note that in LEACHM, RWU is calculated with $RWU_i = \dfrac{\psi_{s,i} - \psi_{r,i}}{R_{sr,i}}$, without considering the root resistance. The resistance terms R_p, R_{min}, $R_{r,i}$ are all normalized by the land surface domain area. All calibrated and reported R_p, R_{min}, R_r have units of d (abbreviation for day), which are integration results of resistivity (d/mm) multiplied by Δx (mm).

2.2.1.4 Storage dynamics of trees

Root water uptake (RWU) is assumed to be equal to transpiration (T) in hydrologic models. In fact, there is a mismatch timing between RWU and T due to tree storage buffering (Cermak et al., 2007) . Sap flow rate rises earlier in the tree's upper crown than in its stem base in the morning for quick transpiration in response to radiation. In the afternoon, sap flow at its stem base persists when transpiration has reduced significantly (Cermak et al., 2007). That is, you would see a larger sap flow flux at the upper crown than that at the stem base in the early morning, the extra amount of the sap flux at upper crown is released from the crown and stem storage; while in the afternoon, with transpiration at crown ceases, the crown and stem are gradually refilled with water and the sap flux will gradually recess to zero from crown to the stem base. The largest contribution of tree storage to transpiration occurs in the morning, and the storage contribution accounts to 10% to 50% of daily transpiration among different tree species and ecosystems (Scholz et al., 2011). To represent this process, a capacitance term is included in v-SPAC to simulate the dynamic plant water storage. Transpiration is hence different from root water uptake due to the transient process of loss or gain of the storage in a tree.

Water is stored in xylem fibers, bark, and primary tissues of a tree. Time scales for water release from tree storage component can be seconds to hours (Pirson and Zimmermann, 1982). The storage change is accompanied with a change in xylem water potential (ψ_x) (Sperry et al., 1998).

$$\Delta S = C \cdot \Delta \psi_x \qquad\qquad (2\text{-}11)$$

where C is a lumped capacitance of the plant storage compartment. Hunt et al. (1991) reported C range of 1×10^{-6} m$^3 \cdot$MPa^{-1} to 350×10^{-6} m$^3 \cdot$MPa^{-1} in grass, softwood, to

hardwood. The capacitance varies with species, age, and water status (or relative water content) (Pirson and Zimmermann, 1982). As there is general scarcity of data on capacitance, a constant capacitance of the plant is used for simplicity. Worth to note is in porous media models, C is assumed to reduce with the drop of xylem water potential ($C = \dfrac{c}{-\psi_x}$, in which c is a constant) (Chuang et al., 2006; Janott et al., 2011; Kumagai, 2001). In v-SPAC, both forms are enabled to calculate the storage change. Here, for model testing, a constant capacitance is used.

Unlike LEACHM, where the actual transpiration (T) equals the root water uptake (RWU), in v-SPAC, both RWU and plant storage change (ΔS) will contribute to T (in which ΔS in positive represents storage refilling of the trees).

$$T = RWU - \Delta S \tag{2-12}$$

2.2.1.5 Transpiration reduction function (significance of ψ_x)

In addition to resistance in soil, roots or stem xylem, water transfer in SPAC is also controlled by leaves. A reduction function is used to represent the stomatal control on transpiration. A similar approach can be found in Hentschel et al.(2013). The reduction function is used to represent the stress of environmental conditions on transpiration. In this preliminary study, the reduction function is associated with plant water potential, similar to the stress function in Hydrus which is based on soil water potential. Instead of using an exponential function as in Hentschel et al., (2013), we apply a simple piecewise linear function. The reduction function $f(\psi_x)$ is derived from correlation between the maximum sap flow rate in a day and its concurrent xylem water potential (ψ_x).

$$
f(\psi_x) = \begin{cases} 1 & (\psi_x \geq p_1) \\ \dfrac{x - p_2}{p_1 - p_2} & (p_2 \leq \psi_x < p_1) \\ 0 & (\psi_x < p_2) \end{cases}
\qquad (2\text{-}13)
$$

where $f(\psi_x)$ is the transpiration reduction function, describing reduced transpiration rate with decreasing plant water potential. p_1 denotes stem water potential (ψ_x) above which transpiration retains a constant optimal transpiration rate, p_2 denotes ψ_x below which, transpiration drops to zero with increased water stress. p_1 and p_2 are obtained from observation of the maximum transpiration rate of a day and its corresponding stem water potential.

2.2.2 Model flowchart

The model is built upon LEACHM soil water transport component. The model starts with initial soil moisture profile ($\psi_{s,i}$), a prescribed upper flux boundary and a lower boundary at the bottom of the soil profile (see Figure 2-2). A given xylem water potential (ψ_x) will be iterated till both the water flux and water potential converge. The soil and plant resistance/conductivity and capacitance will be updated in each iteration step. Figure 2-2 below illustrates the modelling flow chart of v-SPAC for transpiration and plant water status modelling.
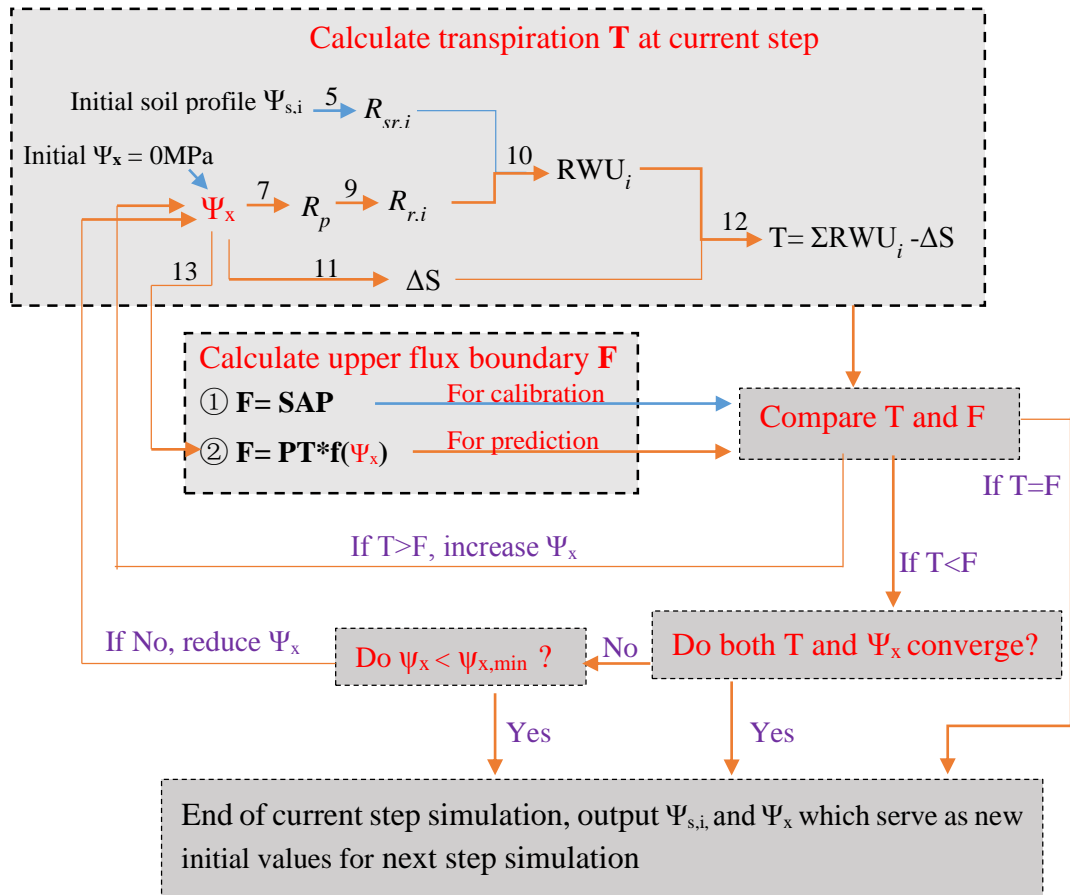
Figure 2-2: Flow chart of v-SPAC simulation for plant water flux/water status. F is the upper flux boundary. SAP is observed sap flux. PT is calculated potential transpiration. Refer to the equations in the text for other symbols.

Note: the orange arrows identify the terms need to be updated in each iteration within one simulation step. The blue arrows are determined values in each simulation step. The numbers above the arrows indicate the equation number in the text.

There are two options in prescribing the upper transpiration flux boundary (F). In option ①, the observed sap flow rate (SAP) is used as flux boundary (F= SAP) to parameterize the SPAC hydraulic system which will be used for model calibration. The parameterized plant hydraulic system embraces all the resistances occurred in water transfer from the root surface to the point where the water potential is measured. In option ②, a reduced potential transpiration (F=PT*f(ψ_x)) is applied as a flux boundary to predict the actual transpiration. Therefore, option ② is used for model

34

testing. The potential evapo-transpiration (PET) is first calculated with FAO method (Allen et al. 1998) and then partitioned to potential transpiration (PT) and potential evaporation (PE). PE is prescribed as the upper boundary condition of the soil surface (also in option ①). PT, reduced with the transpiration reduction function $f(\psi_x)$ is used as the upper boundary of the tree canopy, and is updated with each iteration of ψ_x. To be strict, the predicted flux is actually the sap flow rate (SAP) where the sap flow meter is installed rather than the transpiration (T) from the canopy. However, SAP will be a good approximation of actual T if the sap flow meter is installed at the bottom of the crown (highest position in stem before branching), as ΔS from the crown is usually neglected due to limited storage buffering of leaf water content (Micco and Aronne, 2012). So, interpretation of the observed or predicted sap flow rate depends on where the sap flow meter is installed. The higher the installation point, the closer SAP approaches to T; the lower the installation point, the closer SAP approaches RWU.

In summary, the v-SPAC model retains the soil water transport routine in LEACHM. Soil water extraction by the root remains as a sink term in the equation in both models but the RWU function itself is modified (see Eq. 2-10 and Eq. 2-12 for v-SPAC model vs. Eq. 2-2 for LEACHM model). The dynamics of plant resistance (Eq. 2-3 through Eq. 2-9) and storage (Eq. 2-11) are added in v-SPAC. In LEACHM, PT is calculated based on the FAO method or Penman-Monteith equations in which a constant maximum stomata conductance/minimum stomata resistance is used. However, v-SPAC prescribes a transpiration boundary condition that depends on plant water status in addition to environmental factors. Specifically, PT will be further reduced with a scaling function depending on plant water stress (see Eq. 2-13). The convergence criteria of simulation thus diverse between the two models. In LEACHM, the root water potential will iterate until RWU is equal to the prescribed boundary (PT) or less

than PT when the root water potential reaches a minimum value ($\psi_{r,min}$); while, in v-SPAC, the sum flux (RWU-ΔS) will be compared to the prescribed boundary. The minimum root water potential ($\psi_{r,min}$) is prescribed in both LEACHM and v-SPAC and is often assigned the minimum value of observed or reported ψ_x time series. Here, $\psi_{r,min}$ is assigned as -5.0 MPa.

2.3 Field experiments and data

Two field experiments were used to test the models with datasets for soil moisture, stem xylem water potential and sap flow rate. One site was located in a natural landscape, where *Acacia pycnantha* is abundant and native to the local environment. The experiment was conducted from spring to summer (Oct, 2012 to Feb, 2013). Another site was located in Armidale, New South Wales, where six potted *Eucalyptus crenulata* saplings were water controlled during the growing season (Sep to Oct, 2013).

The largest difference between the two experiments was the soil water condition, in that *Eucalyptus crenulata* experienced sudden and severe artificial droughts while the *Acacia pycnantha* experienced gradual water stress from spring to summer under natural conditions. *Acacia pycnantha* is reputed to be drought tolerant, while *Eucalyptus crenulata* is highly sensitive to water stress.

The two cases also differed in their modelling settings in that the root length distribution of potted trees can be simplified to a uniform distribution, soil texture was uniform, and the lower boundary could be treated as free drainage. The natural field site had more unknowns such as root depth, soil properties and lower boundary conditions. It is interesting to compare the modelling capacity and capabilities under different climate, soil texture, and tree species and data availability.

2.3.1 Field experiment in SA

The experiment was conducted on an *Acacia pycnantha* tree (3.8 m tall) and a *Eucalyptus microcarpa* (6.6 m tall) on a hill slope (138.573 ºE, 35.031 ºS) at Flinders University campus, South Australia. One PSY1 stem psychrometer (ICT international) was installed at about 1.5 m height on each tree to obtain stem xylem water potential at 15 min or 30 min interval from Jan, 2012 to May, 2013. However, because acacia trees released resin after one to two weeks of an installation wound, good data were collected for only part of the measurement period. Since the sensor of the eucalyptus tree was often soaked in rain water that infiltrated through the rough barks. Recalibration and installation were therefore conducted frequently in the lab (see Appendix I for psychrometer recalibration and comparison to a PMS chamber measurement on leaf water potential). The installation of PSY1 stem psychrometers were different between the two tree species. For the acacia tree, we followed the standard procedure, using a clamp to fix the sensor on the stem (http://www.ictinternational.com/products/psy1/psy1-stem-psychrometer/); while, for the eucalyptus tree, because the size of the stem (DBH=14.6 cm) exceeded that of the largest clamp, the sensor was fastened to the stem with a belt. Such installation of psychrometer on big trees is shared experience among other users (personal communications with experts from ICT international company).

Two sets of SFM1 sap flow meter (ICT international) were installed at breast height (1.3 m) at northern and southern directions to get sap flow velocity in each tree stem. Each set of the sap flow meters had two thermistor sensors that are 15 mm apart (see Appendix II for the detail of SFM1 installation). The sapwood cross section area, the depth of thermistor sensors, sapwood density and sapwood water content were calculated from tree cores drilled at or near to the installation site at the end of the

experiment with increment borers. The heat velocity of each tree was converted to sap flux following (Burgess et al., 2001). The observation of sap flow started in Mar, 2012. However, sap flow meter were reinstalled for both trees in Oct, 2012. The sap velocity was not comparable between the two time series before and after the reinstallation date as the sap velocity varied significantly, especially for the eucalyptus tree. The sap flow rate since Oct, 2012 are only used for the modelling of the acacia tree. The *Eucalyptus microcarpa* tree is thus not modelled in this chapter due to an obvious shift in sap flow rate which may be caused by growth around the installation wound (massive growth was observed at the end of the experiment).

A weather station (provided by MEA company, see mea.com.au) was set up at the open site on the slope from 21 Mar, 2012 with an anemometer at 5.49 m height, a pyranometer at 5.45 m height, a T/RH sensor at 4.85 m height and a tipping bucket rain gauge at the ground level. All recording was at 15 min interval.

The soil layers at the site were abundant in clay content (20-50 %, based on Australian soil texture classification) with one layer at 20-50 cm depth heavily enriched in clay content (60-90 %). One capacitance-based soil moisture probe (Sentek, Australia) was installed one metre downslope of the acacia tree with three observation depths (10, 30, 50 cm) and logged from 15 Oct, 2012. Three soil cores were taken within one metre around the acacia tree. The soil hydraulic parameters of van Genuchten water retention curve were estimated from pedo-transfer function of Minasny et al. (1999). Saturated soil hydraulic conductivity (K_s) was calculated from ROSETTA which is a software to calculate soil water retention and hydraulic properties from soil texture database (UNSODA soil database (Leij et al., 1996) as default) (Schaap et al., 2001). The parameter ranges are shown in numbers in bracket (see Appendix III).

Figure 2-3: Experimental setting up of Acacia *pycnantha* site on a slope near Flinders University campus, South Australia

2.3.2 The controlled experiment in NSW

The experiment was conducted from August to Oct, 2013 in Armidale, New South Wales (151.7764 °E, 30.7056 °S) (see Figure 2-4) (experiment conducted and data provided by Michael Forster, ICT international). Seven potted *Eucalyptus crenulata* saplings (1.5-2 metres tall) were randomly divided into two groups: "wet treatment" group includes sapling 1, 3 & 5; "drought treatment" have 4 replicates (sapling 2, 4, 6 & 7). All saplings were irrigated with 1.5 L of water every other day, except that the drought treatment trees had water withheld for 5-20 days. Stem psychrometers (PSY1 model, ICT international) and sap flow meters (SFM1 model, ICT international) were used to monitor the water status and water flux of the saplings. Soil moisture content was measured with EC-5 capacitance based sensors (Decagon Devices) and soil water potential by a WP4C Dewpoint Water Potential Meter and a 2100F Tensiometer with a dial gauge (Soil moisture Equipment Corp). The saturated hydraulic conductivities of the sandy soil in each pot vary in the range of 3-10 m/d (measured at -5 cm/s suction rate with Campbell infiltrometer) although the soil were

well mixed and assumed uniform over all pots. Leaf area was measured with CI-202 Leaf Area Meter (CID Biosciences, US). The bark thickness and the sapwood area were measured at the end of the experiment by cutting the stems at the point where the SFM1 needles were installed. See detailed experimental set up carried out by Michael Forster in Appendix IV.

Figure 2-4: Experiment settings of *Eucalyptus crenulata* saplings in Armidale, New South Wales (photo courtesy of Michael Forster, the experiment was conducted by Michael Forster).
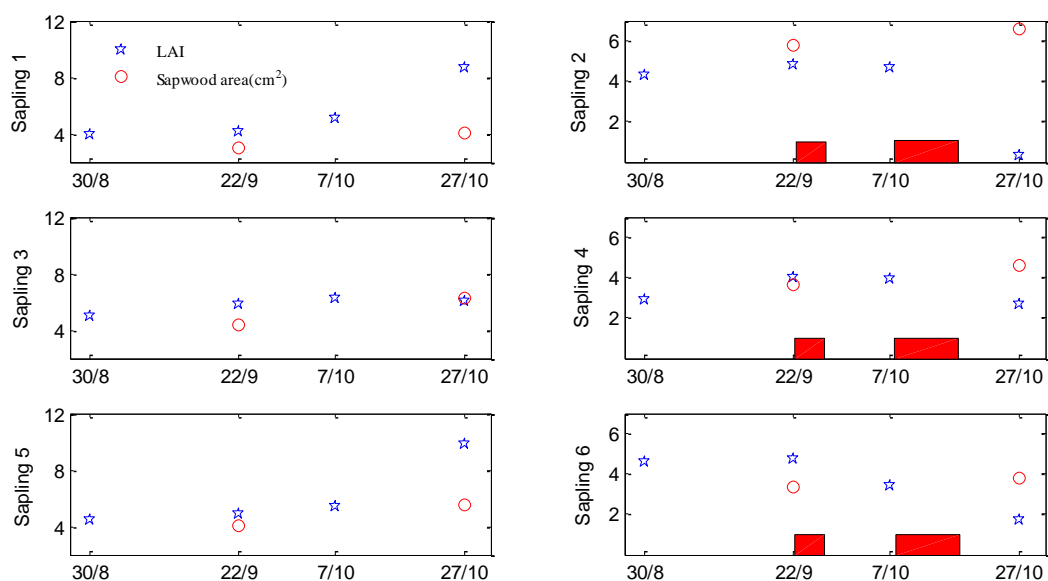
Figure 2-5: Leaf area index (LAI, normalized by pot opening area) and sapwood area (cm^2) of six *Eucalyptus crenulata* saplings over the growing season in year 2013 (x–axis in date

40

format dd/mm). The red boxes denote the periods when the saplings had water withheld.

2.4 The integrated vulnerability curve and model parameterization

A vulnerability curve (VC) describes the dependence of plant hydraulic conductivity loss (HCL) on reduced xylem water potential (ψ_x). Here we propose to parameterize the curve with a plot of sap flow rate (SAP) versus stem ψ_x (SS plot). Only the night-time data were used for the plot since ψ_x is much more stable in night-time than in the day-time and both SAP and ψ_x changes fast in the day-time which will result in large uncertainty in the later calculation. The obtained VC represents the total resistance from soil-root interface to the point where stem ψ_x is measured, thus is not the traditional VC derived for one xylem segment. We name it integrated vulnerability curve (IVC). IVC is from the SS plot as shown in Figure 2-6. It is assumed that soil water potential (ψ_s) is constant within a few days so that ψ_x at zero night-time SAP from weekly observation is assumed be equilibrium with the corresponding ψ_s. Supporting evidence for the observation can be found in (Bucci et al., 2004). The plant resistance (R_p) at each ψ_x is then calculated as the slope of the SS plot (i.e. $R_p(\psi_x)=(\psi_s - \psi_x)/$SAP). The resulted ($\psi_x$, R_p) points will then be used to obtain the parameters R_{min}, d, b by fitting the IVC (see Eq.2-7). The points (ψ_x, R_p) are converted to percentage value (ψ_x, HCL), in which HCL=1- R_{min}/R_p*100%; then the points form the HCL curve.

The idea is applied on two tree species: Acacia *pycnantha* (Figure 2-6) and Eucalyptus *crenulata* (Figure 2-7). It shows that the IVC of *Acacia pycnantha* approximates those of the *Acer negundo*'s root reported in Sperry et al., (1998) (see lower panel in Figure 2-6). The curve is likely to be a good approximation of *Acacia pycnantha* root VC as the root usually contributes much larger resistance than does the stem (Hunt et al.,

41

1991, note that the resistance of a long stem may be the same magnitude as root resistance if normalized over land surface). The dominant role of root over stem in plant hydraulics is also supported by the comparison between the VCs of the same species in Sperry et al. (1998) where the increase of root resistance (or HCL) is much earlier and faster than the stem resistance in terms of ψ_x.
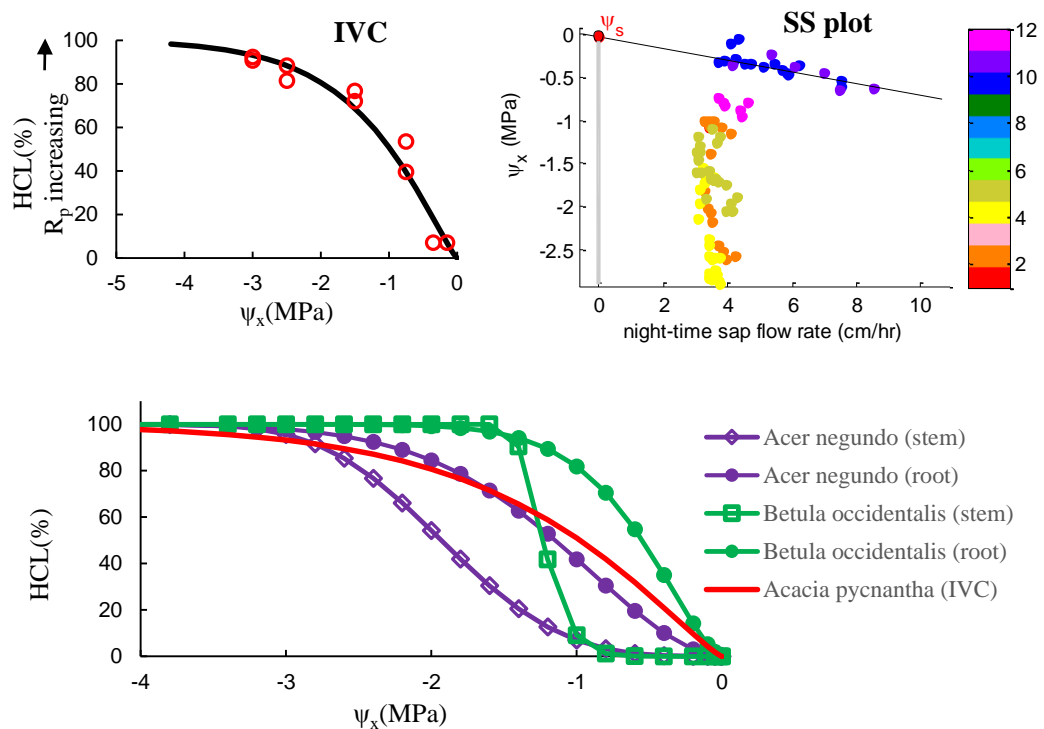
Figure 2-6: Illustration of the acquisition of the integrated vulnerability curve (IVC) of *Acacia pycnantha* (upper panel) and comparison of the acacia IVC to VCs of other tree species (lower panel).

Note: the black line in SS plot demonstrates how to obtain root zone ψ_s; the slope of the line in SS plot corresponds to R_p (at -0.1MPa) in red circles in IVC plot. It is common that the xylem water potential data were not continuous through the month. The soil water potential may also have changed significantly through the month. For each month, we computes two rough estimates of the slope (see two points cluster at -0.2MPa, -0.8MPa, -1.5MPa, -2.5MPa and -3MPa) by regressing through the first week and last week data points to represent the highest and lowest possible values of R_p (the slopes). Remember that it is only a rough estimation of the R_p. The shape parameters of vulnerability curve will be obtained by optimizing through these R_p points. The most sensitive parameter R_{min} of the curve will be further adjusted by model calibration. In the lower panel, VCs of stem and root segments on *Betula occidentalis* and *Acer negundo* are measurements from Sperry et al. (1998).

For *Eucalyptus crenulata* sapling, IVCs were obtained similarly as the *Acacia pycnantha* tree. The land surface domain area is fixed as the pot opening area; and the resistance is normalized by sapwood area/ pot opening area.
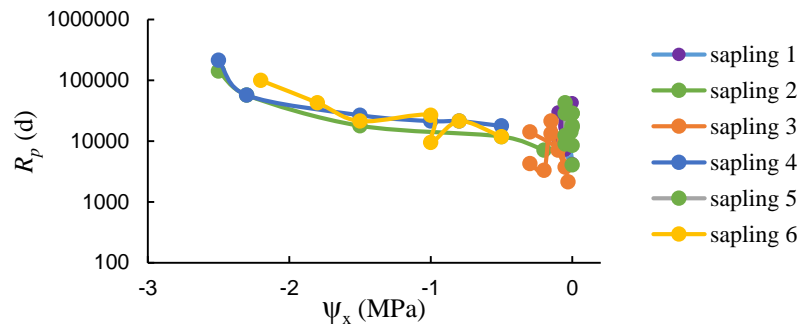
Figure 2-7: The integrated vulnerability curve (IVC) of saplings *Eucalyptus crenulata*. The IVC is represented in the form of resistance rather than HCL.

Soil water retention curves were derived from pedo-transfer functions (see Appendix III) or from direct ψ_s-θ measurements (see Appendix IV). Other unknown parameters were inversely optimised using Markov chain Monte Carlo (MCMC) sampling scheme with the DiffeRential Evolution Adaptive Metropolis (DREAM) algorithm (Vrugt et al., 2008). The algorithm posts the inverse problem in a Bayesian inference, so that a posterior distribution is produced of the sampling parameters, given a known prior distribution of the parameters. The posterior probability distribution function (pdf) describes the likelihood of the parameters within the calibration range in light of the observation data, which helps us to understand the uncertainties of the optimised results. In this study, a uniform distribution is assigned to all unknown parameters within the calibration range since we have no prior knowledge of the distribution but only the possible range of parameters from literature. Usually, an analytical form of the posterior pdf cannot be obtained with complex models such as Hydrus, LEACHM, therefore, we approximate the posterior pdf from the generated samples with the DREAM algorithm. Similar practises for hydrological applications and geo-statistics

using DREAM can be found in Scharnagl et al. (2011) and Minasny et al. (2011).

For parameterization, the measured sap flow rate was used as known upper flux boundary (F=SAP in Figure 2-2). The model was trained over stem water potential (ψ_x) in year 2013 and validated over ψ_x in summer, 2012 for the *Acacia pycnantha* tree (note, sap flow rate in 2012 was not measured in summer). For the potted saplings, ψ_x of sapling 4 (before the severe drought) was used to the train the model. The optimised parameters, scaled with the sapwood area or leaf area, were tested using all other saplings regardless of their different water treatments. Soil moisture content were not used for calibration due to large uncertainty in the soil hydraulic properties of the acacia site. The efficiency of model calibration using stem water potential (ψ_x) was tested with parameter identifiability. Here, we refer to a parameter as identifiable if the uncertainty is reasonably small as defined in Scharnagl et al. (2011).

Table 2-1 shows the details of modelling settings and calibration. The calibration range is wide enough to cover all possible range. K_s can be measured or inferred, but we choose to calibrate the parameter in consideration of the soil heterogeneity of the acacia site and large variation of K_s in potted sandy soils. The acacia site has three distinct soil layers with varying K_s (see Appendix III). One effective hydraulic conductivity K_s was applied to the whole soil profile to minimize model dimension. Capacitance (C) is calibrated between 0 and 5 mm·MPa^{-1} (normalized over land surface domain area), which is wide enough to cover full range of storage contribution to transpiration. Root zone depth L is hard to determine for the acacia site. A range of [0.5 2] metres is reasonable based on the soil core sampling. After one metre, the soil seems to be poorly drained (light grey colour). The depth of 70-90 cm is the transition area from red colour of top soil (20-50 cm) to the grey colour below. The bedrock

locates at 1.5-2 m depth. The root distribution function (RDF) is even more difficult to determine, thus the parameters of RDF were determined by calibration. Root depth (*L*) of the potted saplings was fixed at the pot depth of 250 mm and RDF of the potted saplings was set as a uniform distribution owing to the confined space.

Table 2-1: Parameter settings and calibration range of v-SPAC for the two field experiments

Numerical settings	*A. pycnantha* (natural)	*E. crenulata* (potted)
Training period	Oct 15, 2012 to Feb 10, 2013	Sep 23 to Oct 16, 2013 (sapling 4, before the end of second drought treatment)
Validation period	Jan 8 to Feb 9, 2012	Oct 16 to Oct 27, 2013 of sapling 4 and Sep 23 to Oct 16, 2013 for all other saplings (with or without leaf area or sapwood area scaled of C and R_{min})
Optimization target	Stem xylem water potential	Stem xylem water potential
Soil profile (mm)	2000	250
Soil segment (mm)	100	10
Fixed variables		
Land surface domain area (cm^2)	12000*	471.2 (the pot opening area)
Sapwood area (cm^2)	35	3.66 (sapling 4)
d (MPa) (in VC)	1.33	1.0
b (/) (in VC)	1.3	0.74
α (kPa^{-1}) (in WRC)	See Appendix III	0.145
n (/) (in WRC)	See Appendix III	1.323
$θ_s$ (/) (in WRC)	See Appendix III	0.33
$θ_r$ (/) (in WRC)	See Appendix III	0.004
p_1 (MPa) (in f($ψ_x$))	-0.5	-1.5
p_2 (MPa) (in f($ψ_x$))	-8	-3.5
Parameters	*Calibration range*	
K_s (mm/d)	[10 500]	[500 10000]

Δx (mm)	[0.0001 10]	[0.0001 10]
R_{min} (d)	[100 100000]	[100 10000]
C (mm·MPa^{-1})	[0 5]	[0 5]
β (/) (in RDF)	[0.001 1]	1 (fixed)
L (mm) (in RDF)	[500 2000]	250 (fixed)

Note: * land surface domain area of the acacia tree is roughly the projected crown area.

Initial conditions: the initial soil water profile was estimated by exceeding the model with climatic forcing data for several months before the starting date of simulation. The **lower boundary** is set as free drainage. The **upper boundary condition** varied for different simulation purposes. For model parameterization, the sap flow observation was used (F= SAP in Figure 2-2), while to test the predictive capacity of the model, potential transpiration was used (F= PT*f(ψ_x) in Figure 2-2) as the flux boundary. Potential evapotranspiration (PET) was calculated with the FAO method. PET was partitioned into PT and PE based on leaf area index (LAI). The PT/PET ratio was assumed as 1 at LAI=6. The ratio is linearly scaled between 0 to 1 corresponding to LAI =0 to 6. For example, PT/PET=4/6 at LAI of 4. The maximum PT was constrained by 1.2*PET. For the acacia site, PT/PET was set to 0.5, a rough estimation of vegetation coverage following the photography method in Deng et al., (2013).

2.5 Results and discussion

2.5.1 Model calibration and validation

Figure 2-8 shows the calibration results for *Acacia pycnantha* stem water potential from Oct 15, 2012 to Feb 10, 2013. The soil moisture is shown to indicate the soil moisture depletion from spring to summer. The calibration results indicate that the model can simulate the site water condition reasonably well even only using stem water potential as the optimization target. The lower panel of the figure shows the

correlation between the optimised parameters, with different colours denoting the posterior samples generated with DREAM. If the points all clustered into a small range within the parameter space, it means that the parameter is identifiable or within small uncertainty (have a posterior pdf with reasonably small standard deviation). We see from Figure 2-8 that all parameters are narrowed down to a small range without apparent correlation, indicating the sufficiency of the dataset in identifying the parameters.
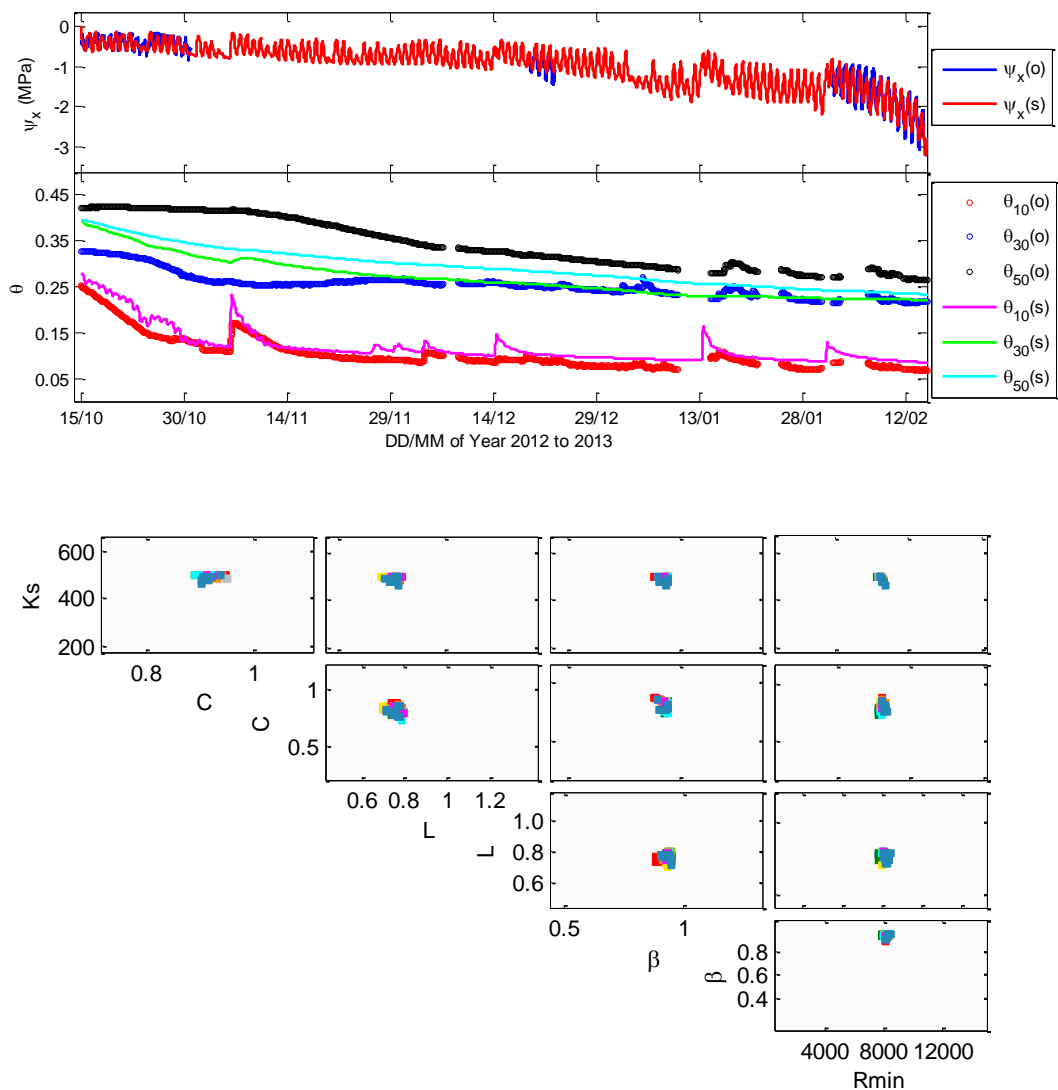
Figure 2-8: Calibration results of *Acacia pycnantha*. The lower panel shows the optimised sets of parameters with different colours denoting the posterior samples generated with DREAM. "(o)" denotes observed, "(s)" denotes simulated.

The optimised parameter setting is shown in Table 2-2. Capacitance is calibrated at 0.8 mm·MPa^{-1}, approximating a maximum storage contribution being 30 % of the daily transpiration.

Table 2-2: Calibrated parameter values for the *Acacia pycnantha* tree with several independent optimization runs

Parameters	Optimised	Range
K_s (mm/d)	500	400-500
Δx (mm)	0.0*	0.0-0.0018
R_{min} (d)	8100	8000-10000
C (mm·MPa^{-1})	0.8	0.4-0.9
L (mm)	800	700-900
β	0.9	0.7-0.9

The calibrated model of the *Acacia pycnantha* tree is then validated over stem water potential (ψ_x) observed from Jan to Feb, 2012. Figure 2-9 shows reasonably good fit with the observed ψ_x. Soil water trend was also well captured if compared to the same period in year 2013 when the timing of the first rainfall in Jan, 2012 event accidently matched that of Jan, 2012. Sap flow rate was obviously wider than midday only. The mismatch cannot be corrected by adjusting the transpiration reduction function ($f(\psi_x)$) parameters. The actual transpiration would always follow the shape of potential transpiration (under non-water-stressed conditions) which is of sinusoid shape and different from the observed "rectangle shape" of sap flow. The unusual rectangle shape may imply a conservative water use strategy of *Acacia pycnantha*. Flat top sap flow rate at midday was also reported in Australian native species (*Eucalyptus victrix*) in semi-arid environment (Pfautsch et al., 2011). In addition to the similarity in day time sap flow shape, both *Acacia pycnantha* and *Eucalyptus victrix* have high night-time

sap flow rate. The mechanism behind this may involve tree-specific physiology. It is also possible that the sap flow meter failed to capture the high flow at midday due to misalignment of the needles at installation. However, the chance of this is small (personal communication with the experts in ICT international). Worth noticing is that the wood basic density of *Acacia pycnantha* is around 0.8 g·cm^{-3}, similar to that of *Eucalyptus victrix* (0.73 g·cm^{-3}), but quite large compared to the *Eucalyptus crenulata* saplings (0.4-0.6 g·cm^{-3}). The wood density is an important determinant of xylem water transport properties, with larger wood density corresponding to lower hydraulic conductivity in the same tree group (such as angiosperms or conifers) (Meinzer, 2003). The flat top sap flow rate may reflect the constraint by the maximum transport ability of the dense xylem.
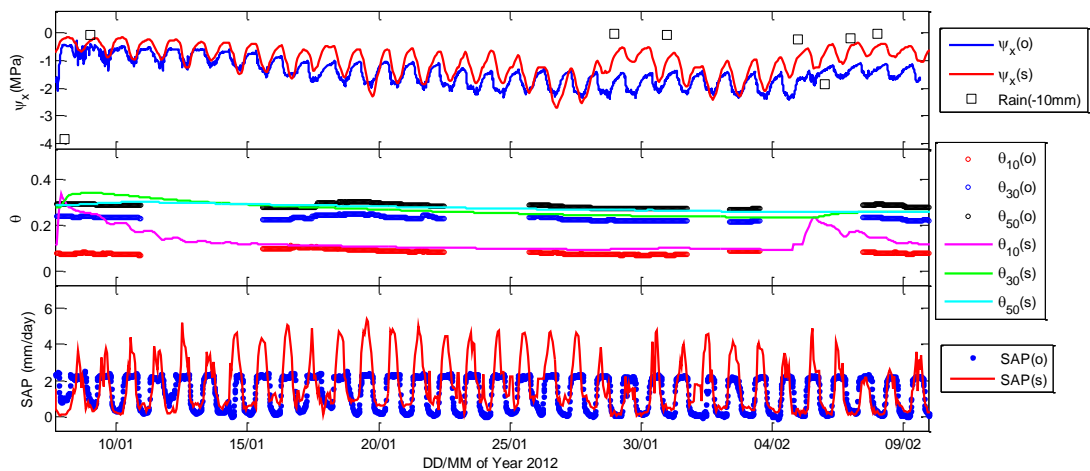
Figure 2-9: Validation of the v-SPAC model on *Acacia pycnantha* ψ_x in summer, 2012.
Note: θ and SAP were not observed in summer, 2012; the observations in Jan, 2013 are only used as reference for 2012. RMSE=0.50 MPa for ψ_x prediction.

The data for *Eucalyptus crenulata* sapling 4 was used for model calibration. The optimal parameter sets were validated on the other five saplings with or without scaling of the resistance/capacitance based on LAI and sapwood area (see Appendix V). The results show that the v-SPAC model reproduced ψ_x as well as θ (although θ not used

for calibration) (see Figure 2-10). It indicates that soil moisture sensors captured the root zone water status in the confined pot space. Table 2-3 gives the optimised parameter sets. It shows that K_s fits in well the measured range 3-10 m/d. Using ψ_x and SAP seems sufficient for inverse modelling to obtain the soil hydraulic conductivity (K_s). The optimised capacitance (C) is at 0.03 mm·MPa^{-1} approximating 3% of the total plant volume (assuming sapwood area is the same all through the main stem). The calibrated R_{min} is in the range of 1900 to 2200 d, comparing well with those inferred from the SS plot (1500-3000 d). Worth noticing that the parameter Δx approaches zero (<2um), implying the marginal contribution of soil-root interfacial resistance (R_{sr}) to the total hydraulic resistance in the soil-plant continuum. However, it is more likely that the integrated vulnerability curve (IVC) derived from the SS plot already integrates the soil-root interfacial resistance (R_{sr}), as the plant resistance is inferred over the water potential gradient from the bulk soil to the stem which may have embraced the water path from bulk soil to root surface (the site R_{sr} occurs). Since Δx is at a micrometre scale for both tree species, the parameter (R_{sr}) in the v-SPAC model could be eliminated. More details about Δx parameter identifiably will be provided in the next section.

Table 2-3: Optimized parameters for *Eucalyptus crenulata* sapling 4 (with several independent optimization runs)

Parameters	Optimized values	Estimated
K_s (mm/d)	5200	3000-10000
Δx (mm)	0.0*	/
R_{min} (d)	2300	1500-3000
C (mm·MPa^{-1})	0.03	/
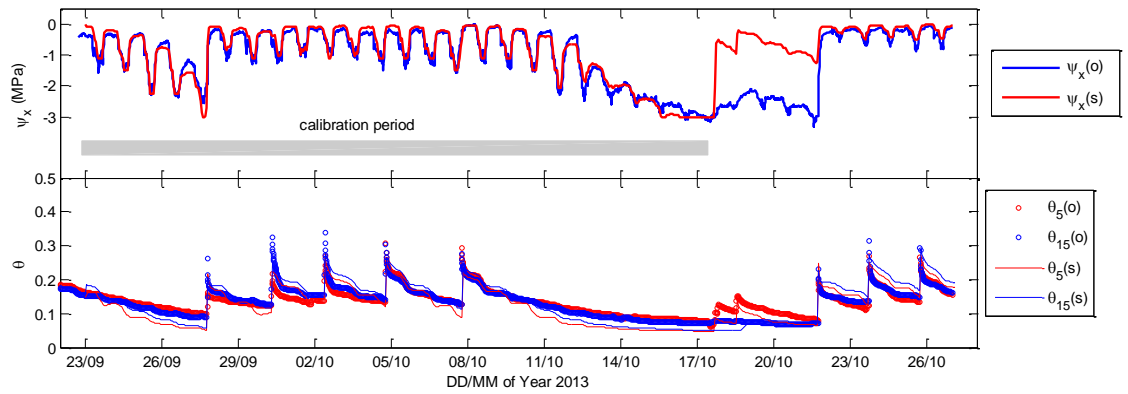
Figure 2-10: Calibration results of *Eucalyptus crenulata* (sapling 4).

The model was validated over the period from the end of the second controlled drought (since 17 Oct, 2013). Prediction of sap flow rate and stem water potential of sapling 1 from the well watered group and sapling 2 from the drought treatment group are shown in Figure 2-11 (results of other saplings are shown in Appendix V).
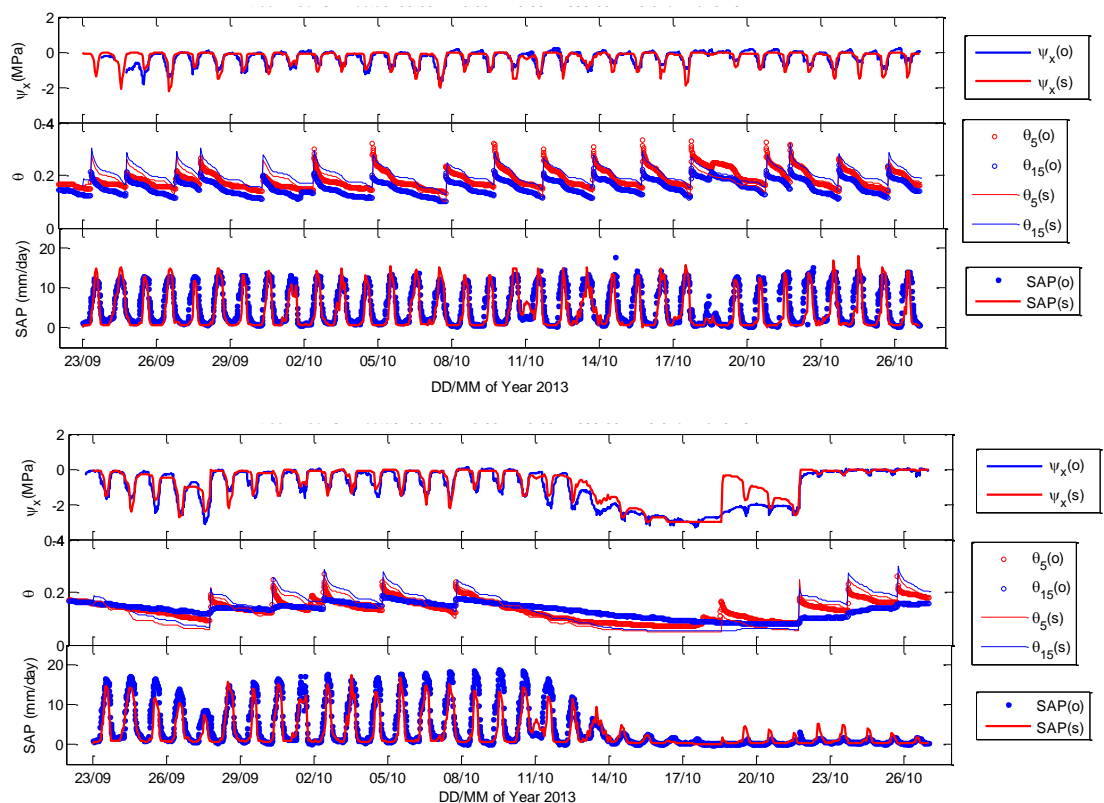
Figure 2-11: Prediction of ψ_x, θ, and SAP of *Eucalyptus crenulata* sapling 1 (upper panel) and sapling 2 (lower panel) with optimised parameters from sapling 4 calibration.

The modelling results demonstrate the good capacity in simulating sap flow rate and

51

soil moisture content for all irrigation schedules. However, the model overestimates ψ_x of the saplings in the drought treatment group during the first four days since rewatering on 18 Oct, 2013. One possible reason is that the plant resistance increased significantly after the severe drought so that R_{min} or the vulnerability curve parameters do not fit any more. Plants can adapt to drought by growth of root casparian bands which will increase root resistance permanently (Aroca and Ruiz-Lozano, 2012). Plant may also go through reversible anatomic change such as embolism of xylem that can be repaired gradually after rehydration (Tyree and Zimmermann, 2002). The rehydration may take from hours to weeks depending on the severity of the dehydration. The gap between soil and root can also enlarge due to shoot/soil shrinkage which can be gradually refilled after rewatering (Carminati et al., 2009). Since the simulation matches well again after 4 days of rewatering, this suggests that the anatomic change of plant is reversible and the soil-root gap may have gone through the cycle of enlarging and narrowing during the drought and rewatering.

Another reason that the model failed to simulate the immediate rewatering period might be due to the simplification of the plant hydraulic system. The v-SPAC model simplifies the plant part from a partial differential equation to an ordinary differential equation problem in which the time variable is eliminated. As v-SPAC only has space variables for the plant part, the recovery process (storage gain and loss from root to stem) is then deemed as an immediate process. The porous media (PM) model instead includes both time and space variables and is expected to capture the time delay of the stem water potential recovery. However, to simulate the recovery of stem with PM model may also be problematic. It is demonstrated in Janott et al. (2011) that there is an apparent transition in the plant water retention curve (WRC) of European beech (*Fagus silvatica L.*) below -3.0 MPa. This indicates that without prior knowledge of

the plant WRC under severe stress conditions, the PM model is unable to predict the transition of the water potential and water flux under severe drought and rewatering conditions. Importantly, Hunt and Nobel (1987) reported that it took 100 times longer for a stem (*Ferocactus acanthodes*) to rehydrate from 85 % to 95 % in relative water content than the root (within 1000 min vs 10 min), indicating that the xylem vulnerability curves (VC) and the water retention curves (WRC) must all be treated differently along the plant hydraulic path to correctly simulate the time response. It appears that a simple model such as v-SPAC that does not require detailed hydraulic properties of plant is especially advantageous in simulating plant water status and flux under modest stress condition which is the case for the *Acacia pycnantha* tree and for the first drought treatment of the *Eucalyptus crenulata* saplings. In the future, v-SPAC can be improved by adding other parameters, which, however, will inevitably increase the model dimension (such as three more parameters for plant WRC and an additional three for each VC).

The simulation of the six *Eucalyptus crenulata* saplings raises the long-held issue: the upscaling challenge. The saplings differed in size and irrigation treatments. It shows that SAP and ψ_x of sapling 1, 2 & 5 can be reproduced with the same parameter sets of sapling 4. But sapling 3 & 6 prediction can be greatly improved if the capacitance and the resistance are scaled with sapwood area or leaf area index (see Appendix V). Upscaling with sapwood area or leaf area index is a common method to calculate stand sap flux rate from individual trees (Asbjornsen et al., 2011). Other information on individual difference may be valuable for the upscaling consideration. For example, sapling 3 growth seems to be suppressed although it was well watered while sapling 2 already showed negative growth after the first controlled modest drought from the LAI time series (see Figure 2-5). It is worth mentioning that sapling 2 & 3 had the largest

53

leaf-specific hydraulic conductivities (normalized by leaf area) at the beginning of the water treatments (from 23 Sep, 2013).

2.5.2 Model comparison between LEACHM and v-SAPC

The v-SPAC model shows advantages in easy parameterization with concurrent stem water potential and sap flow measurements. It can capture a more realistic picture in soil /plant water balance and water status compared to other hydrologic models that ignore root resistance dynamics. We showcase the significance of the transient root resistance in v-SPAC model by comparing to LEACHM model.

From previous modelling experience, we see that Δx can be neglected in v-SPAC modelling for the *Eucalyptus crenulata* saplings. Calibration of *Eucalyptus crenulata* sapling 4 is performed with Δx set to zero (see Figure 2-12). It shows that the parameters can be all identified (narrowed down and no correlation between the parameters, see the left panel), indicating the sufficiency of stem water potential as the optimization target and the robustness of the model structure.
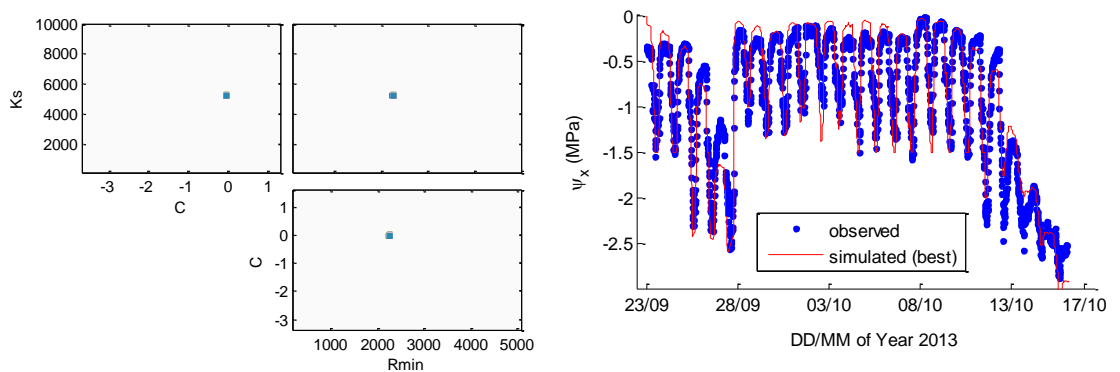
Figure 2-12: Calibration of *Eucalyptus crenulata* sapling 4 under conditions that soil to root resistance (R_{sr}) is ignored ($\Delta x=0$, $R_{sr}=0$). RMSE=0.18 MPa.

LEACHM model is optimized with soil moisture as is common with hydrologic models. The calibration results show that LEACHM can capture the overall trend of

the plant water status but fail to depict the diurnal pattern (see Figure 2-13). It gives a far too narrow diurnal range of root water potential during wet condition. The root-mean-square error (RMSE) of ψ_x is much larger than that of the v-SPAC model (0.46 vs 0.18 MPa). This is due to the neglect of root resistance in LEACHM model. It implies that diurnal patterns of plant water potential cannot be predicted if the root resistance dynamics are not characterized in models. A careful look at the parameterization results shows that K_s and Δx are not identifiable in LEACHM (see left panels in Figure 2-12 vs Figure 2-13), as is also indicated in corresponding Table 2-4 on posterior probability of parameters between the two simulations. Previous studies also suggest that parameterization (such as for water retention curve) with only soil moisture may be insufficient (Scharnagl et al., 2011). For example, for a simple soil evaporation experiment (even without root water uptake), Zhang et al. (2003) showed that a soil moisture dataset was not sufficient for soil hydraulic parameterization unless soil water potential was added. This suggests that stem water potential provides a good constraint for model calibration, especially for cases when soil water potential is not available.
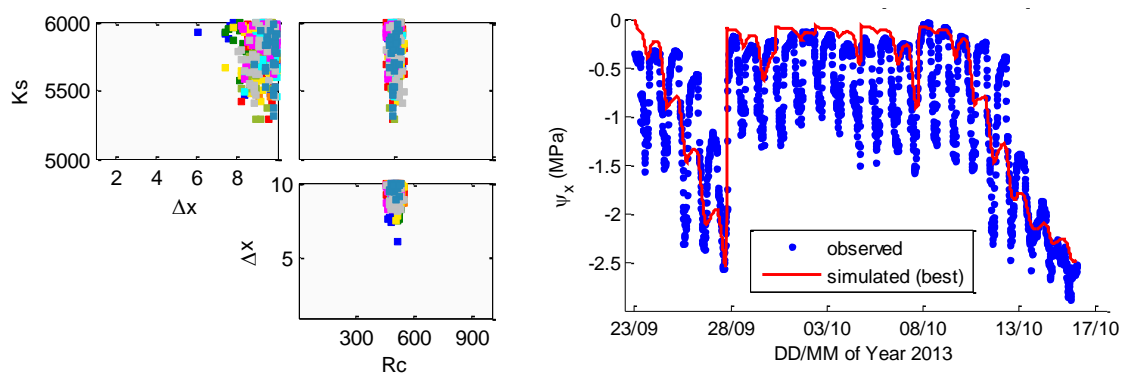
Figure 2-13: Calibration results of *Eucalyptus crenulata* sapling 4 with LEACHM. RMSE=0.46 MPa.

Table 2-4: Posterior moments of parameters for *Eucalyptus crenulata* sapling 4 between the

v-SPAC and LEACHM simulations with DREAM.

v-SPAC	K_s (mm/d)	C (mm/MPa)	R_{min} (d)	Observed ψ_x (MPa)	Simulated ψ_x (MPa)
Best fitting	5200	-0.08	2300	-0.92	-0.92
Standard deviation	260	0.03	130	0.75	0.83
0.25 percentile	4700	-0.10	2000	-2.55	-2.94
Median	4700	-0.08	2000	-0.68	-0.69
97.5 percentile	6800	-0.03	2300	-0.10	-0.06
LEACHM	K_s (mm/d)	Δx (mm)	R_C (/)	Observed ψ_x (MPa)	Simulated ψ_x (MPa)
Best fitting	5800	9.03	510	-0.92	-0.76
Standard deviation	210	1.40	70	0.75	0.80
0.25 percentile	5200	4.17	450	-2.55	-2.37
Median	5800	9.53	500	-0.68	-0.30
97.5 percentile	6000	10.00	730	-0.10	-0.07

Comparison on the acacia tree reveals some interesting information on plant response to rain events (see Figure 2-14). LEACHM simulation indicates that the plant will be immediately hydrated (ψ_x approaches zero) after a rainfall, while, v-SPAC shows a weakened or even no apparent response during the drought period (no quick rise of ψ_x, see the indication by the arrow). This suggests that the plant resistance (R_p) of the acacia tree plays a significant role in regulating its water flux/water status. The large R_p may level off the advantages of taking up rain water infiltrated into the shallow soil layer compared to taking up water in the deeper soil layers.
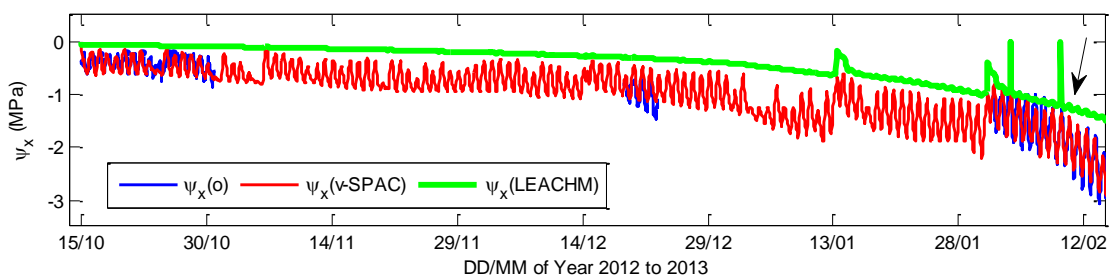
Figure 2-14: Comparison of predicted plant water status between v-SPAC and LEACHM.

Water balance calculation were also compared between the two models (see Table 2-5 and Table 2-6). LEACHM and v-SPAC show marginal differences in soil water balance over potted saplings but a more significant difference for the acacia tree. In the sapling case, the confined root space and the fast drainage of the sandy soil make soil moisture the dominant factor limiting transpiration, which reduced the significance of plant resistance, hence, the difference between the two simulation results of water flux on the saplings.

Table 2-5: Plant and soil water balance of *Eucalyptus crenulata* sapling 4 calculated with v-SPAC and LEACHM (numbers in brackets) (unit: mm)

		Drought 1 23/09-27/09	Post-drought 27/9-10/10	Drought 2 10/10-17/10	Post-drought 17/10-27/10
Plant water balance (mm)	RWU	22.38 (21.02)	62.89 (61.14)	17.91 (16.91)	11.99 (11.70)
	T	-22.41 /	-61.93 /	-18.05 /	-11.92 /
	ΔS	-0.03 /	0.96 /	-0.13 /	0.07 /
Soil water balance (mm)	IN	0.00 (0.00)	159.15 (159.15)	0.00 (0.00)	104.29 (104.29)
	D	-1.02 (-0.98)	-45.88 (-47.85)	-0.10 (-0.10)	-28.56 (-29.62)
	E+RWU	-29.89 (-28.86)	-90.98 (-90.04)	-23.85 (-22.84)	-27.93 (-27.79)
	ΔS	-30.87 (-29.84)	22.42 (21.27)	-23.90 (-22.88)	47.75 (46.86)

Note: the numbers in bracket are with LEACHM, numbers outside with v-SPAC.

Table 2-6: Plant and soil water balance of *Acacia pycnantha* calculated with v-SPAC and LEACHM (unit: mm).

		v-SPAC	LEACHM
Plant water	RWU	200.00	235.95

balance (mm)	T	-202.71	/
	ΔS	-2.70	/
Soil water balance (mm)	IN	66.64	66.64
	D	-89.48	-82.11
	E+RWU	-309.15	-355.87
	ΔS	-333.78	-374.38

A more obvious contrast is seen in root water uptake profile of the acacia site (see Figure 2-15). As the resistance term in LEACHM is purely based on soil hydraulic conductivity, the resistance is much larger in shallow soil layer than the deeper layer due to evaporation and drainage. The root density is also commonly higher in the shallow soil, making it drying out more quickly. Therefore, the deepest root will inevitably contribute the most water to the transpiration stream. It is known that trees may access deeper water source progressively (Meinzer et al. 1999). However, the way larger water consumption by deepest root segments seems indicating shallow groundwater table which is not common on a hill slope. It shows that although the two models both reproduced the soil moisture profile, but the root water uptake partitioning in the soil layers are very different.
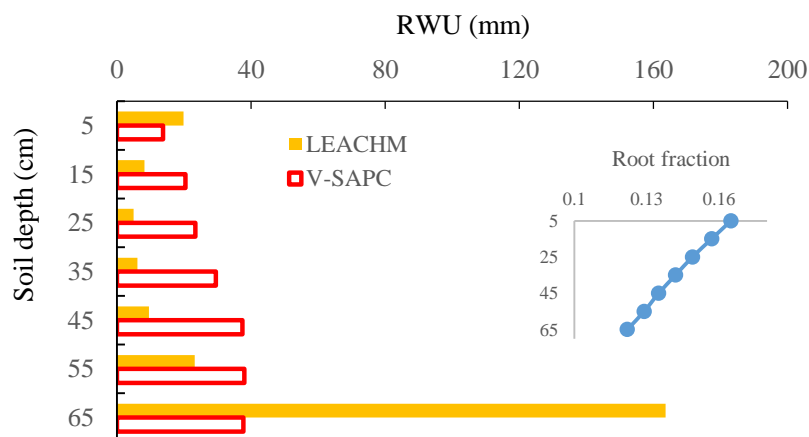
Figure 2-15: Root water uptake (RWU) in soil profile simulated with v-SPAC (hollow bar) and LEACHM (filled bar) at the acacia site. Embedded figure is prescribed root fraction.

The minimum required forcing data for the two models are summarized in (Table 2-7). In v-SPAC, the stem water potential is the key dataset. Alternatively, leaf water potential can be used instead of stem water potential. But the midday or the pre-dawn and minimum leaf water potential are required to quantify the plant hydraulic properties. Sap flow rate can be replaced if not available with potential transpiration (PT). However, the uncertainty from PT calculation may be introduced into the modelling and the sap flow measurement of trees such as *Acacia pycnantha* will be critical in predicting the true water use pattern. Soil moisture is not required in the v-SPAC model and can be calibrated, however, soil texture measurement will be of great value to constrain the WRC. LEACHM have less requirement on plant data. It can be calibrated with soil water content or the plant flux. WRC can also be calibrated in LEACHM. However, as mentioned previously, soil water content may not be sufficient to parameterize WRC. The meteorological measurement is required for PET calculation. Leaf area index or vegetation coverage over land is used for PT and PE partitioning.

Table 2-7: Minimum required forcing data for parameterization of v-SPAC and LEACHM.

Data requirement	v-SPAC	LEACHM
Plant measurement	stem water potential	plant water flux*
	sap flow rate (with sapwood area)	root distribution function (RDF)*
	leaf area index	leaf area index
Soil measurement	WRC (e.g soil texture)*	soil water content
		WRC (e.g soil texture)*
Meteorological measurement	rainfall	rainfall
	radiation, relative humidity, wind speed, air temperature*	radiation, relative humidity, wind speed, air temperature*

Note: * denotes dataset that may not be required if calibrated or there is other data source, for example, sap flow can be replaced with transpiration, inferred from soil moisture depletion etc. The radiation etc can be replaced with evapotranspiration.

2.6 Conclusions and Future work

In this study, we present a new coupled soil-plant-atmosphere continuum model (v-SPAC) in which the plant's control of water transfer in the continuum is emphasized. The v-SPAC model incorporates a dynamic plant resistance and capacitance system to represent plant's hydraulic regulation on water flux and water status. A so-called integrated vulnerability curve is proposed to characterize the whole plant resistance system from in-situ measurement which facilitates the model parameterization. The testing results with two sets of experimental data demonstrate the capacity of the v-SPAC model in predicting the diurnal pattern of both sap flow and stem xylem water potential.

This study underscores the importance of integrating plant hydraulic properties into hydrologic models. Comparison between LEACHM and v-SPAC shows that hydrologic model LEACHM can capture the overall evolution of soil and plant water status based on known soil hydraulic properties, while v-SPAC, by integrating plant hydraulic properties can simulate plant water status and water flux at sub-daily resolution. The comparison highlights the data sufficiency in model calibration. It is insufficient to use soil moisture for constraining the LEACHM model, while v-SPAC model identifies the plant water status data as the key dataset to constrain hydraulic properties of the soil-plant continuum.

Models are only capable of performing well if necessary mechanisms are incorporated and they are well parameterized. The improvement of the current models' capacity to simulate the plant's response in severe drought and its hydraulic recovery relies on a profound understanding of the underlying mechanisms. The model capacity is traded-off with model efficiency, depending on how detailed microscopic mechanisms can be

practically represented in models. Prediction of unique tree water use pattern such as those of *Acacia pycnantha* in natural landscapes requires more focus on physiological regulation of transpiration compared to those examined in the laboratory with space or water limited conditions.

References

Allen, R.G.; Pereira, L.S.; Raes, D.; Smith, M. (1998). Crop Evapotranspiration: Guidelines for Computing Crop Water Requirements. FAO Irrigation and drainage paper 56. Rome, Italy: Food and Agriculture Organization of the United Nations.

Aroca, R., Ruiz-Lozano, J.M., 2012. Regulation of Root Water Uptake Under Drought Stress Conditions In: Aroca, R. (Ed.), Plant Responses to Drought Stress Springer Berlin Heidelberg, pp. 466.

Asbjornsen, H. et al., 2011. Ecohydrological advances and applications in plant-water relations research: a review. Journal of Plant Ecology, 4(1-2): 3-22

Besharat, S., Nazemi, A.H., Sadraddini, A.A., 2010. Parametric modeling of root length density and root water uptake in unsaturated soil. Turkish Journal of Agriculture and Forestry, 34(5): 439-449.

Braud, I., Dantasantonino, A.C., Vauclin, M., Thony, J.L., Ruelle, P., 1995. A simple soil-plant-atmosphere transfer model (sispat) development and field verification. Journal of Hydrology, 166(3-4): 213-250.

Bucci, S.J., Scholz, F.G., Goldstein, G., Meinzer, F.C., Arce, M.E., 2009. Soil water availability and rooting depth as determinants of hydraulic architecture of Patagonian woody species. Oecologia, 160(4): 631-641.

Bucci, S.J. et al., 2004. Processes preventing nocturnal equilibration between leaf and soil water potential in tropical savanna woody species. Tree Physiology, 24(10): 1119-1127.

Burgess, S. S., Adams, M. A., Turner, N. C., Beverly, C. R., Ong, C. K., Khan, A. A., & Bleby, T. M. 2001. An improved heat pulse method to measure low and reverse rates of sap flow in woody plants. Tree Physiology, 21(9), 589-598.

Carminati, A., Vetterlein, D., Weller, U., Vogel, H.-J., Oswald, S.E., 2009. When Roots Lose Contact. Vadose Zone Journal, 8(3): 805-809.

Cermak, J., Kucera, J., Bauerle, W.L., Phillips, N., Hinckley, T.M., 2007. Tree water storage and its diurnal dynamics related to sap flow and changes in stem volume in old-growth Douglas-fir trees. Tree Physiology, 27(2): 181-198.

Chuang, Y.L., Oren, R., Bertozzi, A.L., Phillips, N., Katul, G.G., 2006. The porous media model for the hydraulic system of a conifer tree: Linking sap flux data to transpiration rate. Ecological Modelling, 191(3-4): 447-468.

Deng, Z. Priestley, S.C., Guan, H., Love, A. J., Simmons, C. T. Canopy enhanced chloride deposition in coastal South Australia and its application for the chloride mass balance method. Journal of Hydrology 2013: 62-70. doi: 10.1016/j.jhydrol.2013.05.040

Doussan, C., Pierret, A., Garrigues, E., Pages, L., 2006. Water uptake by plant roots: II - Modelling of water transfer in the soil root-system with explicit account of flow within the root system - Comparison with experiments. Plant and Soil, 283(1-2): 99-117.

Draye, X., Kim, Y., Lobet, G., Javaux, M., 2010. Model-assisted integration of physiological and environmental constraints affecting the dynamic and spatial patterns of root water uptake from soils. Journal of Experimental Botany, 61(8): 2145-2155.

Domec, J. C., Scholz, F. G., Bucci, S. J., Meinzer, F. C., Goldstein, G., and VILLALOBOS-VEGA, R., 2006. Diurnal and seasonal variation in root xylem embolism in neotropical savanna woody species: impact on stomatal control of plant water status. Plant, Cell & Environment, 29(1), 26-35.

Dunbabin, V.M. et al., 2013. Modelling root-soil interactions using three-dimensional models of root growth, architecture and function. Plant and Soil, 372(1-2): 93-124.

Feddes, R.A., Kowalik, P.J., Zaradny, H., 1978. Simulation of Field Water Use and Crop Yield. John Wiley & Sons, New York.

Franco, A.C. 2009, Tree functional strategies in Brazilian savannas. In: Erick De La Barrera,

Smith, W.K. (Eds.), Perspectives in Biophysical Plant Ecophysiology: A Tribute to Park S. Nobel, Mexico : Universidad Nacional Autonoma de Mexico, pp. 400.

Hentschel, R. et al., 2013. Simulation of stand transpiration based on a xylem water flow model for individual trees. Agricultural and Forest Meteorology, 182: 31-42.

Hopmans, J.W., Bristow, K.L., 2002. Current capabilities and future needs of root water and nutrient uptake modeling. Advances in Agronomy, Vol 77, 77: 103-183.

Hunt, E.R., Nobel, P.S., 1987. Non-steady-state Water Flow for Three Desert Perennials with Different Capacitances Aust. J. Plant Physiol., 14: 363-375.

Hunt, E.R., Running, S.W., Federer, C.A., 1991. Extrapolating plant water-flow resistances and capacitances to regional scales. Agricultural and Forest Meteorology, 54(2-4): 169-195.

Hutson, J.L., Wagenet, R.J., 1995. A multiregion model describing water-flow and solute transport in heterogeneous soils. Soil Science Society of America Journal, 59(3): 743-751.

Jackson, R.B., Sperry, J.S., Dawson, T.E., 2000. Root water uptake and transport: using physiological processes in global predictions. Trends in Plant Science, 5(11): 482-488.

Janott, M. et al., 2011. A one-dimensional model of water flow in soil-plant systems based on plant architecture. Plant and Soil, 341(1-2): 233-256.

Jones, H.G., 2004. Irrigation scheduling: advantages and pitfalls of plant-based methods. Journal of Experimental Botany, 55(407).

Jones, H.G., 2008. Irrigation scheduling - Comparison of soil, plant and atmosphere monitoring approaches. In: Goodwin, I., Oconnell, M.G. (Eds.), Proceedings of the Fifth International Symposium on Irrigation of Horticultural Crops. Acta Horticulturae, pp. 391-403.

King, E., Caylor, K., 2011. Ecohydrology in practice: strengths, conveniences, and opportunities. Ecohydrology, 4(4): 608-612.

Kramer, P.J., Boyer, J.S., 1995. Water Relations of Plants and Soils. Nature.

Kumagai, T. 2001, Modeling water transportation and storage in sapwood - model development and validation, Agricultural and Forest Meteorology, 109(2), 105-115.

Leij, F.J., aLVES, W.J. van Genuchten, M.Th., Williams, J.R., 1996. Unsaturated Soil Hydraulic Database, UNSODA 1.0 User's Manual. Report EPA/600/R-96/095, US Environmental Protection Agency, Ada, Oklahoma, 103pp.

Mart ñez-Vilalta, J., Prat, E., Oliveras, I., and Pi ñol, J. (2002). Xylem hydraulic properties of roots and stems of nine Mediterranean woody species. Oecologia,133(1), 19-29.

Meinzer, F. C. 2003. Functional convergence in plant responses to the environment. Oecologia, 134(1), 1-11.

Meinzer FC, Andrade JL, Goldstein G, Holbrook NM, Cavelier J, Wright SJ (1999) Partitioning of soil water among canopy trees in a seasonally dry tropical forest. Oecologia 121:293–301

Micco, V.D., Aronne, G., 2012. Morpho-Anatomical Traits for Plant Adaptation to Drought Plant Responses to Drought Stress. Springer Berlin Heidelberg.

Minasny, B., McBratney, A.B., Bristow, K.L., 1999. Comparison of different approaches to the development of pedotransfer functions for water-retention curves. Geoderma, 93(3-4): 225-253.

Minasny, B., J. A. Vrugt, and A. B. McBratney (2011). Confronting uncertainty in model-based geostatistics using markov chain monte carlo simulation. Geoderma 163, 150–162.

Mualem, Y., A new model for predicting the hydraulic conductivity of unsaturated porous media, Water Resour. Res., 12(3), 513-522, 1976.

Nimah, M.N., Hanks, R.J., 1973. Model for Estimating Soil Water, Plant, and Atmospheric Interrelations: I. Description and Sensitivity. Soil Sci. Soc. Am. J., 37: 522–527.

Nobel, P.S., Cui, M., 1992. Shrinkage of attached roots of opuntia ficus-indica in response to lowered water potentials predicted consequences for water-uptake or loss to soil. Annals of Botany, 70(6): 485-491.

Pfautsch, S. et al., 2011. Diurnal patterns of water use in Eucalyptus victrix indicate

pronounced desiccation-rehydration cycles despite unlimited water supply. Tree Physiology, 31(10): 1041-1051.

Pirson, A., Zimmermann, M.H. (Eds.), 1982. Encyclopedia of Plant Physiology. Physiological Plant Ecology II, Water relations and carbon assimillation, 12B, New York, 747 pp.

Passioura, J. B. 2010. Plant–Water Relations. eLS.

Schaap, M.G., Leij, F.J., van Genuchten, M.T., 2001. ROSETTA: a computer program for estimating soil hydraulic parameters with hierarchical pedotransfer functions. Journal of Hydrology, 251(3-4): 163-176.

Scharnagl, B., Vrugt, J.A., Vereecken, H., Herbst, M., 2011. Inverse modelling of in situ soil water dynamics: investigating the effect of different prior distributions of the soil hydraulic parameters. Hydrology and Earth System Sciences, 15(10): 3043-3059.

Scholz, F. G., Phillips, N. G., Bucci, S. J., Meinzer, F. C., & Goldstein, G. 2011. Hydraulic capacitance: biophysics and functional significance of internal water sources in relation to tree size. In Size-and age-related changes in tree structure and function (pp. 341-361). Springer Netherlands.

Šimůnek, J., K. Huang, and M. Th. van Genuchten, The HYDRUS code for simulating the one-dimensional movement of water, heat, and multiple solutes in variably-saturated media. Version 6.0, Research Report No. 144, U.S. Salinity Laboratory, USDA, ARS, Riverside, California, 164 pp., 1998.

Sperry, J.S., Adler, F.R., Campbell, G.S., Comstock, J.P., 1998. Limitation of plant water use by rhizosphere and xylem conductance: results from a model. Plant Cell and Environment, 21(4): 347-359.

Tardieu, F., & Simonneau, T. (1998). Variability among species of stomatal control under fluctuating soil water status and evaporative demand: modelling isohydric and anisohydric behaviours. Journal of experimental botany,49(Special Issue), 419-432.

Tuzet, A., Perrier, A., Leuning, R., 2003. A coupled model of stomatal conductance, photosynthesis and transpiration. Plant Cell and Environment, 26(7): 1097-1116.

Tyree, M. T., & Zimmermann, M. H. 2002. Xylem structure and the ascent of sap. Springer.

Verburg, K., Ross, P., Bristow, K.L., 1996. SWIMv2.1 user manual, CSIRO Division of Soils, Adelaide.

Vrugt, J.A., Stauffer, P.H., Woehling, T., Robinson, B.A., Vesselinov, V.V., 2008. Inverse modeling of subsurface flow and transport properties: A review with new developments. Vadose Zone Journal, 7(2): 843-864.

Vrugt, J.A., van Wijk, M.T., Hopmans, J.W., Simunek, J., 2001. One-, two-, and three-dimensional root water uptake functions for transient modeling. Water Resources Research, 37(10): 2457-2470.

Wang, H., Guan, H., Deng, Z., & Simmons, C. T. 2014. Optimization of canopy conductance models from concurrent measurements of sap flow and stem water potential on Drooping Sheoak in South Australia. Water Resources Research, 50(7), 6154-6167.

Yang, Y., Guan, H., Hutson, J. L., Wang, H., Ewenz, C., Shang, S., & Simmons, C. T. 2013. Examination and parameterization of the root water uptake model from stem water potential and sap flow measurements.Hydrological Processes, 27(20), 2857-2863.

Zhang, Z.F., Ward, A.L., Gee, G.W., 2003. Estimating Soil Hydraulic Parameters of a Field Drainage Experiment Using Inverse Techniques. Vadose Zone Journal, 2(2): 201-211.

Appendices

Appendix I: Calibration of PSY1 stem psychrometers and comparison to a PMS chamber.

Calibration of the stem psychrometer in the lab is to be practised before reinstallation. The readings of psychrometer are compared to a series of standard NaCl solutions of known concentrations (see Table AI.1 and Figure AI.1 below). A small filter paper (around 5 mm in diameter) is firstly quickly soaked in the solution and then put into a small hole of a chamber. The psychrometer sensor (attached to another half of the chamber) will touch slightly the surface of the filter paper when chamber is closed. The sealing of the chamber is secured with grease oil surrounding the opening. The chamber is placed in a water bus fixed at 25 ℃. The readings are recorded until the chamber temperature reaches equilibrium with the water bus temperature. See procedure online (http://www.ictinternational.com/content/uploads/2014/05/PSY1-stem-psychrometer-manual-ver.-4.4.pdf).

Table AI.1: The NaCl standard solutions for calibrating PSY1 psychrometers

NaCl Molality	Mass of NaCl (g)	Mass of Water (g)	Water Potential (MPa) @ 25 degree
0.1	0.2922	50	0.462
0.2	0.5844	50	0.915
0.3	0.8766	50	1.368
0.4	1.1688	50	1.823
0.5	1.461	50	2.281
1	2.9221	50	4.64
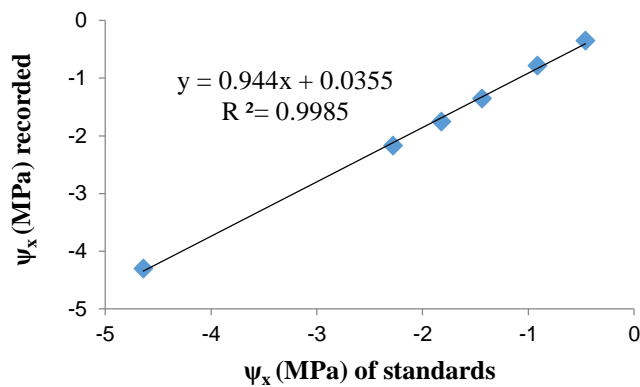
Figure AI.1: One example of the calibration curve of one PSY1 sensor (sensor label PSY1610)

The stem water potential measured by PSY1 psychrometers is also compared to leaf water potential measured by a PMS chamber (Model 615, PMS Instrument Company, US) at pre-dawn (The experiment was conducted by a group of Master student in Hunan, China).
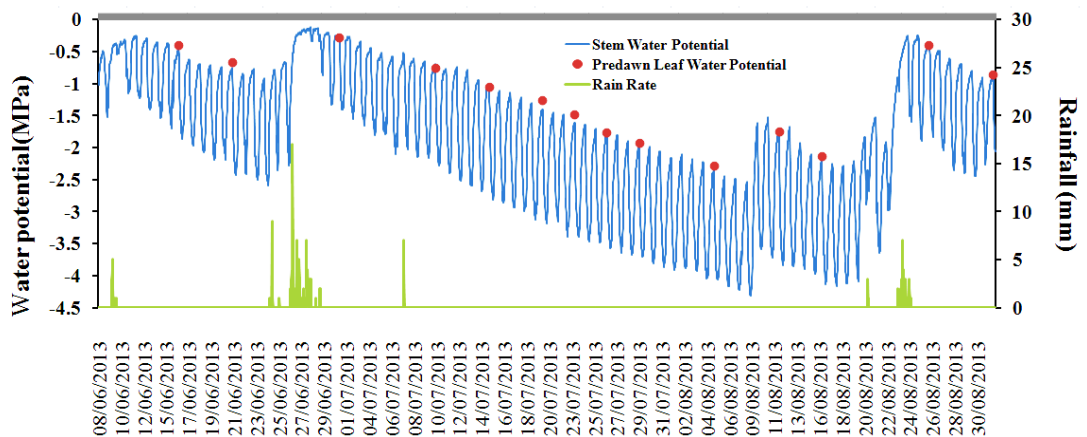
Figure AI.2: Comparison of stem water potential with PSY1 stem psychrometer to pre-dawn leaf water potential with a PMS chamber on an *Osmanthus fragrans* tree in Hunan, China (figure courtesy of Zhang Cicheng).

Appendix II: SFM1 sap flow meter configuration and sap flow rate calculation.
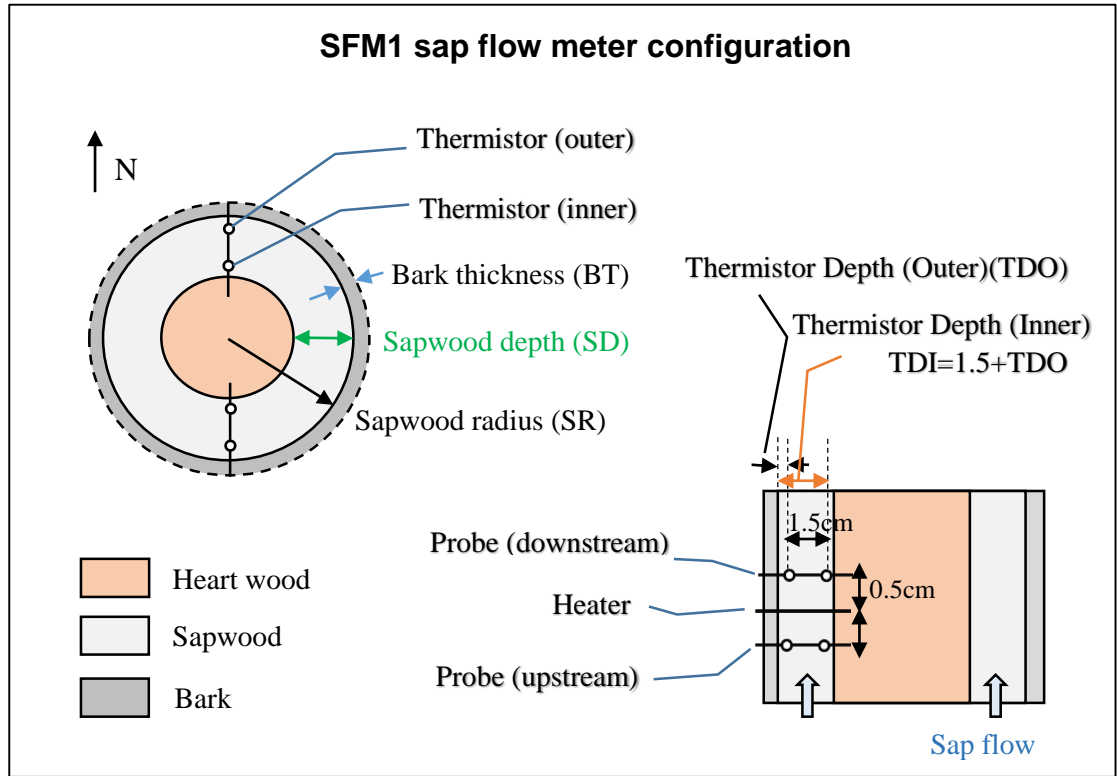
Figure AII.1: The configuration of a set of SFM1 sensors at one side of a tree stem.

The sap velocity (V_s) is calculated from the heat velocity that is obtained from SFM1 sensor following equation below.

$$V_s = \frac{V_c \rho_b (c_w + m_c c_s)}{\rho_s C_s}$$
(AII.1)

where, V_s is sap velocity (cm/hr). V_c is the corrected heat velocity (cm/hr); ρ_b is basic sapwood density g·cm^{-3} (dry weight/fresh sapwood volume); ρ_s is the density of water; m_c (g/g) is water content of sapwood (water weight/dry weight); c_w and c_s are specific heat capacity of wood matrix (1200 J·kg^{-1}·℃$^{-1}$) and water (4182 J·kg^{-1}·℃$^{-1}$), respectively. Refer to Burgess et al., (2002) for the detail on converting the recorded raw temperature to V_c.

The sap velocity is then linearly scaled between the two thermistor sensors (and beyond) through the sapwood depth. The total sap flux will then be the integral of the sap velocity over the sapwood annulus. The sapwood area and sensor depth are recorded in Table AII.1 below.

Table AII.1: Tree wood properties and SFM1 installation settings.

Study site	Tree species	Wood properties	SFM1 parameters
Flinders Campus, Adelaide, SA, Australia (E 138.573 °, S 35.031 °)	*Acacia pycnantha* (3.8 m)	BT: 0.75 cm SR: 2.7 cm SD: 1.5 cm m_c: 0.52 g/g ρ_b: 0.88 g·cm^{-3}	Northern: TDO: 0.2 cm Southern: TDO: 0.2 cm
	Eucalyptus macrocarpa (6.4 m)	BT: 1.3 cm SR: 6.0 cm SD: 2.6 cm m_c: 0.43 g/g ρ_b: 0.96 g·cm^{-3}	Northern: TDO: 0.5 cm Southern: TDO: 0.5 cm
Armidale, New South Wales, Australia (E 151.776 °, S 30.706 °)	*Eucalyptus crenulata* (6 saplings of 1.5-2.2 m)	BT: (0.11, 0.07, 0.13, 0.11, 0.12, 0.1) cm SR: (0.49, 0.68, 0.59, 0.54, 0.565, 0.515) cm SD: (0.49, 0.65, 0.59, 0.54, 0.565, 0.515) cm m_c: (1.2, 0.93, 0.97, 0.81, 0.94, 0.99) g/g ρ_b: (0.47, 0.55, 0.52, 0.53, 0.59, 0.47) g·cm^{-3}	TDO: (0.245, 0.34, 0.295, 0.27, 0.2825, 0.2575) cm *

Note: BT is bark density (cm); SR is sapwood radius (cm); SD is sapwood depth (cm); TDO is the depth into xylem of the outer thermistor sensor. *: the sapwood depth of *Eucalyptus crenulata* is smaller than the space of the two thermistors (1.5cm), so that only one set of SFM1 is used to obtain sap flow rate and the TDO denotes the location of first thermistor at one side of the stem and the other one is 1.5 cm into the sapwood (which is on the other side of the stem).

Appendix III: Soil hydraulic properties at the acacia site

Table AIII.1: Soil water retention parameters estimated from pedo-transfer functions for the acacia tree site.

Soil depth/texture	θ_r	θ_s	α (1/kPa)	n	K_s (mm/d)*
0-20 cm Clay loam	0.05-0.18	0.4-0.5	0.07-0.14	1.3-1.5	50(80)
	0.05	0.4	0.14	1.28	/
20-50 cm Clay	0.13-0.35	0.45-0.6	0.11-0.26	1.2-1.5	100(150)
	0.1	0.6	0.22	1.27	/
50-70 cm Silty clay loam	0.10-0.26	0.4-0.5	0.06-0.13	1.2-1.5	50(110)
	0.05	0.45	0.13	1.27	/
70-90 cm Silty loam	0.08-0.14	0.35-0.45	0.04-0.15	1.3-1.5	25(180)
	0.05	0.4	0.08	1.27	/

Note: Upper line shows WRC parameters θ_r, θ_s, α, n estimated from pedo-transfer functions following (Minasny et al., 1999) based on Australian soil classification and lower lines show the values used in the model. K_s is estimated with WRC parameters with ROSETTA (Schaap et al., 2001).

Appendix IV: Water control experiment of the *Eucalyptus crenulata* saplings (provided by Michael Forster)

Seven *Eucalyptus crenulata* saplings were obtained from a commercial nursery in August, 2013, and were retained in pots at the study site in Armidale, New South Wales, Australia (151.7764 °E, 30.7056 °S). Saplings were chosen from individuals sown at a common date. At time of purchase saplings were 18 months old and ranged in height from 1.52 to 2.21m. Three of the saplings were randomly assigned to a well-watered treatment and four of the saplings were randomly assigned to a water withheld treatment. The total number of measured saplings was restricted by availability of instruments, and four were assigned to the stress treatment as insurance against mortality. Until the 22nd September, all seven saplings were kept well watered, with 1.5L of water given every other day. Between the 22nd and 27th September all water

was withheld from the low water treatment. Between the 27th and 7th October all saplings were once again well watered. Between the 7th and 21st October all water was withheld from the saplings in the low water treatment. From the 21st October, trees were well watered until harvest on the 26th October. During the water withheld periods only one rainfall event occurred. Saplings were grown in 24.5 cm diameter by 25 cm height for a volume of 11.8 L.

Volumetric soil water content (%) and soil water potential (MPa) were measured with a capacitance based sensor, 5cm in length, and 0.3L measurement volume (EC-5 Sensor, Decagon Devices, Pullman, WA, USA). Two sensors were installed in the middle of each pot at an angle to cover a depth between 5 and 8 cm and 15 and 18 cm respectively. Each sensor was individually calibrated for soil specific volumetric soil water content (%) and soil water potential (MPa). Soil used during the study was air dried for 21 days and then partitioned into 10 separate containers with volume of 0.573L. The first container remained air dry, a portion of water was added to the second container, and so on until the 10th container was saturated. Soil in each container was thoroughly mixed so that moisture was evenly distributed throughout the volume of the soil. Moisture levels were checked with an EC-5 Sensor to ensure there was a spectrum of moisture contents across the 10 containers from dry to wet, and to ensure consistency of measurements within the container. Every EC-5 Sensor deployed in this study then measured each container five times and an average taken. Immediately following measurements, a portion of the soil was then carefully moved to a SC4 Stainless Steel Cup (Decagon Devices, Pullman, WA, USA) and placed into a WP4C Dewpoint Water Potential Meter (Decagon Devices, Pullman, WA, USA) for a water potential measurement. The wettest soil sample was outside of the specifications for accurate measurements by the WP4C therefore a 2100F Tensiometer

with a dial gauge (Soil moisture Equipment Corp, Goleta, CA, USA) was used to measure soil water potential in the container. Once measurements had been made with the WP4C, soil wet weight was measured and then samples placed in a drying oven at 105 ℃ for 3 days and then dry weight was measured. Volume of the soil was taken as the volume of the SC4 Stainless Steel Cup and actual volumetric water content (%) was calculated. EC-5 Sensor values were then corrected for actual volumetric water content (%). Soil water potential (MPa) at each sensor location was calculated by the moisture release curve.

Meteorological measurements included air temperature (T_{air}) and relative humidity (RH, VP-3 Sensor), wind speed and direction (Davis Cup Anemometer Sensor), and solar radiation (PYR Sensor) connected to a Em50 Data Logger (equipment sourced from Decagon Devices, Pullman, WA, USA). All soil and meteorological data were recorded at 15 minute intervals.

Appendix V: validation of optimised model for potted saplings in predicting SAP and ψx
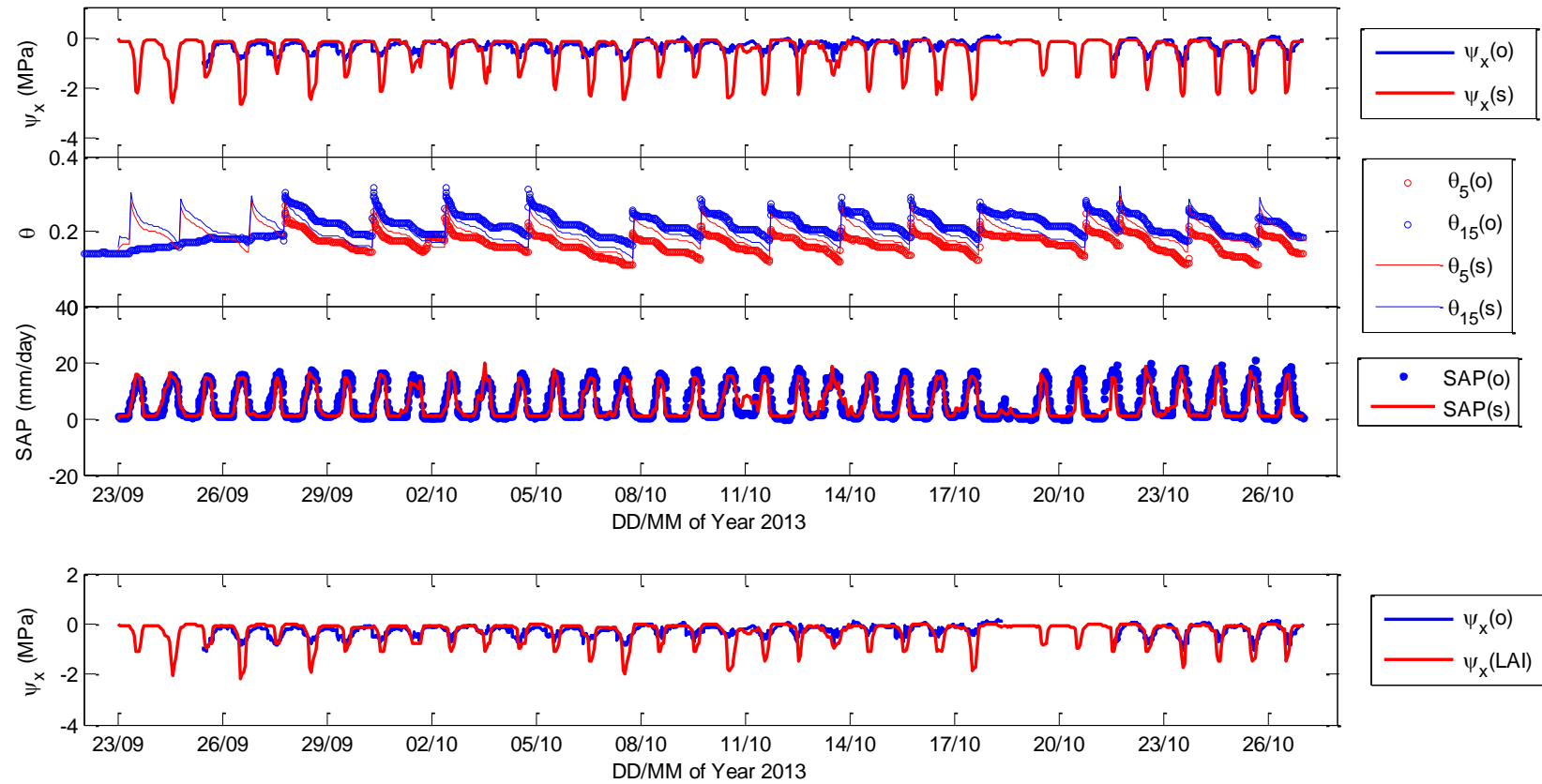
Figure AV.1: Prediction of plant/soil water flux and water status of potted saplings: tree 3 (without scaling (upper panel) and with R_{min} and C scaled with LAI)
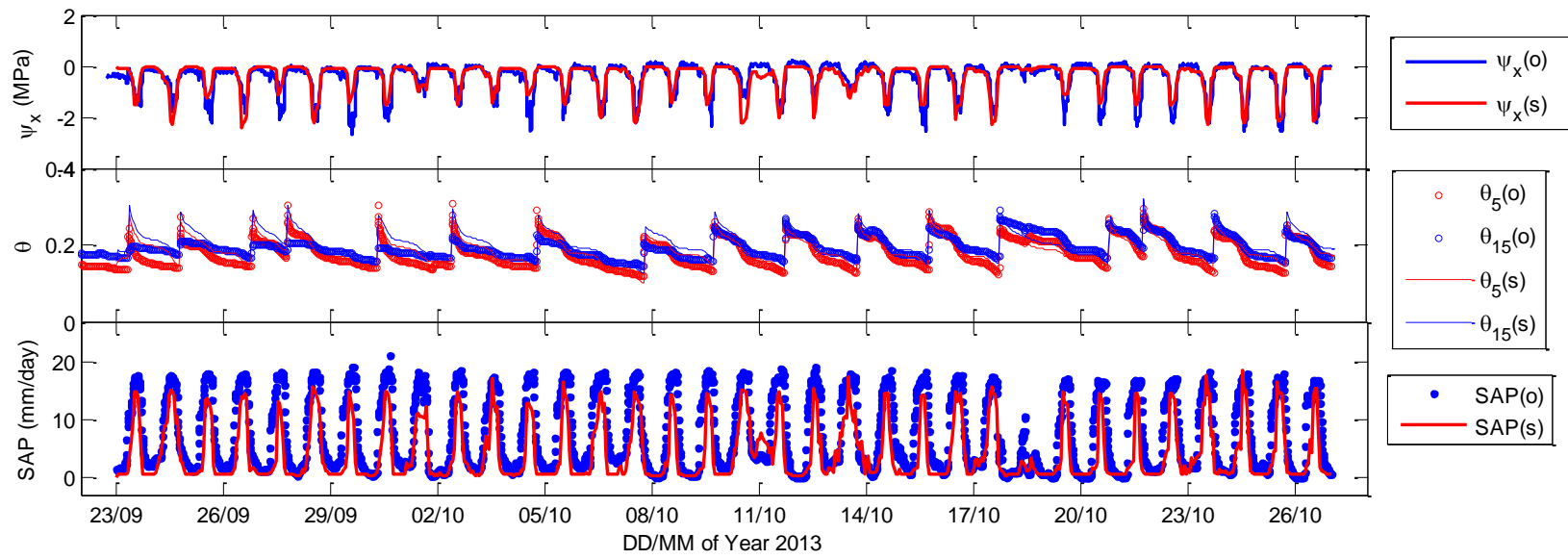
Figure AV.2: Prediction of plant/soil water flux and water status of potted saplings: tree 5 (without scaling of R_{min} and C)
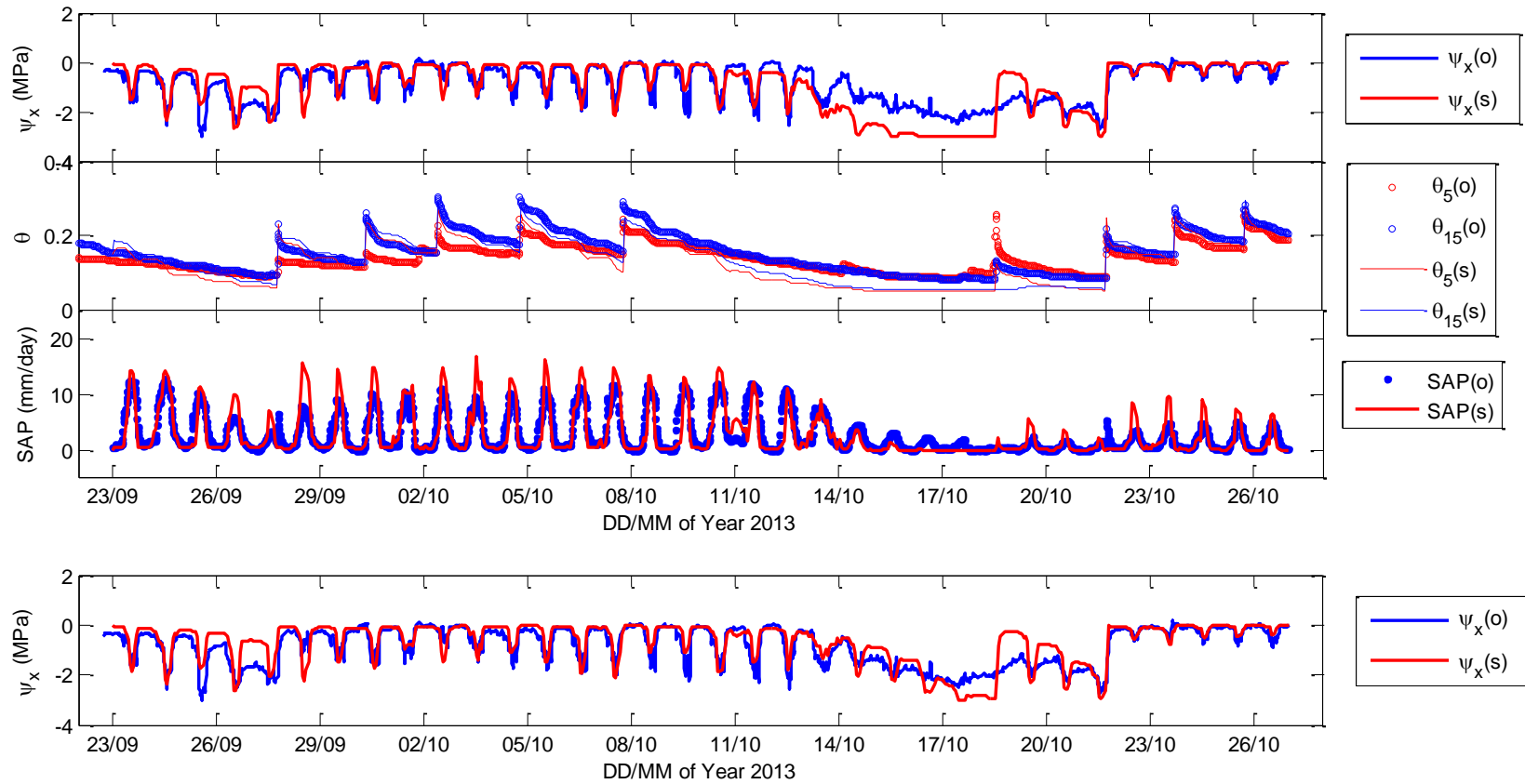
Figure AV.3: Prediction of plant/soil water flux and water status of potted saplings: tree 6 (without scaling (upper panel) and with R_{min} and C scaled with sapwood area

3 EXAMINATION OF NOCTURNAL TRANSPIRATION FROM SAP FLOW MEASUREMENT AND ITS INFLUENCING ENVIRONMENTAL FACTORS

Abstract

Nocturnal transpiration is observed over diverse ecosystems and is a significant component of total ecosystem water use. Direct measurement of the nocturnal transpiration (Tn) is a big challenge. Sap flow measurement is common practice for measuring tree water use. However, the nocturnal sap flux may result from both tree storage recharge and nocturnal transpiration. Various methods are available for partitioning the two components, but often come to different results. In this chapter, a brief review of these different methods is provided. The focus is given to two types of "baseline" methods, with an aim to compare the performance of these methods and to examine the associated uncertainties with modelling technique. The study is based on the sap flow measurement of an *Acacia pycnantha* tree. The results show that the uncertainty of the Phillips baseline method is majorly attributed to tree storage dynamics and the method may underestimate Tn for 15-30 % for the *Acacia pycnantha* tree. With storage dynamics and soil/plant water stress being accounted, the Phillips baseline method can reach a universal function for Tn estimation, which calculate similar results as the Buckley baseline method and the v-SPAC modelling. The atmospheric vapour pressure deficit (VPD) and the soil water stress (Θ) are dominant influencing factors on Tn of the *Acacia pycnantha* tree. VPD and Θ in total explain 90 % of Tn variations of the *Acacia pycnantha* tree. The canopy conductance (g_c) seem insensitive to VPD, indicating a lack of stomata regulation for Tn. However, g_c reduced with increased water stress from wet spring to dry summer. By accounting for

Θ variation, the Tn vs VPD relations converges across seasons. It suggests that an integrated analysis of the environmental factors will help to clarify our understandings on concerned behaviours of Tn.

3.1 Introduction

Nocturnal transpiration is vegetation transpiration water loss occurring from sunset till predawn of the next day (defined here as global radiation < 2 $W \cdot m^{-2}$). Nocturnal transpiration is commonly 5-15% of day-time transpiration and can be as high as 30% for some species (Caird et al. 2007). Nocturnal transpiration should therefore be counted into the ecosystem water use budget. Because of this importance, it has attracted continuous attention in terms of its quantification and its controlling factors (Dawson et al., 2007; Phillips et al., 2010).

Nocturnal transpiration of tree species is primarily calculated from sap flow measurement. For example, sap flow measurement was used to estimate the nocturnal transpiration at the ecosystem level for more than 50 % cases in a summary study by Dawson et al. (2007). More than one third of nocturnal transpiration studies for tree species was estimated from sap flux in Caird et al. (2007). Nocturnal sap flow has found occurring across many taxa, seasons and biomes (Forster 2014). Sap flow measurement is thus an important practice to monitor nocturnal tree water use. However, the nocturnal sap flux can be resulted from transpiration, storage recharge or a mixture of both (Caird et al. 2007; Dawson et al., 2007; Zeppel et al., 2013). It is therefore necessary to separate the two components in sap flow in order to quantify and characterizing the nocturnal transpiration.

Different approaches have been used to diagnose whether the nocturnal sap is driven by nocturnal transpiration or results from storage recharge (Zeppel, et al., 2010; Daley

and Phillips, 2006; Dawson et al., 2007). The first type is to directly measure transpiration or stomata conductance (representative technique: gas exchange chamber method) (Caird et al., 2007; Dawson et al., 2007). This method directly tells if leaf-level transpiration truly occurs, but it is difficult to scale leaf-level measurement to the whole canopy due to variation between leaves. Usually, a chamber may be large enough to cover bushes (as summarized in Caird et al., 2007), but not for tall trees in natural landscape. The same problem exists with the methods trying to minimize nocturnal transpiration by covering the whole canopy with bags (e.g. Donovan, et al., 2001). Eddy covariance measurement can indicate nocturnal transpiration at ecosystem level, however, the results are unreliable due to low turbulence in the night (Fisher et al., 2007).

The second method is correlation analysis between sap flow rates and the driving forces such as vapour pressure deficits (VPD) (Cermak et al., 2007; Dawson et al., 2007; Phillips et al., 1997). If the peak of sap flow matches that of VPD in time, the sap flux can be assumed as driven by nocturnal transpiration (Cermak et al., 2007; Dawson et al., 2007); if the sap flow rate lags, one hour for example, behind the peak VPD, it suggests that the tree capacitance takes effects, and the nocturnal transpiration should be smaller than the measured nocturnal sap flow (Cermak et al., 2007; Phillips et al., 1997). This method provides a rough estimate of nocturnal transpiration and may be only useful for qualitative analysis.

The third method is to compare sap fluxes at two cross sections along the tree stem (Cermak et al., 2007; Zeppel et al., 2010). The sap flux measured at the upper crown of a tree is deemed as transpiration due to its proximity to the canopy. The storage buffering of leaf water content can be neglected (Micco and Aronne, 2012; Scholz et

al., 2011). The sap flux at the base of the tree stem (such as 50 cm above ground in Zeppel et al., (2010)) is assumed to be primarily root water uptake. The difference of the sap fluxes between the crown and the stem base reflects water recharge/discharge in the stem. Once the storage dynamics is known, it can be extrapolated to other trees of which sap flow is measured at only one cross section of the stem. This method requires careful comparison between the two sap fluxes while scaling the sap velocity from point measurement to the whole cross section, which may introduce a large uncertainty (Caylor and Dragoni et al., 2009; Cermak and Nadezhdina 1998; Phillips et al., 1996).

On cases when only one level of sap flow is measured, the baseline method can be used to estimate nocturnal transpiration by comparing sap fluxes between two consecutive nights (Phillips et al., 2010). The two nights need to be carefully selected. Firstly, one night should be under low VPD, so that the nocturnal sap flux can be assumed as storage recharge only and serves as the "baseline". After the baseline is extracted, the remaining nocturnal sap flux of the other night (under high VPD) is considered to be the nocturnal transpiration. This method may overestimate storage recharge, thus give a conservative estimate of nocturnal transpiration (Phillips et al., 2010). The baseline method is subject to uncertainties of storage change from one night to another (Buckley et al., 2011).

By simulating the baseline (nights under low VPD <0.1 kPa) using time-constant concept (Phillips et al., 1997), Buckley et al., (2011) developed a simple numerical method that can be applied for all conditions. Hereafter, we refer the simple baseline method as Phillips baseline method and the other as Buckley baseline method. There are other types of baseline methods, such as those of Fisher et al., (2007). However,

those baseline methods used a fixed time period (e.g. several hours since sunset) to quantify storage refilling which did not account for various day-time conditions, while, the time-constant reflects the inherent tree hydraulic properties (Buckley et al., 2011). The Buckley baseline method is built upon a Resistance-Capacitance (RC) model concept, but requires no parameter calibration as RC models do (Buckley et al., 2011). Without prior knowledge on plant hydraulic or storage properties, the Buckley baseline method will give a possible range of the nocturnal transpiration.

Apart from the above methods based on simple data analysis, numerical modelling provides a more comprehensive interpretation of sap flow. Resistance-Capacitance models (Verbeeck et al., 2007) or porous media (PM) models (Chuang et al., 2006; Kumagai, 2001) can simulate water flow and storage change in plant. The storage compartment is represented in different forms in RC models. The water flow conduit (xylem) is connected with a tree storage pool through a storage resistance term (e.g. Verbeeck et al., 2007) or is parallel to the storage compartment with the same water potential gradient (e.g. Phillips et al., 1997). The storage resistance and water flow resistance are assumed constant in these RC models and assigned with empirical or calibrated values. In PM models, water flow in xylem is simulated as in porous media, and the storage recharge/discharge occurs simultaneously with water transferring in the xylem conduits (e.g. Kumagai, 2001; Chuang et al., 2006). The PM model has advantages over RC model in modelling the details along the transport continuum, but have intensive data requirement. The PM model is thus not easy to apply in field conditions (Chapter 2). A new model (v-SPAC), which simulates the soil water flow in PM mode but simplifies the plant water flow in RC mode, is more flexible to apply in field conditions (Chapter 2) to account for transient soil water conditions. Unlike most RC models with constant resistances, the v-SPAC model characterizes the

dynamic plant hydraulic system with easily parameterized vulnerability curve functions.

Various methods were attempted to estimate Tn but gave very different results (Fisher et al., 2007). It is thus necessary to address the uncertainties of those methods. With the quantification of nocturnal transpiration (Tn), the influencing factors can then be examined. Nocturnal VPD (nVPD) have been commonly reported as the dominant driving force (Buckley et al., 2011; Dawson et al., 2007; Phillips et al., 2010; Zeppel et al., 2010). However, the sensitivity of Tn with nVPD varies over seasons (Phillips et al., 2010; Rosado et al., 2012). Soil moisture could be the secondary factor that limits Tn (Dawson et al., 2007; Zeppel et al., 2010). Wind speed did not show obvious impact on Tn (Buckley et al., 2011; Zeppel et al., 2010) as reported in Phillips et al., (2010). In summary, Tn may be regulated similarly as day-time transpiration (Caird et al., 2007). We hypothesize that difference in soil moisture explains the seasonal variation of Tn response to VPD, and a universal function between Tn and external factors can be derived across the seasons.

In this chapter, we aim 1) to examine the uncertainties of the two baseline methods in estimating Tn; 2) to examine the effect of environmental factors on nocturnal transpiration; 3) to derive a universal function for estimating Tn by accounting for the environmental factors.

3.2 The baseline methods

3.2.1 The Phillips baseline method

The discrepancy between nocturnal sap flow rates (nSAP) and the nocturnal transpiration (Tn) is caused by the transient storage change in trees (ΔS). The interpretation of sap flux (SAP) thus depends on where the sap flow meter is installed.

The nearer it approaches the crown, the closer it represents transpiration, vice versa, the nearer it is to the ground, the closer it matches the root water uptake (see Figure 3-1). Figure 3-1 demonstrates the methods to obtain Tn or ΔS with sap flow measurements. **Eq. 3-1** corresponds to the method of comparing two sap fluxes at cross sections immediately under the crown and at the base of the stem (Cermak et al., 2007; Zeppel et al., 2010). It is more common that sap flow is measured only at one level (e.g. at breast height, see SAP_2), not too high for the ease of installation and not too low for preventing disturbance from the ground. **Eq. 3-2** formulates the Phillips baseline method that can be used to analyse SAP_2. The sap flux of low VPD night (e.g. DAY 1) is assumed to be primarily storage refilling (Tn$\approx$0) and the storage change (ΔS) over the two nights remains the same ($\Delta S/\Delta t$=0 or $\Delta S_{d1} = \Delta S_{d2}$). Tn in DAY 2 is then calculated by removing the storage recharge which is estimated to be the night-time sap flux in DAY 1 ($T_{n_{d2}} \approx nSAP_{2,d2} - nSAP_{2,d1}$). DAY 1 night-time sap flux serves as the baseline.

Separating T and ΔS in sap flow

Eq. 3-1: $F_1 = SAP_1$, $F_2 = SAP_3$, $\Delta S = \Delta S_2 + \Delta S_3$, $T \approx F_1$ (3-2)

$\Delta S = F_2 - F_1$

Eq. 3-2: $F_1 = T$, $F_2 = SAP_2$, $\Delta S = \Delta S_1 + \Delta S_2$ (3-2)

$SAP_{2, d1} = T_{d1} + \Delta S_{d1}$, $SAP_{2, d2} = T_{d2} + \Delta S_{d2}$

$Tn_{d2} = nSAP_{2, d2} - nSAP_{2, d1} - (\Delta S_{d2} - \Delta S_{d1}) + Tn_{d1}$

Tn is the nocturnal transpiration (T); ΔS is the storage change;
nSAP is the night-time sap flow rate (SAP). SAP_1 is measured under the crown,
SAP_2 at breast height; SAP_3 near to ground; F_1, F_2 denote two fluxes at two cross sections.
Subscript d1, d2 denote "DAY 1" and "DAY 2"

Figure 3-1: Schematic illustration of three methods to calculate nocturnal transpiration (Tn) or storage refilling (ΔS) from sap flow measurement.

3.2.2 The Buckley baseline method

In Buckley et al. (2011), the baseline is simulated based on the night-time SAP (nSAP) under very low VPD (e.g. VPD <0.1kPa). Tn is therefore minimized and nSAP within several hours after sunset (2-3 hours in the paper) is assumed to reflect the storage dynamics (ΔS/Δt) (the baseline). The time-constant (τ) that describes the relaxation of storage refilling is in the form of an exponential function:

$$nSAP \propto \exp(-t/\tau) \tag{3-3}$$

The time-constant (τ) is then estimated from the change rate of nSAP (i.e. $-1/\tau$ takes

the slope of linear regression between ln(nSAP) and t). nSAP is the night-time sap

flow rate in unit of cm/hr, and τ is in unit of hour (hr).

The transpiration (T) is then calculated by

$$\frac{dT}{dt} = \frac{d(SAP)}{\omega dt} + \frac{T - SAP}{\omega\tau} \tag{3-4}$$

where ω is the ratio of storage resistance over the sum of storage and water transport

resistances, which is usually unknown and assumed as constant between 0.04-0.5

(Phillips et al., 1997). T is solved by discretion of the time step (e.g. Δt =15 min) with

initial solution of T=0 or T=SAP.

$$T_{i+1} \approx T_i + \Delta t \cdot [\frac{SAP_{i+1} - SAP_i}{\omega\Delta t} + \frac{SAP_i - T_i}{\omega\tau}] \tag{3-5}$$

where i denotes the time step number. At extremes cases, e.g. ω =0, T is solved with

$T_i \approx SAP_i + \frac{\tau(SAP_{i+1} - SAP_{i-1})}{2\Delta t}$ (Buckley et al., 2011) ; at ω =1, when the storage

resistance is extremely large, T=SAP.

3.3 The v-SPAC modelling techniques

The v-SPAC model is a recently developed soil-plant-atmospheric-continuum model

for simulating soil/plant water fluxes and water states (see Chapter 2). The model

describes hydraulic system with a vulnerability curve (Sperry et al., 1998).

$$R_p = R_{min} \cdot \exp[(-\psi_x/d)^b] \tag{3-6}$$

where ψ_x is the stem xylem water potential of root or stem. R_p is total plant resistance

(day), R_{min} is the minimum plant resistance (equivalent to the maximum hydraulic

conductance at full hydration). The parameters d and b can be obtained by measuring

single root/stem segment. To derive the vulnerability curve for the whole plant, night-time sap flow and stem water potential are used (see details in section 2.4, Chapter 2).

The storage component is simulated with constant capacitance:

$$\Delta S = C \cdot \Delta \psi_x \tag{3-7}$$

where, C is a lumped capacitance of the plant storage compartment. Worth to note is C is assumed to reduce with the drop of xylem water potential ($C = \dfrac{c}{-\psi_x}$, in which c is a constant) in PM models (e.g. Chuang et al., 2006; Janott et al., 2011; Kumagai, 2001). In v-SPAC, both forms are enabled to calculate the storage change. Here, for model testing, a constant capacitance is used.

The root water uptake (RWU) is simulated through

$$\sum RWU_i = \sum \frac{\psi_{s,i} - \psi_{r,i}}{R_{r,i} + R_{sr,i}} \tag{3-8}$$

where, the $\psi_{s,i}$ and $\psi_{r,i}$ are the soil and root water potential in soil layer i. $\psi_{r,i}$ is calculated from the stem xylem water potential ψ_x (Eq. 3-6) by accounting for the gravity loss (i.e. $\psi_{r,i} = \psi_x - z$, in which z is the vertical distance from the root to the stem where ψ_x is measured). The soil-root interfacial resistance $R_{sr,i}$ in soil layer i depends on soil hydraulic conductivity and the root density in each soil layer (RDF_i). The root system are assumed in parallel, i.e. $R_{r,i} = \dfrac{R_p}{RDF_i}$, in which, R_p is characterized with vulnerability curve in (Eq. 3-6). The transpiration is then calculated as

$$T = \sum RWU_i - \Delta S \tag{3-9}$$

where ΔS is the storage change of the whole plant ($\Delta S = \Delta S_1 + \Delta S_2 + \Delta S_3 + \Delta S_4$). If the model is calibrated with SAP data, then $SAP = \sum RWU_i - \Delta S$, and $\Delta S = \Delta S_3 + \Delta S_4$ if SAP is observed at the breast height (see Figure 3-1).

The upper flux boundary is prescribed with sap flow rates, or actual transpiration for model calibration. The model is initialized with soil moisture at field capacity and $\psi_{x} = 0$ MPa. ψ_x is iterated until the flux $\Sigma RWU - \Delta S$ meets the prescribed upper flux boundary (SAP or T).

3.4 Materials and methods

3.4.1 Study site

Experiments were conducted on an *Acacia pycnantha* tree (3.8 m, around 5 years old) in South Australia (138.573 ºE, 35.031 ºS). The site is under the Mediterranean climate with high VPD (VPD >2kPa) frequently occurring in spring and summer time. Two sap flow meters (SFM1 meters, ICT international, Australia) were installed on in the southern and northern directions of the main stem. The sap velocity was converted from heat velocity following Burgess et al. (2001). Sap flux were aggregated from the sap velocity by multiplying the averaged sap velocity with sapwood area (the sapwood depth is very thin (15 mm)). The sapwood area was obtained with tree core sampled by an increment borer. The sap fluxes were measured at the breast height (1.3 m), which means that only the baseline methods (e.g. Buckley et al., 2011; Phillips et al., 2010) are useful to quantify the nocturnal transpiration. One stem psychrometer (PSY1, ICT international, Australia) was installed at one branch (ca. 1.9 m height). Soil moisture was observed at three depths 10, 30 and 50 cm with one capacitance-based soil moisture probe (Sentek, Australia) installed 1 m downslope from the tree stem. Meteorological conditions were observed upslope of the acacia tree. For detailed site

description, refer to Chapter 2.

3.4.2 Data selection for the baseline methods

To test the integrity of the Phillips baseline method, we set 8 different scenarios for selecting the two consecutive days based on soil moisture saturation (Θ) and VPD (see Table 3-1). Day-time VPD is not used as selecting criteria as in the original method (Phillips et al., 2010) since mostly two consecutive day-time sap flow rates were similar for both study sites except rainy or overcast days. Scenarios 1 to 4 follow the strict criteria for data selection in the baseline method, having at least one day with maximum night-time VPD <0.6 kPa (when Tn is assumed negligible). Scenarios 4-8 are to examine the method under high VPD Days. A difference by a factor of two in VPD between the two nights is to ensure a sufficient contrast in two nocturnal sap flow rates. At the acacia site, the maximum night-time VPD is hardly as low as 0.1 kPa (the criteria as in Buckley et al., (2011)) under Mediterranean spring and summer in South Australia. We set 0.6 kPa as the criteria based on the observation that the sap flow showed linear increase with VPD above the threshold after several hours since sunset, which is often viewed as nocturnal transpiration (Dawson et al., 2007).

Table 3-1: 8 scenarios to evaluate the uncertainty of baseline method

Scenarios	Θ	Night-time maximum VPD
1	0.4-0.8	$VPD_{d1}<=0.6kPa$ & $VPD_{d2}>2\times VPD_{d1}$
2	0.4-0.8	$VPD_{d2}<=0.6kPa$ & $VPD_{d1}>2\times VPD_{d2}$
3	0.2-0.4	$VPD_{d1}<=0.6kPa$ & $VPD_{d2}>2\times VPD_{d1}$
4	0.2-0.4	$VPD_{d2}<=0.6kPa$ & $VPD_{d1}>2\times VPD_{d2}$
5	0.4-0.8	$VPD_{d1}>0.6kPa$ & $VPD_{d2}>VPD_{d1}$
6	0.4-0.8	$VPD_{d2}>0.6kPa$ & $VPD_{d1}>VPD_{d2}$
7	0.2-0.4	$VPD_{d1}>0.6kPa$ & $VPD_{d2}>VPD_{d1}$
8	0.2-0.4	$VPD_{d2}>0.6kPa$ & $VPD_{d1}>VPD_{d2}$

Note: subscript d1 denotes Day 1, d2 denotes Day 2

The 8 scenarios are visualized in Figure 3-2 for the acacia tree. Tn is directly calculated with the baseline method under scenarios 1-4. Storage change is simulated with v-SPAC modelling (shown later). Days outside scenarios 1-8 are assumed as primarily storage refilling and not considered in Tn calculation.
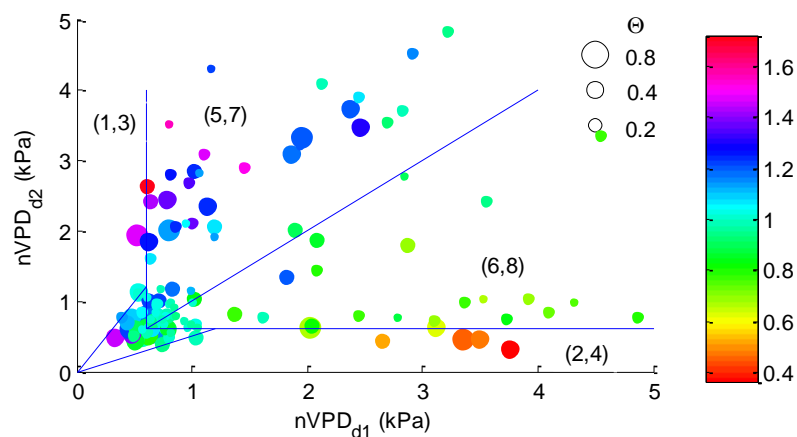
Figure 3-2: Different scenarios for data selection based on maximum night-time VPD of two consecutive days for the Phillips baseline method at the acacia site.

Note: the numbers in brackets are the scenario numbers. The colorbar shows the ratio of nSAP of Day 2 over that of Day 1; the size of circles shows the magnitude of soil moisture saturation (Θ); subscripts d1, d2 in x, y-axis denote Day 1 and Day 2.

The resulted Tn is used to evaluate its influencing factors, such as VPD and Θ. It is reported that the relation between Tn and VPD varies with seasons (Phillips et al., 2010) which we hypothesize is due to plant/soil water stress (Θ or ψ_x). Here, this hypothesis is tested with v-SPAC simulation if a universal scheme to calculate Tn can be derived based on VPD and Θ/ψ_x. With the baseline established from scenarios 1-4, we then examine Tn for days that do not fulfil the selecting criteria for the baseline method such as scenarios 5-8. For the Buckley baseline method, we also select the nights under 0.6 kPa for the time-constant evaluation. The averaged time-constant is used for simulating the baseline. The calculated Tn is at 15 min interval as observed

sap flux.

3.4.3 The v-SPAC model calibration

A 2 m soil column was set up in the v-SPAC model. Rainfall and potential evaporation were the upper flux boundary of the soil column. The lower boundary was prescribed as free drainage. The observed sap flux was used for the upper flux boundary in the tree stem. The water flux at the interface of plant-soil was calculated with root water uptake function (see Eq. 3-8). The tree hydraulic parameters (resistance and capacitance terms) were calibrated with optimization target of the observed stem water potential (ψ_x) using DREAM algorithm (Vrugt et al., 2008). Please refer to Chapter 2 for the details on model calibration.

3.5 Results

3.5.1 Calculating Tn with the baseline methods

A total of 65 pairs of days were selected from the acacia sap flow time series under the 8 scenarios for Tn calculation, in which 7 pairs were under the scenarios 1-4 when at least one night VPD did not exceed 0.6 kPa. For scenarios 1-4, Tn of the high VPD night ($VPD_{d2} > VPD_{d1}$) is calculated as $Tn_{d2} = nSAP_{d2} - nSAP_{d1}$, with an assumption of $\Delta S / \Delta t \approx 0$ over the two nights and $Tn_{d1} \approx 0$ (see the hollow symbols in Figure 3-3). The averaged nightly Tn rate (unit: cm/hr, normalized by sapwood area) follows a linear relation with averaged nightly VPD for scenarios 1-4.

For scenarios 5-8, Tn is calculated similarly by subtracting the sap flux of low VPD night (>0.6 kPa). However, both nights may have sap flux comprised of significant Tn proportion, using sap flow extraction may underestimate the true Tn of high VPD days (see Eq. 3-2). The calculated Tn for scenarios 5-8 thus should be used as the lower

boundary of possible Tn ranges.
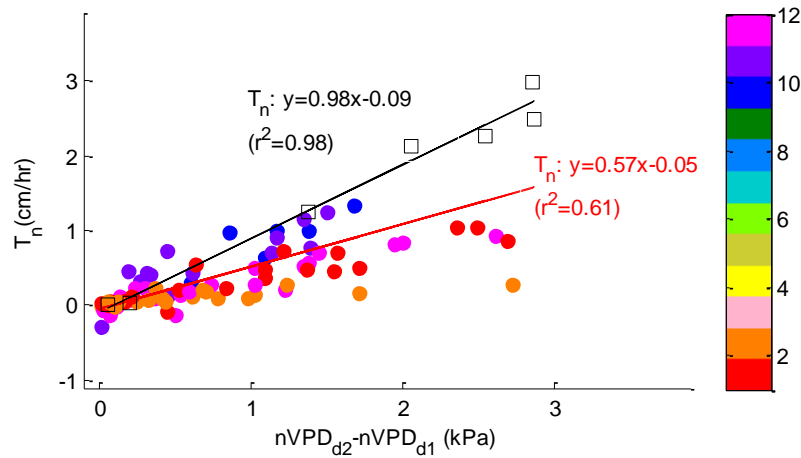
Figure 3-3: Relation between average nVPD and the calculated Tn for scenarios 1-4 (hollow squares) and for scenarios 5-8 (filled circles) based on the Phillips baseline method

Note: Tn is the average nocturnal transpiration rate normalized by the sapwood area. The colorbar indicates the month number. Subscripts d1, d2 denote DAY 1 and DAY 2.

Figure 3-3 indicates different sensitivities of Tn to nVPD between scenarios 1-4 (Eq. 3-10) and scenarios 5-8 (Eq. 3-11). The lower ratio of Tn over nVPD of summer months from Dec, 2012 to Feb, 2013 seem to reflect the increased soil water stress from Dec to Feb (most summer data fall into scenarios 7, 8 corresponding to Θ<0.4).

$$Tn_{d2}=0.98*(nVPD_{d2}-nVPD_{d1})-0.09 \qquad \text{(scenarios 1-4)} \qquad (3\text{-}10)$$

$$Tn_{d2}=0.57*(nVPD_{d2}-nVPD_{d1})-0.05 \qquad \text{(scenarios 5-8)} \qquad (3\text{-}11)$$

In which, Tn_{d2} denotes Tn of higher VPD night (nominal DAY 2).

The Buckley baseline method also relies on SAP analysis of the nights under very low VPD conditions. We selected the low VPD nights from scenarios 1-4 and used the averaged time-constant (τ) calculated for each night. Figure 3-4 shows an example of the calculation of τ which is estimated at around 2.4 hours (slope of ln(SAP) over time

(hours) is around -0.42).
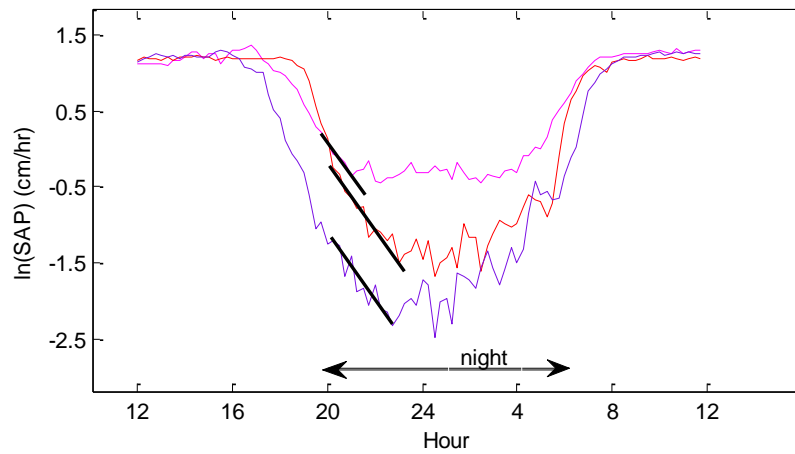
Figure 3-4: Time-constant (τ) calculated based on the Buckley baseline method for low VPD nights. Colour lines show three selected dates of 4 Nov (purple), 17 Nov (magenta), 17 Dec (red), 2012.

Without prior knowledge of relations between the resistance terms (ω), Buckley baseline method will not give a determined Tn, rather a range of Tn with varied ω from 0 to 1. It was suggested that ω =0.5 was reasonable for the tree species *Eucalyptus pauciflora* in Buckley et al., (2011) and ω is usually in the range of 0.04 to 0.5 (Phillips et al., 1997). Figure 3-5 shows the possible Tn results at ω =0.3, 0.5 and 0.8. The calculated Tn demonstrates the quick storage loss for early morning transpiration and storage refilling after sunset as observed in (Cermak, et al., 2007). It is noted that negative Tn occurs in Oct at ω =0.3 and 0.5. Negative Tn is believed not happening at the acacia site based on meteorological observation. Therefore, ω should be no less than 0.6 in Oct, 0.85 in Dec and 0.95 in Feb to avoid negative Tn. It suggests that the resistance of storage refilling accelerated faster compared to water flow resistance with increasing soil water stress from spring to summer.
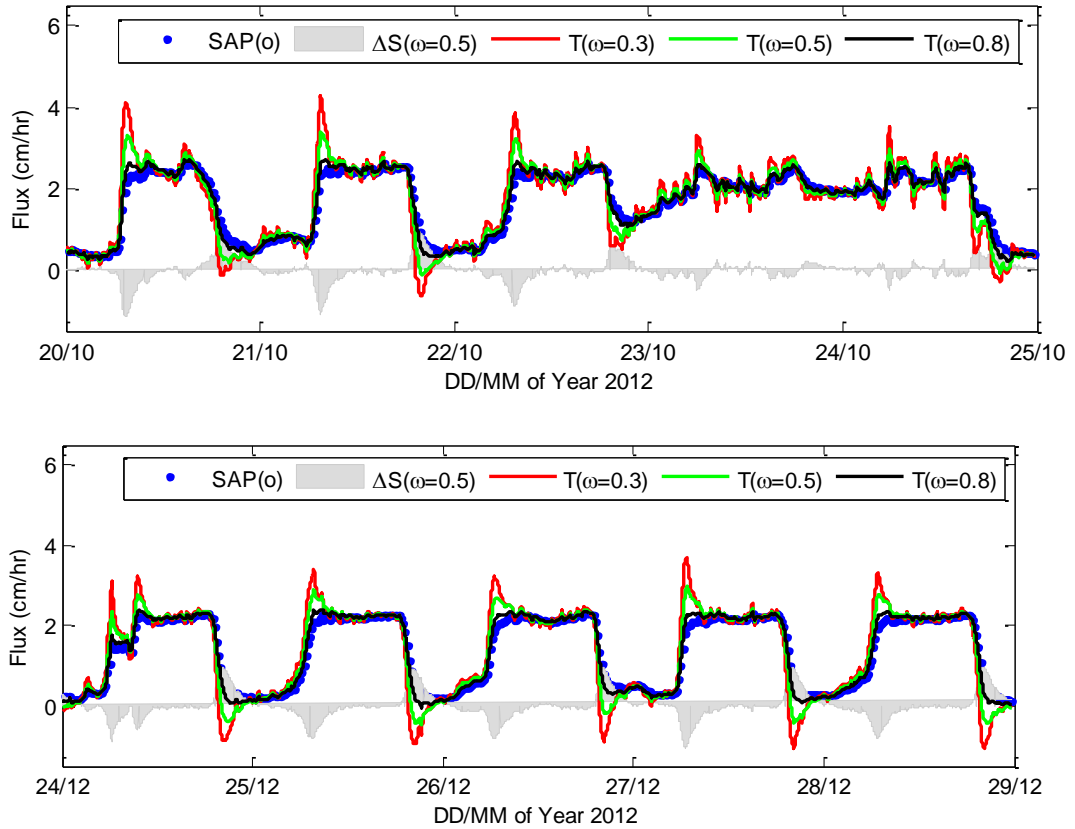
Figure 3-5: Tn calculated with the Buckley baseline method at τ =2.4 hr and ω=0.3, 0.5 or 0.8. The storage change (ΔS) of the crown is shown in shaded grey block.

Comparison of the estimated Tn between the Buckley baseline method and the Phillips baseline method for scenarios 1-4 nights (Figure 3-6) shows that the two methods are consistent with each other. Variation of ω does not result in apparent difference at high Tn rate for scenarios 1-4. At low Tn rate, the difference is marginal. Thus we take ω =0.5 as in Buckley et al. (2011).
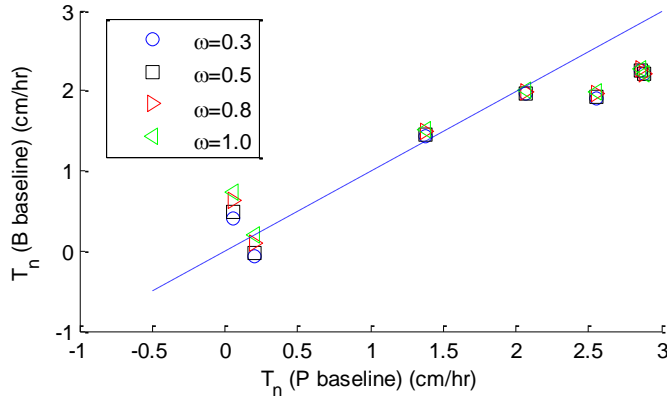
Figure 3-6: Comparison between Tn calculated with the Buckley baseline method Tn(B) and Tn with the Phillips baseline method Tn(P) under scenarios 1-4. The blue line is 1:1 line.

3.5.2 Uncertainty evaluation of the baseline method

The storage dynamics over nights will induce uncertainty to the Phillips baseline method. We derive ΔS time series from the calibrated v-SAPC model for the acacia tree (Chapter 2) in which, $\Delta S = \Delta S_3 + \Delta S_4$, representing the storage change in root and stem below the breast height. From Buckley baseline method, we can also get the ΔS time series which is the storage change of crown and stem above the breast height ($\Delta S = \Delta S_1 + \Delta S_2$). For scenarios 1-4, the night-time SAP is assumed to be storage refilling for the low VPD nights (nSAP=$\Delta S_1 + \Delta S_2$), which we used as night-time storage refilling. Figure 3-5 shows the relation between nVPD and the ΔS. The figure indicates that the Buckley baseline method may overestimate the storage refilling for low VPD nights. The v-SPAC simulated ΔS gives the same magnitude as that estimated from the Phillips baseline method for scenarios 1-4 with an assumption that the storage refilling are the same in the tree above or below the breast height ($\Delta S_1 + \Delta S_2 = \Delta S_3 + \Delta S_4$). Based on this, the v-SPAC simulated ΔS is then used as the benchmark ΔS time-series. The resulting function for ΔS is

$$\Delta S = -0.15 * nVPD + 0.76 \qquad \text{(all scenarios)} \qquad (3\text{-}12)$$

92

The ΔS dynamics $\Delta S/\Delta t$ is expressed over the difference of nVPD between the two nights as follows (see also Appendix I)

$$\Delta S/\Delta t = -0.25*(nVPD_{d2}-nVPD_{d1})+0.11 \qquad \text{(scenarios 1-4)} \qquad \text{(3-13)}$$
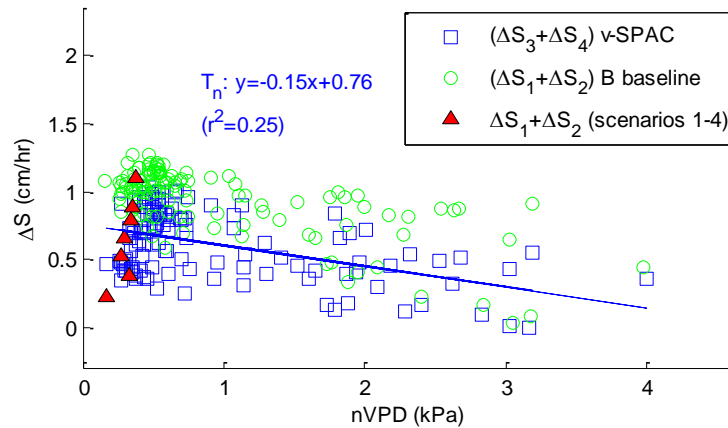
Figure 3-7: Relation between nVPD and ΔS ($\Delta S=\Delta S_3+\Delta S_4$) simulated with v-SPAC (squares), ΔS ($\Delta S= \Delta S_1+\Delta S_2$) simulated with Buckley baseline method (circles) and observed storage recharge (triangles, nSAP= $\Delta S_1+\Delta S_2$) of low VPD nights under scenarios 1-4 of the acacia tree.

It is found that the calculated Tn is correlated with the one night-time VPD as well ($r^2=0.97$, see Figure AI.2 in appendix I). Thus, Tn is expressed with one night VPD as follows:

$$Tn_{d2}=1.02*nVPD_{d2}-0.47 \qquad \text{(scenarios 1-4)} \qquad \text{(3-14)}$$

where $nVPD_{d2}$ is the night with higher VPD. From this equation, Tn will be around zero at $nVPD_{d2}=0.6$ kPa, which is consistent with the assumptions for the data selection for the baselines. The similarity of Eq. 3-10 and Eq. 3-14 indicates that Eq. 3-14 also applies on low VPD nights.

From section 2.1, we recall Eq 3-2 that $Tn_{d2} = (nSAP_{d2} - nSAP_{d1}) - \Delta S/\Delta t + Tn_{d1}$

in which $\Delta S/\Delta t = \Delta S_{d2} - \Delta S_{d1}$ is the storage change over the two nights. The Phillips baseline method give $Tn_{d2} = (nSAP_{d2} - nSAP_{d1})$ and $-\Delta S/\Delta t + Tn_{d1}$ is the error term. Suppose the two night-time VPD vary by 2.0 kPa, the Phillips baseline method would give $Tn_{d2} = 1.02*3 - 0.47 = 2.5$ cm/hr at $nVPD_{d2} = 3$ kPa; the error term would be at $[- (-0.25*2 + 0.11)] + [1.02*(3-2) - 0.47] = 0.9$ cm/hr using Eq. 3-13 and Eq. 3-14. The error is around 30% of the estimated Tn_{d2}. If Tn_{d1} is estimated similarly as Tn_{d2}, then the only uncertainty term is $-\Delta S/\Delta t$, which will induce around 15% underestimation at a night-time VPD difference of 2 kPa.

For scenarios 5-8, if we assume that Tn follows the same equation as that for scenarios 1-4, with the error terms corrected following Eq. 3-13 and Eq. 3-14, we reproduce the Tn time-series with

$$Tn_{d2} = (nSAP_{d2} - nSAP_{d1}) - [-0.25 \times (nVPD_{d2} - nVPD_{d1}) + 0.11] + (1.02 \times nVPD_{d1} - 0.47)$$

$$\text{(all scenarios)} \qquad \text{(3-14b)}$$

It shows that Tn calculated for scenarios 5-8 (see the red line in Figure 3-8) still does not converge to the same Tn function derived for scenarios 1-4 (see the black line) except for the spring months (Oct and Nov). It suggests that Tn is likely to be limited by soil moisture in summer months (see Figure 3-3 vs Figure 3-8), which cannot be accounted by the error terms.
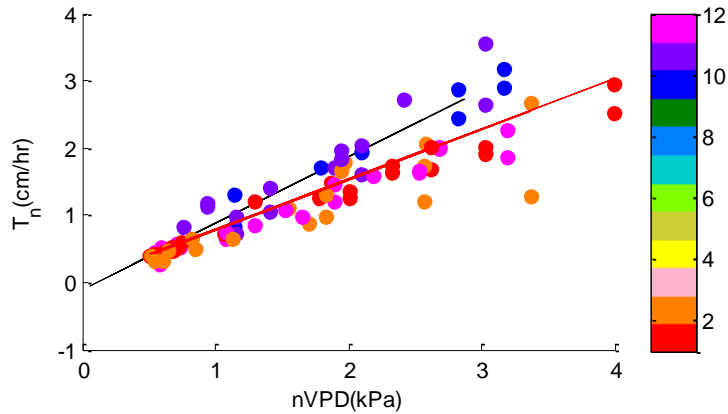
Figure 3-8: Tn calculated for scenarios 5-8 (solid circles) of the acacia tree with the Tn function (black line) derived for scenarios 1-4 and ΔS simulated with v-SPAC modelling (see Figure 3-4).

3.5.3 Environmental factors controlling Tn

To examine if the water stress accounts for the reduced Tn sensitivity to VPD in summer than in spring, the soil water stress indicated by soil moisture saturation (Θ) and plant water stress by pre-dawn stem water potential (ψ_{pd}) are used to reanalyse the sap flow time-series. Tn calculated for scenarios 1-4 is used as benchmark, Tn for scenarios 5-8 are calculated with the error terms corrected (similar to Figure 3-8) but plotted over the space of $nVPD \times \sqrt{\Theta}$ or $nVPD \times \psi_{pd,n}$. The resulted Tn converges to a universal function across the seasons (including all scenarios) (see Figure 3-9). $\psi_{pd,n}$ is normalized ψ_{pd} value linearly scaled between 0 to 1, corresponding to ψ_{pd} at -2.3 and 0 MPa respectively. ψ_{pd} was gap filled between Oct, 2012 to Feb, 2013 with the v-SPAC modelling outputs. Θ is weighted over three soil moisture contents at 10, 30 and 50 cm by [0.2, 0.3, 0.5]. The weight is based on the soil layering at the acacia site.
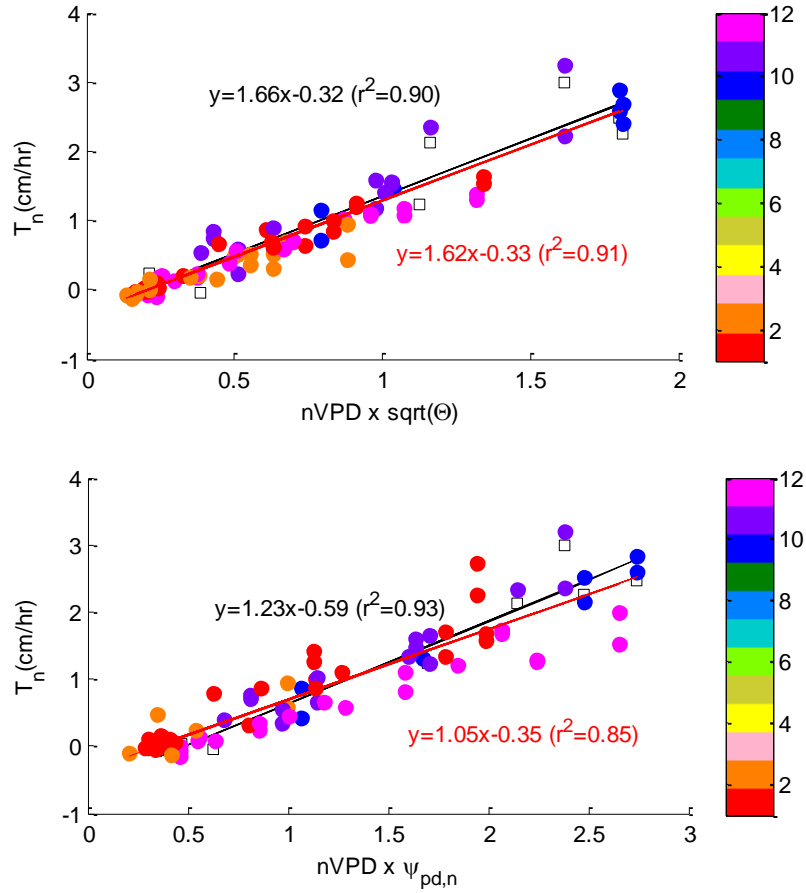
Figure 3-9: Convergence of Tn functions for all scenarios over $nVPD \times \sqrt{\Theta}$ (upper panel) and $nVPD \times \psi_{pd,n}$ (lower panel) of the acacia tree.

Note: the black line is fitted over hollow squares, representing scenarios 1-4; the red line is fitted over filled circles representing any days with VPD>0.6kPa. $\psi_{pd,n}$ is the normalized ψ_{pd} between 0 to 1, corresponding to -2.3 MPa and 0 MPa respectively.

The universal Tn functions based on VPD and soil/plant water stress are:

$$Tn = 1.62 \times [nVPD \times \sqrt{\Theta}] - 0.33 \qquad \text{(all scenarios)} \qquad (3\text{-}15)$$

$$Tn = 1.05 \times [nVPD \times \psi_{pd,n}] - 0.35 \qquad \text{(all scenarios)} \qquad (3\text{-}16)$$

where $\psi_{pd,n}$ and Θ are in the range of [0, 1], nVPD is the averaged night-time VPD in unit of kPa; Tn is the averaged nocturnal transpiration normalized over the sapwood cross section, in unit of cm/hr. The two Tn functions indicate the dominance of VPD and soil/plant water stress over Tn. The two factors VPD and Θ/ $\psi_{pd,n}$ combined,

96

explain around 90% variation of Tn for the *Acacia pycnantha* tree. The figure suggests that soil moisture explains the different sensitivities of Tn to VPD across the seasons.

3.5.4   Comparing the baseline methods with the v-SPAC modelling

If the calibrated results of v-SPAC model (calibration over stem water potential and sap flow data) in Chapter 2 is adopted with an assumption that the storage change of the tree are the same in crown and root ($\Delta S_3 + \Delta S_4 = \Delta S_1 + \Delta S_2$), Tn can then be estimated from Tn= $SAP_2 - (\Delta S_3 + \Delta S_4)$, in which $\Delta S_3 + \Delta S_4$ is simulated with the v-SPAC model. Figure 3-10 shows the comparison results between the Buckley baseline method and that from the v-SPAC modelling. The result shows consistency between the two methods, which may be due to that both methods are based on the Resistance-Capacitance model concept (see Figure 3-10). The difference relies on the different assumptions behind; in the Buckley baseline method, the storage and transport resistances are assumed to follow a fixed ratio (constant ω), while, in the v-SPAC model, the storage contribution of the tree are assumed the same above and below the sap flow meter installation point.
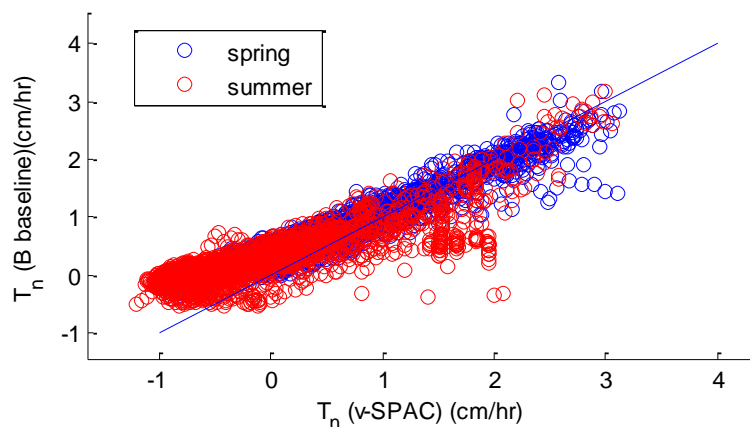
Figure 3-10: Comparison of Tn between the Buckley baseline method (y-axis) and the v-SPAC model (x-axis). The blue line is 1:1 line. Tn is at 15 min interval.

To evaluate the robustness of all methods in estimating Tn, we assign the upper boundary of Tn as the nSAP (no storage refilling, see the black dash line in Figure 3-11) and the lower boundary as Tn simulated for scenarios 5-8 with the Phillips baseline method ($Tn_{d2}=nSAP_{d2}-nSAP_{d1}$, see the black dots) without correction of the error terms. Figure 3-11 shows that nightly Tn calculated with the Phillips baseline method using VPD and Θ as dependence (red triangles) are mostly within the upper and lower boundaries. Tn calculated with the Buckley baseline method (blue circles) shows slight underestimation of Tn and follows perfect linear correlation with nSAP (r^2=0.998). It is due to the assumption that the storage recharge occurs primarily in early night (see Figure 3-5). The v-SPAC modelling seems to underestimate Tn for low nSAP rate, which corresponds to the summer time. It suggests that the assumption of the storage refilling being the same in root as in the crown may not be valid in summer. The storage in crown is likely to be much smaller than in root.
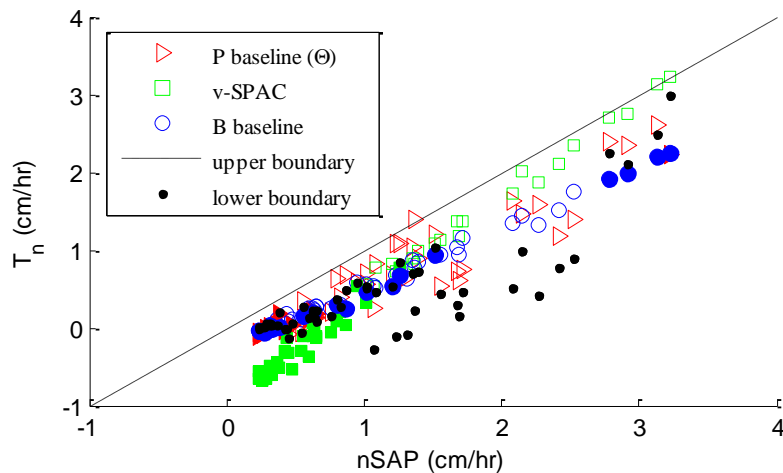
Figure 3-11: Comparison of nightly Tn among the Phillips baseline method with VPD and Θ as dependence (red triangles, see Figure 3-9), the Buckley baseline method (blue circles) and the v-SPAC modelling (green squares).

Note: the dash black line shows the upper boundary of Tn (Tn=nSAP), the black dots are the lower boundary calculated with $Tn_{d2}=nSAP_{d2}-nSAP_{d1}$. All filled symbols represents the estimated Tn exceeding the lower boundary.

3.6 Discussion

The Phillips baseline methods (Phillips et al., 2010) is very simple in calculating nightly Tn, but may underestimate Tn for 15-30%; while, the Buckley baseline method (Buckley et al., 2011) can simulate sub-daily Tn under all conditions with assumptions of a certain range of storage versus water flow resistance. The storage resistance may not be stationary over seasons but varied storage resistance only result in slight discrepancy in Tn estimation, which is consistent with the statement in Buckley et al., (2011). The v-SPAC with observed sap flow as flux boundary can eliminate the uncertainty of the upper flux boundary, but may overestimate storage recharge of crown in summer time under assumption of the same storage dynamics in crown and root. Calibrating the v-SPAC model with observed Tn or with those inferred from the Phillips baseline method for scenarios 1-4 may be useful to cross out the uncertainty from the assumption. However, the selected dates for scenarios 1-4 occurred in wet conditions, such that the model is not well constrained under dry conditions, resulting also large uncertainty in the model calibration for summer time (data not shown). Despite the differences in Tn calculation, the three methods show similar results (the Phillips baseline method are corrected with storage dynamics and soil water stress), estimating Tn of 80% to 100% of night-time sap flow rate. Combining the methods give more confidence in interpreting the Tn results. The Tn function based on VPD and Θ (Eq. 3-15 & Eq. 3-16) seems to give reasonable estimation of Tn which falls in the upper and lower boundaries and approximates the results of the Buckley baseline method. The function reveals the quantitative relation between the controlling factors (VPD, Θ) and Tn.

VPD and Θ, all together explain around 90% of the Tn variation (see Figure 3-9).

These results are in accordance with previous studies showing that Tn is sensitive to VPD and soil moisture (Dawson et al., 2007; Zeppel et al., 2013). The soil/plant water stress indeed accounts for the seasonable variation of Tn to VPD. In addition, it indicates that the night-time canopy conductance (g_c) remained constant with VPD within one month ($\mathrm{Tn} \propto g_c \times D$, D is bulk air VPD to replace leaf to air VPD under low aerodynamic resistance, g_c is constant within one month, see Figure 3-8). When Θ is considered, the slope of each month converges (see Figure 3-8 vs Figure 3-9, larger slope corresponds to larger g_c). It suggests a lack of response of night-time g_c to VPD, which is different from day-time g_c. The night-time g_c seems to be only sensitive to water stress. Such phenomena was mostly reported for those dry sclerophyllous forest (Rosado et al., 2012). However, non-linear relation between Tn and VPD (g_c responses to VPD) also exists in eucalyptus (Phillips et al., 2010) and montane forests (Rosado et al., 2012). The different Tn vs VPD behaviours may be site-specific or tree-specific. This study shows that the soil/plant water stress may have complicated the relation between Tn and VPD (see Figure 3-8 vs Figure 3-9). Combined analysis of environmental factors on Tn behaviours is thus suggested.

3.7 Conclusions

In this study, the nocturnal transpiration of an *Acacia pycnantha* tree was calculated with the baseline methods and the v-SPAC modelling. The results show that the nocturnal transpiration (Tn) accounts for 80 % -100% of the night-time sap flux, given by different calculation methods. The Phillips baseline method is useful to constrain the lower boundary in estimating Tn. Diagnosed with the v-SPAC modelling, the Phillips baseline method may underestimate Tn for 15-30 % for the studied acacia tree. The Buckley baseline method calculates Tn at a fixed ratio to night-time sap flow rate if using the same storage resistance for the whole period. The v-SPAC modelling

method underestimates Tn at low night-time sap flow rate, while calculates the largest Tn than the two baseline methods at high sap flow rate. Direct validation such as using controlled lysimeter experiment will be of great value to examine the robustness of the different methods.

The nocturnal transpiration (Tn) is driven by atmospheric vapour pressure deficit (VPD) and reduced with increased soil water stress (Θ). Tn showed strong linear relation with VPD in each month. The Tn vs VPD relation converges to one universal function when Θ is accounted. The two factors VPD and Θ combined explain 90% of the variation of Tn over the experimental period of Oct 2012 to Feb 2013. The results indicate that the night-time canopy conductance of *Acacia pycnantha* lacks response to VPD, but is sensitive to water stress. It suggests that the demand of integrated analysis of the environmental drivers (such as VPD, Θ) on Tn behaviours. Developing comprehensive quantitative tools accounting for both environmental and tree-specific characteristics will help us to clarify or enhance our understanding on the diverse behaviours of the nocturnal transpiration.

References

Buckley, T.N., Mott, K.A., Farquhar, G.D., 2003. A hydromechanical and biochemical model of stomatal conductance. Plant Cell and Environment, 26(10): 1767-1785.

Buckley, T.N., Turnbull, T.L., Adams, M.A., 2012. Simple models for stomatal conductance derived from a process model: cross-validation against sap flux data. Plant Cell and Environment, 35(9): 1647-1662.

Buckley, T., Turnbull, T., Pfautsch, S., Adams, M. 2011. Nocturnal water loss in mature subalpine Eucalyptus delegatensis tall open forests and adjacent E. pauciflora woodlands. Ecology and Evolution, 1(3), 435-450

Burgess, S. S., Adams, M. A., Turner, N. C., Beverly, C. R., Ong, C. K., Khan, A. A., & Bleby, T. M. 2001. An improved heat pulse method to measure low and reverse rates of sap flow in woody plants. Tree Physiology, 21(9), 589-598.

Caird, M. A., Richards, J. H., and Donovan, L. A. 2007. Nighttime stomatal conductance and transpiration in C3 and C4 plants. Plant Physiology, 143(1), 4-10.

Caylor, K. K., & Dragoni, D. 2009. Decoupling structural and environmental determinants of sap velocity: Part I. Methodological development. agricultural and forest meteorology, 149(3), 559-569.

Cermak, J., Kucera, J., Bauerle, W.L., Phillips, N., Hinckley, T.M., 2007. Tree water storage and its diurnal dynamics related to sap flow and changes in stem volume in old-growth Douglas-fir trees. Tree Physiology, 27(2): 181-198.

Cermak, J., and Nadezhdina, N. 1998. Sapwood as the scaling parameter-defining according to xylem water content or radial pattern of sap flow?. InAnnales des Sciences forestieres (Vol. 55, No. 5, pp. 509-521). EDP Sciences.

Chuang, Y.L., Oren, R., Bertozzi, A.L., Phillips, N., Katul, G.G., 2006. The porous media model for the hydraulic system of a conifer tree: Linking sap flux data to transpiration rate. Ecological Modelling, 191(3-4): 447-468.

Daley, M. J., & Phillips, N. G. 2006. Interspecific variation in nighttime transpiration and stomatal conductance in a mixed New England deciduous forest. Tree Physiology, 26(4), 411-419.

Dawson, T. E., Burgess, S. S., Tu, K. P., Oliveira, R. S., Santiago, L. S., Fisher, J. B., and Ambrose, A. R. 2007. Nighttime transpiration in woody plants from contrasting ecosystems. Tree Physiology, 27(4), 561-575.

Donovan, L.A., Linton, M.J., Richards, J.H., 2001. Predawn plant water potential does not necessarily equilibrate with soil water potential under well-watered conditions. Oecologia, 129(3): 328-335.

Donovan, L. A., Sperry, J. 2000. Scaling the soil–plant–atmosphere continuum: from physics to ecosystems. Trends in plant science, 5(12), 510-512.

Fisher, J. B., Baldocchi, D. D., Misson, L., Dawson, T. E., & Goldstein, A. H. 2007. What the towers don't see at night: nocturnal sap flow in trees and shrubs at two AmeriFlux sites in California. Tree Physiology, 27(4), 597-610.

Forster, M. A. 2014. How significant is nocturnal sap flow?. Tree physiology, 34(7), 757-765.

Janott, M. et al., 2011. A one-dimensional model of water flow in soil-plant systems based on plant architecture. Plant and Soil, 341(1-2): 233-256.

Kumagai, T. 2001, Modeling water transportation and storage in sapwood - model development and validation, Agricultural and Forest Meteorology, 109(2), 105-115.

Micco, V.D., Aronne, G., 2012. Morpho-Anatomical Traits for Plant Adaptation to Drought Plant Responses to Drought Stress. Springer Berlin Heidelberg.

Phillips, N., Nagchaudhuri, A., Oren, R., & Katul, G. 1997. Time constant for water transport in loblolly pine trees estimated from time series of evaporative demand and stem sapflow. Trees, 11(7), 412-419.

Phillips, N. G., Lewis, J. D., Logan, B. A., & Tissue, D. T. 2010. Inter-and intra-specific variation in nocturnal water transport in Eucalyptus. Tree physiology, 30(5), 586-596.

Phillips, N., Oren, R., & Zimmermann, R. 1996. Radial patterns of xylem sap flow in non-, diffuse-and ring-porous tree species. Plant, Cell & Environment,19(8), 983-990.

Rosado, B. H. P., Oliveira, R. S., Joly C. A., Aidar M. P. M., and Burgess S. S. O., 2012. Diversity in nighttime transpiration behavior of woody species of the Atlantic Rain Forest, Brazil, Agricultural and Forest Meteorology, 158, 13-20.

Scholz, F. G., Phillips, N. G., Bucci, S. J., Meinzer, F. C., & Goldstein, G. 2011. Hydraulic capacitance: biophysics and functional significance of internal water sources in relation to tree size. In Size-and age-related changes in tree structure and function (pp. 341-361). Springer Netherlands.

Zeppel, M., Logan, B., Lewis, J. D., Phillips, N., & Tissue, D. 2013, June. Why lose water at night? Disentangling the mystery of nocturnal sap flow, transpiration and stomatal conductance-when, where, who?. In IX International Workshop on Sap Flow 991 (pp. 307-312).

Zeppel, M., Tissue, D., Taylor, D., Macinnis-Ng, C., & Eamus, D. 2010. Rates of nocturnal transpiration in two evergreen temperate woodland species with differing water-use strategies. Tree Physiology, 30(8), 988-1000.

Appendices

Appendix I: Nocturnal transpiration (Tn) estimation with the Phillips baseline method for acacia tree

For scenarios 1-4, the estimated Tn with the Phillips baseline method are shown in Figure AI.1. The storage dynamics ($\Delta S/\Delta t$) are estimated with v-SPAC modelling (see Chapter 2) under assumption of the same storage change in root and crown.

$$Tn_{d2}=0.98*(nVPD_{d2}-nVPD_{d1})-0.09 \qquad \text{(scenarios 1-4)} \qquad (A.1)$$

$$\Delta S/\Delta t =-0.25*(nVPD_{d2}-nVPD_{d1})+0.11 \qquad \text{(scenarios 1-4)} \qquad (A.2)$$
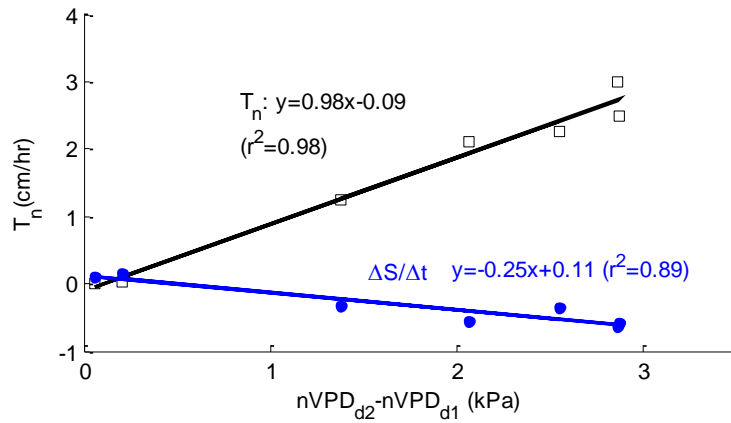
Figure AI.1: Relation between average nVPD and the calculated Tn (hollow squares) based on the Phillips baseline method and storage change ($\Delta S/\Delta t$, ($\Delta S=\Delta S_3+\Delta S_4$) filled circles) simulated with v-SPAC under scenarios 1-4 of the acacia tree.

Note: Tn is the average nocturnal transpiration rate normalized by the sapwood area.

Tn and $\Delta S/\Delta t$ can be also expressed with one nVPD as follows (see also Figure AI.2):

$$Tn_{d2}=1.02*nVPD_{d2}-0.47 \qquad \text{(scenarios 1-4)} \qquad (A.3)$$

$$\Delta S/\Delta t =0.27*nVPD_{d2}+0.22 \qquad \text{(scenarios 1-4)} \qquad (A.4)$$
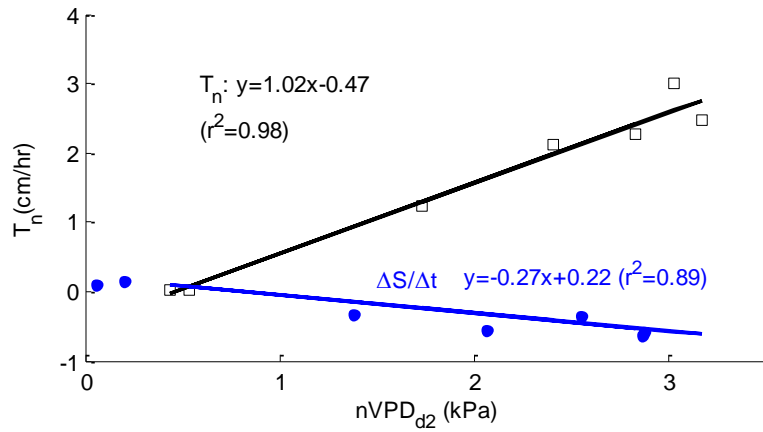
Figure AI.2 Relation between average nVPD of Day 2 and the calculated Tn (hollow squares) based on the Phillips baseline method and storage change ($\Delta S/\Delta t$, filled circles) simulated with v-SPAC under scenarios 1-4 of the acacia tree.

Note: Tn is the average nocturnal transpiration rate normalized by the sapwood area.

4 AN INNOVATIVE METHOD TO OBTAIN IN-SITU ROOT ZONE SOIL WATER-RETENTION CURVES FROM SOIL-STEM HYDRAULIC CONTINUUM MEASUREMENTS

Abstract

Soil water retention curves (WRC) are required for unsaturated hydrologic modelling. It is traditionally obtained from direct soil-core measurements, pedo-transfer functions (PTFs) based on soil texture, or from inverse modelling. Here, we propose a new method to obtain root zone WRC directly from concurrent plant and soil water content measurements (referred to **RWRC method**). In the method, xylem water potential (ψ_x) is used as a substitute for soil water potential (ψ_s) under the assumption of soil/plant hydraulic equilibrium. For disequilibrium condition, a so called equivalent water potential ($\psi_{s,v}$) is proposed for WRC establishment by inferring from extra sap flow measurement. We test the method with the v-SPAC modelling experiments on synthetic soil columns of different soil/plant hydraulic properties. Two study sites provide us a great opportunity to test the method in field conditions with contrast soil texture, plant hydraulic properties and climate. The modelling results show that the RWRC method is capable to predict WRC within uncertainty of ± 0.05 in moisture content (θ), or within 50% deviation of water potential on clayey and silty soils. The method can be used with high confidence when the data pairs (ψ_x, θ) are carefully selected. The field case studies show that the proposed method can give comparable WRC with those obtained from the PTF method or from direct measurement. By lumping the soil moisture at all depths (θ_{wt}), the data pairs (ψ_x, θ_{wt}) improve the performance of the RWRC method. The method provides a potential upscaling scheme for effective hydraulic properties estimation for land surface modelling.

4.1 Introduction

Water retention curve (WRC) describes the relationship between soil water content and soil water potential, which is a premise to simulate the soil water dynamics in vadose zone hydrology (Vereecken et al., 2010). The traditional measurement methods are usually labour-intense and may not be readily usable for modelling purposes. For example, the hydraulic test of soil cores is a direct method to obtain WRC, but the method is very time-consuming. It is common that the small soil columns or soil samples in lab conditions fail to represent field conditions, due to heterogeneity of the soil texture and the boundary conditions of the site, or the preferential flow paths in the field being disturbed in the lab samples (Scharnagl et al., 2011). Pedo-transfer functions (PTFs) is an alternative to bridge the gap between hydraulic characteristics to those more easily measurable soil properties such as soil texture (Vereecken et al., 2010; Wosten et al., 2001). From PTFs, WRC and the relative hydraulic property can be modelled based on existing database such as those of Rawls et al. (1982), UNSODA soil database (Leij et al., 1996) and Australian soil database (Minasny et al., 1999). However, using different soil database can result in great discrepancy in WRC description, so does with different PTF methods (Minasny et al., 1999; Vereecken et al., 2010). In-situ WRC are assumed to capture water dynamics more realistically, which can be obtained from inverse modelling (Scharnagl et al., 2011; Zhang et al., 2003). Inverse modelling, however, requires information more than soil water states and the model should be soundly described including the boundary conditions (Vrugt et al., 2008). Inverse modelling is more easily defined for simple cases, such as bare soil evaporation or drainage experiments (Zhang et al., 2003). The presence of vegetation will induce larger uncertainty into the modelling with involvement of root zone processes (Shin et al., 2012). It is therefore valuable to develop an in-situ method

to obtain representative WRC of the whole root zone for vegetated landscape. WRC of the whole root zone is not only useful for root zone hydraulic modelling, but also required for large scale land surface modelling.

In this study, we propose a method to obtain root-zone WRC from plant water status and concurrent soil water state measurements. Pre-dawn stem water potential (or leaf water potential) is commonly used as an indicator of plant water status (Jones, 2004). Stem water potential can be approximated as soil water potential if hydraulic equilibrium between the soil and plant has reached, indicated by zero sap flow rate (Zeppel et al., 2010). However, recent studies show that pre-dawn stem water potential is not necessarily in equilibrium with soil water potential largely due to night-time transpiration (Donovan et al., 2001; Donovan et al., 2003). Bucci et al., (2004) reported that leaf water potential of exposed leaves extrapolated to zero sap flow rate will give comparable values to those of covered leaves of which, the night-time transpiration is minimized. This suggests that it is possible to approach the soil water potential by extrapolating the pre-dawn stem xylem water potential to zero sap flow rate with additional sap flow measurements. We refer to the extrapolated water potential as the "equivalent soil water potential" ($\psi_{s,v}$).

Therefore, plant stems function as observation 'wells' to keep track of the root zone water potential. Combined with concurrent root-zone soil water content measurements, root-zone WRC can be established. This root-zone based WRC has a spatial scale equivalent to the whole root zone (metres), much larger than those by conventional methods based on soil core samples or in situ soil moisture or water potential sensors (centimetres). For land surface modelling, larger areal and deeper soil water status revealed by these plant stems, offer a particularly important supplement to the remote

sensing products which can only detect near surface soil hydraulic properties (within 10 cm) (Mohanty and Skaggs, 2001; Shin et al., 2012; Walker et al., 2001). Therefore, the proposed method provides not only an alternation for WRC establishment but also a potential upscaling scheme for land surface modelling.

The root-zone based WRC method (refer to RWRC method) is firstly tested qualitatively across different types of soil/plant hydraulic properties and environment settings through synthetic numerical simulations with the v-SPAC model. The simulation will be prescribed both zero and high night-time flux boundary to test the hypothesis that the night-time transpiration is the major reason for soil-stem disequilibrium. Another important aim of the synthetic tests is to identify precisely the relation between the xylem water potential (ψ_x) and the soil water potential (ψ_s). Does the ψ_x indicate the average wetness of the whole root zone, or does it couple with ψ_s of the wettest root zone or the soil layer that contributes the most of water? With these answers clear, then we can interpret and apply ψ_x with reasonable confidence. The method is then examined over two study sites. One site is on an *Acacia pycnantha* tree, of which an apparent disequilibrium between soil and plant is indicated by its high night-time sap flow rates. The other site is on *Eucalyptus crenulata* saplings, which give flat zero sap flow at midnight to predawn. The two study sites differ in plant hydraulic properties, soil texture and climate, providing two contrast cases to test the RWRC method with other techniques for WRC derivation. Finally, the uncertainty of the RWRC method is estimated by quantitative analysis. The favourable conditions for the application of the method will be summarized and discussed within the context of other available WRC methods.

4.2 Methodology

The RWRC method, to estimate root zone WRC with plant stem water potential is readily applicable under the assumption that the soil/plant has reached hydraulic equilibrium. We first test this favourable condition by doing synthetic modelling experiments in which both soil/plant water flux and water status are simulated. The model is prescribed zero flux boundary at night. Different combinations of soil types, plant hydraulic properties, and vapour pressure deficit (in atmospheric demand) are simulated using the v-SPAC model. As mentioned earlier, the RWRC method is challenged largely by non-zero night-time transpiration conditions. To reproduce such scenarios, the simulation is prescribed a high night-time flux boundary to induce non-equilibrium states. The equivalent soil water potential ($\psi_{s,v}$) is then calculated by the ψ_x time-series with v-SPAC simulation and tested by comparing to the corresponding ψ_s (the week in preceding). This group of tests is to check the closeness of inferred $\psi_{s,v}$ to soil water potential under the non-equilibrium cases. Finally, real cases are analysed to test the applicability of the RWRC method in field conditions. The method is compared to traditional techniques such as direct measurement of soil water content and soil water potential or from pedo-transfer functions based on soil texture measurements. The purpose of this section is to show if the RWRC method can serve as an alternation to those traditional ones.

4.2.1 The equivalent soil water potential ($\psi_{s,v}$) calculation

As mentioned previously, water retention curve (WRC) is not directly obtained from ψ_x-θ points if there is night-time transpiration. The equivalent soil water potential $\psi_{s,v}$ represents the xylem water potential at non transpiration state, thus needs to be inferred from the observed SAP- ψ_x curve (see the SS plot in Chapter 2). Figure 4-1 and Figure 4-2 shows two ways to obtain $\psi_{s,v}$. For the *Acacia pycnantha* tree, the averaged SAP

and ψ_x between 3 and 6 am are used to calculate $\psi_{s,v}$. A pair of (SAP, ψ_x) of one day determines a point in the plot (Figure 4-1). The slope is obtained by plotting data points within a week without rainfall, during which soil water potential are assumed stationary. For the *Eucalyptus crenulata* saplings, the curve is obtained from concurrent SAP and ψ_x measurement from 7 pm to 7 am the next day. For most of the days, the data points within a day follow a line (see the points with the same colour in Figure 4-2). The soil water potential (in diamond symbol) is calculated from corresponding soil water content (at 5 and 15 cm) with WRC from an independent experiment (see Appendix I). The figure clearly demonstrates that ψ_x at zero sap flow rate agrees with those inferred ψ_s. It suggests that ψ_x has nearly reached equilibrium with ψ_s when the night-time sap flow rate approaches zero (see the arrow in the middle figure pointing the reduction of SAP rate from 7 pm to 7 am the next day). The intercept of the fitted line is the so called equivalent soil water potential $\psi_{s,v}$. The former way (for the acacia tree) is suitable for cases when pre-dawn leaf water potential is observed for consecutive days on maybe clayey soils. The latter one works for cases in which bulk soil ψ_s changes quickly, such as sandy soils. The equivalent soil water potential is introduced for application under non-equilibrium hydraulic states which will be artificially generated with synthetic modelling experiments (described in the next section).
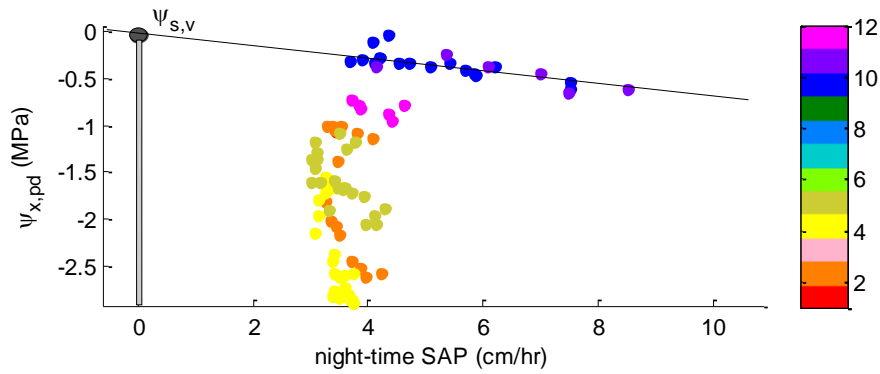
Figure 4-1: Predawn stem xylem water potential ($\psi_{x,pd}$, averaged value between 3-6 am) vs. the night-time sap flow rate (SAP) of *Acacia pycnantha.*
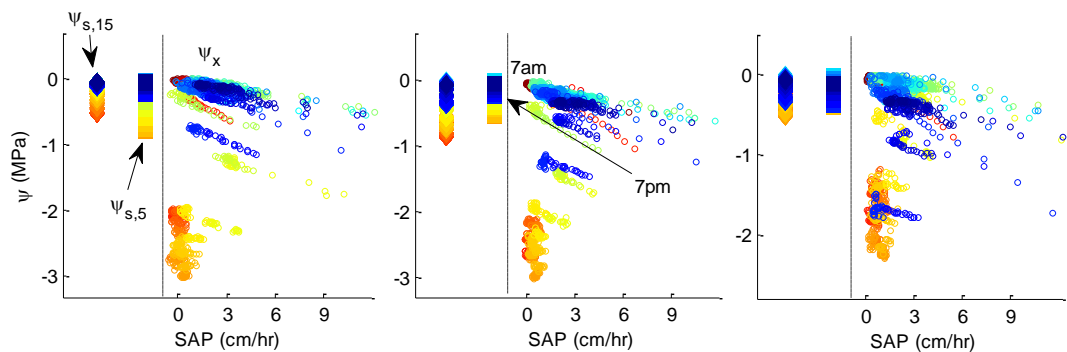
Figure 4-2: Concurrent night-time sap flow rate (SAP) vs. stem xylem water potential (ψ) three *Eucalyptus crenulata* saplings (sapling 2, 4, 6) from 7 pm to 7 am the next day.

Note: data within a week are ploted in one colour. The points of each day appear in a line of the same color; ψ_x is shown in circles, inferred ψ_s from soil moisture with measured WRC is shown in squares ($\psi_{s,5}$ denotes soil water potential at 5cm) and diamond ($\psi_{s,15}$ at 15cm) to the left of the dash line; The warm colour days are under water withheld conditions.

4.2.2 Synthetic soil/plant experiments

Soil profile and WRC

The proposal RWRC method is firstly examined by synthetic numerical experiment with the v-SPAC model. A soil column of 200 cm with uniform soil texture and hydraulic properties is prescribed for the v-SPAC simulation. Parameters of the water retention curves and the hydraulic conductivities of the soil types are derived from pedo-transfer function code ROSETTA (Schaap et al., 2001) based on the UNSODA soil database (Leij et al., 1996). The WRC parameters are described in van Genuchten

(1980) function (see Table 4-1).

Table 4-1: Water retention curve parameters in van Genuchten function for soil types from the UNSODA database with ROSETTA simulation.

Soil type	θ_r	θ_s	α (1/kPa)	N	K_s (mm/d)
1 Clay (C)	0.1	0.46	0.15	1.25	150
2 Clay loam (CL)	0.08	0.44	0.16	1.41	80
3 Loam (L)	0.06	0.4	0.11	1.47	120
4 Loamy sand (LSD)	0.05	0.39	0.35	1.75	1050
5 Sand (SD)	0.05	0.37	0.35	2.0	6430
6 Sandy clay (SDC)	0.12	0.39	0.33	1.21	110
7 Sandy clay loam (SDCL)	0.06	0.38	0.21	1.33	130
8 Sandy loam (SDL)	0.04	0.39	0.27	1.45	380
9 Silt (ST)	0.05	0.49	0.07	1.68	440
10 Silty clay (STC)	0.11	0.48	0.16	1.32	100
11 Silty clay loam (STCL)	0.09	0.48	0.08	1.52	110
12 Silty loam (STL)	0.06	0.44	0.05	1.66	180

Plant hydraulic properties: the vulnerability curve

We choose plant vulnerability curves **(VC)** of two tree species from Sperry et al. (1998): *Betula occidentalis* (Bo) and *Acer negundo* (An) and the two species in our study sites: *Eucalyptus crenulata* (Ec) and *Acacia pycnantha* (*Ap*). The VCs of the four species represent a wide range of water sensitivities: water stress sensitive riparian trees (Bo and Ec) to less sensitive trees (An) (Sperry et al., 1998) and drought tolerant trees (Ap) (Chapter 2) (see Table 4-2). The vulnerability curves, in the form of hydraulic conductivity loss (1- k_p/k_s)*100%, is shown in Figure 4-3. The saturated xylem hydraulic conductivity (k_s) in Sperry et al. (1998) is the reciprocal of minimum plant hydraulic resistance (R_{min}) in this study. For v-SPAC modelling, all resistances are based on the land surface domain area, which is unknown for the Bo and An trees. We then prescribe the same R_{min} (normalized over the land surface domain area) for

Bo as Ec to represent the riparian trees and the same R_{min} for An as Ap to represent the drought tolerant trees. We preserve the shape parameters (*d, b*) of root VCs for Bo and Ec from Sperry et al. (1998) since we know that the root resistance is the dominant resistance and R_{min} is the most sensitive parameter. The R_{min} of Ec and Ap are taken from the calibration results from Chapter 2.

Table 4-2: Plant hydraulic properties prescribed in the modelling setting

Tree species	Native habitat	Vulnerability curve $k_{\mathrm{p}} = k_{\mathrm{s}} \cdot e^{-(-\psi_x/\mathrm{d})^b}$ *
Acacia pycnantha (Ap)	Mediterranean, South Australia	k_s=0.9 mmol·s^{-1}·MPa^{-1}, d=1.33 MPa, b=1.3, R_{min}=9000 d·mm^1·mm^{-1},
Eucalyptus crenulata (Ec)	Riparian alluvium, New South Wales	k_s =7.6±2.5 mmol·s^{-1}·MPa^{-1}, d=1.0 MPa, b=0.74, R_{min}=2208 d·mm^1·mm^{-1}
Betula occidentalis (Bo)	Riparian, Western US	**k_s =2.18±0.76 mmol·s^{-1}·MPa^{-1}, d=0.7 MPa, b=1.5,**
Acer negundo (An)	/	**d=1.41 MPa, b=1.78**

Note: * shows the original vulnerability curve form and the parameter values (**in bold font**) of the root vulnerability curves in (Sperry et al., 1998). k_p, k_s are the reciprocal of R_p and R_{min} (see Chapter 2). In the following v-SPAC simulation, Bo use the same R_{min} as Ec and An use the same R_{min} as Ap due to the unknown land surface area of Bo and An site.
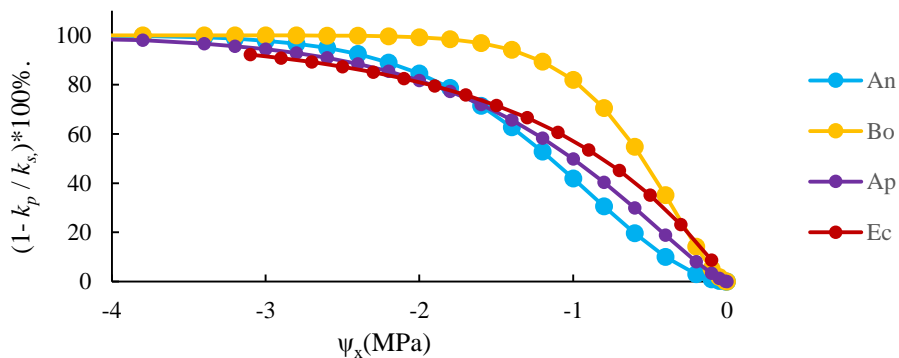
Figure 4-3: The vulnerability curves of the four different tree species used in the synthetic modelling experiment. An, Bo, Ap, Ec are abbreviations of the tree species (see Table 4-2)

Root zone depth (*L*) and root distribution function (RDF)

Root zone depth influences total available water that can be extracted by roots, and RDF determines the proportion of root water uptake from specific soil layers. Four different root zone depth and root density distribution are applied to reflect the effects of the root zone on the method performance. The root zone depth is set to either 50 or 100 cm depth and RDF is set as a uniform or exponential shape.
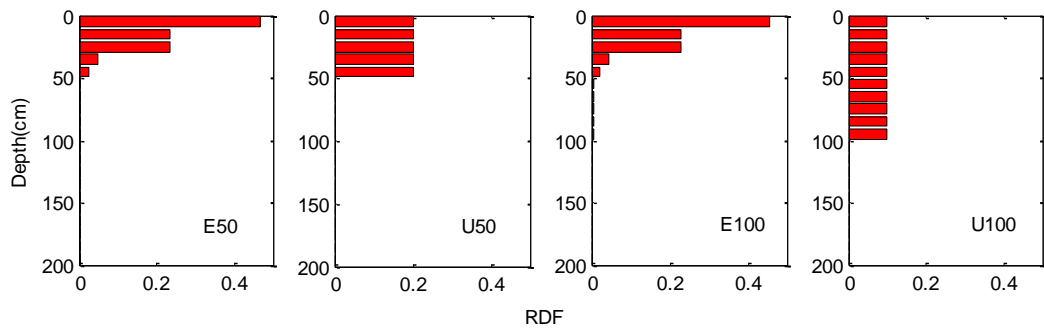
Figure 4-4: RDF in the soil profile, E50 denotes exponential root density decreasing from soil surface to soil depth at 50 cm, U100 denotes uniform root density from top to 100 cm. 200cm is the soil column depth.

Upper flux boundary: potential transpiration and night-time transpiration

A sinusoid function is used to characterize the potential transpiration (PT) for the upper flux boundary of the model. Zero night-time flux is set by forcing the value to zero during night-time (6 pm to 6 am next day), while non-zero night-time flux is adopted from observed sap flow time series of the *Acacia pycnantha* tree (see Figure 4-5).

115
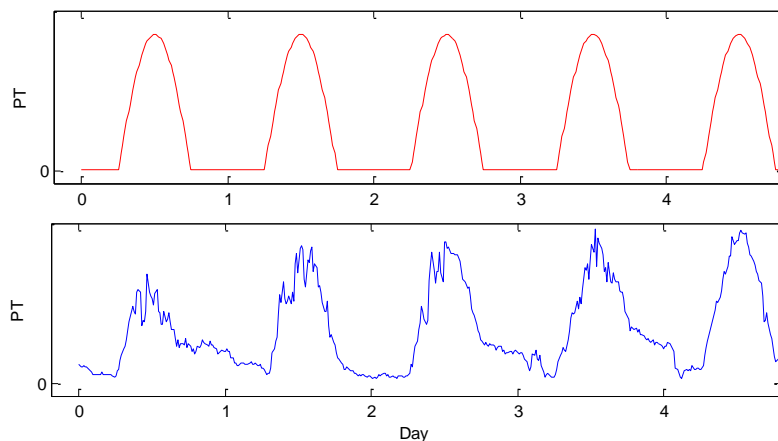
Figure 4-5: Schematic illustration of two types of PT boundary: zero night-time flux (the upper panel) and non-zero night-time flux (the lower panel). The y-axis unit is relative. The x-axis is days, integers indicate 12:00 am.

A range of climate conditions are applied by prescribing a gradient of atmospheric demands, including P/PT=0.3, 0.5, 0.7 and 1.0 (P is precipitation, PT is potential transpiration). The time series is derived from the observations in 230 days from Oct to May at the acacia site. The total precipitation value is fixed at 179 mm as observed, daily PT is then scaled correspondingly. The resulting T/PT ratios are between 0.3-1.2. The lower boundary of the soil column is set as free drainage (FD) and reduced drainage is realized by prescribing less permeable bottom soil layers under FD condition. For example, modest drainage (MD) is realized by setting the soil saturated hydraulic conductivity (K_s) of the bottom 40 cm soil being 1/10 of the original K_s of the soil column, and low drainage (LD) as being 1/100 of the K_s.

4.2.3   The field experiments

The two study sites include an *Acacia Pycnantha* tree of around 5 years on clayey soil in South Australia; and six *Eucalyptus crenulata* saplings of 18 months old in potted sands in Armidale, New South Wales. For the acacia site, the soil water retention curve is obtained from pedo-transfer functions based on the soil texture. Three disturbed soil cores were taken with auger on 4/10/2012 (soil moisture probe installation date), 8/08/2013 and 13/08/2013 at the acacia site. Three undisturbed samples were taken at 8 to 30 cm depths on 13/08/2013. The soil texture is determined with particle-size analysis protocol following Van Reeuwijk LP (2002). Water content (by mass) at 1500 kPa is determined for most samples using pressure plates. The soil water retention curve is then inferred with the pedo-transfer function (function ENR7) following Minasny et al. (1999).

Table 4-3: Soil texture and water content measurement at the acacia site (Australian criteria)

Date	Soil depth (cm)	Sand % (>20um)	Silt % (2-20um)	Clay % (<2um)	BD[1] (g/cm³)	θ(1500)[2]
8/08/2013	0-28	43.796	17.967	38.237	1.0-1.3	0.183
8/08/2013	28-38	11.702	8.191	80.106	1.0	0.341
8/08/2013	38-42	11.778	4.627	83.595	1.0	0.326
8/08/2013	42-45	11.768	9.281	78.952	1.0	0.331
8/08/2013	45-54	27.869	32.236	39.895	1.1-1.3	0.125
8/08/2013	54-59	36.382	36.683	26.935	1.1-1.3	0.131
8/08/2013	59-65	37.034	34.534	28.431	1.1-1.3	0.179
13/08/2013	8-17*	43.358	20.790	35.852	0.954	0.159
13/08/2013	17-25*	37.395	14.368	48.238	1.022	0.250
13/08/2013	25-30*	13.763	7.865	78.372	0.939	0.320
13/08/2013	25-30*	14.149	6.773	79.079	1.106	0.320
13/08/2013	0-34	39.121	16.860	44.020	1.0-1.3	0.177
13/08/2013	34-45	8.106	5.161	86.733	1.0	0.357
13/08/2013	45-50	42.582	27.157	30.261	1.0	0.327
13/08/2013	50-60	37.425	32.075	30.500	1.1-1.3	0.104
13/08/2013	60-66	38.198	28.974	32.828	1.1-1.3	0.111
13/08/2013	66-70	50.124	28.054	21.822	1.1-1.3	0.111
13/08/2013	70-80	46.626	30.936	22.438	1.1-1.3	0.083
4/10/2012	0-10	50.000	10.000	40.000	1.0-1.3	0.184
4/10/2012	10-20	41.000	17.000	42.000	1.1-1.3	0.222
4/10/2012	20-30	21.000	9.000	70.000	1.1-1.3	0.289
4/10/2012	30-40	13.000	7.000	80.000	1.0	0.293
4/10/2012	40-50	17.000	8.000	75.000	1.0	0.311
4/10/2012	50-60	28.000	32.000	40.000	1.1-1.3	0.256
4/10/2012	60-70	40.000	28.000	32.000	1.1-1.3	0.215
4/10/2012	70-80	47.000	31.000	22.000	1.1-1.3	0.136
4/10/2012	80-90	47.000	31.000	22.000	1.1-1.3	0.121
4/10/2012	90-100	47.000	31.000	22.000	1.1-1.3	0.136

Note: *are undisturbed soil cores; others are disturbed soil cores; data shaded with light purple colour are directly measured; shaded orange are obtained from (Minasny, 1999); others are inferred from matching the location of the soil, photos of soil texture and the soil water content at the 1500 kPa. BD[1] is bulk density; θ(1500)[2] is water content (by mass) under suction pressure of 1500 kPa.

For potted saplings, the soil water retention curve was obtained by fitting van Genuchten function with measured soil moisture and water potential in an independent experiment (see detailed description of the experiment in Appendix I).

Table 4-4: Soil water retention curve of the *Eucalyptus crenulata* pot soil

θ (%)*	17.74	11.40	8.25	6.64	6.23	5.07	3.40	2.40	1.97	1.41
ψ_s(MPa)	0.05	0.20	0.37	0.83	1.00	1.54	11.09	31.87	57.04	89.78

Note: * by volume.

4.2.4 Criterion evaluating the RWRC method

To test the robustness of the RWRC method for WRC derivation, an evaluation criteria is defined based on the uncertainty range of the pedo-transfer function (PTF) method. We set the maximum allowed uncertainty range to be no more than that of the PTF method, which is commonly estimated at around ±0.05 in soil water content (θ) away from the prescribed WRC (Vereecken et al., 2010). The defined upper boundary (refer as D_{PTF}) is thus the curve above the WRC by offsetting θ with -0.05 while keeping the water potential the same (see the solid red line in Figure 4-6) and the lower boundary by +0.05 (the solid blue line). We see that the uncertainties of D_{PTF} at the wet and dry ends are quite large, we then constrain the boundaries in the direction of the water pressure head (h), by setting a upper boundary having twice the h at a given θ (see dashed red line) and the lower boundary as half of h (see the dashed blue line). Within the two types of boundaries, we further narrow down the space by half the distance in θ direction (see UB(50%) and LB(50%), the dashed black lines), which corresponds to an uncertainty around ±0.03 in θ from the prescribed WRC. The newly defined boundary is now D_B (the dashed black line).
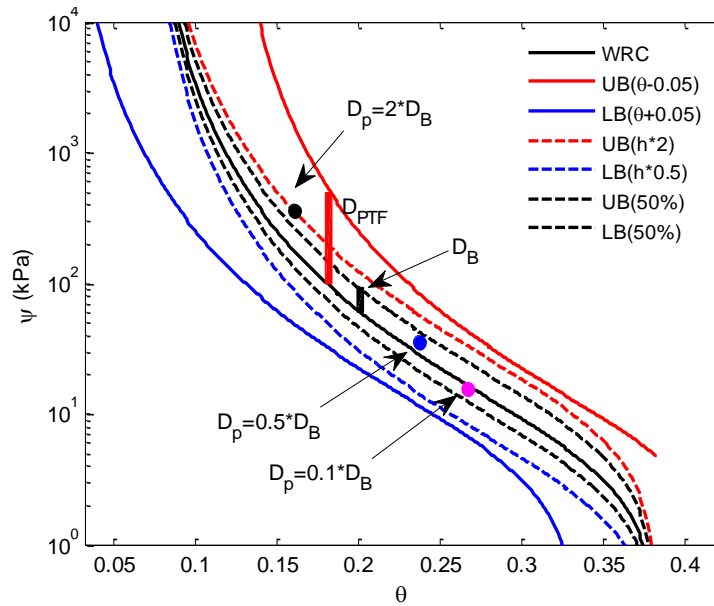
Figure 4-6: Criteria of selecting ψ_x-θ data points for WRC estimation. Only those points within the defined narrow boundaries (the black dash lines) are viewed as passing the criteria.

Note: D_B is the distance from the defind boundary to the prescribed WRC at a specific θ; "D_{PTF}" is the distance from the uncertainty boundary of the PTF method to the prescribed WRC; "D_p" is the evaluated distance from the data points (ψ_x-θ) to WRC. For all WRC plots following on, the water potential (ψ) is plotted with the minus sign omitted and the axis upside down.

The usefulness of the ψ_x-θ time-series, produced from the synthetic simulation experiments under various scenarios are then checked by counting the acceptable ψ_x-θ data points (within the defined boundary D_B). The distance of the ψ_x-θ points to the prescribed WRC (along ψ direction) is D_p. The proximity of the points to the WRC is then evaluated by the ratio of D_p/D_B. The smaller the D_p/D_B ratio, the nearer the points to the WRC, suggesting a better performance of the RWRC method. From preliminary modelling tests, we know that some data points should be discarded under extreme cases such as during a drought or a recovery period or during a rainfall or right after a rainy event. The rest data points will still be sufficient to obtain WRC. We then define a criterion by allowing less a quarter of the data useless, that is, the probability that the ψ_x-θ points fall within D_B should be higher than 0.75 ($p(D_p/D_B<=1)>=0.75$). Based on

this criterion, the RWRC can be quantitatively evaluated and the favariable conditions for RWRC application are summarized.

4.3 Results

4.3.1 Synthetic soil/plant experiment under zero night flux

With 12 soil types, 4 types of root distribution, 4 different vulnerability curves and 6 cases of different upper /lower boundary conditions, we have overall 1154 simulation results. We assume that these 1154 results include a large range of relations between stem water potential (ψ_x) and soil water potential (ψ_s) in uniform soil texture cases. Figure 4-7 shows one example of the relations between ψ_x and ψ_s of sandy clay loam with RDF=E50 (see Figure 4-4 for RDF) and vulnerability curve of *Eucalyptus crenulata.* Figure 4-8 shows the cases of different soil types. Figure 4-9 and Figure 4-10 shows the influence of different VCs and RDF options on the ψ_x - ψ_s relations.
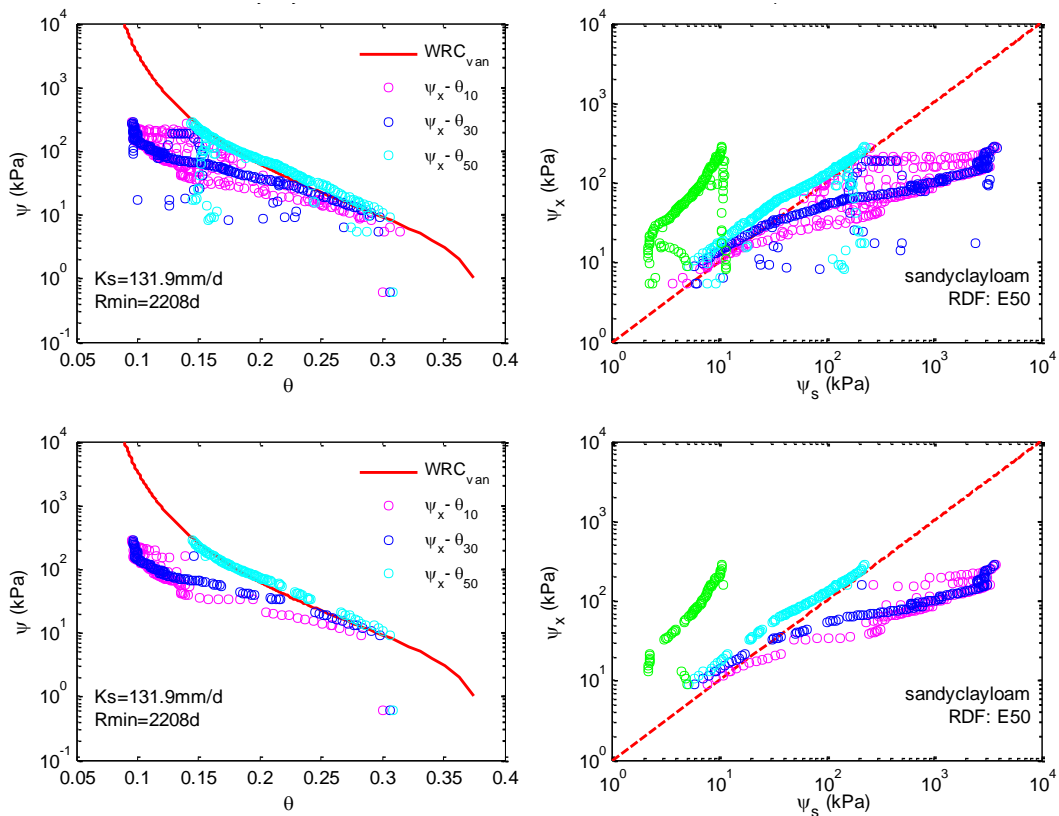
Figure 4-7: Simulated $\psi_{x,pd}$-θ pairs compared against prescribed WRC on all days (upper

panel) and those excluding rainy days (lower panel) (VC: Ec, RDF: E50). Average soil water potential (ψ_s) of 50-200 cm is shown in green circles in the right panels.

Figure 4-7 shows the noise from rainy days. For sandy soils, the data points that within 3 days following a rainfall seem to be not useful to infer the soil water potential. Therefore, the following disucssion will focus on the results with rainy days excluded.

Soil types and WRC
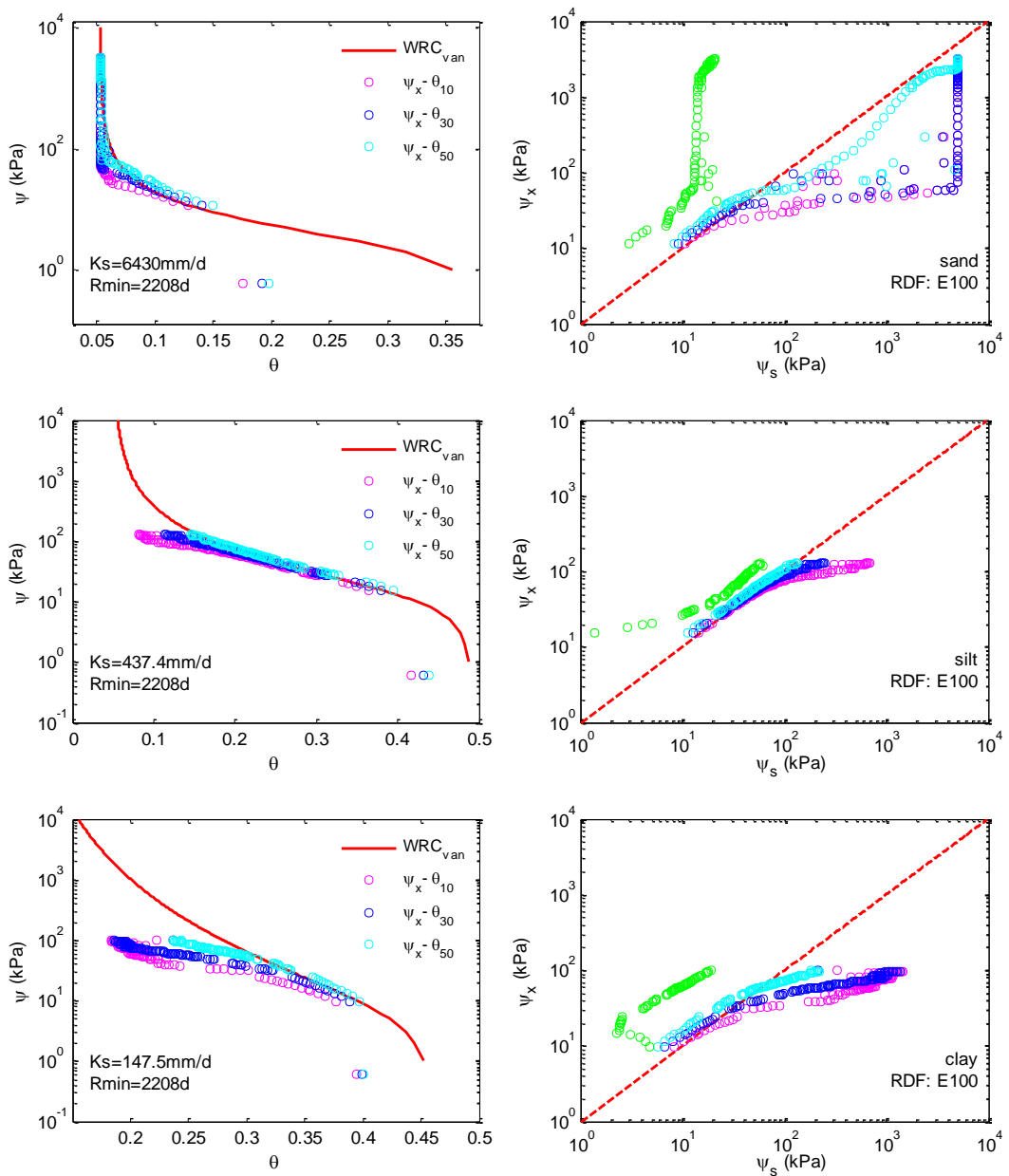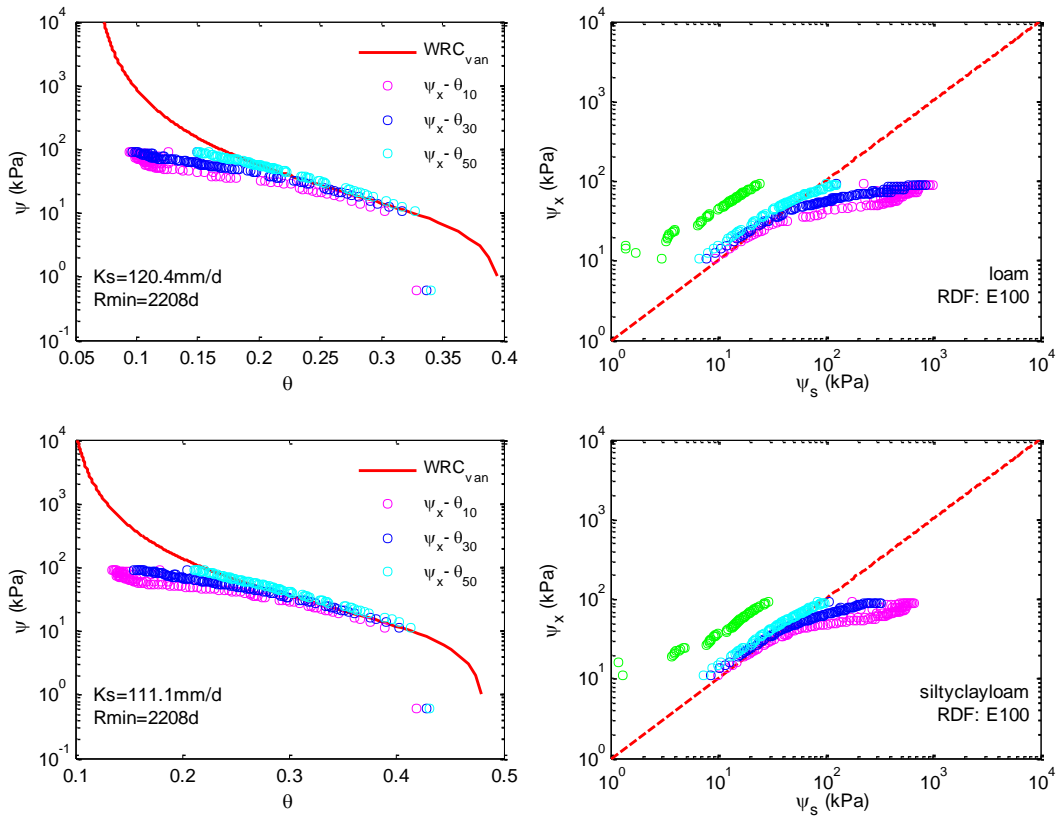
Figure 4-8: Simulated $\psi_{x,pd}$-θ of different soil types at fixed VC (Ec) and RDF (E100).

Figure 4-8 of different soil types indicates that silty soil gives most reliable prediction of ψ_s with pre-dawn stem water potential ($\psi_{x,pd}$). In the drier period the pairs of ψ_s-$\psi_{x,pd}$ deviate from the 1:1 line (see the right panels). $\psi_{x,pd}$-θ pair of deeper soil layer within root zone (50 cm) seem to best represent the WRC, while using the shallow soil layer θ is likely to overestimate the ψ_s due to evaporation at the surface.

Plant vulnerability curve (VC)

The vulnerability curves of *Acacia pycnantha* (Ap) and *Eucalyptus crenulata* (Ec) are firstly compared to demonstrate the influence of plant hydraulic properties. Note that Ap gives four times larger resistance than Ec.
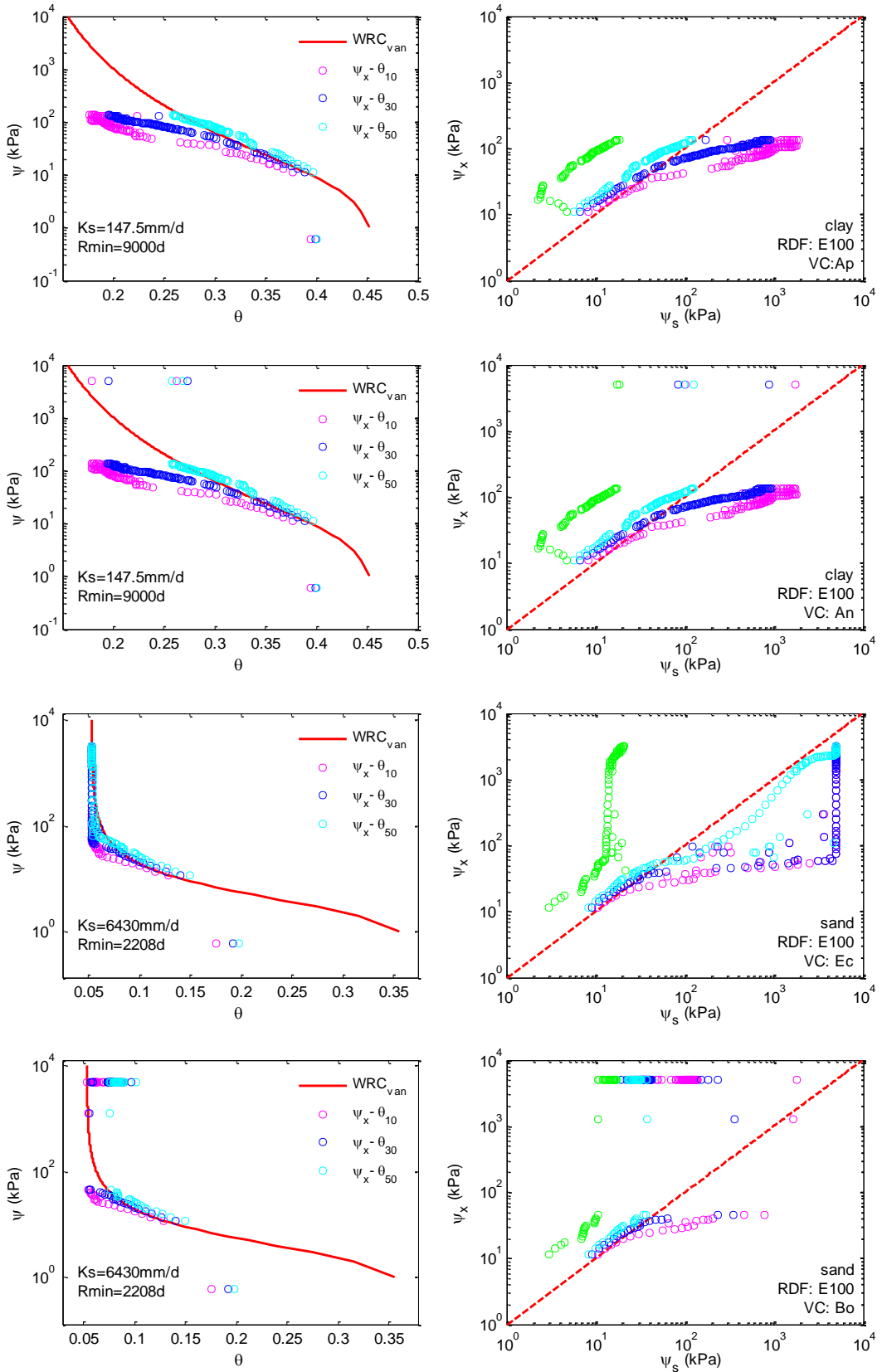
Figure 4-9: Simulated $\psi_{x,pd}$-θ of different VCs in clay and sand. VCs from top to down are Ap, An, Ec, Bo.

The results shown in Figure 4-8 and Figure 4-9 do not indicate much influence of VCs

on the relation between ψ_x and ψ_s. The difference between soil hydraulic properties seem to exert much larger uncertainty in the soil/plant water status correlation than the plant hydraulic properties.

Root distribution (RDF) and root depth (L)
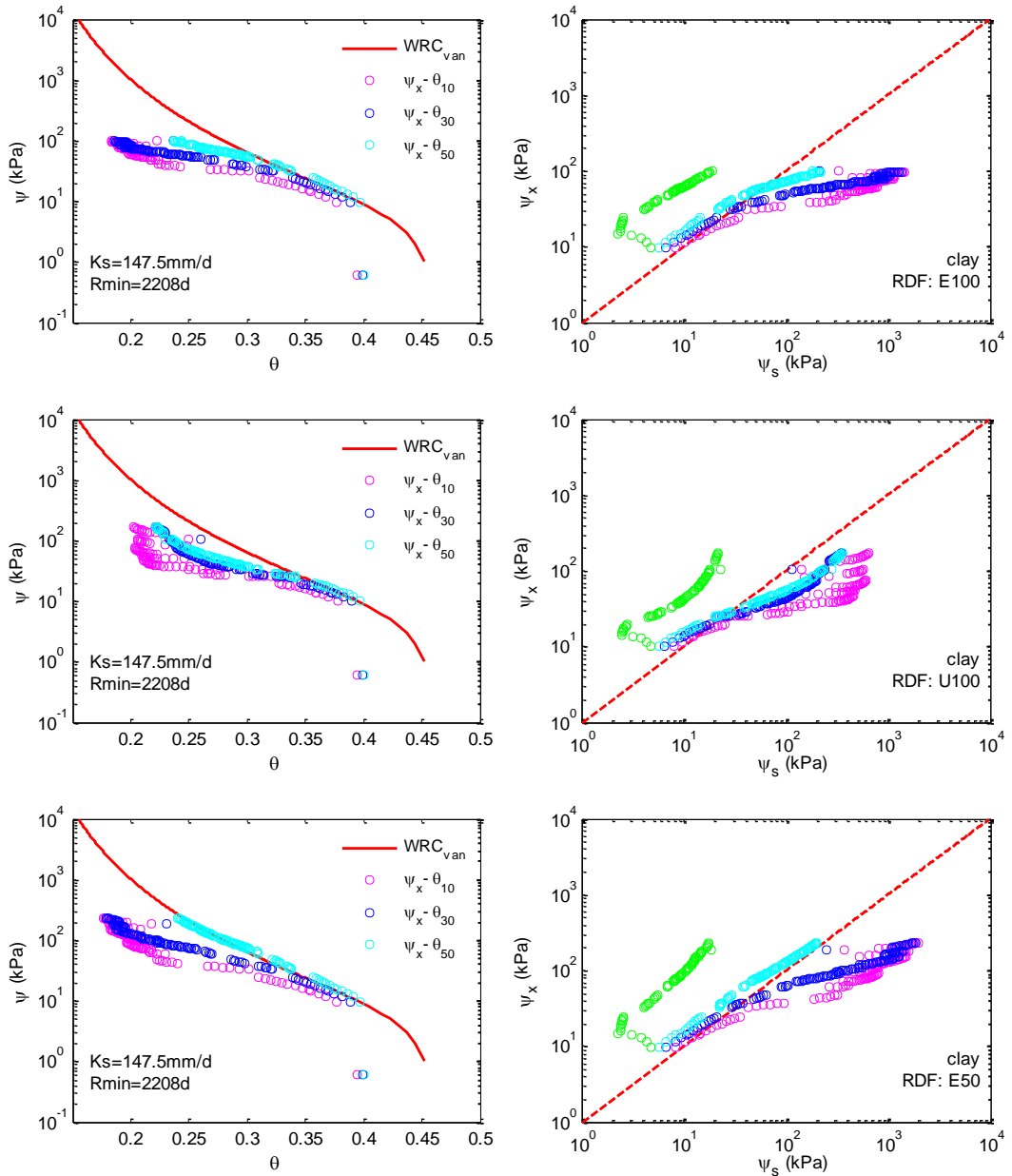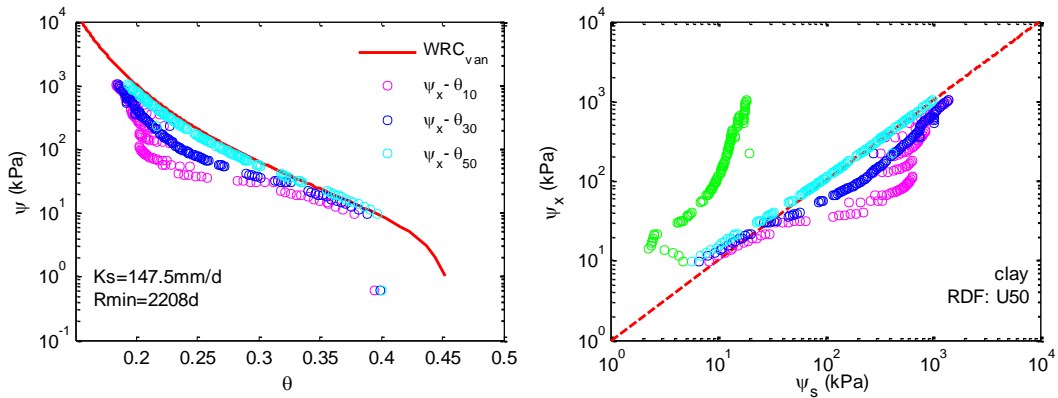
Figure 4-10: Simulated $\psi_{x,pd}$-θ of different RDF and root depth (VC: Ec).

Figure 4-10 indicates that soil moisture at depth of 50 cm is able to capture the root zone water status within 0-50 cm, but not for a root zone that is much deeper (see U100 and E100 cases). This is supported by the simulation results that the ψ_x is much more negative than the ψ_s at 10-50 cm depth in drier periods, indicating that roots are extracting most of the water from the root zone below 50 cm.

The upper and lower boundaries

The upper boundary – potential transpiration (PT) defines the maximum water uptake from the soil in SPAC models. By prescribing larger PT will make soil moisture depleting faster, thus inducing higher chances of disequilibrium between soil and plant. Free drainage can also induce fast water depletion in sandy soils due to their high hydraulic conductivity at saturation. Figure 4-11 shows no much difference for clay soil among cases with either low or high PT demand, and large or low drainage, which is likely due to the low hydraulic conductivity of clayey soils. While for sandy soil, the points show better converge to 1:1 ψ_s-ψ_x line for a low PT demand than a high PT demand. The lower boundary does not seem to exert much influence on the ψ_s-ψ_x equilibrium. It is likely due to the sufficient soil moisture in the 200 cm soil column

for sustaining transpiration starting with soil moisture at field capacity and a quickly

fall out of hydraulic conductivity of sandy soils as the soil dries out.
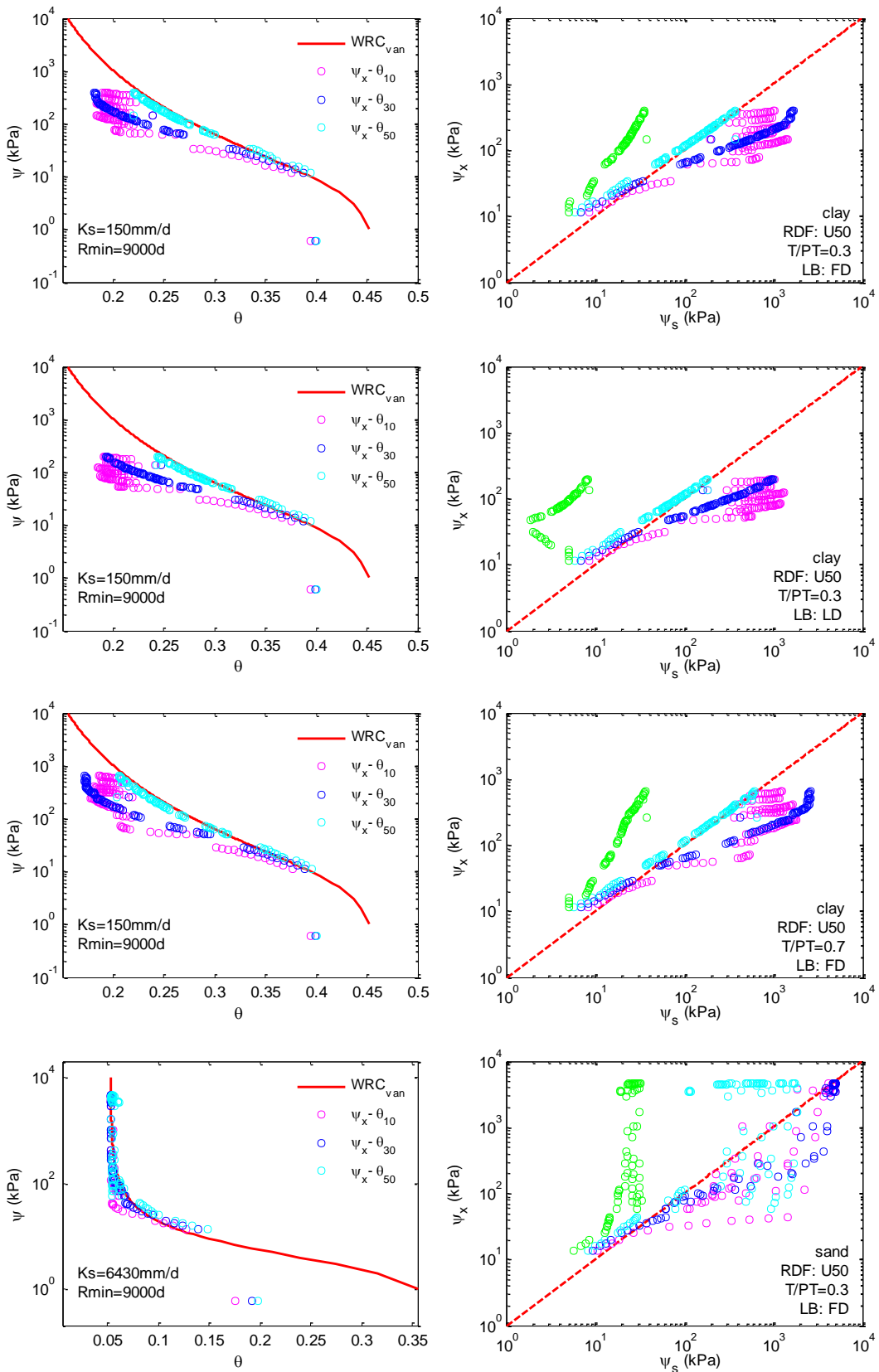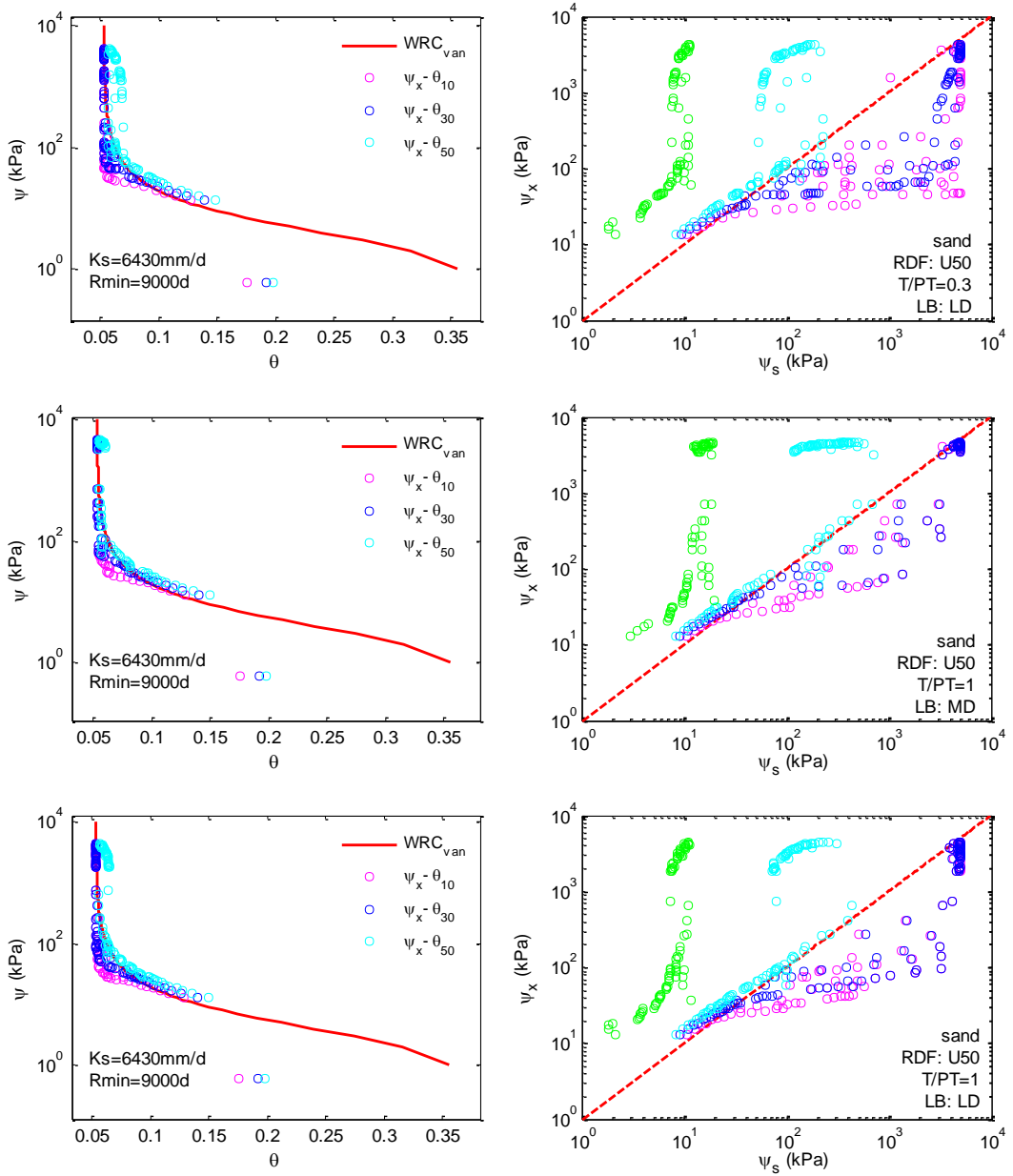
Figure 4-11: Simulated $\psi_{x,pd}$-θ of different upper and lower boundary conditions of sand and clay (VC: Ap).

Note: T/PT shows the upper boundary, LB shows the lower boundary.

Summarization over the modelling results over settings of various soil types, plant VCs, root traits and upper/lower boundary conditions, we conclude qualitatively that the stem water potential together with the 50-cm soil moisture observation at wetter period can be more reliably used to infer the soil WRC under zero night-time flux.

4.3.2 Synthetic experiment under non-zero night-time flux

The non-zero night-time flux boundary is realized by prescribing the real time series of sap flow rate (SAP) of *Acacia pycnantha* of which, the night-time SAP displays more than 50% of day-time SAP. For detailed modelling setting, please refer to Chapter 2. Figure 4-12 shows contrasting results from previous figures that produced under zero night-time flux. There are many more data pairs of ψ_x-ψ_s scattering away from the 1:1 line. The data under night-time flux seem to approach the WRC at the drier period rather than the wetter period, especially for the sandy soil. The reason could be that the night transpiration is also limited by the soil moisture availability, so that the night-time transpiration is much larger in spring than in dry summer for this Mediterranean climate site. The larger the night-time transpiration, the larger the water potential discrepancy between soil and plant. Another example of such similar phenomena was reported on *Eucalyptus victrix* in semi-arid climate which also has higher night-time transpiration in wetter period (Pfautsch et al., 2011).
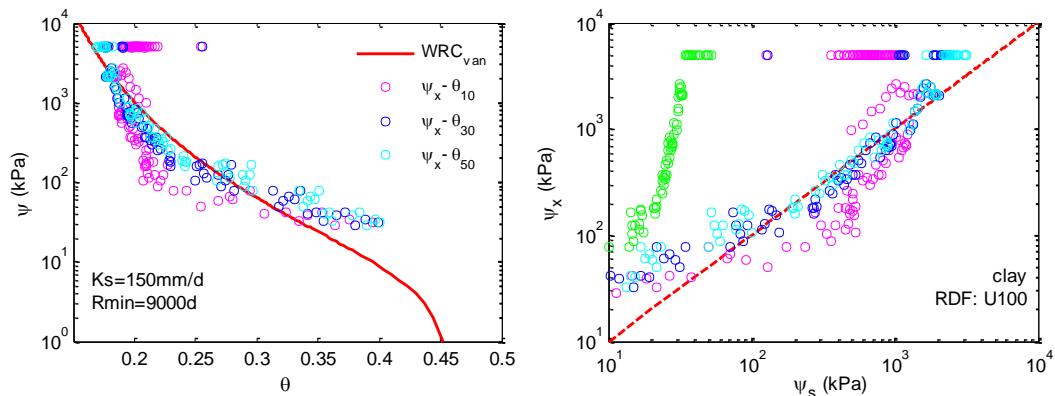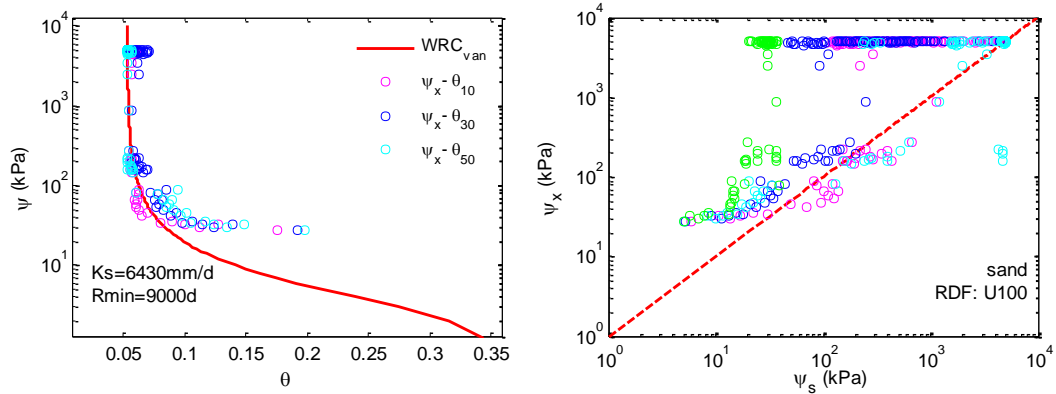
Figure 4-12: Simulated $\psi_{x,pd}$-θ under night-time sap flow (VC: Ap, P/PT=0.3).

Under a disequilibrium state due to night-time transpiration, the equivalent soil water potential ($\psi_{s,v}$) is then inferred following Figure 4-2. The time series of ψ_x-SAP or $\psi_{x,pd}$-SAP are trimmed to segments of 5-7 days between two rainfalls to avoid occasions that the bulk soil moisture changes too quickly. Figure 4-13 shows one example of how $\psi_{s,v}$ is inferred and its distance to the "observed" ψ_s at different depths in the model. The figure indicates that during a wetter period (from Oct to Nov), the $\psi_{s,v}$ reveals the root zone ψ_s; while in a drier period when both ψ_s and ψ_x drop fast within a week (see b4, c4 panel), the inferred $\psi_{s,v}$ is not used and should be discarded. As the soil dries out, $\psi_{s,v}$ gradually approaches the ψ_s (inferred from measured WRC) at a deeper layer (see panel a1, d3, d4 for example).
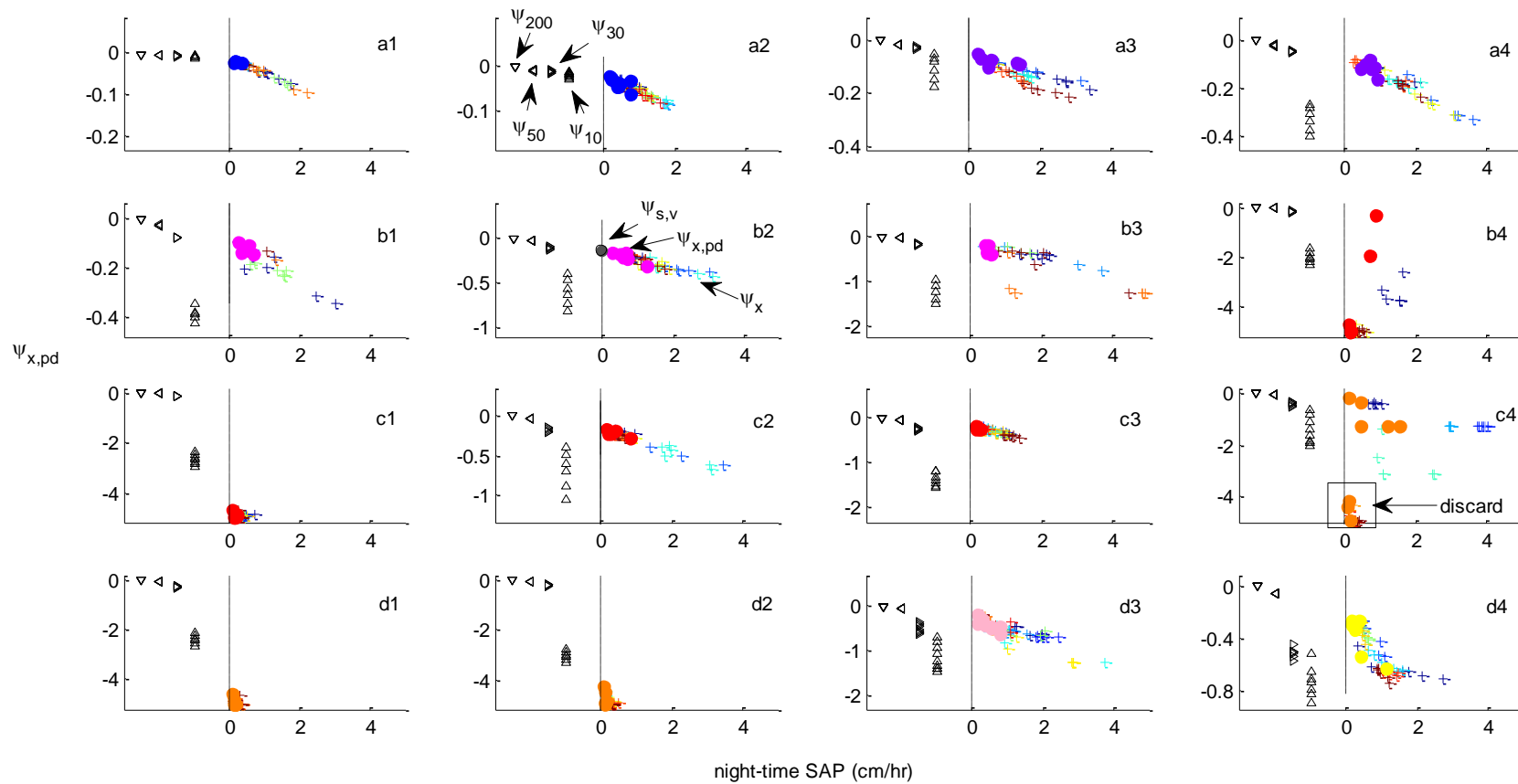
Figure 4-13: Temporal evolution of $\psi_{x,pd}$ with the night-time SAP and the inferred $\psi_{s,v}$ correspondingly (see b2 panel for the $\psi_{s,v}$ inference).

Note: cross (+) are concurrent ψ_x-SAP in the night (one colour indicates one day); solid circles are daily value of $\psi_{x,pd}$-SAP averaged between 3:00 to 6:00 am; the colour of solid circles indicate the month: Dec, Nov, Oct, Jan, Feb, Mar, Apr; black triangles show observed ψ_s at depth 10, 30, 50 and 200 cm from left to right (see a2 panel).

130

The time series of ψ_x with ψ_s at different depths demonstrate the dynamic evolution of ψ_x with root zone water status (see Figure 4-14). It shows that ψ_x starts with close proximity to ψ_s of shallow soil layer (at 10cm), then gradually approaches to ψ_s of the second deep soil layer (at 30cm) with the shallower soil drying out, and finally approaches the deepest soil layer (at 50cm) when the upper soils ψ_s drops quickly to wilting points. The connection between ψ_x and ψ_s of the shallow soil layer resumes immediately after rainfall. The figure demonstrate a gradual root water uptake process from the surface to the depth, and the dynamic relations between ψ_x and ψ_s at different depths. It suggests that the RWRC method is able to capture the effecitve root zone hydraulic characteristics with time as the ψ_x always couples well with the ψ_s of the soil layer that contributes the most of water for transpiraiton.
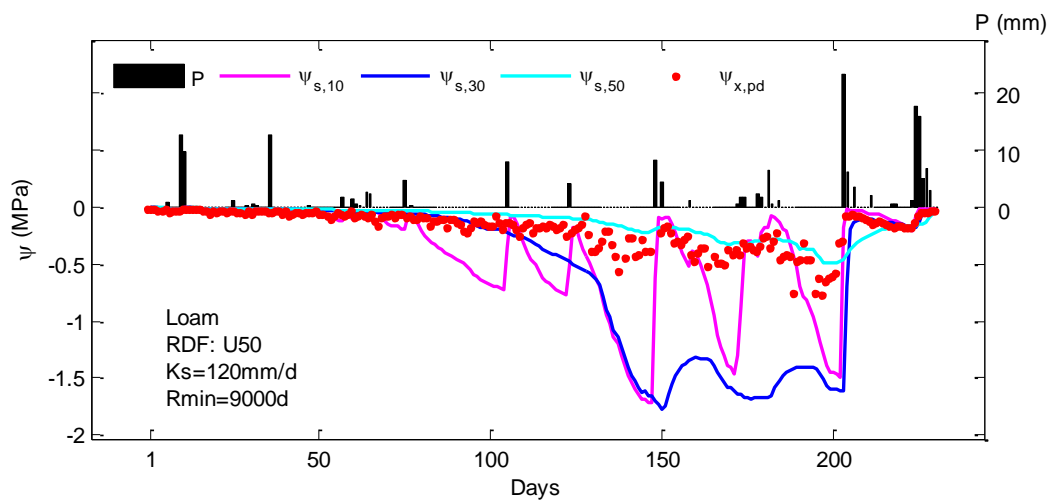
Figure 4-14: Evolution of ψ_x and ψ_s at three depth 10, 30 and 50 cm of a simulation on loamy soil.

4.3.3 Comparing RWRC method with other WRC methods in field conditions

The soil column of *Acacia pycnantha* site is multi-layered. The top 20 to 30 cm soil texture is clay to clay loam. Between 20 to 50 cm is a heavy clayey layer. Below 50 cm, the soil becomes gradually silty (see Appendix I in Chapter 2). The WRC obtained

131

from the PTF method (WRC$_{PTF}$) is shown in Figure 4-15. The inferred equivalent soil water potential $\psi_{s,v}$-θ fall between the WRC$_{PTF}$ lines, especially for the deeper soil layers. The embedded figure in Figure 4-15 shows the good match between the lumped $\psi_{s,v}$-θ_{wt} and WRC$_{PTF}$ of the whole profile (weighting θ of depth 10, 30, 50 cm with [0.2 0.3 0.5] at the same ψ_s). It indicates that the lumping method offers a good up-scaling scheme of root zone WRC with vertical heterogeneity in soil texture.
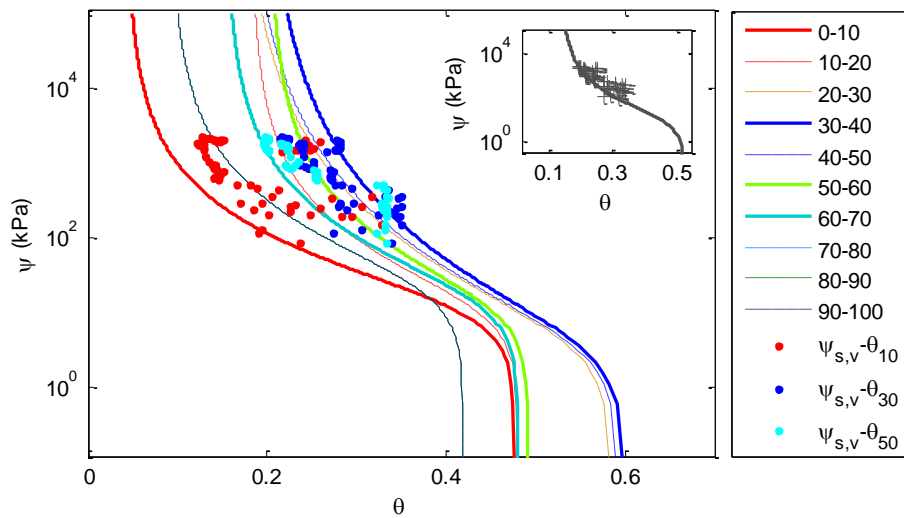
Figure 4-15: Comparison between $\psi_{s,v}$-θ and WRC$_{PTF}$ (lines) of acacia site.
Note: The different colours show the WRC$_{PTF}$ from soil core at different depth (cm).

For *Eucalyptus crenulata*, the sandy soil WRC is obtained from direct measurement of ψ_s and θ (we call it WRC$_m$). Previously, Figure 4-2 shows that the pre-dawn xylem water potential ($\psi_{x,pd}$) almost reached equilibium at pre-dawn with ψ_s except for the drought period. Thus, we compare $\psi_{x,pd}$-θ directly to WRC$_m$. Figure 4-16 shows that the data points fall around WRC$_m$. $\psi_{x,pd}$ approaches to ψ_s within 0.2 MPa uncertainty at $\psi_{x,pd} >$ -1.0 MPa, which is in accordiance with the uncertainty of $\psi_{s,v}$ inferred from the $\psi_{x,pd}$-θ (see panel b2 in Figure 4-13). $\psi_{x,pd}$ is not usable for ψ_s indication at $\psi_{x,pd} <$ -1.0 MPa when $\psi_{x,pd}$ drops too fast during the drought (see panel d1, d2 in Figure 4-13). In this case, we just prescribe ψ_s at wilting point of -1.5 MPa for the WRC estimation.
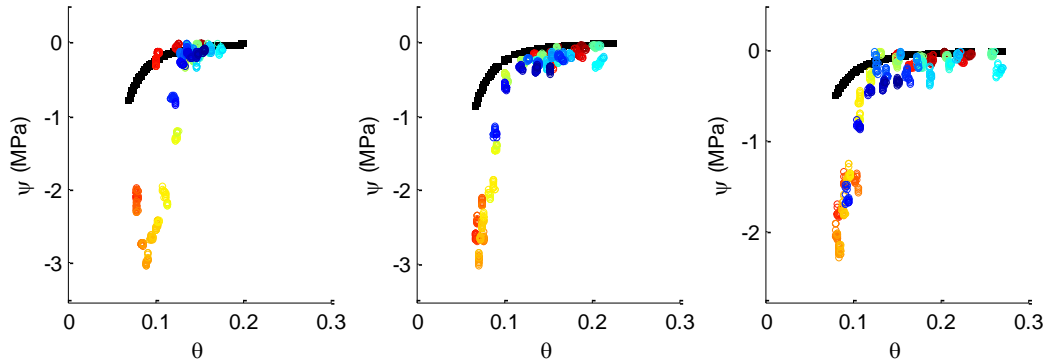
Figure 4-16: Comparison between $\psi_{x,pd}$-θ and measured WRC (black lines) of three potted saplings (circles).

4.3.4 Conditions that favour the application of RWRC

Figures above illustrate that, overall, ψ_x-θ at a deeper soil layer matches better with the prescribed WRC. The ψ_x couples closest with the ψ_s of the soil layer that contributes the most of root water uptake. Soil water extraction (or root water uptake) is a function of the atmospheric demand PT, the soil/plant hydraulic properties K_s, R_p, and the root distribution RDF, root depth L and the soil water availability θ; that is RWU=f(PT, $K(\theta)$, $R_p(\psi_x)$, RDF, L, θ). Smaller atmospheric demand, larger soil/plant conductivity, denser root and larger moisture will all favour the coupling between the soil/plant water potential at the corresponding soil layer. However, it is common that only soil moisture at certain depths, and pre-dawn leaf water potential or stem water potential are available for crude estimate of soil/plant hydraulic conductivity. It is then meaningful to reach a general rule for the WRC establishment based on rough soil classification and expert knowledge on tree species.

To quantify the uncertantiy range of the RWRC method, we employ the criterion introduced in section 4.2.4. The results are shown in the following bar figures. The value of the bar is calculated as 2*(1-D_p/D_B), so that the positive value (>0) denotes that 75% of the data are within the defined boundary D_B. Bar value of 2.0 indicates

that the ψ_x-θ points are on the reference WRC curve, value of 1.0 denotes that the point is half way between the boundary D_B and the WRC. Negative values means that less than 75% data points are within D_B boundary and value $>$-2.0 means that 75% data points are within the uncertainty with of PTF method (($\pm$0.05 in θ). It should be noted that the uncertainty range ($\pm$0.03 θ) we use is much stricter than PTF method, especially for the extreme dry and wet ends. In most cases, 75% of data points are within the PTF boundary (D_{PTF}) (see bar value $>$ -2.0) while outside the defined boundary (D_B) (see bar value $>$0).

Figure 4-17 shows the evaluation result with complete time-series ψ_x-θ. Figure 4-18 and Figure 4-19 show the results with filtered data points. Figure 4-18 demonstrates the results by filtering out the wet and dry end of the time series (ψ_x outside the range of 50-800 kPa is trimmed out). The remaining time series ψ_x within the range of 50-800 kPa) is analysized to see if the filtering process can cross out the "bad" data points that are far away from the prescribed WRC. Similarly, Figure 4-19 shows another filtering method based on θ, in which data points with $\theta < \theta_{min}$*2 are discarded. Here, θ_{min} is the observed minimum θ of the shallow soil layer.

Both Figure 4-18 and Figure 4-19 show apprarent improvement of WRC prediction than Figure 4-17 when all data points are used. Figure 4-18 shows dramatic improvement for the ψ_x-θ at 50 cm depth with U50 root setting when both dry and wet end are trimmed out based on ψ_x. Figure 4-19 shows that by crossing out the dry end data below θ_{min}*2, the 10 cm and 30 cm θ can be also used for clayey and silty soil WRC prediction. Among all types of root distriction, the uniform and shallow root system (U50) seem to have most reliable prediciton. Among all soil types, silt and silty loam (soil type 9 and 12) show consistently good prediction of WRC. It suggests that

the proposed RWRC method is applicable for almost all conditions on uniform silty and loamy soils.

By lumping ψ_x-θ at three θ observation depths (10, 30 and 50 cm), we come to one time-series of ψ_x-θ_{wt} to represent the WRC for the whole root zone. There are three different weighting schemes for θ_{wt}: [4 3 3] denotes heavier weighting on shallow θ (θ_{wt} =0.4*θ_{10}+ 0.3*θ_{30}+ 0.3*θ_{50}), while [2 3 5] denotes heavier weighting on deeper θ (θ_{wt} =0.2*θ_{10}+ 0.3*θ_{30}+ 0.5*θ_{50}). Figure 4-20 shows that all three lumped ψ_x-θ_{wt} schemes improves the prediction capability for all cases. Almost all data points are within D_{PTF} (see value >-2.0) and the performance improves greatly over E100 and E50 cases. Similarly, we compare the performance of ψ_x-θ_{wt} over a gradient of climate aridity by setting P/PT =0.3 to P/PT=0.9 (see Figure 4-21). Again, all cases are within D_{PTF} boundary and the largest improvement occurs on cases with E100 and wet climate (P/PT=0.9). When the atmospheric demand is large (P/PT=0.3), the heavier weighting of shallow soil layer does not seem to improve the performance. The shallow soil may have depleted water near to the wilting point commonly under such large atmospheric demand, which does not contribute much to the root water uptake. It indicates that the water retention curve should be derived with heavier weighting of deeper soil layers with increased aridity of the local climate.
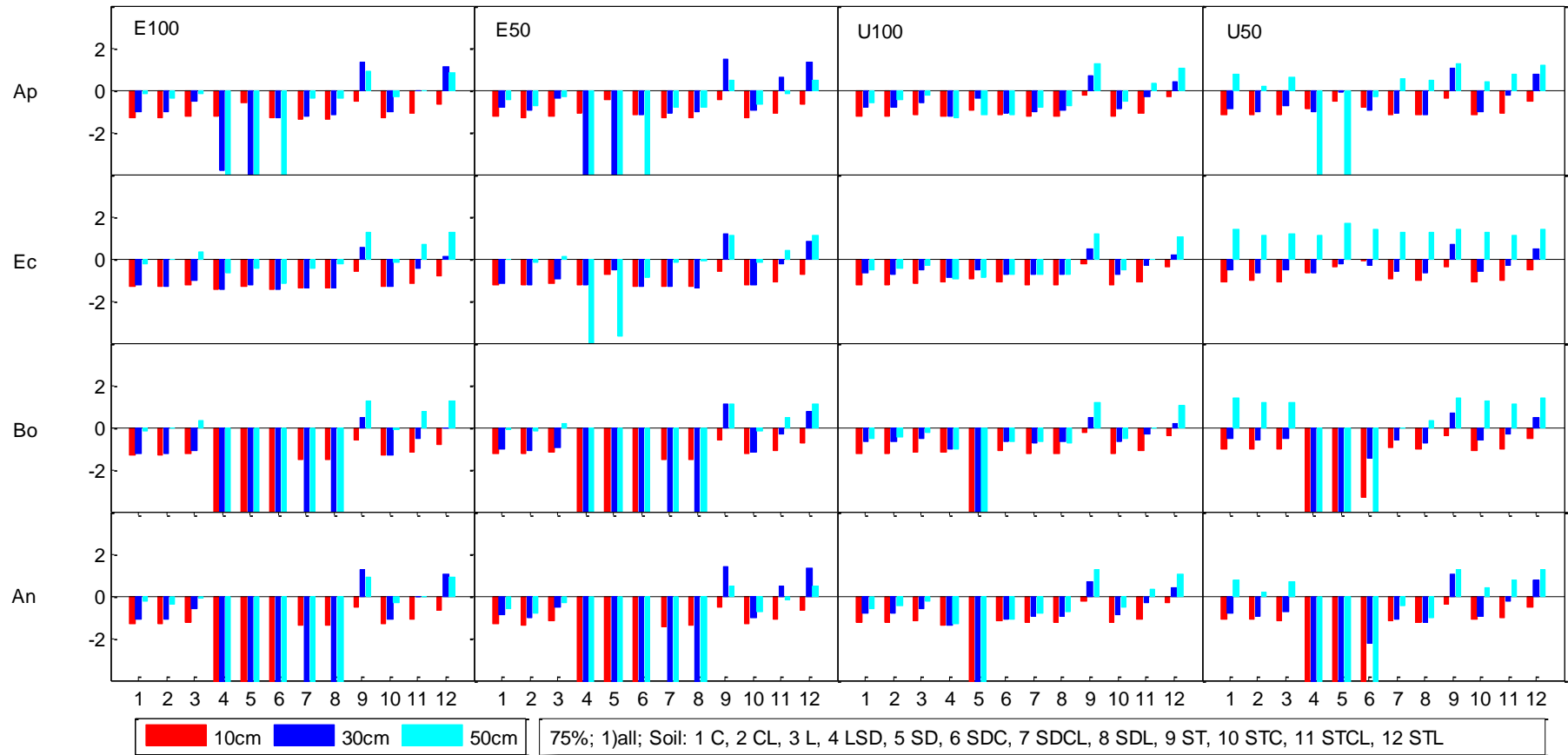
Figure 4-17: Cases of ψ_x-θ with 75% of data points pass criteria (positive bars) and those not (negative bars) under P/PT=0.9 and zero night-time flux.

Note: the more positive of the bar value, the nearer the ψ_x-θ points to the prescirbed WRC line, the more negative, the further away the ψ_x-θ points from the WRC. The x-axis represents 12 types of soil listed in Table 4-1. The red, blue and cyan bars showing ψ_x-θ at 10, 30 and 50cm depth. Ap, Ec, Bo, An are tree species abbravation. E100, E50, U100, U50 show the root architecture.

136
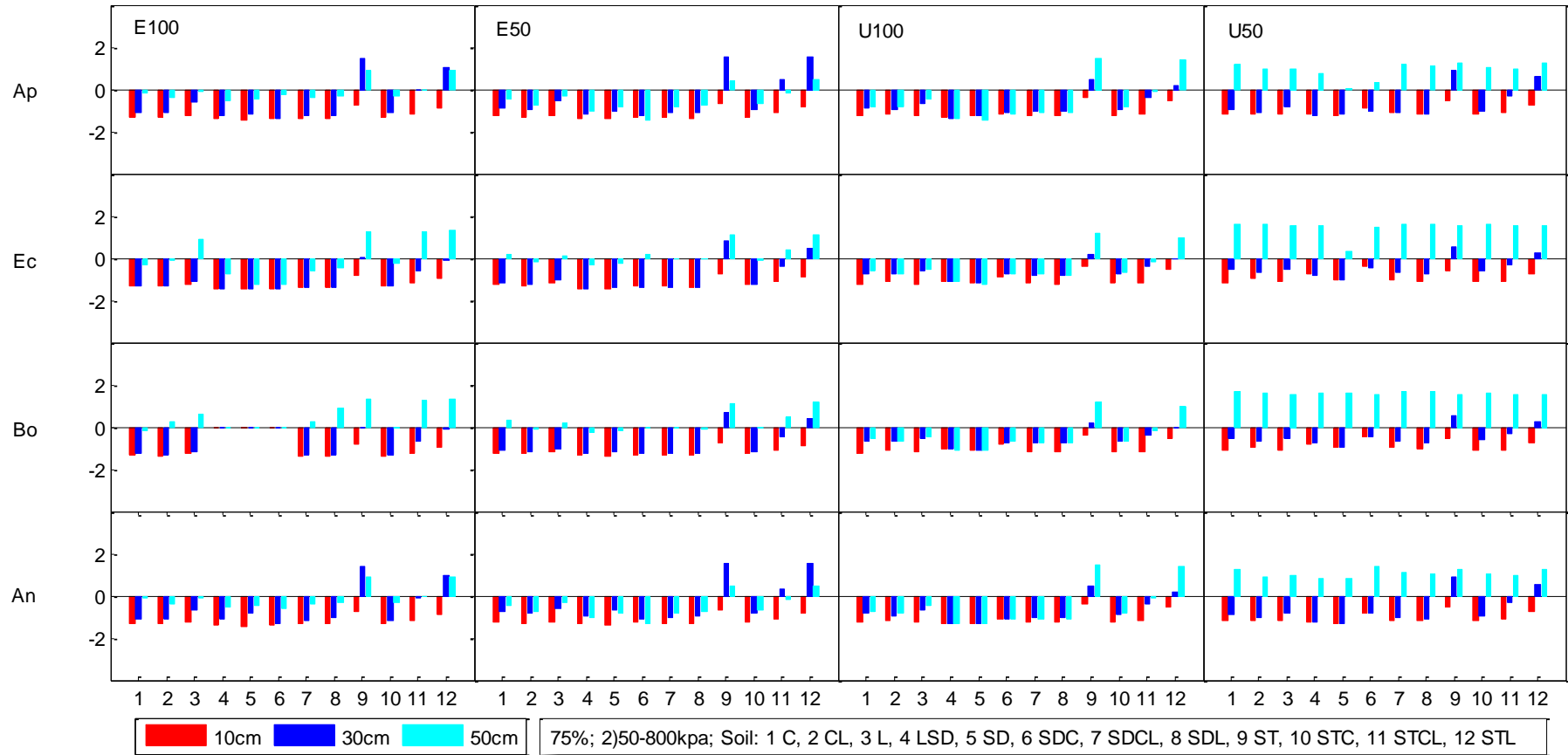
Figure 4-18: The same as Figure 4-17 but data points (ψ_x-θ) outside 50-800 kPa (ψ_x) is discarded before the analysis.
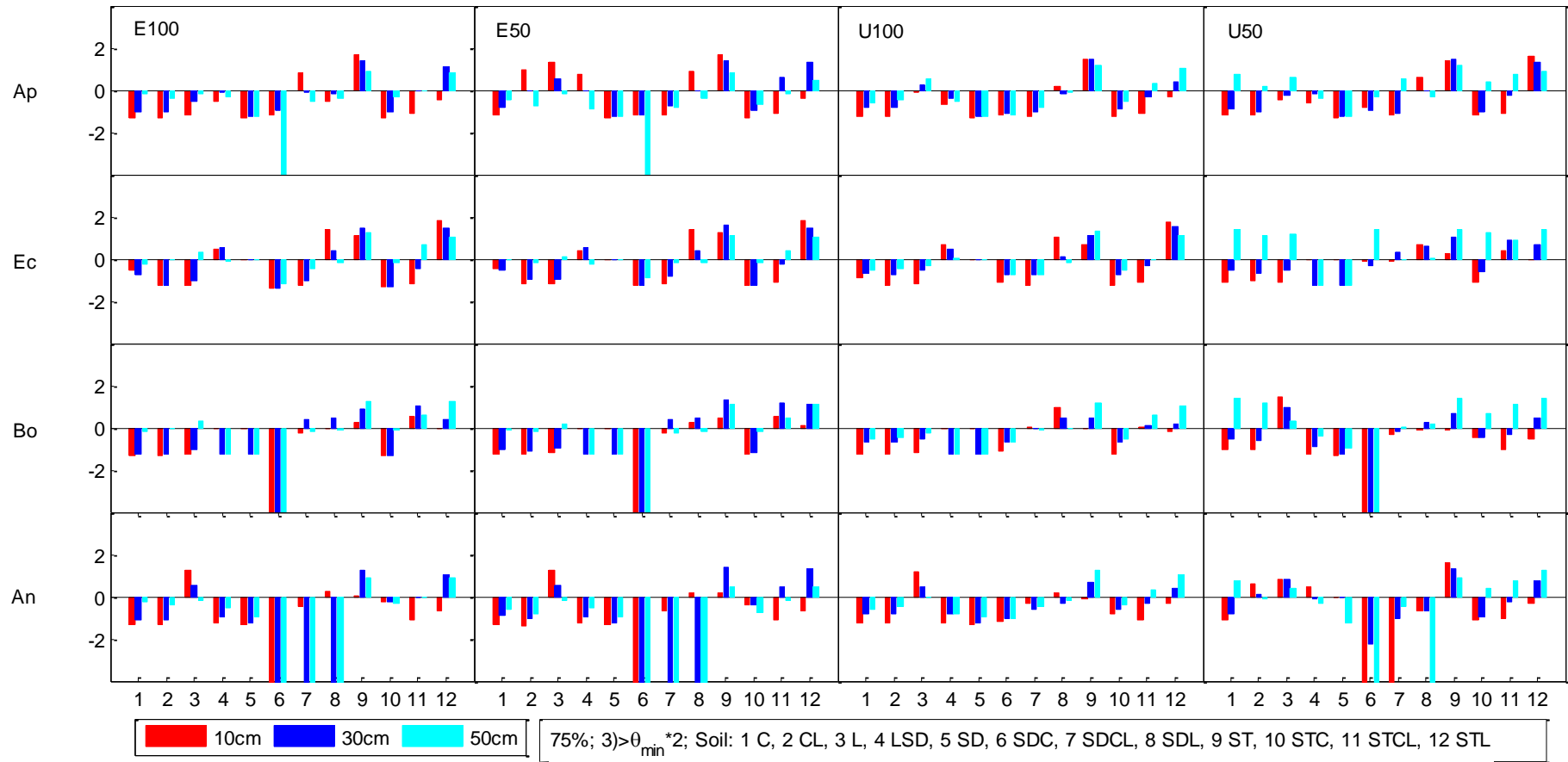
Figure 4-19: The same as Figure 4-17 data points (ψ_x-θ) below θ_{min}*2 is discarded before the analysis.
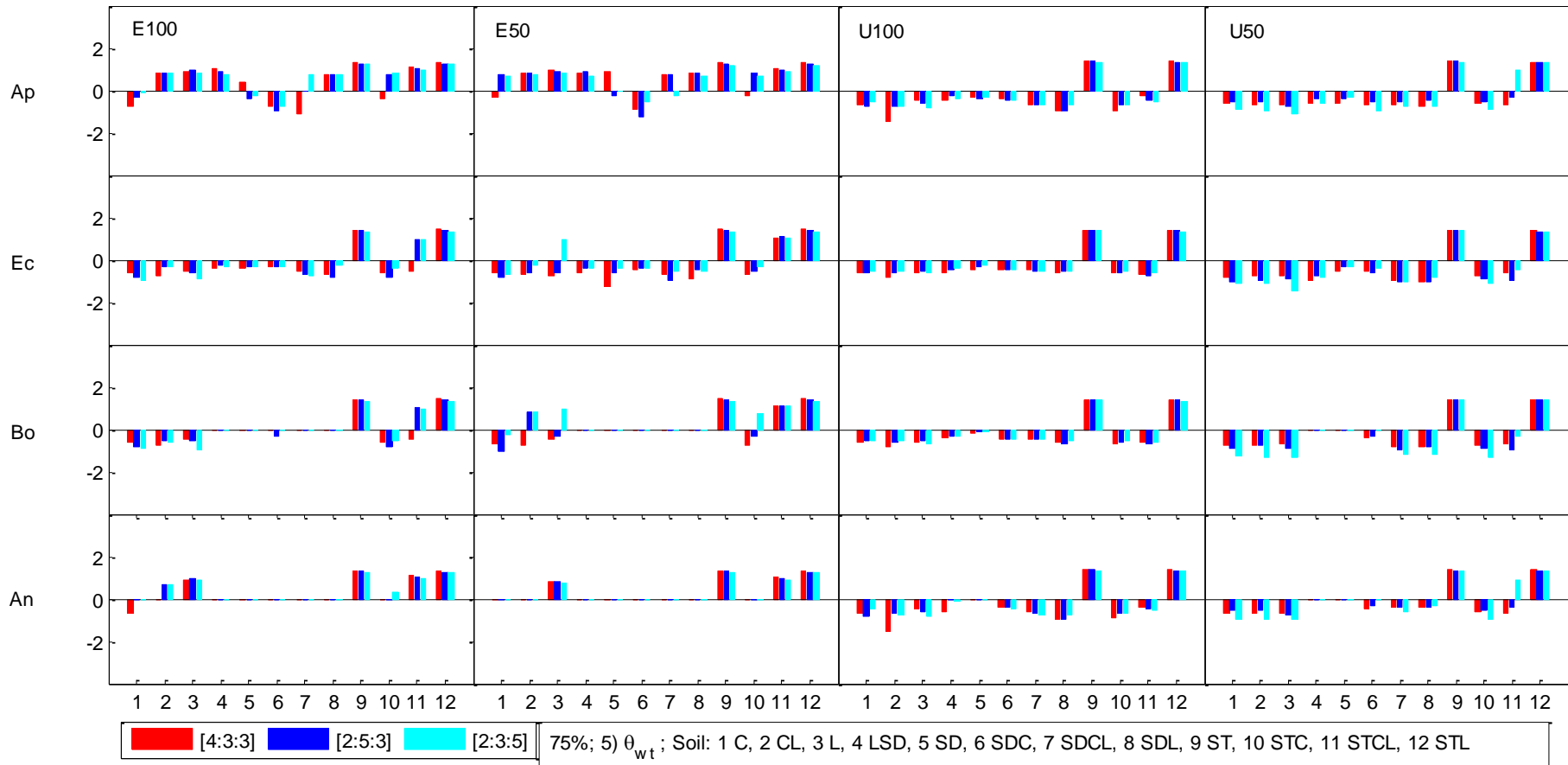
Figure 4-20: Cases of ψ_x -θ_{wt} with 75% of data points pass criteria (positive bars) and those not (negative bars) with same setting as Figure 4-17.

Note: θ_{wt} is the lumped soil moisture over three depth. The three different colors red, blue and cyan indicates different weighting scheme of the soil profile.

 [4:3:3] means that $\theta_{wt} = 0.4*\theta_{10}+ 0.3*\theta_{30}+ 0.3*\theta_{50.}$
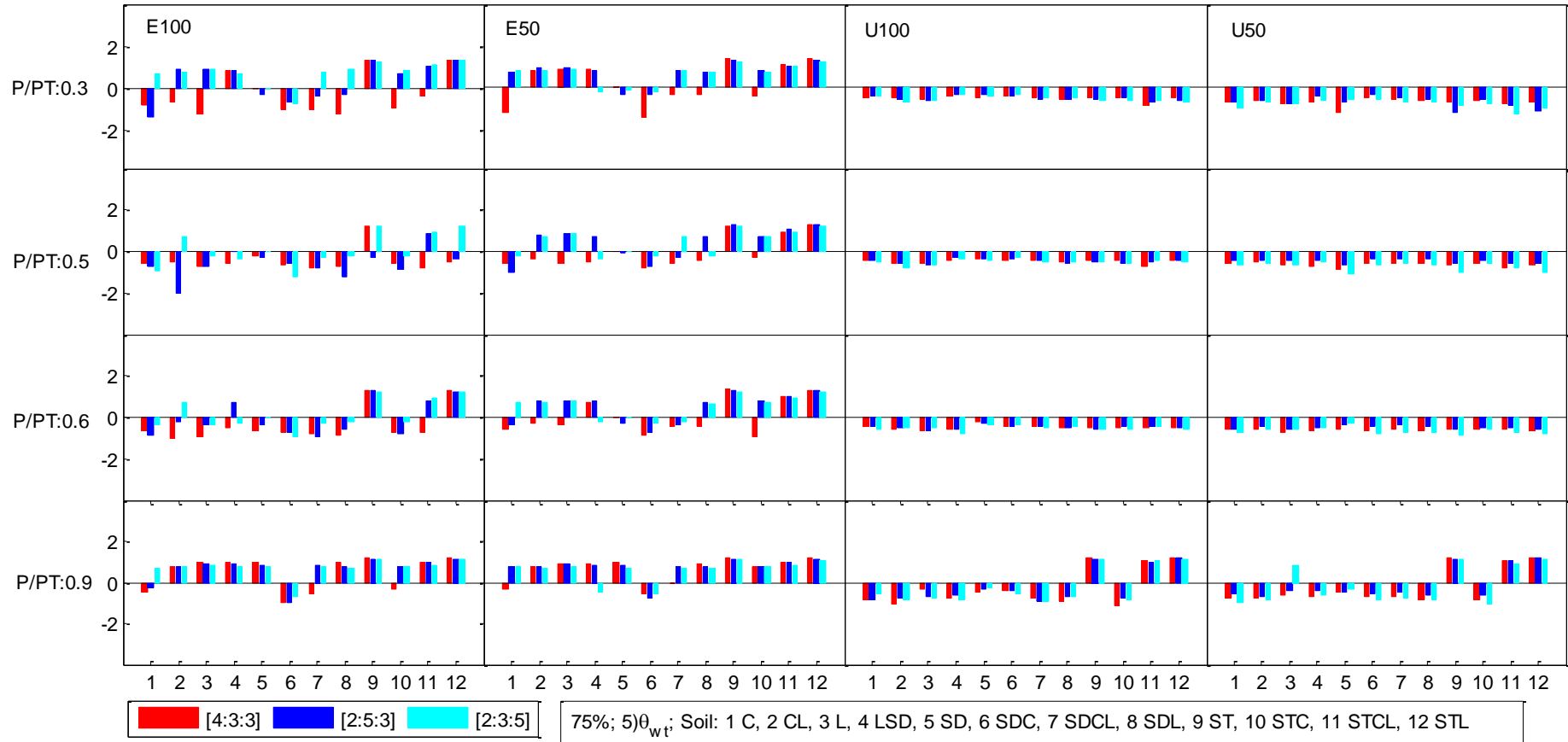
Figure 4-21: Cases of ψ_x -θ_{wt} with 75% of data points pass criteria (positive bars) and those not (negative bars) under different atmoshperic demand (VC:Ap).

4.4 Discussion

The xylem water potential gives one single information for multiple depths of soil water content. Then how the xylem water potential (ψ_x) should be used in WRC derivation? Figure 4-14, for example, shows that during the initial dry out (see simulation date 60 to 100), the ψ_x is closest to the ψ_s in the middle layer, while, in the water stressed period (see simulation date 100 to 200), the ψ_x couples with that of the deepest soil layer (also the wettest layer), and immediately after rainfall, it approaches to surface layer. It suggests that ψ_x always couples closely with the ψ_s of the soil layer that contributes the most of water. The soil layering and their relative contribution in root water uptake, however, are almost unknown without inverse modelling, the lumping of soil water content then provides a handy way to give a good approximation of the root zone WRC (see Figure 4-20 & Figure 4-21). From both the synthetic and field experiments (Figure 4-20 & Figure 4-15), we see that the prediction of WRC with lumped water contents performs better with reduced uncertainty.

The soil water retention curve describes the ability of the soil to retain water. For agriculture purposes, for example, irrigation, the tensiometer may be sufficient for the purpose of monitoring as its measurement range matches the range of crop water stress for high yield requirement (above -100 kPa). Below -100 kPa, other technique to measure soil water potential has to be applied for monitoring to get the full range of WRC, for example, most importantly for soil water flow simulation in arid land hydrology or forestry studies. There is, however, a lack of sensors that are available for field soil water potential measurement in the range of -100 kPa to -1.0 MPa with both high precision and wide range (personal communication with soil experts). It is common that combining techniques of the field (such as tensiometer with scale of -10

kPa to -100 kPa) and that of the lab (such as WP4 sensor, measurement range -0.5 to <-5 MPa) are required to capture the full range of WRC. It is then easy for us to see the advantage of the proposed RWRC method which provides a good approximation of WRC between the range of -50 and -800 kPa.

4.5 Conclusions and Future work

This study examines a novel method (RWRC) to obtain root-zone soil water retention curve from field-based observations with stem water potential and concurrent soil moisture measurement. The results from both synthetic soil column modelling experiments and real field cases suggest a good potential of the method. The results show that the RWRC method is capable to obtain WRC on clayey and silty soils with high confidence, but not on sandy soils. With careful data selection, such as excluding data on rainy days, those in dry periods ($\psi_x < -800$kPa, or $\theta < 2 * \theta_{min}$), the performance improves greatly.

By lumping multiple soil moisture observations of the synthetic experiments and the field experiment of the acacia site, the resulted ψ_x-θ_{wt} or $\psi_{s,v}$-θ_{wt} provides another way to improve the performance of the RWRC method. The ψ_x-θ_{wt} may become an vertical up-scaling scheme for root zone hydraulic properties, which is meaningful to explore in the future.

From the experience with data selection processes, we recommend that the plant water potential is observed between two rainfalls. For example, ψ_x is measured between 3-7 days after a big rainfall so that the soil moisture are not too wet or too dry. ψ_x is measured within 2 days after a small rainfall to capture the reponse of ψ_x to the shallow soil layer.

References

Bucci, S.J. et al., 2004. Processes preventing nocturnal equilibration between leaf and soil water potential in tropical savanna woody species. Tree Physiology, 24(10): 1119-1127.

Donovan, L.A., Linton, M.J., Richards, J.H., 2001. Predawn plant water potential does not necessarily equilibrate with soil water potential under well-watered conditions. Oecologia, 129(3): 328-335.

Donovan, L.A., Richards, J.H., Linton, M.J., 2003. Magnitude and mechanisms of disequilibrium between predawn plant and soil water potentials. Ecology, 84(2): 463-470.

Jones, H.G., 2004. Irrigation scheduling: advantages and pitfalls of plant-based methods. Journal of Experimental Botany, 55(407).

Leij, F.J., aLVES, W.J. van Genuchten, M.Th., Williams, J.R., 1996. Unsaturated Soil Hydraulic Database, UNSODA 1.0 User's Manual. Report EPA/600/R-96/095, US Environmental Protection Agency, Ada, Oklahoma, 103pp.

Minasny, B., McBratney, A.B., Bristow, K.L., 1999. Comparison of different approaches to the development of pedotransfer functions for water-retention curves. Geoderma, 93(3-4): 225-253.

Mohanty, B.P., Skaggs, T.H., 2001. Spatio-temporal evolution and time-stable characteristics of soil moisture within remote sensing footprints with varying soil, slope, and vegetation. Advances in Water Resources, 24(9-10): 1051-1067.

Mohanty, B. P., & Zhu, J. 2007. Effective hydraulic parameters in horizontally and vertically heterogeneous soils for steady-state land-atmosphere interaction.Journal of Hydrometeorology, 8(4), 715-729.

Pfautsch, S. et al., 2011. Diurnal patterns of water use in Eucalyptus victrix indicate pronounced desiccation-rehydration cycles despite unlimited water supply. Tree Physiology, 31(10): 1041-1051.

Scharnagl, B., Vrugt, J.A., Vereecken, H., Herbst, M., 2011. Inverse modelling of in situ soil water dynamics: investigating the effect of different prior distributions of the soil hydraulic parameters. Hydrology and Earth System Sciences, 15(10): 3043-3059.

Shin, Y., Mohanty, B.P., Ines, A.V.M., 2012. Soil hydraulic properties in one-dimensional layered soil profile using layer-specific soil moisture assimilation scheme. Water Resources Research, 48.

van Genuchten, M. Th., 1980. A closed-form equation for predicting the hydraulic conductivity of unsaturated soils, Soil Sci. Soc. Am. J., 44, 892-898.

Van Reeuwijk LP 2002 (ed.). Procedures for soil analysis (6th ed.). Tech. Pap. 9, ISRIC, Wageningen

Vereecken, H. et al., 2010. Using Pedotransfer Functions to Estimate the van Genuchten-Mualem Soil Hydraulic Properties: A Review. Vadose Zone Journal, 9(4): 795-820.

Vrugt, J.A., Stauffer, P.H., Woehling, T., Robinson, B.A., Vesselinov, V.V., 2008. Inverse modeling of subsurface flow and transport properties: A review with new developments. Vadose Zone Journal, 7(2): 843-864.

Walker, J. P., Willgoose, G. R., & Kalma, J. D., 2001. One-dimensional soil moisture profile retrieval by assimilation of near-surface observations: a comparison of retrieval algorithms. Advances in Water Resources, 24(6), 631-650.

Wosten, J.H.M., Pachepsky, Y.A., Rawls, W.J., 2001. Pedotransfer functions: bridging the gap between available basic soil data and missing soil hydraulic characteristics. Journal of Hydrology, 251(3-4): 123-150.

Zeppel, M., Tissue, D., Taylor, D., Macinnis-Ng, C., & Eamus, D. 2010. Rates of nocturnal transpiration in two evergreen temperate woodland species with differing water-use strategies. Tree Physiology, 30(8), 988-1000.

Zhang, Z.F., Ward, A.L., Gee, G.W., 2003. Estimating Soil Hydraulic Parameters of a Field Drainage Experiment Using Inverse Techniques. Vadose Zone Journal, 2(2): 201-211.

Appendices

Appendix I: Soil water retention curve experiment of potted *Eucalyptus crenulata* saplings (provided by Michael Forster)

Volumetric soil water content (%) and soil water potential (MPa) were measured with a capacitance based sensor, 5cm in length, and 0.3L measurement volume (EC-5 Sensor, Decagon Devices, Pullman, WA, USA). Two sensors were installed in the middle of each pot at an angle to cover a depth between 5 and 8cm and 15 and 18cm respectively. Each sensor was individually calibrated for soil specific volumetric soil water content (%) and soil water potential (MPa). Soil used during the study was air dried for 21 days and then partitioned into 10 separate containers with volume of 0.573L. The first container remained air dry, a portion of water was added to the second container, and so on until the 10th container was saturated. Soil in each container was thoroughly mixed so that moisture was evenly distributed throughout the volume of the soil. Moisture levels were checked with an EC-5 Sensor to ensure there was a spectrum of moisture contents across the 10 containers from dry to wet, and to ensure consistency of measurements within the container. Every EC-5 Sensor deployed in this study then measured each container five times and an average taken. Immediately following measurements, a portion of the soil was then carefully moved to a SC4 Stainless Steel Cup (Decagon Devices, Pullman, WA, USA) and placed into a WP4C Dewpoint Water Potential Meter (Decagon Devices, Pullman, WA, USA) for a water potential measurement. The wettest soil sample was outside of the specifications for accurate measurements by the WP4C therefore a 2100F Tensiometer with a dial gauge (Soil moisture Equipment Corp, Goleta, CA, USA) was used to measure soil water potential in the container. Once measurements had been made with the WP4C, soil wet weight was measured and then samples placed in a drying oven at 105 ℃ for 3 days and then dry weight was measured. Volume of the soil was taken as

the volume of the SC4 Stainless Steel Cup and actual volumetric water content (%) was calculated. EC-5 Sensor values were then corrected for actual volumetric water content (%).

5 POTENTIAL OF USING LEAF TEMPERATURE FOR VEGETATION WATER STRESS INDICATION OF TWO NATIVE TREE SPECIES UNDER MEDITERRANEAN CLIMATE

Abstract

Leaf temperature has been widely used to monitor plant water stress. Previous studies mainly focus on homogeneous agriculture crops and are often based on intermittent observations at certain time windows within a day. Few studies of continuous observations have been reported, especially on plants in natural ecosystems. In this study, potential of using leaf temperature (T_c) as a water stress indicator (thermal indices) is tested on two native vegetation species (*Acacia pycnantha* and Eucalyptus *macrocarpa*) on a hill-slope in South Australia. A simplified thermal index based on adjusted intra-crown variability of leaf temperatures ($aStd(T_c)$) is proposed and compared to published thermal indices against soil moisture content and pre-dawn stem water potential. Monte Carlo sampling technique is applied to check the identifiability of all thermal indices on detecting temporal evolution of plant water stress. The results show that the new index ($aStd(T_c)$) performs as well as canopy to air temperature difference (T_c-T_a) and the crop water stress index (CWSI), while remaining much simpler than CWSI. The intra-crown temperature variation index ($Std(T_c)$) does not perform consistently over seasons for *Acacia pycnantha*. Overall, the three published thermal indices are able to detect increasing water stress from spring to summer. By examining the non-water-stress baseline (NWSB) commonly reported for crops, we find that the empirical CWSI reflects water stress resulting from both root zone moisture and vapour pressure deficit. A modified CWSI is suggested

based on the stomata sensitivity to VPD, which improves the performance in indicating root-zone moisture condition. This result also implies that the linear interpolation for root-zone wetness or transpiration between the wet and dry reference temperatures may not be justified.

5.1 Introduction

Thermal imaging is a low cost, efficient way to detect plant water stress in large scale (Jones, 2007). It proves to be the most reliable remote method to detect plant water status (Zarco-Tejada et al., 2012) and has been applied widely for spatial patterns such as mapping identify heterogeneous drip irrigation effect (Gonzalez-Dugo et al., 2013) and stomata conductance mapping in crop field (Berni et al., 2009). Application of satellite thermal remote sensing for vegetation water stress assessment is also useful for catchment scale water management and for natural ecosystem health monitoring (Moran et al., 1994).

First application of leaf temperature to indicate plant water stress dates back to 1960s' (Idso et al., 1981; Jackson et al., 1981). The simplest thermal index (based on infrared leaf temperature), canopy to air temperature difference (T_c-T_a), has been successfully applied to indicate water stress on crops (Idso et al., 1980). The index was later found unstable with varying atmospheric conditions (Idso et al., 1981). Crop water stress index (CWSI) was then proposed for more stable performance (Idso, 1982; Jackson et al., 1981). The index is normalized with the linear non-water-stress baseline (NWSB) established on well irrigated vegetation plots (see Figure 5-1). For partially vegetated catchments, Moran et al. (1994) argued that CWSI is not valid as the remotely sensed temperature does not distinguish leaf temperature from the soil background, thus CWSI can only be used on fully covered crops. They proposed to solve the problem

147

by combing remotely sensed vegetation index to decompose pixel temperature to estimate leaf temperature and suggested a new water deficit index (WDI). The idea has been adopted for evapotranspiration estimation with satellite remote sensing products. For ground-based thermal imaging, leaf/canopy temperature is directly resolved from the pixel because of its high spatial resolution (Jones et al., 2002) (see Appendix I for example).

Natural ecosystems differ from crop fields. It is sometimes impractical to transfer the same technique from agriculture fields to natural ecosystems in terms of the cost and efficiency. For example, to obtain the wet reference temperature required for CWSI calculation, manual operation such as irrigation practise is required. The intra-crown temperature variation index ($Std(T_c)$) stands out in this respect as it does not require extra measurement other than leaf temperatures. The index was proven effective on almond trees (Gonzalez-Dugo et al., 2012), but reported to be insensitive to water stress on citrus trees (Ballester et al., 2013; Villalobos et al., 2009).

Jackson et al. (1981) developed CWSI theoretically providing an alternative option to obtain the reference temperature through modelling. However, the index becomes difficult to apply in a heterogeneous landscape where aerodynamic resistance and stomata conductance across diverse tree species are usually unknown. It may not be an issue for spatial comparison of water status in homogenous crop fields where the atmospheric conditions can usually be assumed relatively uniform at one snapshot in time. It is more of a concern to detect water stress onset of a natural ecosystem, that is, the temporal evolution of soil or plant water status. However, the thermal method is often a function of local meteorological conditions (Moran et al., 1994), limiting its capacity to indicate water stress variation with time. The thermal method may be more

148

robust for spatial rather than temporal application.

Recent advances in several tree-crop studies seem to pose an additional challenge to the thermal remote sensing method, particularly in a Mediterranean climate. Villalobos et al. (2009) observed that stomata conductance can reduce significantly at midday due to high vapour pressure deficit (VPD) and thus the thermal indices suggest water stress even when the citrus trees are actually well irrigated. Ballester et al. (2013) also pointed out that leaf temperature became indistinguishable between well-irrigated and water-stressed tree crops beyond a VPD threshold (ca 2.7 kPa in the paper). This finding poses a question on the applicability of using leaf temperature in the Mediterranean climate zone where VPD is often high and water is most deficit in summer. Although VPD is considered in CWSI calculation, but only as a driving force, its impact on stomata conductance is not included. To relate the thermal index exclusively to plant water status, VPD effect on stomata conductance becomes critical in the calculation of thermal indices.

In this study, we aim to examine if leaf temperature in various thermal index forms are applicable as a water stress monitoring tool in a study site of Mediterranean climate and if VPD is the limiting factor in this applicability. We discuss the capacity of the thermal imaging method for temporal water status indication for two native species in a heterogeneous landscape.
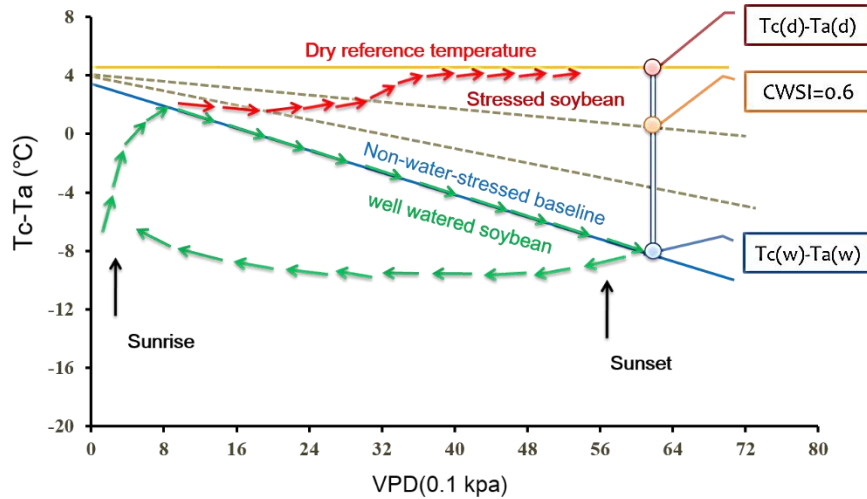
Figure 5-1: Schematic illustration of dependence of canopy temperature on plant water stress.

Note: T_c-T_a is the canopy to air temperature difference; $T_{c(d)}$ is the dry canopy temperature; $T_{c(w)}$ is the wet canopy temperature. The red arrows show the evolution of T_c of the stressed soy bean. The green arrows show the change of T_c of well irrigated plot over a day. The linear blue line is the non-water-stressed baseline (NWSB). Grey dashed lines are isolines indicating the same level of water stress (Jackson, 1982).

5.2 Materials and methods

5.2.1 Experimental setting up

The experiment was conducted on a hill slope (E 138.57 °, S 35.0317 °, sloping 20-30 °) in Flinders University campus, South Australia from 5 Jan, 2012 till 30 May, 2013. The two native tree species selected for investigation are *Eucalyptus microcarpa* and *Acacia pycnantha*, both of which are widely distributed in South Australia. The eucalyptus tree is 6.3 m tall with a large dense crown. The acacia tree is 3.8 m tall with very scattered branches, located 20 m upslope from the eucalyptus tree. Two thermal cameras (DALI company, 120×160 pixels, field of view 13 °×18 °) were positioned upslope from the trees, one at 6 m away from the eucalyptus tree to capture more than 80 % of the north-facing crown, the other camera was installed 2.4 m away to target one branch of acacia (to maximize the leaf area in the thermal image frame). Both

150

cameras were mounted on two fixed tripods so that the images have virtually the same view angle and distance to the targets throughout the whole experimental period. Leaf temperatures were taken every one min on most clear days from Jan, 2012 to May, 2013. The thermal images were at leaf level resolution (within 2 cm). Stem xylem water potentials were monitored with two stem psychrometers (ICT International, Australia) from Jan, 2012 to May, 2013 at interval of 15min (dry season) or 30min (wet season). One capacitance-based soil moisture probe (Sentek, Australia) was installed one metre downslope from each tree since Oct, 2012. Weather station was installed 21 Mar, 2012 several metres upslope of Acacia tree.

5.2.2 Data

Thermal cameras were set up from around 10 am to 4 pm on most of the clear days. The emissivity of the two cameras was fixed at 0.96. As infrared radiactive temperature of canopy surface can change quickly with wind speed, leaf temperautres within 30-min interval (30 data points) were averaged for all thermal indices calculation. For example, leaf temperaute at noon in this analysis is actually the averaged value of images taken from 11:45 am to 12:15 pm. The temperatures of leaves were extracted from the soil and sky background in thermal images with the expectation-maximation algorithm according to Wang et al. (2010) (see Appendix I).

Soil moisture satuation was estimated by scaling between the saturated and residual moisture content. The soil has three distinct horizons. The top layer is 10-30 cm loam, middle layer is 20-30 cm thickness of clay, and bottom layer is silty clay of 50-80 cm thickness. The overall soil moisture saturation of the root zone is calculated by summing up the three depth reading at 10, 30 and 50 cm by weight of [0.2, 0.3, 0.5] at the acacia site and by weight of [0.1 0.2, 0.2, 0.5] at eucalyptus site (a fourth sensor

151

at 100 cm depth). The weight is based on the soil layering (for example, at acacia site, 20 cm clayer is underlaid by 30 cm heavy clay and the bottom is silty clay). The heavier weight on the soil moisture at 50 cm depth (or 100 cm for the eucalyptus site) is to emphasize the larger contribution of deep water source. The priliminary results also indicate that the linear correlation between the thermal indices and deepest soil moisture content is most significant.

5.2.3 Thermal indices

Idso et al. (1981) observed that the canopy to air temperature difference (T_c-T_a) follows a linear relationship with VPD if the crops are well irrigated (the regression line is called non-water-stress baseline (NWSB), see Figure 5-1 and Eq. 5-1).

$$T_{c(w)} - T_{a(w)} = a \cdot \text{VPD} + b \tag{5-1}$$

where $T_{c(w)}$ is the wet reference temperature, taken from canopies of well irrigated plot (subscript "w" means "wet" plot with no water stress). $T_{a(w)}$ is the air temperature at the wet plot. "a" and "b" are empirical coefficients by the linear regression. A water stress index (CWSI) is then calculated following Idso et al., (1981).

$$\text{CWSI} = \frac{(T_c - T_a) - (T_{c(w)} - T_{a(w)})}{(T_{c(d)} - T_{a(d)}) - (T_{c(w)} - T_{a(w)})} \tag{5-2}$$

where, T_c is the canopy temperature of the target vegetation plot. T_a is the air temperature above that plot. $T_{c(d)}$ is the dry reference temperature, taken from the canopies of the dry plot (most stressed) and $T_{a(d)}$ is the air temperature correspondingly. Usually, common air temperature $T_a = T_{a(w)} = T_{a(d)}$ is used for simplicity under the assumption of little change of air temperature across the plots. $T_{c(d)}$ is usually assumed as a constant positive value which is obtained from upper limit of stressed plants (see

Eq 5-4).

Without baseline observation, CWSI can be modelled by combining Penman-Monteith equation and energy conservation equation (Jackson et al., 1981). The wet leaf temperature is modelled by assigning the zero canopy resistance (r_{cp}) following Jackson et al. (1981) or a certain value if it's known.

$$T_{c(w)} - T_{a(w)} = \frac{r_a R_n}{\rho_a C_p} \cdot \frac{\gamma(1 + r_{cp}/r_a)}{\Delta + \gamma(1 + r_{cp}/r_a)} - \frac{VPD}{\Delta + \gamma(1 + r_{cp}/r_a)} \qquad (5\text{-}3)$$

where R_n is the net radiation (W m^{-2}), ρ_a is the density of air (kg m^{-3}), C_p is the heat capacity of air (J kg^{-1} $^{\circ}$C^{-1}), r_a is the aerodynamic resistance (s m^{-1}), γ is the psychrometric constant (Pa $^{\circ}$C^{-1}). The dry leaf temperature is obtained by assuming infinitely large canopy resistance (replace r_{cp} with $r_c = +\infty$), then we have dry leaf temperature as

$$T_{c(d)} - T_{a(d)} = \frac{r_a R_n}{\rho_a C_p} \qquad (5\text{-}4)$$

Therefore, CWSI calculated with the baseline observation is referred to empirical CWSI$_v$; theoretical modelling with Eq. 5-3 & 5-4 is referred to theoretical CWSI$_t$ (Moran et al., 1994). The term r_a is calculated with

$$r_a = \frac{\{\ln[(z-d)/z_o]/k\}^2}{U} \qquad (5\text{-}5)$$

where z is the height of wind speed measurement (m), d is the displacement height (m), z_0 is the roughness length (m), k is the von Karman constant (~0.4), and U is wind speed (m s^{-1}). d and z_0 are calculated from tree height (d=0.66, zo=0.13h, where h is tree height). Parameter d and z_0 is tricky to obtain over heterogeneous landscape such

153

as the one in this study. The empirical function seems reasonable compared to r_a value from inverse modeling of Eq. 5-4 with dead leaf temperature of acacia tree (assuming $r_c = +\infty$). The value of r_a for eucalyptus trees will be discussed in the next section.

Canopy temperature is a statistical mean of leaf temperatures, distribution of leaf temperature may be more suitable to indicate the water stress level (Fuchs, 1990). Only a few studies have explored the leaf temperature distribution and until recently, a study has explicitly validated a related index on the almond tree crop − the intra crown leaf temperature variation (Std(T_c)) (Gonzalez-Dugo et al., 2012) .

$$\text{Std}(T_c) = \sqrt{\frac{\sum (T_{c,i} - \overline{T_c})^2}{n-1}} \tag{5-6}$$

$T_{c,i}$ is the temperature of a leaf pixel i, and $\overline{T_c}$ is the average temperature of all leaf pixels with total number of n. However, standard deviation of canopy temperature is a non-monotonic function of water stress; for example, it displays peak value at modest stress and lower values at either severely stressed or non-stressed trees (Gonzalez-Dugo et al., 2012). To solve this problem, we suggest a new index: adjusted standard deviation of leaf temperatures (aStd(T_c)) (see Eq. 5-7). By multiplying Std(T_c) with $\dfrac{\overline{T_c} - T_a}{\overline{T_c}}$, the new index distinguishes the situations between severe water stressed (T_c-T_a is positive) or non-water stressed conditions (T_c-T_a is negative).

$$\text{aStd}(T_c) = \sqrt{\frac{\sum (T_{c,i} - \overline{T_c})^2}{n-1}} \cdot \frac{\overline{T_c} - T_a}{\overline{T_c}} \tag{5-7}$$

The capacity of the thermal indices in detecting water stress is commonly evaluated by simple comparison against plant or soil water status such as linear regression

analysis. However, for water management purposes, more acute quantitative tool should be applied to detect the occurrence of water stress with the thermal method. We here suggest to use Monte Carlo sampling technique to test if the thermal indices can capture the temporal evolution of plant water stress. The time-series of leaf temperature are separated into segments of around one week length, resulting in 20 representative points of each thermal index over the observation period. The performance of the indices are then tested against benchmark water stress indicators (observed soil moisture content or stem water potential). Identifiability of the thermal indices is defined as rejection of the null hypothesis that the observation of one segment comes from a normal distribution of another segment at a significance level of 0.1 (z test with Matlab). For example, if CWSI shows a mean value of 0.5 over a week, while CWSI of another week shows large variation (three observation points: 0.5, 0.4, 0.6) with also a mean value of 0.5, CWSI is then not identifiable between the two segments, indicating that it fails to capture the water stress evolution over the weeks. The Monte Carlo sampling technique will be used to randomly choose any two segment and to test the identifiability of the indices over various water stress conditions.

5.3 Results and discussion

5.3.1 Thermal indices evaluation

From Jan 2012 till to Jan 2013, Adelaide experienced an average meteorological year of the local Mediterranean climate (compared to long term average). Soil moisture content (θ) and pre-dawn stem water potential ($\psi_{x,pd}$) reveal a dry to wet (Jan, 2012 to Sep, 2012) and wet to dry cycle (Oct, 2012 to Apr, 2013). The hottest month of the period is Feb, 2013 and driest month is Apr, 2013.
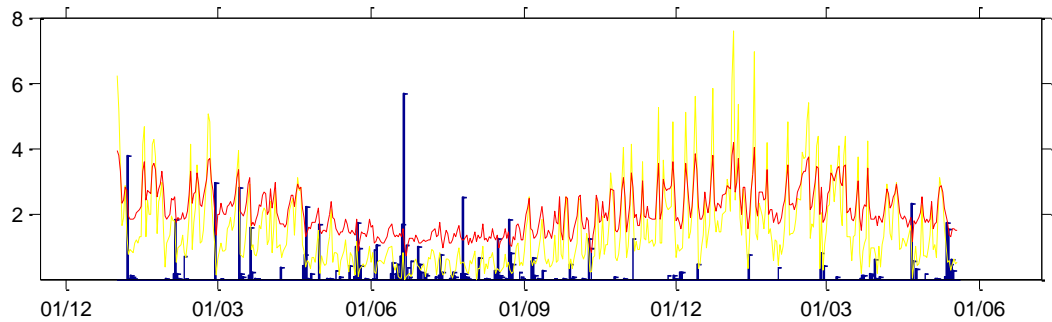
Figure 5-2: Daily rainfall (cm, blue bar), air temperature (divided by 10 °C, red line), and VPD (kPa, yellow line) from 1 Dec, 2011 to 1 Jun, 2013 (date format: dd/mm from year 2011 to 2013)

The pre-dawn stem water potential ($\psi_{x,pd}$) was observed in a small range from -0.2 to -0.5 MPa during winter time and in a much larger range from -1.0 to -3.0 MPa during hot summer. Soil moisture content (θ) instead shows much smaller variation in summer than winter. Both $\psi_{x,pd}$ and θ indicate increasing water stress of the trees from Oct 2012 to Feb 2013.

The continuous observation with thermal imaging during a day provides an opportunity to examine the best time window for applying thermal indices. To allow a fair comparison, only those images taken on clear days with complete continuous measurements of leaf temperature from 10:30 am to 15:30 pm are included, resulting in 28 observation points. Figure 5-3 shows the sensitivity of thermal indices varying over the time of day for different tree species. For the acacia tree, morning time does not seem to be a good observation time window, while for the eucalyptus tree, all indices except the standard deviation of leaf temperatures Std(T_c) perform in a rather stable manner throughout the day. For an individual thermal index, the sensitivity also varies temporally. Std(T_c) seem to show increasing significant correlation with $\psi_{x,pd}$ or Θ into the afternoon with highest significance (R<-0.6) at 15:30 pm (see the upper right panel). While other indices follow the same temporal pattern with early afternoon as the best time window. Overall, the new index, the adjusted standard deviation

156

aStd(T_c), performs as well as other indices for the acacia tree and the best for the eucalyptus tree. As water stress increased, leaf temperature variation (std(T_c)) would increase as well as the mean leaf temperature (T_c); multiplying the two would magnify the effect of water stress, which may explain for the good performance of the new index. Although involving local weather normalization, $CWSI_v$, does not show any advantage over simple indices such as T_c -T_a or aStd(T_c). Std(T_c) does not perform well on the acacia tree whether compared to $\psi_{x,pd}$ or θ.
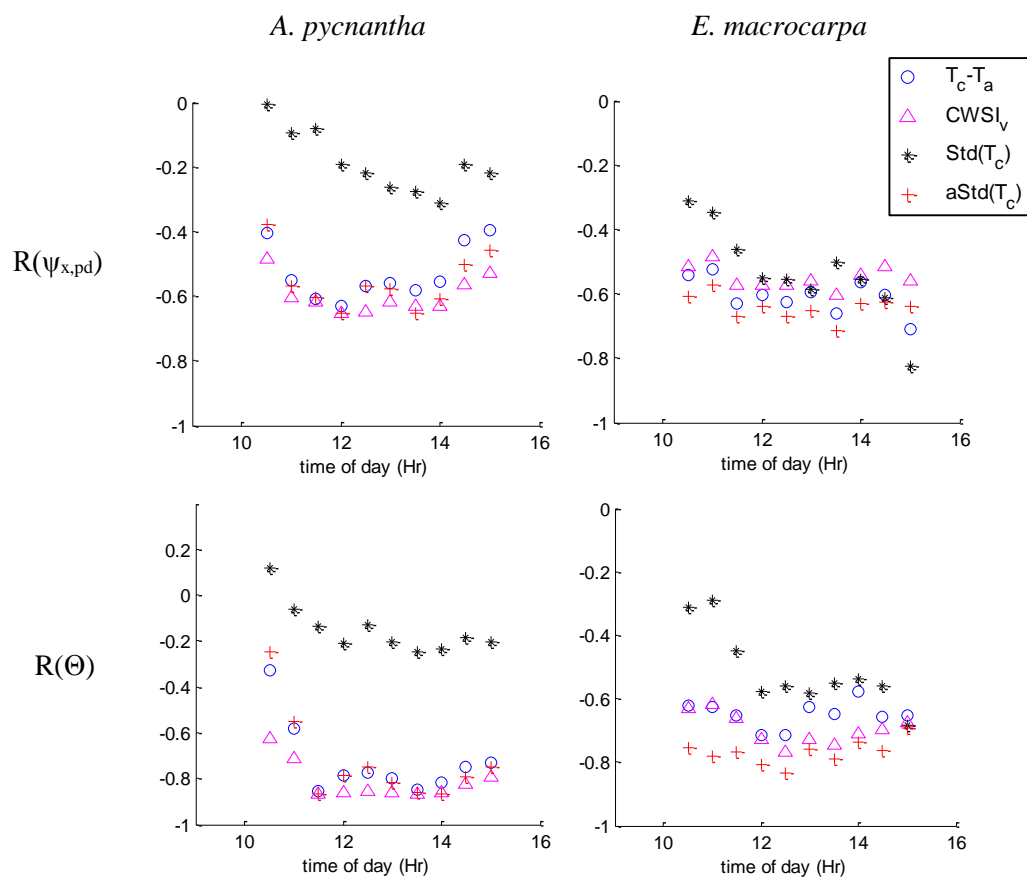
Figure 5-3: Pearson correlation coefficient (R) between thermal indices (in legends) and pre-dawn stem water potential ($\psi_{x,pd}$) (upper panels) and soil moisture saturation (Θ) (lower panels) through the day. The left column is on the acacia tree and right is on the eucalyptus tree. Correlation is significant when R < -0.5 (at 0.05 level).

The thermal indices show optimal performance at different times over the day; to maximize the observation data points, midday leaf temperature from 11:45 am to 12:15 pm are selected for daily water stress comparison. Figure 5-4 shows time series of all

thermal indices calculated with midday observation. It is found that the temporal evolution of soil water status can be captured by all thermal indices except for $Std(T_c)$. The depression of $Std(T_c)$ on acacia corresponds to the hottest months of Jan and Feb in year 2013 (see the upper left panel). However, the phenomena is not observed on the eucalyptus tree (see lower left panel). It may be due to their different responses to heat. The highly dynamic weather condition can induce large uncertainty in thermal indices performance. In the top left graph, the 1 min T_c-T_a (grey background) displays large temperature fluctuation around the 30 min mean value due to frequent wind strokes. It suggests that thermal indices based on canopy temperature at one snapshot may result in unreliable water stress indication. Using average values appears to smooth out the temperature fluctuation. Besides, cloudy conditions deteriorate the performance (see hollow circles), and should thus be avoided for thermal indices calculation. $\psi_{x,pd}$ observation covers two summers on the acacia tree and reveals a wetter summer in year 2012 than 2013. However, the thermal indices do not show the water stress difference between the two summers (see the upper left panel).
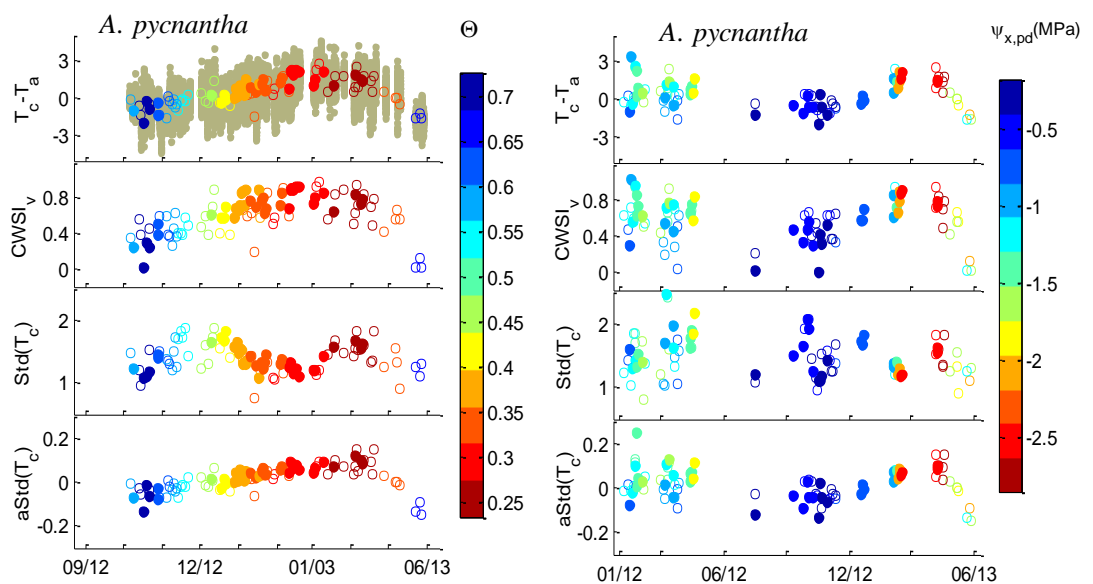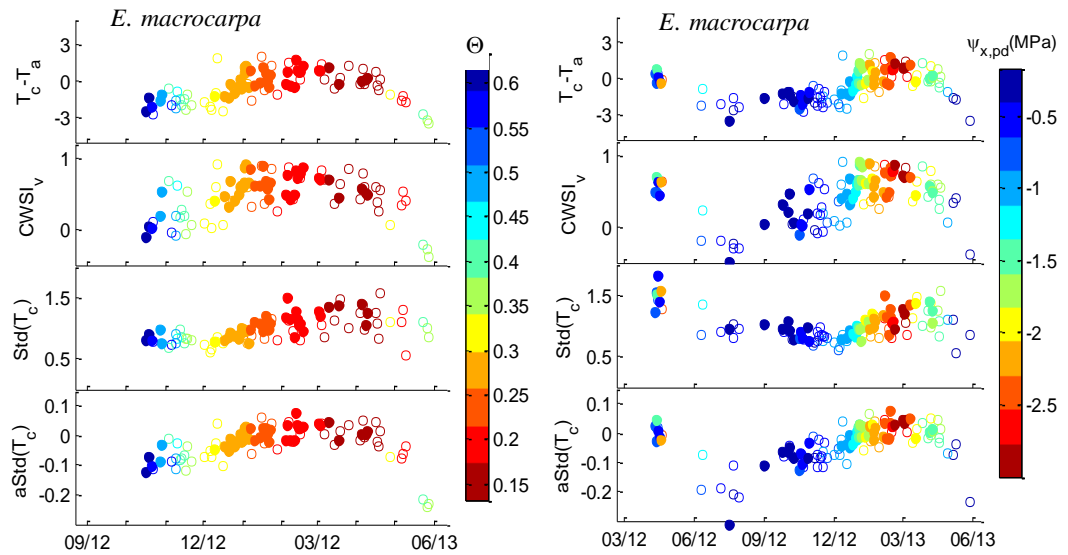
Figure 5-4: Temporal evolution of thermal indices in comparison to water status indicated by Θ (left panels) and $\psi_{x,pd}$ (right panels).

Note: The x-axis shows the date in a format of mm/yy. $CWSI_v$ is calculated from NWSB: $T_{c(w)} - T_a = -2 \times VPD + 1$ (A.*pycnantha*) and $T_{c(w)} - T_a = -2 \times VPD$ (E. *macrocarpa*), dry reference for both is set as constant $T_{c(d)} - T_a = 3\,^{\circ}C$. The grey dots of the upper left panel shows 1 min $T_c - T_a$ around the 30 min average. The filled circles are data under clear sky condition; hollow circles are data of days with intermittent cloudy conditions.

To examine the capability of thermal indices for temporal water stress detection quantitatively, the time series are separated into segments between rainfall events (further decomposition to keep segments within 1 week, see Figure 5-5). Only segments that include at least three observation points at clear sky window are counted as a useful one. The water status within one segment is deemed stationary. The v-SPAC (see chapter 2) is used to fill the data gap of soil moisture and stem water potential. The gap-filled dataset is used to compare the wetting cycle (from Jan 2012 to Sep, 2013) and the drying cycle (from Oct, 2012 to Mar, 2013).
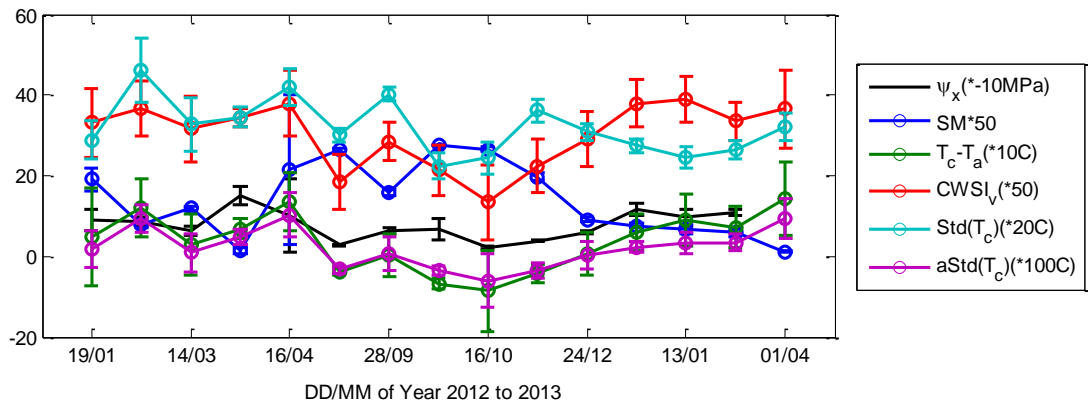
Figure 5-5: Segmentation of time series of thermal indices, Θ and $\psi_{x,pd}$ (gap filled by v-SPAC modelling for the acacia site). Circles represent averaged values. Error bars show the standard deviation of observation in each segment.

Note: soil moisture before 16/10/2012 is filled by v-SPAC modelling. The stem xylem water potential is also filed in times other than summer.

Thermal indices in each segment are compared against soil water status or stem water potential in Figure 5-6. All data are linearly scaled to 0 to 1 over the whole sampling period for normalization between the trees. The thermal indices indicate comparable relative water status between the acacia and eucalyptus trees although the absolute values differ. The empirical crop water stress index $CWSI_v$ does not perform better than simple indices as T_c-T_a or $aStd(T_c)$. The intra-crown leaf temperature variation $Std(T_c)$ of the acacia tree does not show significant correlation with Θ or $\psi_{x,pd}$, but it seems to work on eucalyptus when compared to Θ during the wet to dry cycle. The new index $aStd(T_c)$ works for both trees and performs consistently as well as other indices, while keeping its simplicity without involvement of the reference temperatures. Gap-filled time-series are sufficient long to capture the trend in each segment, so that, the correlation is analysed with the de-trended data (all data are subtract a best-fit line to remove the linear trend). Thus, Figure 5-7 shows much smaller standard deviation than Figure 5-6. However, both figures essentially show the same capacity of the thermal indices.

160
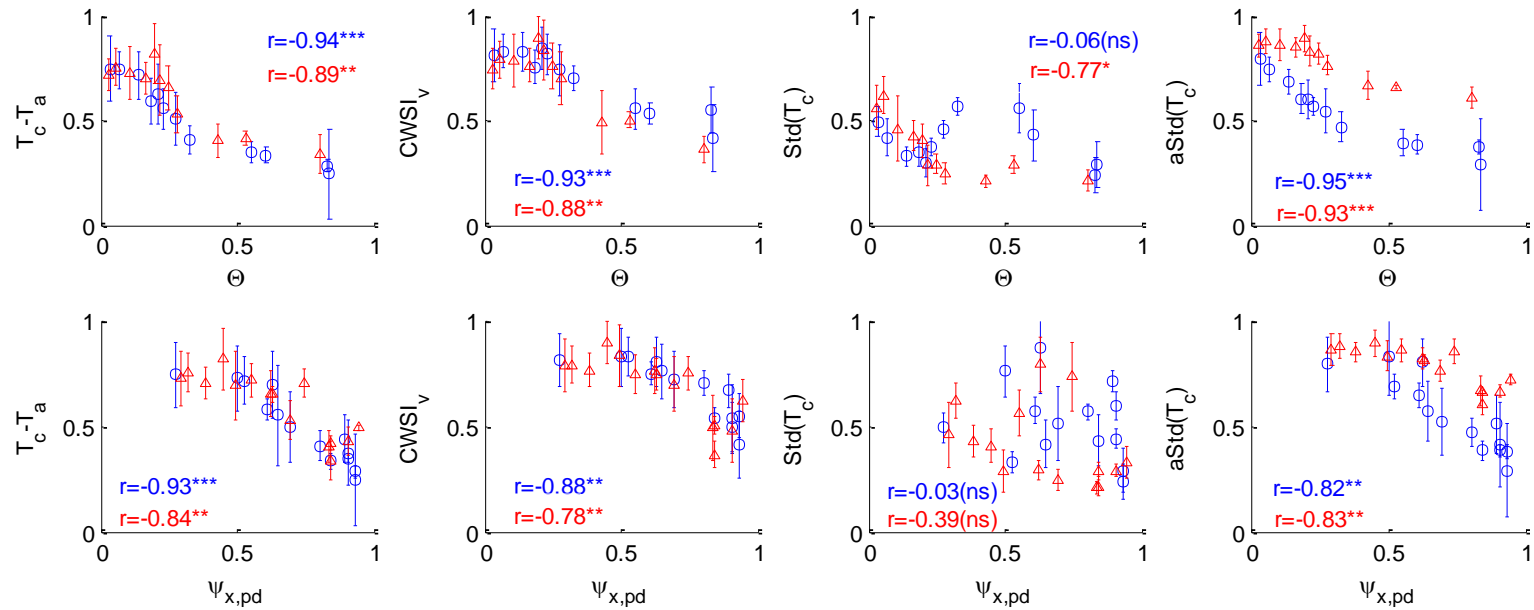
Figure 5-6: Thermal indices versus Θ and ψ$_{x,pd}$ on clear days, blue circles are for the *A. pycnantha* tree, red triangles are for the *E. macrocarpa* tree.

Note: The x-axis are normalized between maximum and minimum values to allow comparison between the two tree species. Error bars plot the standard deviation within the segment; r shows the Pearson correlation coefficient; ***means significance level of 0.001, ** at the level of 0.05 and * at 0.1 level and "ns" means no significance at 0.1 level.
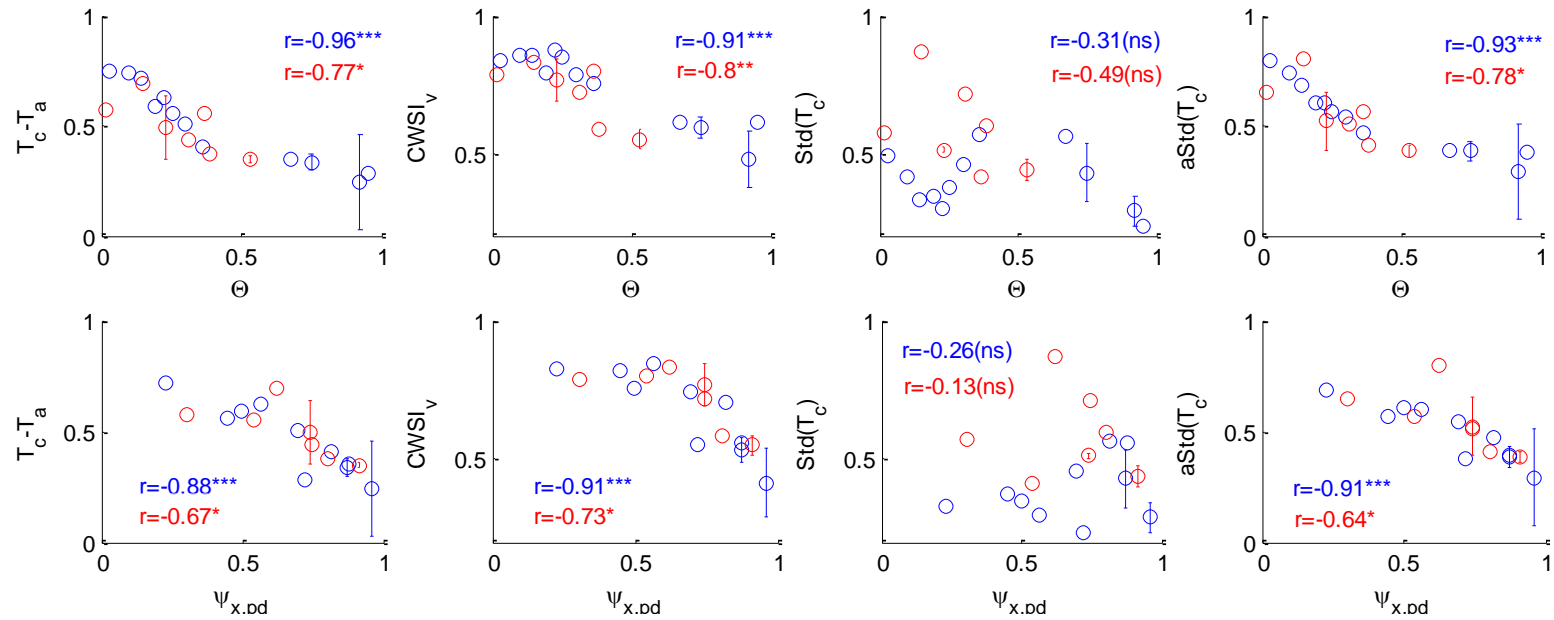
Figure 5-7: Thermal indices compared against v-SPAC model gap filled Θ and $\psi_{x,pd}$ over clear days of the *A. pycnantha* tree.

Note: blue shows drying cycle from Oct, 2012 to Mar, 2013, red circles shows wetting cycle from Jan 2012 to Apr 2012 (leaf temperature of 2012 winter is not measured); error bars show the standard deviation from de-trended time-series; r shows the Pearson correlation coefficient; ***means significance level of 0.001, ** at level of 0.05 and * at 0.1 level and "ns" means no significance at 0.1 level.

The results above indicate that three of the four thermal indices (T_c-T_a, CWSI, aStd(T_c)) capture the temporal evolution of water stress for the two tree species. However, as mentioned previously a large variation of thermal indices can occur within days even under a similar root-zone water condition and identifiably of the thermal indices should be tested with the Monte Carlo sampling technique. The simulation results show that the water status from Jun 2012 to Sep 2012 is not identifiable from $\psi_{x,pd}$ measurements (see Figure 5-5), while Θ is not identifiable from Jan 2013 through to Mar 2013. It indicates that during the dry seasons, stem water potential shows higher sensitivity to plant/soil water status than soil moisture content.

Table 5-1 shows the Monte Carlo simulation results of the thermal indices. The thermal indices are tested on conditions when the difference in Θ or $\psi_{x,pd}$ is identifiable. This implies that the thermal indices are not capable of detecting the slowly developing water stress (by comparing adjacent time segments), unless the water status differs by more than 0.15 in Θ or more than 0.5 MPa in $\psi_{x,pd}$. This indicates that thermal indices may only be reliable to detect water status between months when water stress progress apparently. An improvement in the confidence of the thermal indices detection capacity will occur with more frequent observations from which a reliable trend can be seen.

Table 5-1: Probability of giving identifiable thermal indices when soil moisture or stem water potential are significantly different (>=0.9 means identifiable at significance level of 0.1)

	E. macrocarpa				*A. pycnantha*			
Θ	Tc-Ta	$CWSI_v$	Std(T_c)	aStd(T_c)	Tc-Ta	$CWSI_v$	Std(T_c)	aStd(T_c)
0.10	0.7	0.8	0.6	0.8	0.7	0.7	0.1	0.7
0.15	**0.9**	**0.9**	0.6	**0.9**	0.8	**0.9**	0.1	**0.9**
0.20	**0.9**	**0.9**	0.5	**0.9**	**0.9**	**0.9**	0.2	**0.9**

0.22	**0.9**	**0.9**	0.7	**0.9**	**0.9**	**0.9**	0.1	**0.9**
0.25	**1.0**	**1.0**	0.7	**1.0**	**0.9**	**0.9**	0.2	**0.9**
$\Psi_{x,pd}$ (MPa)								
0.2	0.6	0.4	0.4	0.6	0.3	0.3	0.3	0.3
0.5	0.6	0.5	0.4	0.7	0.4	0.3	0.3	0.4
0.8	0.6*	0.4	0.5	0.7*	0.5	0.4	0.4	0.5
1.0	0.7*	0.5*	0.5	0.8*	0.6	0.5	0.4	0.6

Note: the first column are criteria set for the Monte Carlo running. For example, 0.20 under Θ is set when two segments differ beyond 0.20 in Θ; 0.5 under $\psi_{x,pd}$ sets the condition when the two segments have $\psi_{x,pd}$ difference larger than 0.5 MPa. The bold figures show that the thermal indices are identifiable at significance level of 0.1. The stars * indicate that thermal indices are identifiable when only the drying cycle (Oct, 2012 to Feb, 2013) of $\psi_{x,pd}$ are considered.

The experiment further confirms that Std(T_c) does not perform consistently across tree species (Ballester et al., 2013). The difference between the two tree species may be explained by a numerical modelling study of an ideal tree of spherical distribution of leaf inclination angles (Fuchs, 1990). The modelling shows the case that when the viewing plate is perpendicular to the solar zenith angle, leaf temperature variation due to water stress increases with solar zenith angle. Mid-afternoon time may be the best time to indicate water stress with Std(T_c) for tree species such as *Eucalyptus macrocarpa* which has a dense sphere crown. *Acacia pycnantha*, instead, has near vertical leaf orientation which may account for the Std(T_c) failure. Grant et al. (2007) reported that Std(T_c) did not work in a grapevine in which the vertical profile of the crown or branch was taken in thermal images. The sampling size of the leaves could be another reason. Sampling one branch of leaves may not be sufficient to reveal the overall tree water status in some cases, such as the case of the acacia tree in this study and the grapevine in Grant et al.(2007). However, general conclusions on factors affecting the performance of Std(T_c) cannot be drawn as studies investigating the leaf

temperature distribution are limited. The various mechanisms behind this are yet to be quantified, such as canopy structure, viewing angle and sampling size. Numerical modelling of tree canopies for species such as *Acacia pycnantha* is worth further investigation in order to better understand the mechanisms.

5.3.2 CWSI$_t$ evaluation

The theoretical crop water stress index CWSI$_t$ is evaluated separately from other thermal indices as the value is non-unique and dependent on parameterization of aerodynamic resistance (r_a) and potential stomata resistance (r_{cp}) (see Figure 5-8). As shown in Eq. 5-5, the empircal equations of displacement height and roughness length is established for homogeneous land cover which is difficult to apply on individual trees on a hillslope. r_{cp} is usually assumed as zero (such as Jackson et al. (1981)) or a constant value (Berni et al., 2009) in CWSI calculations for simplicity.
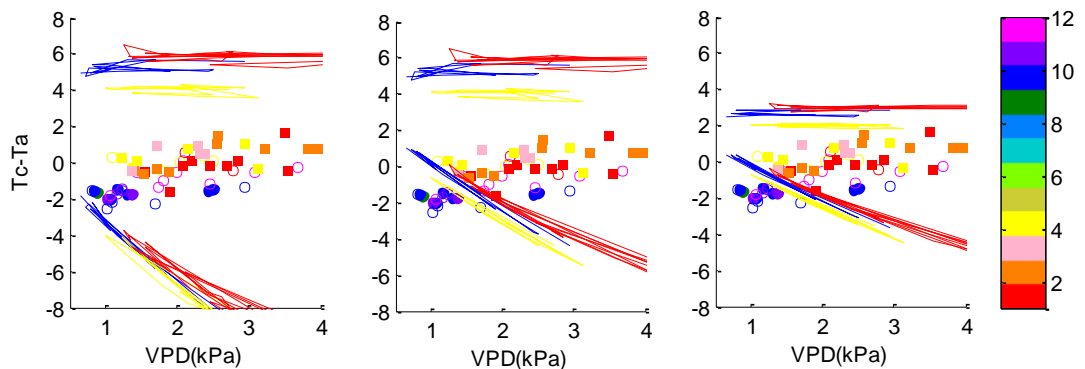
Figure 5-8: T$_c$-T$_a$ versus VPD of the *E. macrocarpa* tree with different wet and dry reference temperatures. Colour bars show the month number.

Note: the solid line at the top of panels are the theoretical upper limits (T$_{c(d)}$ -T$_a$) calculated with Eq. 4 for month Jun, Oct and Jan and lines at the bottom are NWSB calculated with Eq. 3. Pair parameters (r_a, r_{cp}) are r_a=10, r_{cp} = 0; r_a=10, r_{cp} =10; and r_a =5, r_{cp} =20 s/m from left to right panels. Filled circles represent non-water-stressed days ($\psi_{x,pd}$>-0.5MPa), hollow circles between -0.5 and -1.5MPa, indicating mild to modest water stress, and filled squares at $\psi_{x,pd}$ < -1.5MPa showing modest to severe water stress of the year.

The empirical CWSI$_v$ is actually the simpler form of CWSI$_t$ without involing the

complex calculation of aerodynamic resistance r_a and net radiation R_n. $CWSI_t$ can be reduced to a VPD dominated equation when r_a is relatively small which is common for open tree canopies (Villalobos et al., 2009). For the eucalyptus tree, including varied r_a does not show improvement of $CWSI_t$ over $CWSI_v$ (not shown). It could be due to the local heteogeneity of the wind field. $CWSI_t$ only improves the empirical $CWSI_v$ marginally for the acacia tree (Pearson correlation R increased from 0.93 to 0.95 when compared to Θ).

5.3.3 VPD impact on thermal indices performance

Figure 5-8 shows that the baselines may give reasonable CWSI values for conditions at VPD < 2 kPa, but unreasonable high water stress when VPD >2 kPa for data points with $\psi_{x,pd} >-0.5$MPa (see Oct data points), indicating a "false alarm" of water stress. We presume that it's due to the stomata conductance reduction in response to high VPD (beyond 1.5 kPa). Lange et al. (1987) reported a midday depression of stomata conductance of well watered *Acacia longifolia* and *Acacia melanoxylon* during summer and autumn. However, this phenomenon was only observed in their Portugal experiment but not on *Acacia ligulata* and *Acacia melanoxylon* in their Australia experiment. The maximum leaf to air VPD was much lower (< 2 kPa) in the experiment in Australia than in Portugal (2-4 kPa). This suggests that there might be a VPD threshold beyond which the G_s to VPD behaves differently. Villalobos et al. (2009) observed that G_s reduced dramatically at midday on *Clementina mandarin*, and Ballester et al. (2013) showed that the leaf temperature was not sensitive to water stress when VPD was higher than 2.7 kPa. These results indicate that VPD induced stress may dominate the water stress after a particular threshold.

A photosynthetic experiment with LI-6400XT photosynthesis analyser (LI-COR

Biosciences, USA) near this study site shed some light on G_s response to VPD on the Australian native species (see Figure 5-9). The experiment was carried out on other acacia trees (same species) and another eucalyptus tree species (*Eucalyptus torquata*) within 100 metres of the measurement site from 16 Apr to 29 May, 2013 (see details in Appendix II). Leaf temperature is fixed around 20ºC which can exclude the temperature influence on G_s. The experiment was intended for light response curves. To exclude the influence of light, only those observed under light saturation condition are plotted (Photosynthetic active radiation intensity >= 1000 μmol photon m^{-2} s^{-1}) against VPD.
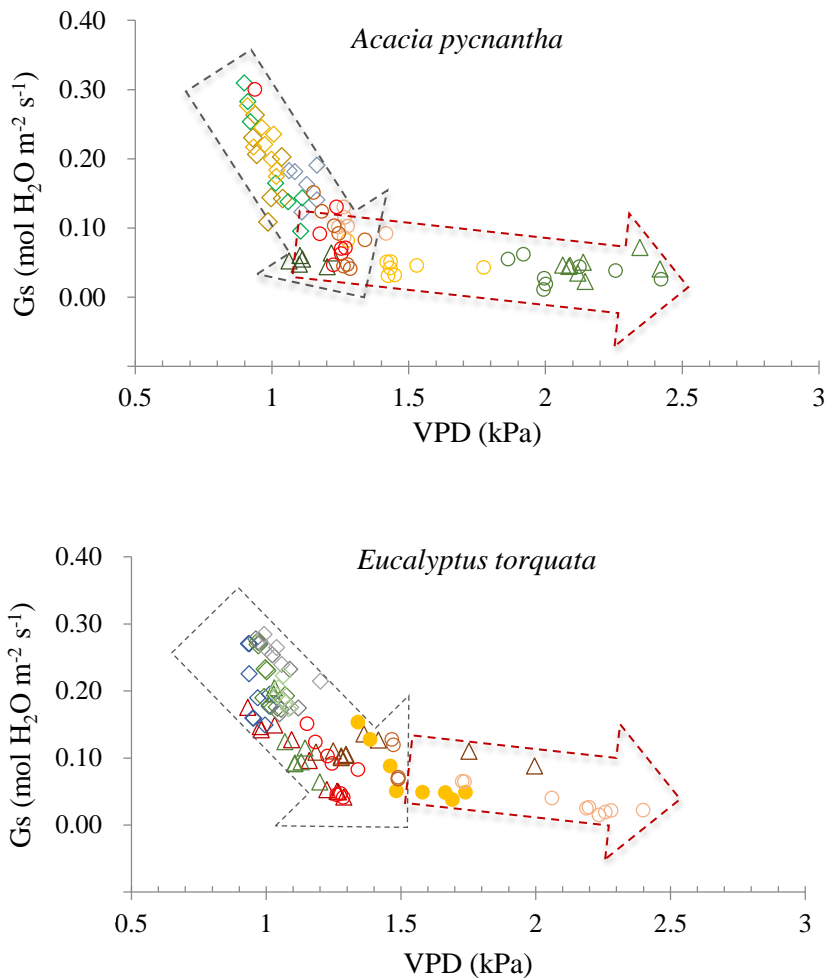
Figure 5-9: Stomata conductance (G_s) in response to VPD of *A. pycnantha* and *E. torquate*. Note: different symbols represent different days; triangle represent water stressed days ($\Theta <$ 1/3, indicated by soil moisture probe at the acacia site), circles at $\Theta =$ 1/3 - 2/3 and diamond

at $\Theta > 2/3$.

The measured stomata conductance (G_s) may reflect the differences between leaves. However, a one day measurement on *Eucalyptus torquate* clearly shows the transition of G_s response to VPD after 1.5 kPa (see solid orange points). G_s shows different sensitivity to VPD at different ranges: G_s reduced more than 5 fold when VPD increased from 0.9 to 1.2 kPa at 2/3 Θ, which is at the same magnitude of G_s reduction from 2/3 to 1/3 Θ. G_s seems to be much less sensitive to VPD beyond around 1.0 kPa for the *A. pycnantha* trees and 1.5 kPa for the *E. torquate* trees. This may explain the better performance of the thermal indices in the drier months (see Figure 5-6), as G_s in wet months (correspond to lower VPD) will change dramatically over a small variation of VPD (see Figure 5-9). It implies that r_{cp} should not be assigned a fixed value but varied with sensitivity to VPD. Assuming T_c-T_a is proportional to G_s (see Figure 5-1), and the rate of G_s reduction after VPD > 1.5 kPa is 1/10 of that when VPD < 1.5 kPa (or 1.0 kPa for the acacia), the baseline slope is changed accordingly (see Figure 5-10).
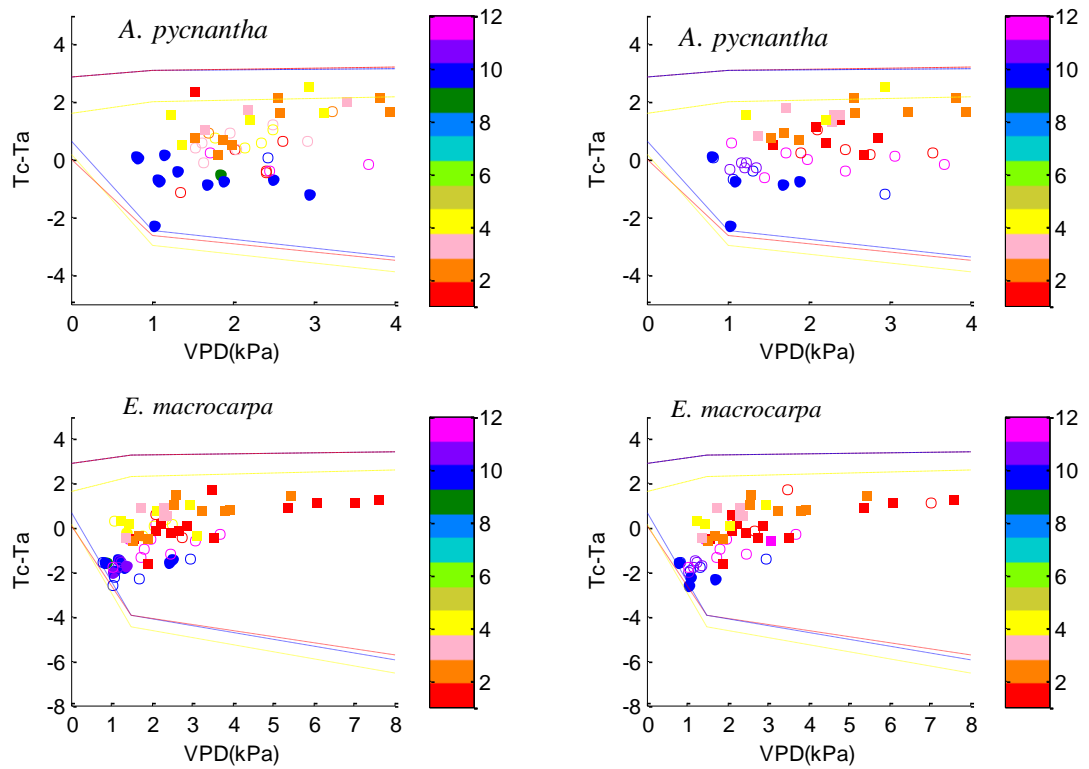
Figure 5-10: T_c-T_a versus VPD of the *A. pycnantha* tree and the *E. macrocarpa* tree with new non-water-stressed baseline (NWSB).

Note: The dashed lines above the points show the dry reference temperature and lines below the points are the wet reference temperature. The left panels indicate water stress level with $\psi_{x,pd}$, the right panels with Θ: filled circles are points with $\Theta > 2/3$ or $\psi_{x,pd} > -0.5$MPa, hollow circles are points with $\Theta = 1/2 - 2/3$ or $\psi_{x,pd}$ between $-0.5 \sim -1.5$MPa, filled squares are $\Theta < 1/3$ or $\psi_{x,pd}$ below -1.5MPa. The slope of NWSB is reduced to $1/10$ beyond VPD threshold (1.5 kPa for the eucalyptus tree and 1.0 kPa for the acacia tree).

The CWSI$_v$ index is then recalculated with the new baseline (Figure 5-10). The resulting CWSI$_v$ performs similarly to the CWSI$_t$ with Pearson correlation coefficient increasing from 0.93 to 0.97 (see Figure 5-11). The good fitting obtained by linear regression indicates that, correction for the VPD effect with the new baseline makes the new CWSI$_v$ index comparable over the whole soil wetness range. The plateau of the old CWSI$_v$ index over the dry condition ($\Theta < 0.3$) and larger variation in the wet condition ($\Theta > 0.6$), indicates that the linear interpolation that is commonly used in interpolating soil wetness with satellite imaging may not be appropriate (see Figure 5-11).
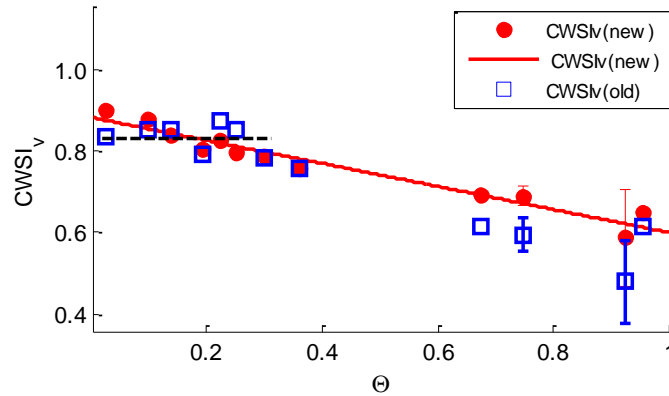
Figure 5-11: Performance of the new CWSI$_v$ obtained from the new NWSB (red dots) compared against CWSI$_v$ from the linear NWSB (blue rectangle).

It is interesting to note that no studies have reported midday depression of leaf temperature in herb crops. The herb crops usually have high decoupling factors (Ω) from the bulk air (such as soy bean $\Omega >0.8$ (Campbell and Norman, 1998) and typical value of 0.6 in wheat (Jarvis and McNaughton, 1986)), the actual VPD at leaf-air interface may have reduced to an equilibrium value that is much lower than the bulk air VPD (Jarvis and McNaughton, 1986). The microclimate can be modified by irrigation, preventing VPD at leaf-air interface to go beyond the VPD threshold where G_s sensitivity to VPD changes. The trees, instead, often have low decoupling factor (Campbell and Norman, 1998); the bulk air VPD can be used as substitute of leaf to air VPD, and it will experience a wide range of VPD in which G_s sensitivity may change. Therefore, it is meaningful to detect the G_s response to VPD of tree canopies before CWSI is used for water stress detection.

5.3.4 Implication on scaling issues

Thermal indices and related infrared remote sensing methods have been increasingly used to estimate large scale soil moisture condition, or ecosystem water requirements (like CWSI or WDI index) (Anderson et al., 2012, Moran et al., 1994, Yang and Shang, 2013). Linear interpolation between wet and dry reference temperatures are commonly

used to upscale transpiration for regional landscape using satellite images. In addition, to obtain the whole year water balance requires temporal up-scaling of soil moisture condition between satellite images. The results of this study imply that the linear interpolation scheme may not be appropriate to update the soil wetness of the satellite bypass gaps when large VPD variation is likely to occur. The in-phase change of water stress of both the acacia and eucalyptus trees shows reliability to interpolate soil water status linearly of the drier period, but not in wetter period due to leaf temperature insensitivity to soil moisture saturation (see Figure 5-6). It is thus recommended that the sensitivity of the leaf temperature over whole range of soil wetness is tested before applying the linear upscaling scheme.

5.4 Conclusions

In this study, the thermal imaging method is tested against plant water stress indicators on two tree species under the Mediterranean climate. Three of the four examined thermal indices (T_c–T_a, CWSI, aStd(T_c)) capture the overall temporal evolution of water stress indicated by soil moisture content and pre-dawn stem water potential. Early afternoon is found to be the best time window for leaf/canopy temperature observation. The proposed index - adjusted leaf temperature variation aStd(T_c) proves to work as well as other existing indices and remains simpler. The intra-crown leaf temperature variation index Std(T_c) does not work for the *Acacia pycnantha* tree but is comparable on the Eucalyptus *macrocarpa* tree for the drying cycle from Oct 2012 to Mar 2013. The widely-used crop water stress index (CWSI) reflects stress lumped from soil water depletion and high VPD stress. Instead of using one straight line as the non-water-stressed baseline, a new spline is proposed that the slope decreases 10 fold beyond the VPD threshold at 1.5 kPa (for the *Eucalyptus macrocarpa* tree) and 1.0 kPa (for the *Acacia pycnantha* tree). Based on the new spline, the empirical CWSI$_v$

171

performance improves over the whole range of soil wetness. It is suggested that the stomata conductance sensitivity to VPD should be examined before applying the thermal method over seasons. In addition, the results of this study suggest that linear interpolation schemes requires justification for the purpose of soil/root zone water status updating between two satellites images.

References

Anderson, M. C., Allen, R. G., Morse, A., and Kustas, W. P. 2012. Use of Landsat thermal imagery in monitoring evapotranspiration and managing water resources. Remote Sensing of Environment, 122, 50-65.

Ballester, C., Jimenez-Bello, M.A., Castel, J.R., Intrigliolo, D.S., 2013. Usefulness of thermography for plant water stress detection in citrus and persimmon trees. Agricultural and Forest Meteorology, 168: 120-129.

Berni, J., Zarco-Tejada, P., Sepulcre-Canto, G., Fereres, E., Villalobos, F., 2009. Mapping canopy conductance and CWSI in olive orchards using high resolution thermal remote sensing imagery. Remote Sensing of Environment, 113(11): 2380-2388.

Campbell, G.S., Norman, J.M., 1998. An Introduction to Environmental Biophysics.

Fuchs, M., 1990. Infrared measurement of canopy temperature and detection of plant water-stress. Theoretical and Applied Climatology, 42(4): 253-261.

Gonzalez-Dugo, V. et al., 2012. Almond tree canopy temperature reveals intra-crown variability that is water stress-dependent. Agricultural and Forest Meteorology, 154: 156-165.

Gonzalez-Dugo, V. et al., 2013. Using high resolution UAV thermal imagery to assess the variability in the water status of five fruit tree species within a commercial orchard. Precision Agriculture, 14(6): 660-678.

Grant, O.M., Tronina, L., Jones, H.G., Chaves, M.M., 2007. Exploring thermal imaging variables for the detection of stress responses in grapevine under different irrigation regimes. Journal of Experimental Botany, 58(4): 815-825.

Idso, S., 1982. Non-water-stressed baselines- a key to measure and interpreting plant water-stress. Agricultural Meteorology, 27(1-2): 59-70.

Idso, S., Jackson, R., Pinter, P., Reginato, R., Hatfield, J., 1981. Normalizing the stress-degree-day parameter for environtal variability Agricultural Meteorology, 24(1): 45-55.

Idso, S. et al., 1980. A generalization of the stress-degree-day concept of yield prediction to accommodate a diversity of crops. Agricultural Meteorology, 21(3): 205-211.

Jackson, R.D., 1982. Soil-moisture inferences from thermal-infrared measurements of vegetation temperatures. Ieee Transactions on Geoscience and Remote Sensing, 20(3): 282-286.

Jackson, R.D., Idso, S.B., Reginato, R.J., Pinter, P.J., 1981. Canopy temperature as a crop water-stress indicator. Water Resources Research, 17(4): 1133-1138.

Jarvis, P.G., McNaughton, K.G., 1986. Stomatal control of transpiration - scaling up from leaf to region. Advances in Ecological Research, 15.

Jones, H.G., 2007. Monitoring plant and soil water status: established and novel methods revisited and their relevance to studies of drought tolerance. Journal of Experimental Botany, 58(2): 119-130.

Jones, H.G. et al., 2002. Use of infrared thermography for monitoring stomatal closure in the field: application to grapevine. Journal of Experimental Botany, 53(378): 2249-2260.

Lange, O. L., Ullmann, I., Tenhunen, J. D., & Bannister, P. 1987. Stomatal conductance and transpiration of the two faces of Acacia phyllodes. Trees,1(2), 110-122.

Moran, M.S., Clarke, T.R., Inoue, Y., Vidal, A., 1994. Estimating crop water-deficit using the relation between surface-air temperature and spectral vegetation index. Remote Sensing of Environment, 49(3): 246-263.

Villalobos, F.J., Testi, L., Moreno-Perez, M.F., 2009. Evaporation and canopy conductance of citrus orchards. Agricultural Water Management, 96(4): 565-573.

Wang, X., Yang, W., Wheaton, A., Cooley, N., Moran, B., 2010. Automated canopy temperature estimation via infrared thermography: A first step towards automated plant water stress monitoring. Computers and Electronics in Agriculture, 73(1): 74-83.

Yang, Y., & Shang, S. 2013. A hybrid dual-source scheme and trapezoid framework–based evapotranspiration model (HTEM) using satellite images: Algorithm and model test. Journal of Geophysical Research: Atmospheres,118(5), 2284-2300.

Zarco-Tejada, P.J., Gonzalez-Dugo, V., Berni, J.A.J., 2012. Fluorescence, temperature and narrow-band indices acquired from a UAV platform for water stress detection using a micro-hyperspectral imager and a thermal camera. Remote Sensing of Environment, 117: 322-337.

Appendices

Appendix I: Leaf temperature extraction of thermal images following Wang et al.

(2010)
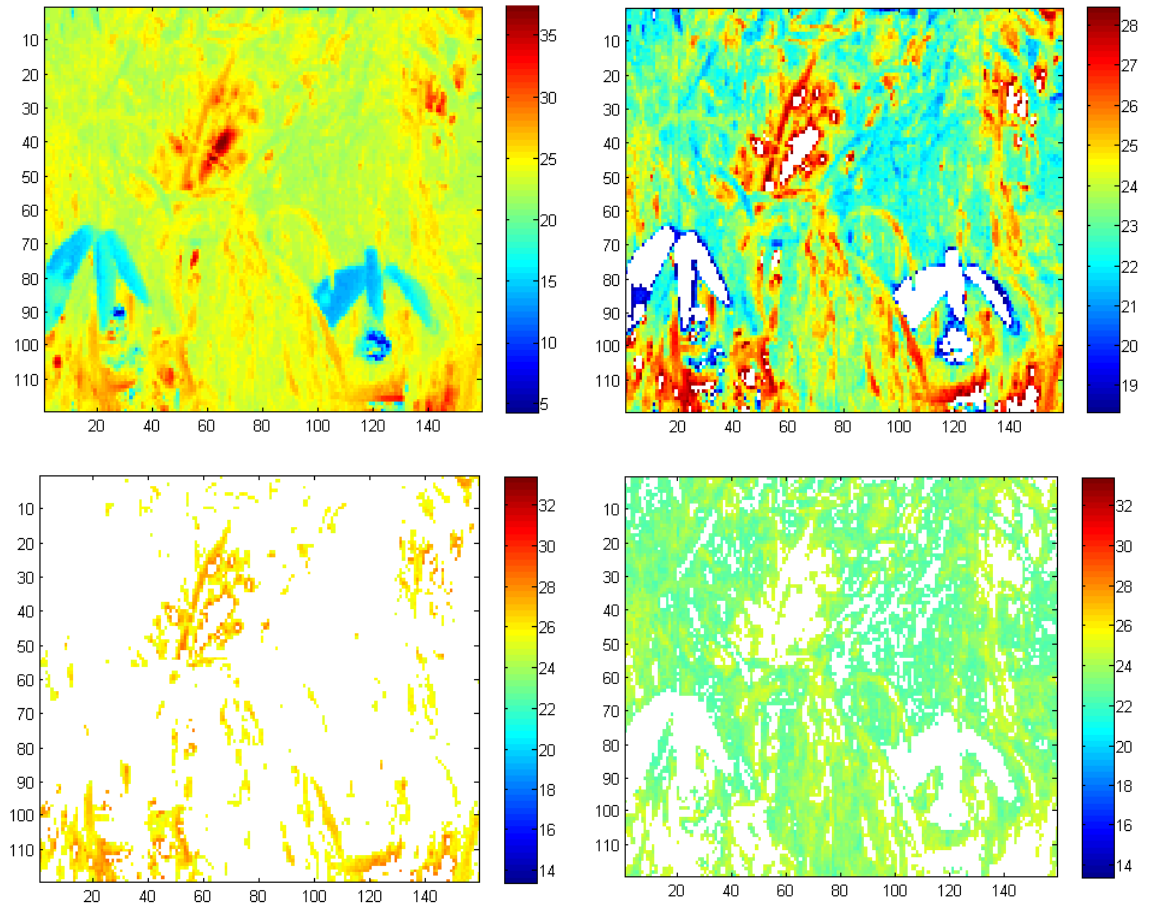
Figure AI.1: Leaf temperature extraction with the expectation-maximation algorithm according to Wang et al. (2010). Colorbar shows the temperature range.

Note: the upper left figure is the whole thermal image with artifical wet leaf (temperature below 15°C is water saturated cotton cloth and alluminum foil). Upper right figure shows artifical wet leaf excluded. Lower left figure shows the temperature extracted of the stems or dry dead leaves. The lower right figure give the final image that is used to obtain the average leaf temperature T_c.

Appendix II: Measurement of leaf stomata conductance of *Acacia pycnantha* and

Eucalyptus torquata

The site is located on a hill slope within 100 m of the *Acacia pycnantha* tree on which

leaf temperatures were monitored. From the 16, Apr to 29 May, 2013, leaf stomata conductance (g_s) were measured on several *Acacia pycnantha* and *Eucalyptus torquata* trees with a portable LI-6400XT photosynthetic analyser (LI-COR Biosciences, USA). The experiment was intended for the light response curves of the leaf photosynthesis. Measurement were conducted on at least 5 leaves on each tree at irregular intervals 3 times a week. For each measurement session, the LI-6400XT analyser was start up and warmed up for at least 30 min. The reference CO_2 and H_2O were levelled off before each measurement of a leaf. The light response curve auto program was used, during which, chamber air temperature was maintained at 20 ℃, airflow rate was fixed at 500 mol/s and PAR reduces in 10 increments from 2000 to 0 μmol photon·m^{-2}·s^{-1}. At each PAR increment, 3 minutes was given for stabilisation and then a reading was taken.

6 SUMMARY AND RECOMMENDATIONS

Soil-plant water relations are shared subject for communities of hydrology, ecology and physiology. To combine the knowledge and strengths from the communities will enhance our understanding of tree water use strategy, such as tree responses to water stress and the night-time transpiration etc. The first part of the thesis describes the development of a new hydraulic model (v-SPAC) that considers water transport limit from both soil and plant hydraulic properties (Chapter 2). The v-SPAC model is then applied in a few cases. Firstly, night-time transpiration is explored with sap flow measurement and v-SPAC modelling in chapter 3. The model can be used as a diagnosing tool for clarify the existing hypothesis. Secondly, a new method to derive root zone water retention curve is proposed from stem-soil hydraulic connection in chapter 4, the v-SPAC is to identify the favourable conditions for the application of the method. And finally, infrared thermography method is tested on its capability of detecting water stress of the two native species in chapter 5. The v-SPAC model provides a gap-filling tool for the observed plant and water stress time series. Summary and recommendations for each piece of work are given as follows.

6.1 The v-SPAC modelling

The v-SPAC model considers both the hydraulic limits of plant/soil porous media and the influencing environmental factors including soil moisture, vapour pressure deficit and radiation. The model is different from either hydrologic models that only consider subsurface processes or ecophysiological models that describe water transport in plant in such detail that subsurface soil water dynamics has to be simplified as steady-state. The v-SPAC is built upon hydrologic model LEACHM with added simple

representation of the dynamic plant hydraulic properties. The model has strengths in easy parameterization in field conditions, good performances in simulating both soil and water plant water status and water flux, and particularly improves the plant water state prediction.

Experimentation with the v-SPAC modelling suggests the great necessity of better quantification of the boundary water fluxes at the soil to root or canopy to air interfaces. For example, nocturnal transpiration should be described at the canopy to air boundary for the model calibration and prediction of transpiration. The root water uptake at the soil - root interface presents tough obscures (for both experimentation and modelling) in differentiating the resistances from bulk soil to root proximity, in the soil-root void or at the root surfaces. Lumping the resistances will not be able to identify the key processes in water stress progression. Charactering the tree hydraulic properties over a wide range of plant water state is also lacking or not easy to implement in models. The challenge therefore remains in simulating the tree responses and consequences to severe and sudden drought. To strengthen the power of the current model capacity requires advances in knowledge and experimental skills. It also requires skills from the modellers in appropriate compromise between model simplicity and model effectiveness when different processes dominate at different scales.

6.2 Nocturnal sap flow and transpiration

The plant's role in regulating transpiration and soil-plant water balance is strongly reflected in the observed high night-time sap flow rate of the *Acacia pycnantha* tree. The night-time vapour pressure deficit (VPD) and soil moisture saturation (Θ) are identified as the dominant factors that explain the nocturnal transpiration (Tn) variation over the seasons. The night-time canopy conductance is found being lack of

response to bulk air VPD but remains sensitive to soil water stress. The strong linear relation between Tn and night-time VPD of the acacia tree were consistent with those reported for dry sclerophyllous forest (Rosado et al., 2012). Non-linear relation were also noted in the study. Synthesizing research outcome on nocturnal transpiration and screening out the proper calculation methods will help to clarify our understanding on the relations between the driving factors and Tn.

Varied Tn results given by different methods of partitioning sap flow calls for a benchmark experiment with thorough instrumentations on soil, plant and atmosphere measurement. For example, using lysimeter, sap flow measurement and eddy covariance data will provide valuable insight into nocturnal transpiration characteristics at tree to ecosystem scales. The associated uncertainties from various methods can be fairly compared and pinned down with such experiment.

6.3 The RWRC method for root zone WRC derivation

A new method (RWRC method) is proposed to estimate root zone effective water retention curve. The method is based on hydraulic connection between the soil and the plant that sense the soil wetness through the "root". The method is deemed as superior than traditional WRC methods in terms of better presentation of the averaged root zone and larger scale coverage (at metre scale) than the soil core measurement (at centimetre scale). The RWRC method is shown to have high reliability on cases of silty and clayey soil sites. The method is particularly useful to constrain the water retention curves at -100 to -800 kPa range that is not captured by tensiometers in the field.

The method is preliminarily tested with v-SPAC modelling experiments on uniform soil texture and two common root density distribution forms. Vertical heterogeneity in soil texture and tree-specific root distribution forms are not considered in the

modelling experiments. One case of vertical heterogeneity is tested of the RWRC method at the acacia field site, showing comparable water retention curves to those of pedo-transfer function based on soil core measurement. The real case validation suggests that the method at least provides a good approximation at the initial stage of soil-plant researches before a thorough soil investigation is conducted. Further investigation on the effectiveness of the RWRC method in land surface modelling. Combined use of the method with remote sensing techniques will be of great potential.

6.4 Using leaf temperature to assess plant water status

Usefulness of the thermal imaging technique on detecting water stress of two native tree species (*Acacia pycnantha* and *Eucalyptus macrocarpa*) is tested under natural heterogeneous landscape. Comparing against standard water stress indicators, the leaf temperature based thermal indices are capable to detect the water stress progression. However, the thermal indices are not acute enough to detect soil moisture depletion within a week. The performance are deteriorated by high variable leaf temperatures caused by cloudy and windy conditions. Therefore, the method till now is more practical to apply under clear sky and relative stable atmospheric conditions. To broaden the usage of the method, more easily implement procedures and numerical analysis to eliminate the contamination factors should be advanced. The study raises the caution on applying the technique under high VPD conditions, such that the linear interpolation between wet and dry ends of the soil/plant water flux or water stress may be questionable and requires further investigation.

6.5 Recommendation for future work

Soil-plant water relations should attract more attention in the context of a changing environment. It's expected that severe droughts become more frequent in the future

(McDowell et al., 2013). The study of plant response to drought and the recovery afterwards require thorough and comprehensive research collaborations across the concerned disciplines. Compilation of large scale study experiences to confront the coming extreme weather is in need. Plant-photosynthetic capacity, transpiration may shift to a new realm with not only rising CO_2 but also higher VPD (Eamus et al., 2013). One piece of our work reveals that the usage of remote sensing technique may be impeded under high VPD conditions. It suggests that our previous experience should be renewed under the changing environment.

Scaling issues reside on both soil hydrologic and eco-physiologic research. The innovative method of deriving root-zone soil moisture (RWRC method) advanced water retention curve estimation from centimetre scale of the soil core point measurements to metre scale. The advancement provides a particularly important complement to the remote sensing method which only shows great advantage in large spatial areal coverage. Future work to test the upscaling scheme of the root-zone water status or transpiration flux with both the RWRC method and remote sensing technique is strongly recommended.

The plant size, architecture can reveal substantial convergence in plant function in multiple scales (Meinzer, 2003), but are less documented for the nocturnal transpiration studies. Synthesizing the nocturnal transpiration research outcome from both biological and environmental aspects will be of great value to build universal scaling model for ecosystem water flux calculation and enhance our understanding on the mechanisms behind.

The v-SPAC model currently only concerns water transport. Combing carbon and water into one integrated model will be the future trend to answer research questions

in the water, soil, plant and atmospheric interaction. For example, why plant lose water at night is an open puzzle for eco-physiologists from an instinct that water loss at night seems a waste of water with no carbon gain (Caird et al., 2007).

References

Caird, M. A., Richards, J. H., and Donovan, L. A. 2007. Nighttime stomatal conductance and transpiration in C3 and C4 plants. Plant Physiology, 143(1), 4-10.

Eamus, D., Boulain, N., Cleverly, J., & Breshears, D. D. 2013. Global change-type drought-induced tree mortality: vapor pressure deficit is more important than temperature per se in causing decline in tree health. Ecology and evolution, 3(8), 2711-2729.

McDowell, N.G. et al., 2013. Evaluating theories of drought-induced vegetation mortality using a multimodel-experiment framework. New Phytologist, 200(2): 304-321.

Meinzer, F. C. 2003. Functional convergence in plant responses to the environment. Oecologia, 134(1), 1-11.

Rosado, B. H. P., Oliveira, R. S., Joly C. A., Aidar M. P. M., and Burgess S. S. O., 2012. Diversity in nighttime transpiration behavior of woody species of the Atlantic Rain Forest, Brazil, Agricultural and Forest Meteorology, 158, 13-20.

Yunusa, I. et al., 2010. Topographical and seasonal trends in transpiration by two co-occurring Eucalyptus species during two contrasting years in a low rainfall environment. Agricultural and Forest Meteorology, 150(9): 1234-1244.